The Scientific World Journal

Application of Discrete Mathematics in Urban Transportation System Analysis

Guest Editors: Baozhen Yao, Bin Yu, Gang Chen, Rui Mu, and Fang Zong

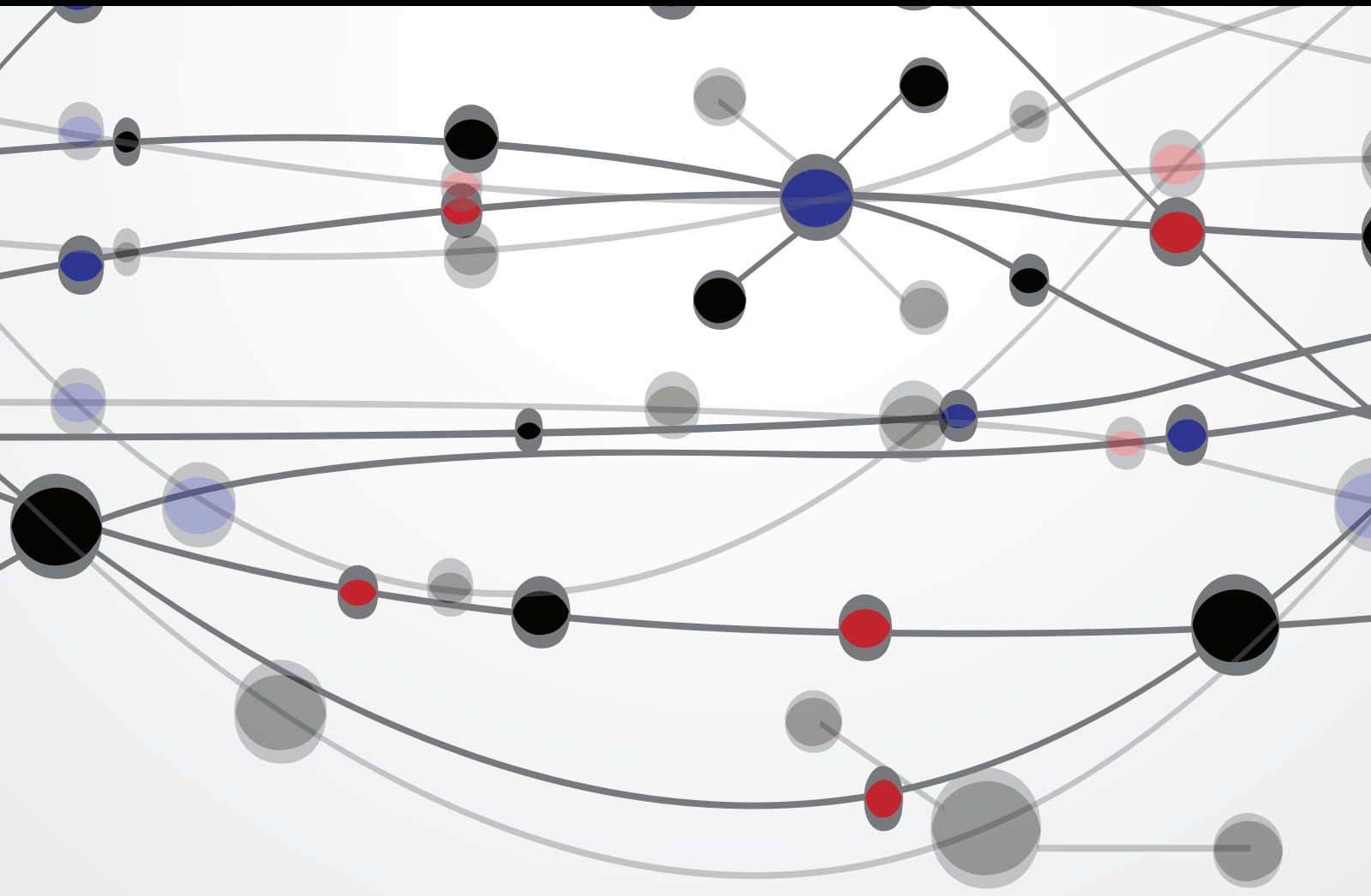

Application of Discrete Mathematics in Urban Transportation System Analysis

Mathematical Problems in Engineering

Application of Discrete Mathematics in Urban Transportation System Analysis

Guest Editors: Baozhen Yao, Bin Yu, Gang Chen, Rui Mu, and Fang Zong

Editorial Board

Contents

Application of Discrete Mathematics in Urban Transportation System Analysis, Baozhen Yao, Bin Yu, Gang Chen, Rui Mu, and Fang Zong
Volume 2014, Article ID 212356, 2 pages

A Hybrid GRASP+VND Heuristic for the Two-Echelon Vehicle Routing Problem Arising in City Logistics, Zheng-yang Zeng, Wei-sheng Xu, Zhi-yu Xu, and Wei-hui Shao
Volume 2014, Article ID 517467, 11 pages

Static and Dynamic Analysis of Railway Reinforced System with Cross-Beams, Bin Peng, Nan Zhang, and Yu Lan Gao
Volume 2014, Article ID 513606, 7 pages

Study on the Weaving Behavior of High Density Bidirectional Pedestrian Flow, Lishan Sun, Zifan Yang, Jian Rong, and Xiaoming Liu
Volume 2014, Article ID 765659, 9 pages

An Initial Implementation of Multiagent Simulation of Travel Behavior for a Medium-Sized City in China, Chengxiang Zhuge, Chunfu Shao, Jian Gao, Meng Meng, and Weiyang Xu
Volume 2014, Article ID 980623, 11 pages

The Effect of Travel Information on Travelers' Choice of Travel Modes and Routes: A Case Study of the Travel between the Campuses, Linjie Gao, Zhicai Juan, Anning Ni, and Peng Jing
Volume 2014, Article ID 781395, 9 pages

Deterioration Prediction of Urban Bridges on Network Level Using Markov-Chain Model, Li Li, Lijun Sun, and Guobao Ning
Volume 2014, Article ID 728107, 10 pages

The Best Path Analysis in Military Highway Transport Based on DEA and Multiobjective Fuzzy Decision-Making, Wu Juan, Lu Huapu, Sun Xu, Liu Xianfeng, and Yang Huijun
Volume 2014, Article ID 206024, 6 pages

Multiobjective Optimization Based Vessel Collision Avoidance Strategy Optimization, Qingyang Xu, Chuang Zhang, and Ning Wang
Volume 2014, Article ID 914689, 9 pages

Lane Changing Trajectory Planning and Tracking Controller Design for Intelligent Vehicle Running on Curved Road, Lie Guo, Ping-Shu Ge, Ming Yue, and Yi-Bing Zhao
Volume 2014, Article ID 478573, 9 pages

Beam Structure Damage Identification Based on BP Neural Network and Support Vector Machine, Bo Yan, Yao Cui, Lin Zhang, Chao Zhang, Yongzhi Yang, Zhenming Bao, and Guobao Ning
Volume 2014, Article ID 850141, 8 pages

Structural Damage Identification of Pipe Based on GA and SCE-UA Algorithm, Yaojin Bao, He Xia, Zhenming Bao, Shuiping Ke, and Yahui Li
Volume 2013, Article ID 101483, 9 pages

Bayesian Network Assessment Method for Civil Aviation Safety Based on Flight Delays,
Huawei Wang and Jun Gao
Volume 2013, Article ID 594187, 12 pages

Transport Turnover with Spatial Econometric Perspective under the Energy Conservation and Emissions Reduction in China, Zhongzhen Yang, Wensi Wang, Hongli Bao, Lu Kong, and Bin Yu
Volume 2013, Article ID 760604, 9 pages

Real-Time Gate Reassignment Based on Flight Delay Feature in Hub Airport, Huawei Wang, Yuxiao Luo, and Zhijian Shi
Volume 2013, Article ID 646241, 10 pages

Damage Detection of Bridge Structure Based on SVM, Yaojin Bao, Chenjin Song, Wensi Wang, Ting Ye, Lu Wang, and Lan Yu
Volume 2013, Article ID 490372, 7 pages

Predicting Severity and Duration of Road Traffic Accident, Fang Zong, Huiyong Zhang, Hongguo Xu, Xiumei Zhu, and Lu Wang
Volume 2013, Article ID 547904, 9 pages

An Improved Particle Swarm Optimization for the Automobile Spare Part Warehouse Location Problem, Zhen Yaobao, Hu Ping, and Yang Shu
Volume 2013, Article ID 726194, 6 pages

Multiobjective Gate Assignment Based on Passenger Walking Distance and Fairness, Yu Jiang, Linyan Zeng, and Yuxiao Luo
Volume 2013, Article ID 361031, 7 pages

Accurate Multisteps Traffic Flow Prediction Based on SVM, Zhang Mingheng, Zhen Yaobao, Hui Ganglong, and Chen Gang
Volume 2013, Article ID 418303, 8 pages

Prediction for Traffic Accident Severity: Comparing the Bayesian Network and Regression Models, Fang Zong, Hongguo Xu, and Huiyong Zhang
Volume 2013, Article ID 475194, 9 pages

Hindawi Publishing Corporation
Mathematical Problems in Engineering
Volume 2014, Article ID 212356, 2 pages
http://dx.doi.org/10.1155/2014/212356

Editorial

Application of Discrete Mathematics in Urban Transportation System Analysis

Baozhen Yao,[1] Bin Yu,[2] Gang Chen,[3] Rui Mu,[4] and Fang Zong[5]

[1] *School of Automotive Engineering, Dalian University of Technology, Dalian 116024, China*
[2] *Transportation Management College, Dalian Maritime University, Dalian 116024, China*
[3] *Department of Mechanical and Manufacturing Engineering, Aalborg University, Denmark*
[4] *Faculty of Technology, Policy and Management, Delft University of Technology, Delft, The Netherlands*
[5] *College of Transportation, Jilin University, Changchun 30022, China*

Correspondence should be addressed to Bin Yu; ybzhyb@163.com

Received 5 May 2014; Accepted 5 May 2014; Published 15 June 2014

Urban transportation system is of foremost importance to support the passengers and freight mobility requirements of urban agglomerations. Transportation in urban areas is highly complex because of the modes involved, the multitude of origins and destinations, and the amount and variety of traffic. Analysing the urban transportation system is the process of attempting to examine the behaviour patterns of the elements of urban transportation system and the interactions among them, which is very critical for urban traffic planning and management. Discrete mathematics is the branch of mathematics dealing with objects that can be assumed by only distinct, separated values. Since the behaviour of travellers and vehicles, which are the main elements in urban transportation system, is in an individual level, compared with traditional aggregated methods, the techniques of discrete mathematics are more suitable to be adopted in urban transportation system analysis. Therefore, discrete mathematics is gradually becoming the popular method to analyse transportation system and has attracted much attention of the researchers.

Within this context, this special issue serves as a forum to highlight the most significant recent developments in the techniques of discrete mathematics, especially discrete choice models, Bayesian network, and so on, and to apply these techniques on urban transportation system analysis, such as travel behaviour, taxi's driving pattern, and delivery route selection.

Some works focus on the application of prediction in urban transportation system; for example, Z. Mingheng et al.'s work "*Accurate multisteps traffic flow prediction based on SVM*" attempted to use support vector machine to predict traffic flow for intelligent traffic management. In the prediction method, a multisteps prediction was adopted to improve the performance of prediction. The results indicated that the proposed support vector machine had a good ability for traffic flow prediction. F. Zong et al.'s paper "*Prediction for traffic accident severity: comparing the Bayesian network and regression models*" tried to predict traffic accident severity by comparing the Bayesian network and regression models. In their paper, there were three severity indicators, that is, number of fatalities, number of injuries, and property damage, which were used. L. Li et al. "*Deterioration prediction of urban bridges on network levelusing Markov-chain model*" aimed to predict urban bridge deterioration with Markov-chain model. In the model, three deterioration circumstances were considered, and the results showed that recoverable repair treatments were important for bridge condition and the prediction method was effective for predicting bridge deterioration. F. Zong et al.'s work "*Predicting severity and duration of road traffic accident*" presented a model system to predict the severity and duration of road traffic accidents. In the model, ordered probit model and hazard model were used, respectively. The results suggested that the ordered probit model had a higher prediction performance than the SVM model.

Some researchers focused on the detection or assessment problem in transportation system. Y. Bao et al.'s paper "*Structural damage identification of pipe based on GA and*

SCE-UA algorithm" wanted to identify structural damage effectively. They proposed genetic algorithm and SCE-UA algorithm to detect platform structure damage in their paper. The results showed that the two algorithms have high identification accuracy and good adaptability. B. Peng et al.'s paper "*Static and dynamic analysis of railway reinforced system with cross-beams*" proposed a static and dynamic analysis of railway reinforced system with cross-beams. Y. Bao et al.'s work "*Damage detection of bridge structure based on SVM*" attempted to detect the damage of bridge pier for bridge management and maintenance. In their paper, support vector machine was used to detect the damage of bridge pier. The results suggested that the support vector machine was an effective method for detecting damage of bridge pier. H. Wang and J. Gao's work "*Bayesian network assessment method for civil aviation safety based on flight delays*" proposed a Bayesian network assessment method for civil aviation safety. In the model, the Bayesian network was used to build the aviation operation safety assessment based on flight delay. B. Yan et al.'s work "*Beam structure damage identification based on BP neural network and support vector machine*" attempted to use BP neural network and support vector machine to identify beam structure damage. The results showed that the two methods had a preferable identification precision.

Also assignment methods in urban transportation system are discussed in some works. Y. Jiang et al.'s work "*Multiobjective gate assignment based on passenger walking distance and fairness*" attempted to shorten the walking distance and balance the airlines' service quality by using a multiobjective gate assignment model. Test results indicated that the optimization model could reduce effectively the walking distance of passenger and improve the number of flights. H. Wang et al.'s work "*Real-time gate reassignment based on flight delay featurein hub airport*" tried to achieve real-time gate reassignment in hub airport. The objective was to minimize the disturbance led by gate reassignment based flight delay feature and ant colony algorithm was used to solve the problem.

There are also some works on the planning problem in this field. W. Juan et al.'s work "*The best path analysis in military highway transport based on DEA and multiobjective fuzzy decision-making*" presented data envelopment analysis and multiobjective fuzzy decision-making to select the best path for military highway transport. L. Guo et al.'s work "*Lane changing trajectory planning and tracking controller design for intelligent vehicle running on curved road*" tried to enhance the active safety and presented lane changing trajectory planning and tracking controller design for intelligent vehicle running on curved road. Z. Yaobao et al.'s work "*An improved particle swarm optimization for the automobile spare part warehouse location problem*" used a particle swarm optimization to solve the automobile spare part warehouse location problem. In the algorithm, acceleration coefficients and crossover operation were used to improve the performance of the algorithm.

Travel behaviour and weaving behaviour are also considered in some papers. L. Sun et al.'s work "*Study on the weaving behavior of high density bidirectional pedestrian flow*" discussed the characteristic of pedestrian weaving behaviour. In the study, video analysis was selected to extract pedestrian moving behaviour. L. Gao et al.'s work "*The effect of travel information on travelers' choice of travel modes and routes: a case study of the travel between the campuses*" attempted to study the travelers' choices of travel modes and routes. In their paper, a case study of the travel between Minhang campus and Xuhui campus of Shanghai Jiao Tong University was conducted. C. Zhuge et al.'s work "*An initial implementation of multiagent simulation of travelbehavior for a medium-sized city in China*" proposed an agent-based simulation of travel behaviour to acquire the travel behaviour features in a medium-sized city in China.

Other methods like transport turnover and vessel collision avoidance strategy are also studied in this special issue. Z. Yang et al.'s paper "*Transport turnover with spatial econometric perspective under the energy conservation and emissions reduction in China*" proposed a spatial econometric model to solve the space correlation of road turnover among 31 provinces in China. Q. Xu et al.'s work "*Multiobjective optimization based vessel collision avoidance strategy optimization*" presented a multiobjective optimization to reduce the human fault and improve the safety of marine traffic. And a multiobjective optimization algorithm NSGA-II was used to solve the problem.

These articles demonstrate the advancement of the recent development in techniques like discrete choice models, Bayesian network, and support vector machine in urban transportation system.

Acknowledgments

We would like to express our gratitude to the many reviewers for their hard work. We would also like to thank the authors for their contributions to the special issue. This special issue could not have been completed without their dedication and support.

Baozhen Yao
Bin Yu
Gang Chen
Rui Mu
Fang Zong

Hindawi Publishing Corporation
Mathematical Problems in Engineering
Volume 2014, Article ID 517467, 11 pages
http://dx.doi.org/10.1155/2014/517467

Research Article

A Hybrid GRASP+VND Heuristic for the Two-Echelon Vehicle Routing Problem Arising in City Logistics

Zheng-yang Zeng, Wei-sheng Xu, Zhi-yu Xu, and Wei-hui Shao

School of Electronics and Information Engineering, Tongji University, Shanghai 201804, China

Correspondence should be addressed to Wei-sheng Xu; xuweisheng@tongji.edu.cn

Received 29 November 2013; Accepted 30 March 2014; Published 23 April 2014

Academic Editor: Baozhen Yao

The two-echelon vehicle routing problem (2E-VRP) is a variant of the classical vehicle routing problem (VRP) arising in two-level transportation systems such as those encountered in the context of city logistics. In the 2E-VRP, freight from a depot is compulsorily delivered through intermediate depots, named satellites. The first echelons are routes that distribute freight from depot to satellites, and the second are those from satellites to customers. This problem is solved by a hybrid heuristic which is composed of a greedy randomized adaptive search procedure (GRASP) with a route-first cluster-second procedure embedded and a variable neighborhood descent (VND), called GRASP+VND hereafter. Firstly, an extended split algorithm in the GRASP continuously splits randomly generated permutations of all customers and assigns customers to satellites reasonably until a feasible assignment appears, and a complete 2E-VRP feasible solution is obtained by solving the first echelon problem subsequently and, secondly, a VND phase attempts to improve this solution until no more improvements can be found. The process above is iterated until the maximum number of iterations is reached. Computational tests conducted on three sets of benchmark instances from the literature show that our algorithm is both effective and efficient and outperforms the best existing heuristics for the 2E-VRP.

1. Introduction

The transportation of freight constitutes an extremely important activity taking place in urban areas, but it is also very disturbing. The increase in the number of freight transportation trucks using urban roads makes a more and more significant contribution to traffic congestion and many associated negative environmental impacts, such as air pollution and noise. For the purpose of preventing the urban environment from getting worse, many municipalities place restrictions on these big trucks to keep them out of their city centers by creating peripheral intermediate facilities, called satellites. External carriers need to supply these satellites from central depots and then smaller and environmentally friendly vehicles would distribute the freight downtown from these satellites [1–3]. Therefore, two distribution echelons are involved in city logistics. With the customer demands, satellite capacities, and vehicle capacities from the two levels known in advance, the two-echelon vehicle routing problem (2E-VRP) [4, 5] consists in building a set of the least-cost trips (the fewest number of vehicles used and least vehicle traveling cost) for the two echelons.

The 2E-VRP is a new two-echelon variant of the well-known vehicle routing problem (VRP). Several models have been proposed and different kinds of algorithms have been designed, including both exact algorithms [4–7] and heuristic algorithms [8–11].

Perboli et al. [4] introduced a family of two-echelon vehicle routing problems and proposed a three-index flow-based formulation for the 2E-VRP. The authors also introduced some valid inequalities and two math-heuristics based on the 2E-VRP model, which were used within a branch-and-cut framework. They were able to solve to optimality instances containing up to 21 customers.

Perboli and Tadei [5] proposed several new classes of valid inequalities based on the traveling salesman problem (TSP) and the VRP and strengthened the previous 2E-VRP formulation with new cuts (including capacity cuts), which allowed their algorithm to solve seven new instances to

optimality and reduce the optimality gap on several other instances.

Jepsen et al. [6] presented an edge flow based model for the 2E-VRP and employed a specialized branching scheme to branch on infeasible integer solutions in their branch-and-cut algorithm to obtain feasible solutions. Their algorithm was able to solve 47 instances to optimality, surpassing previous exact algorithms. They found that the coupling between the two echelons in the 2E-VRP would pose a challenge to incorporate.

Baldacci et al. [7] proposed a new mathematical formulation of the 2E-VRP (used to derive valid lower bounds) and a new exact method. They decomposed the 2E-VRP into a limited set of multidepot vehicle routing problems (MDVRPs) with side constraints. Computational results on extensive benchmark instances showed that their exact algorithm outperformed the state-of-the-art exact methods in terms of size, number of problems solved to optimality, and computing time.

Since exact algorithms are usually computationally expensive for large-scale combinatorial optimization problems, approximate solutions with sufficient accuracy that can be obtained fast are often desired in practice.

Crainic et al. [8] developed a family of multistart heuristics, based on separating the depot-to-satellite transfer and the satellite-to-customer delivery by iteratively solving the two resulting routing subproblems, while adjusting the satellite workloads that linked them. Besides, an intensification phase aiming at improving feasible solutions by local search was followed by a diversification phase to avoid local optimum in their algorithms. Their ideas are very useful to handle the 2E-VRP; however, they obtained relatively poor results even in small-scale instances.

Meihua et al. [9] proposed a hybrid ant colony optimization algorithm which combined three heuristics for the 2E-VRP. They firstly divided the problem into several VRPs by a separation strategy and then applied improved ant colony optimization with multiple neighborhood descent to build better feasible solutions. Computational tests on 22 benchmark instances from the literature showed that their algorithm was better than previous published algorithms.

Hemmelmayr et al. [10] developed an adaptive large neighborhood search (ALNS) heuristic for the 2E-VRP, based on the destroy-and-repair principle in which two different sets of operators (destroy operators and repair operators) are alternated. They used existing operators and new operators designed specifically for the 2E-VRP. Their algorithm was shown to provide better solutions and outperform existing heuristic methods for the 2E-VRP but is much complicated to implement in practice because of adopting too many kinds of operators (8 kinds of destroy operators, 5 kinds of repair operators, and 5 kinds of local search operators) and many parameters.

Crainic et al. [11] proposed a heuristic algorithm based on greedy randomized adaptive search procedure (GRASP) combined with path relinking to address the 2E-VRP. The problem was treated by separating the depot-to-satellite transfer and the satellite-to-customer delivery and iteratively solving the two resulting routing subproblems, while adjusting the satellite workloads that link them; this idea is the same as Crainic et al. [8]. The path relinking procedure with feasibility search was applied to link current solution to elite one. The computational results on instances with up to 50 customers and 5 satellites showed that the proposed heuristic can improve literature results, in both efficiency and accuracy, but their solution quality cannot outperform the ALNS of Hemmelmayr et al. [10].

According to the published computational results of these heuristic methods mentioned above, we can retrieve that the best existing heuristic for the 2E-VRP is the ALNS algorithm of Hemmelmayr et al. [10].

Greedy randomized adaptive search procedure (GRASP) is one of the most well-known multistart heuristics for combinatorial optimization problems. It was introduced by Feo and Resende [12]. Each GRASP iteration consists basically of constructing a feasible solution and then applying a local search procedure to improve it until a local optimum is found, and the best overall solution is kept as the final result [12, 13].

Variable neighborhood descent (VND) is a deterministic version of variable neighborhood search (VNS), originally proposed by Mladenović and Hansen [14]. VNS is a metaheuristic for solving combinatorial optimization problems, whose basic idea is a systematic change of neighborhoods, both within a descent phase to find a local optimum and in a perturbation phase to get out of the corresponding valley [14, 15]. VNS explores an ordered list of neighborhoods. It starts with a given neighborhood and switches to the next one in the list when it finds a local minimum. The search is reinitialized from the first neighborhood whenever a new better solution is found or when all neighborhoods have been checked. VND also changes the neighborhood operators once the search is stuck in a local optimum, but it differs from VNS that no random perturbation is applied.

The hybrid of GRASP and VND has successfully solved several kinds of routing problems, such as pickup-and-delivery traveling salesman problem [16], truck and trailer routing problem [17], traveling repairman problem [18], three-dimensional bin packing problem [19], and school bus routing problem [20]. Because the combinations of GRASP and VND are not only effective and efficient in solving combinatorial optimization problems but also very simple to implement, we design a hybrid GRASP+VND heuristic for the 2E-VRP based on the characteristics of this problem to meet the practical requirements arising in city logistics.

The remainder of this paper is organized as follows. Section 2 first describes the 2E-VRP and its mathematical model. Section 3 gives the details of our hybrid heuristic for the 2E-VRP. Section 4 presents computational results on three sets of instances. Section 5 contains the discussion and Section 6 gives the conclusion.

2. Problem Description and Mathematical Formulation

The definition of 2E-VRP provided here follows those in [4, 7, 10]. 2E-VRP can be defined on a weighted, complete, and undirected graph $G = (V, A)$ with node set V and arc set

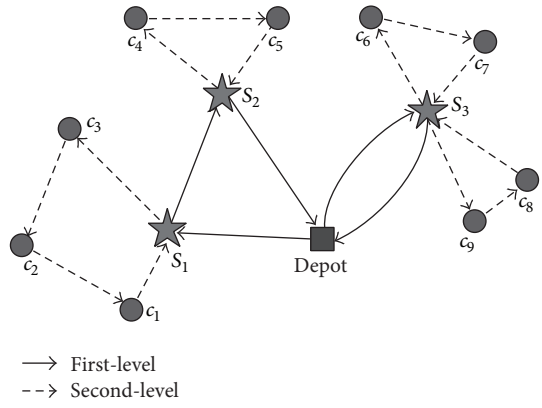

Figure 1: A solution to the 2E-VRP.

A. Node set V is composed of three kinds of nodes: a depot V_0, a subset V_S of n_s satellites, and a subset V_C of n_c customers. In the arc set A, each arc (i, j) represents the shortest path in the actual road network, with a known traveling cost c_{ij}. Costs in both levels are assumed to satisfy the triangle inequalities. Each customer $i \in V_c$ has an associated demand d_i, known in advance, and cannot be split. The demand should not be delivered by direct shipping from the depot but must be consolidated in a satellite. The deliveries to the satellites on the first echelon can be split. Each vehicle has a capacity constraint that has to be respected. This capacity is the same for all vehicles belonging to the same level but may differ for each level. The capacities of the first- and the second-level vehicles are denoted by Q_1 and Q_2, respectively. The total number of vehicles available is given by m^1 for the first level and m^2 for the second. Each satellite $k \in V_S$ has a capacity B_k that limits the total amount of customers' demands that can be delivered to it by first-level routes. Moreover, there are m_k first-level vehicles available at each satellite $k \in V_S$. No additional limitation on the route size, neither in length nor in number of visited customers, is introduced.

Figure 1 illustrates a 2E-VRP solution with a depot, three satellites, and nine customers. The satellites are represented by five-pointed stars and customers by circles and the depot by a square. The routes that serve the satellites from the depot are called the first-level routes. The second-level routes are those that start from a satellite, visit the customers, and return to the same satellite. Vehicle routes of the first and the second echelon are represented by continuous thick lines and dashed thin lines, respectively.

2.1. Mathematical Formulation. Based on the above description, the 2E-VRP can be formulated as follows [7]. Let $\mathscr{M}$ be the index set of all first-level routes, and let $\mathscr{M}_k \subseteq \mathscr{M}$ be the subset of first-level routes serving satellite $k =\in V_S$. Let R_r and $A(r)$ be the subset of satellites visited and subset of arcs traversed by a first-level route $r \in \mathscr{M}$, respectively. Let $\mathscr{R}_k$ be the index of the second-level routes passing through satellite $k \in V_S$, and let $\mathscr{R}_{ik} \subseteq \mathscr{R}_k$ be the subset of routes passing through satellite $k \in V_S$ and customer $i \in V_C$. The subset of customers visited and the subset of arcs traversed by a second-level route $l \in \mathscr{R}_k$ are represented by R_{kl} and $A(l)$, respectively. Let y_r be a binary variable equal to 1 if and only if route $r \in \mathscr{M}$ is in 2E-VRP solution, x_{kl} a binary variable equal to 1 if and only if route $l \in \mathscr{R}_k$ of satellite $k \in V_S$ is in 2E-VRP solution, and d_{kr} a nonnegative integer variable representing the quantity delivered by first-level route $r \in \mathscr{M}$ to satellite $k \in R_r$. And the mathematical model of the 2E-VRP can be stated as follows [7]:

$$\min \quad \sum_{k\in V_S}\sum_{l\in\mathscr{R}_k}\sum_{(i,j)\in A(l)} c_{ij}x_{kl} + \sum_{r\in\mathscr{M}}\sum_{(i,j)\in A(r)} c_{ij}y_r \tag{1}$$

$$\text{subject to:} \quad \sum_{k\in V_S}\sum_{l\in\mathscr{R}_k} x_{kl} = 1, \quad i \in V_C, \tag{2}$$

$$\sum_{l\in\mathscr{R}_k} x_{kl} \le m_k, \quad k \in V_S, \tag{3}$$

$$\sum_{k\in V_S}\sum_{l\in\mathscr{R}_k} x_{kl} \le m^2, \tag{4}$$

$$\sum_{l\in\mathscr{R}_k}\sum_{i\in R_{kl}} d_i x_{kl} \le B_k, \quad k \in V_S, \tag{5}$$

$$\sum_{r\in\mathscr{M}} y_r \le m^1, \tag{6}$$

$$\sum_{r\in\mathscr{M}_k} d_{kr} = \sum_{l\in\mathscr{R}_k}\sum_{i\in R_{kl}} d_i x_{kl}, \quad k \in V_S, \tag{7}$$

$$\sum_{r\in R_r} d_{kr} \le Q_1 y_r, \quad r \in \mathscr{M}, \tag{8}$$

$$x_{kl} \in \{0, 1\}, \quad k \in V_S, \quad l \in \mathscr{R}_k, \tag{9}$$

$$y_r \in \{0, 1\}, \quad r \in \mathscr{M}, \tag{10}$$

$$d_{kr} \in \mathbb{Z}_+, \quad k \in R_r, \quad r \in \mathscr{M}. \tag{11}$$

The objective function (1) aims to minimize the total cost of two echelons. Constraints (2) ensure that each customer $i \in V_C$ must be visited by exactly one second-level route. Constraints (3), (4), and (6) impose the upper bounds on the number of first- and second-level routes in the solution. Constraints (5) specify the capacities of each satellite. The balance between the quantity delivered by first-level routes to every satellite and the customers demands supplied from this satellite is ensured by constraints (7). Constraints (8) impose that the vehicle capacity of the first-level vehicles is not exceeded.

Each second-level route must begin and end at the same satellite, and each customer must be served by exactly one second-level vehicle. The demand of each satellite is the total demand of its assigned customers, so each satellite must receive enough freight from the depot to satisfy the customers of its second-level routes. Besides, any change to the customer-to-satellite assignment affects the first-level routing and therefore has an impact on the first-level transportation costs. The objective function to be minimized is the global transportation costs in both levels. 2E-VRP can be easily seen to be a reduction to the vehicle routing problem (VRP), which

is a special case of 2E-VRP arising when just one satellite is considered, so it is also NP-hard [10].

3. The Hybrid GRASP+VND Heuristic

The proposed algorithm is a memoryless multistart heuristic method in which each iteration consists of two phases: a *greedy randomized adaptive search procedure* (GRASP) construction phase and a *variable neighborhood descent* (VND) improvement phase. Since the solutions generated by the GRASP construction phase are not guaranteed to be locally optimal, it may be very beneficial to apply a local search to further improve each constructed solution [12, 17]. We use the term GRASP+VND to symbolize this hybrid algorithm. GRASP+VND independently creates and improves a number of initial solutions and in the end returns the best solution obtained during the entire search.

3.1. Search Space. The search is restricted to feasible solutions. We do not allow any violations of the constraints on the vehicle capacity, number of vehicles available, and the capacity constraints of the satellites. The reason that we always maintain the feasibility of solutions is that it is quite difficult and time consuming to perform feasibility repairing (due to the constraints of the number and capacity of the second-level vehicles) after the solutions are infeasible in the search.

The initial solutions of GRASP+VND are generated from solutions encoded as random permutations (TSP tours covering the entire n_c customers). Any random permutation T can be converted into a 2E-VRP solution S (with respect to the orders of customers in T) using an extended version of the splitting procedure *split* of Nguyen et al. [21]. Customers are assigned to satellites by this extended *split* according to their orders in T in a relatively reasonable manner and then the demand of each satellite is obtained by the summation of the demands of all its assigned customers.

With the obtained demands of all the satellites, the first-level routes are constructed as follows [10, 22]: we first create as many full-load direct trips from the depot to each satellite as possible until the remaining demand of each satellite is less than the capacity Q_1 of the first-level vehicle and then solve a TSP tour using the saving algorithm of Clarke and Wright [23], as it was handled by Hemmelmayr et al. [10].

3.2. Initial Solution Construction Phase. The goal of GRASP is to create initial feasible solutions for the second phase to further improve them. For the hybrid GRASP+VND algorithm to work well, it is essential that solutions of relatively high quality are constructed during the solution construction phase.

The idea of splitting a good TSP tour to a VRP solution was first introduced by Beasley [24], as a route-first cluster-second heuristic for the VRP. A random permutation T of all customers is first cut into second-level routes by an extended version of the *split* algorithm of Nguyen et al. [21]. The first stage of our extended algorithm consists of minimizing the number of second-level routes, that is, the number of second-level vehicles used. This extension [25] of *split* defines

(1) Initialize random generator;
(2) **repeat**
(3) $T \leftarrow RandomPermutation(V_C)$;
(4) $Trips \leftarrow Split(T)$;
(5) **until** *Trips* are *feasible*
(6) $S \leftarrow CompleteSolution(Trips)$;
(7) **return** the feasible solution S generated;

Algorithm 1: GRASP for the construction of an initial solution.

a second label N_i for the number of arcs on the shortest path (i.e., the number of second-level vehicles used up to j), sets $N_0 = 0$ at the beginning, and tests N_j before L_j (the cost of the shortest path up to j) to minimize first the number of second-level vehicles.

The adoption of this extension is because the number of routes is often considered as the primary objective of VRP and we also need to obtain feasible solutions concerning the upper bound on the number of the second-level vehicles.

Algorithm 1 gives the framework of the initial solution construction procedure in our GRASP+VND.

Algorithm 2 implements the extended *split* for a random permutation T of all the n_c customers. SA_j records the assigned satellite of the jth customer in T and P_j records the predecessor of this customer on the shortest path. $\mathscr{W} \cdot c(k, V_0)$ represents the additional penalty for each second-level route according to the distance between its assigned satellite and the depot. $\mathscr{W}$ is a nonnegative value, it can be adjusted to change the impact of the first-level routes on the complete initial solution, and, as it increases, the first-level routes are given more importance. It is set to 1 as a default value to obtain a compromised consideration on routes of both echelons.

3.3. Solution Improvement Phase. After an initial feasible solution is generated, an attempt is made to improve it exhaustively. We apply a VND approach to perform the solution improvement procedure until no more improvements can be found. VND is a simplified variant of the VNS heuristic, in which the shaking phase is omitted. Therefore, VND is usually completely deterministic contrary to VNS.

The neighborhoods of our VND can be classified into two types: intersecond-level-route and intrasecond-level-route. Traditional VRP local search operators contain interroute and intraroute operators. Intraroute operators search and improve a single route at a time, while interroute operators deal with several routes simultaneously. When handling the 2E-VRP, we slightly modify the name of this classification for the second-level routes. The existing three interroute neighborhood structures *Shift*, *Swap*, and *Cross* and three intraroute neighborhood structures 2-*Opt*, *Or-Opt,* and *Exchange* of Subramanian et al. [26–28] are employed, and we also propose two new neighborhoods *Satellites-Change* and *Satellites-Swap* specially for the 2E-VRP.

Following the representation of Subramanian et al. [26–28], we consider $Shift\,(\lambda, 0)$, $\lambda \in \{1, 2, 3\}$, and $Swap\,(\lambda_1, \lambda_2)$, $\lambda_1, \lambda_2 \in \{1, 2, 3\}$. We restrict that *Shift* moves at most 3 adjacent customers from a second-level route to another; *Swap*

(1) $L_0 \leftarrow 0$; $N_0 \leftarrow 0$;
(2) **for** $i \leftarrow 1$ **to** n_c **do**
(3) $\quad L_i \leftarrow +\infty$; $N_i \leftarrow i$; $SA_i \leftarrow \varnothing$;
(4) **end for**
(5) **for** $i \leftarrow 1$ **to** n_c **do**
(6) $\quad load \leftarrow 0$; $cost1 \leftarrow 0$; $j \leftarrow i$;
(7) $\quad$ **repeat**
(8) $\quad\quad load \leftarrow load + d(T_i)$;
(9) $\quad\quad$ **if** $j = i$ **then**
(10) $\quad\quad\quad cost1 \leftarrow 0$;
(11) $\quad\quad$ **else**
(12) $\quad\quad\quad cost1 \leftarrow cost1 + c(T_{j-1}, T_j)$;
(13) $\quad\quad$ **end if**
(14) $\quad\quad cost \leftarrow cost1 + \min\{c(k, T_i) + c(T_j, k) + \mathscr{W} \cdot c(k, V_0) \mid k \in V_S\}$; Record the best satellite $\mathbf{S_l}$;
(15) $\quad\quad$ **if** $load \leq \mathbf{W_2}$ **then**
(16) $\quad\quad\quad$ **if** $N_j > N_{i-1} + 1$ **then**
(17) $\quad\quad\quad\quad N_j \leftarrow N_{i-1} + 1$; $L_j \leftarrow L_{i-1} + cost$;
(18) $\quad\quad\quad\quad P_j \leftarrow i - 1$; $SA_j \leftarrow \mathbf{S_l}$;
(19) $\quad\quad\quad$ **end if**
(20) $\quad\quad\quad$ **if** $(N_j = N_{i-1} + 1)$ **and** $(L_{i-1} + cost < L_j)$ **then**
(21) $\quad\quad\quad\quad L_j \leftarrow L_{i-1} + cost$; $P_j \leftarrow i - 1$; $SA_j \leftarrow \mathbf{S_l}$;
(22) $\quad\quad\quad$ **end if**
(23) $\quad\quad\quad j \leftarrow j + 1$;
(24) $\quad\quad$ **end if**
(25) $\quad$ **until** $(j > n_c)$ **or** $(load > \mathbf{W_2})$
(26) **end for**
(27) Using vectors P_j and SA_j, return the resulting set *Trips* of second-level routes

Algorithm 2: Procedure *split* for a random permutation T of all n_c customers.

swaps at most 3 adjacent customers from a second-level route with 3 adjacent customers from another. As a result, nine distinct neighborhood structures can be identified, that is, $Shift(1,0)$, $Shift(2,0)$, $Shift(3,0)$, $Swap(1,1)$, $Swap(1,2)$, $Swap(1,3)$, $Swap(2,2)$, $Swap(2,3)$, and $Swap(3,3)$. The neighborhoods of $Swap(\lambda_1, \lambda_2)$ and $Shift(\lambda, 0)$ are shown in Figures 2 and 3, respectively. In $Shift(\lambda, 0)$, λ consecutive customers in a second-level route are moved from a route r_1 to another route r_2. In $Swap(\lambda_1, \lambda_2)$, λ_1 consecutive customers from a second-level route r_1 are interchanged with λ_2 consecutive customers from another second-level route r_2. The *Cross* operator is also called 2-*Opt** in the literature, firstly proposed by Potvin and Rousseau [29], consisting of replacing arc $(i, i+1)$ from a route r_1 and arc $(j, j+1)$ from a route r_2 by arcs $(i, j+1)$ and $(j, i+1)$ (see Figure 4) or by arcs (i, j) and $(i+1, j+1)$ (see Figure 5).

The *Satellites-Change* neighborhood changes the assigned satellite of a second-level route at a time, while *Satellites-Swap* neighborhood swaps the assigned satellites of two distinct second-level routes if they belong to different satellites. Both of them may modify the demands of the satellites and hence may change the total cost of the 2E-VRP. The *Satellites-Change* can be seen as a special case of *Satellites-Swap* when a second-level route swaps its satellite with an empty second-level route. We define both of them as intersecond-level-route neighborhoods. Neighborhoods of *Satellites-Swap* and *Satellites-Change* are shown in Figures 6 and 7, respectively.

Once a new initial feasible solution is generated, an intersecond-level-route move is performed to modify the second-level routes first and then an intrasecond-level-route improvement procedure that uses 2-*Opt*, *Or-Opt,* and *Exchange* neighborhoods sequentially is triggered to improve the modified routes if they are feasible. Details of the three neighborhoods can be found in the survey of Bräysy and Gendreau [30]. 2-*Opt* moves delete two nonadjacent arcs and add two new arcs to generate a new route (see Figure 8); *Or-Opt* moves at most two adjacent customers back and forth in the current second-level route (see Figure 9), while *Exchange* exchanges the positions of two customers or the positions of a customer and two adjacent customers in the same second-level route (see Figure 10). *Or-Opt* used in this paper can be seen as the intraroute version of $Shift(1,0)$ and $Shift(2,0)$, while *Exchange* can be seen as the intraroute version of $Swap(1,1)$ and $Swap(1,2)$.

All the neighborhoods are searched until no more improvements can be obtained, in a first-accept manner, and infeasible move against the capacity of each echelon vehicles is never allowed. When no more moves that improve the current solution can be found in a neighborhood, the search continues with the next neighborhood. VND ends when the current solution is a local optimum with respect to all the applied neighborhoods. The framework of VND [31, 32] is briefly shown in Algorithm 3. Each N_h $(h < h_{\max})$ is actually a combination of an intersecond-level-route neighborhood

```
(1) Define the neighborhood N_h = Shift, Swap, Cross, ...
(2) S* ← S;
(3) repeat
(4)     improve_flag ← false;
(5)     h ← 1;
(6)     while h ≤ h_max do
(7)         S ← LocalSearch(S, N_h);
(8)         if Cost(S) < Cost(S*) then
(9)             improve_flag ← true;
(10)            S* ← S;
(11)            h ← h + 1;
(12)        end if
(13)    end while
(14) until improve_flag = false
(15) return the local optimum S* found;
```

Algorithm 3: VND for the improvement of a solution S.

```
(1) S* ← ∅, Cost(S*) ← +∞
(2) for i ← 1 to max i do
(3)     S ← GRASP();
(4)     S ← VND(S);
(5)     if Cost(S) < Cost(S*) then
(6)         S* ← S;
(7)     end if
(8) end for
(9) return the best solution S* found;
```

Algorithm 4: GRASP+VND for 2E-VRP outline.

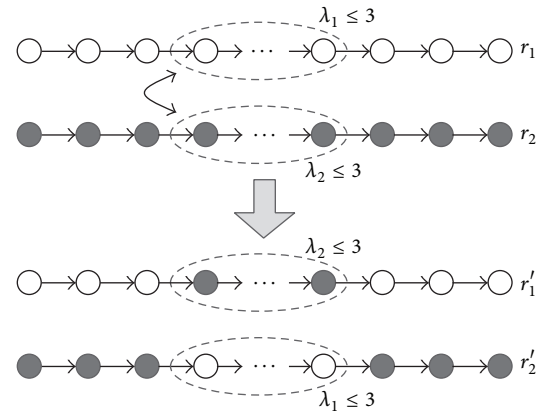

Figure 2: $Swap(\lambda_1,\lambda_2)$ neighborhoods.

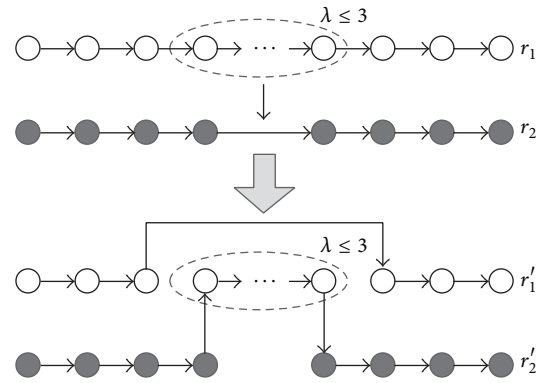

Figure 3: $Shift(\lambda,0)$ neighborhoods.

and the three intrasecond-level-route neighborhoods. But the neighborhood $N_{h_{\max}}$ placed at the end is an exception and it is only composed of the above three intrasecond-level-route neighborhoods, which are searched circularly until none of them can improve every second-level route of current solution. Every time the solution is modified due to a feasible intersecond-level-route move, the three intrasecond-level-route operators are performed sequentially to improve the newly generated second-level routes.

3.4. Framework of the Resulting GRASP+VND. Our hybrid GRASP+VND heuristic for the 2E-VRP combines a GRASP construction phase with a VND improvement phase. Both of them are iterated *maxi* times, and the best solution found of all iterations is kept as the final result. An outline of the proposed hybrid algorithm is shown in Algorithm 4. The term $\mathbf{S}^*$ stands for the global best solution found.

4. Numeric Verification

We conducted computational study on three sets of benchmark instances in order to assess the proposed hybrid GRASP+VND algorithm with respect to solution quality and computing times. Our hybrid algorithm was coded in C++, compiled by Microsoft Visual C++ 6.0, and run on a single core of an Intel Pentium Dual-Core E5500 processor (2.8 GHz) and 2 GB of memory.

4.1. Instance Description. The proposed hybrid algorithm was tested on the 2E-VRP benchmark instances Set 2, Set 3, and Set 4. Instances Set 2 and Set 3 were proposed by Perboli et al. [4] and they are based on the following VRP instances of Christofides and Eilon: E-n22-k4, E-n33-k4, and E-n51-k5. The cost matrix of each instance is given by the corresponding VRP instance. The capacity of the first-level vehicles is 2.5 times the capacity of the second. The capacity and the available number of the second-level vehicles are equal to the corresponding VRP instance. The satellites are located at several randomly chosen customers. Instances in this set range between 21 and 50 customers and consider 2 or 4 satellites. Set 4 was proposed by Crainic et al. [33] and contains 54 instances. Each instance has 50 customers and the number of available satellites is 2, 3, or 5. They were generated using three different customer distributions (*Random*, *Centroids,* and *Quadrants*) and three satellite location patterns (*Random*, *Sliced*, and *Forbidden Zone*). A summary of the characteristics of these instances can be found in Hemmelmayr et al. [10].

4.2. Parameter Setting. The nonnegative weight $\mathscr{W}$ in Algorithm 2 is set to 1 as default, which has been determined

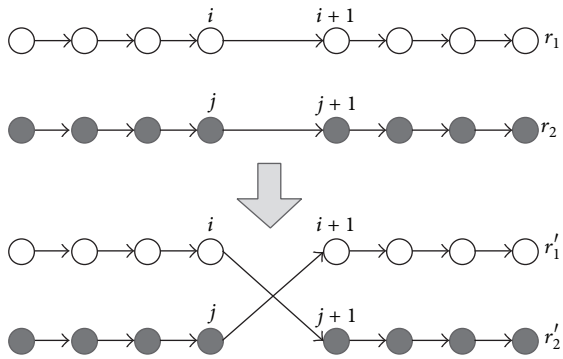

Figure 4: *Cross* neighborhoods type-1.

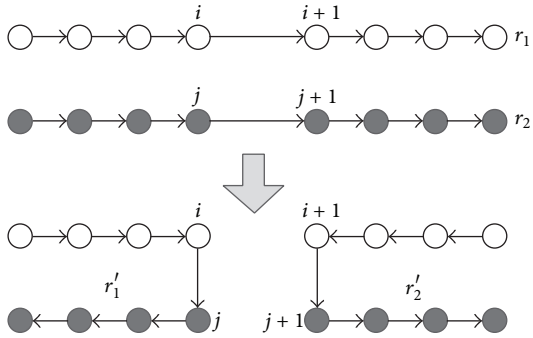

Figure 5: *Cross* neighborhoods type-2.

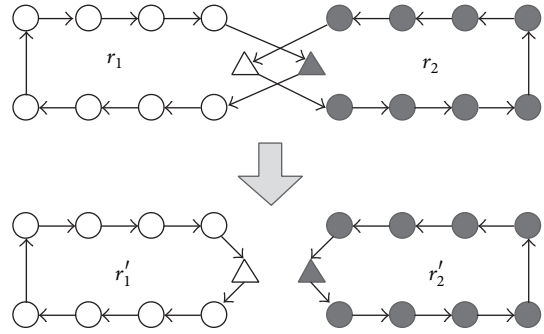

Figure 6: *Satellites-Swap* neighborhoods.

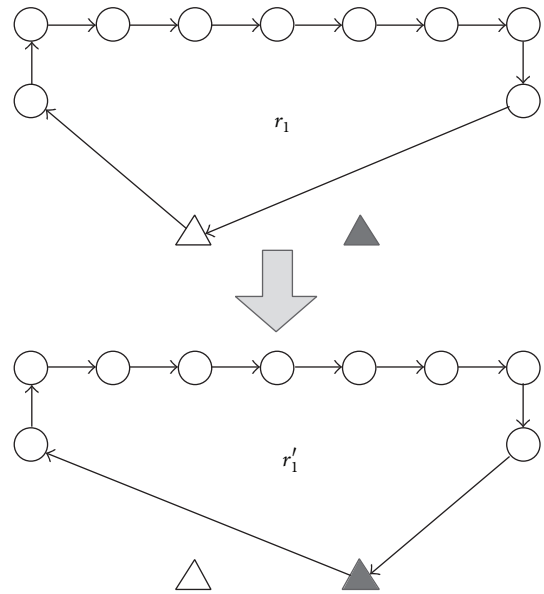

Figure 7: *Satellites-Change* neighborhoods.

by experience. The maximum number of iterations *maxi* (i.e., the number of initial feasible solutions generated and improved by VND) is set to 500, and each instance is conducted on five independent runs, as it was done in [10]. We record the best and average solutions, as well as the average time needed to find the best solution of five runs for each instance.

4.3. Computational Results. In this section, we compare the computational results of our hybrid GRASP+VND heuristic with the best existing heuristic method for the 2E-VRP, that is, the ALNS algorithm of Hemmelmayr et al. [10].

The results of instances Set 2, Set 3, and Set 4 obtained by the two compared heuristics are shown in Tables 1, 2, and 3, respectively. The column instance name gives the names of these instances. The column BKS gives the best-known results of these 2E-VRP instances (published in Baldacci et al. [7]). The columns *ALNS* and *GRASP+VND* report the computational results of the two algorithms, respectively. The ALNS algorithm [10] and our GRASP+VND algorithm both report the best and average solutions (containing their percentage deviation from the best-know solutions), as well as the average time (in seconds) needed to find the best solutions of five runs.

The two heuristics were both implemented in C++ but used different workstations. The ALNS heuristic was tested on a single core of an AMD Opteron 275 processor (2.2 GHz). In order to make a fair comparison, we choose the running times of ALNS as a benchmark and scale the running times of our GRASP+VND according to the CPU performances reported at http://www.cpubenchmark.net/cpu_list.php. Our machine is 1.34 times faster than the AMD Opteron 275 processor (2.2 GHz) used by Hemmelmayr et al. [10]; therefore, our running times are multiplied by 1.34. The times shown in Tables 1, 2, and 3 are already the scaled value of actual running times. Values in bold fonts correspond to those that our GRASP+VND outperforms the ALNS, while those italic mean that our algorithm is worse than the ALNS.

5. Discussion

As seen from Tables 1, 2, and 3, our GRASP+VND and the ALNS can both find the best-known solutions for all the 39 instances in Set 2 and Set 3, and the ALNS can find the best-known 44 solutions for instances in Set 4, while the GRASP+VND can find 52; besides, there are ten better results in the best values found by our GRASP+VND. In terms of the average solutions, the two heuristics obtained the same results in Set 2 and Set 3, but we can see from Table 3 that our GRASP+VND is much better than the ALNS. In regard to

Table 1: Computational results comparison for Set 2 for the 2E-VRP.

Number	Instance name	n_s	BKS [7]	ALNS					GRASP+VND				
				Best	% dev.	Average	% dev.	Time (s)	Best	% dev.	Average	% dev.	Time (s)
1	E-n22-k4-s6-17	2	417.07	417.07	0.00	417.07	0.00	0	417.07	0.00	417.07	0.00	0
2	E-n22-k4-s8-14	2	384.96	384.96	0.00	384.96	0.00	0	384.96	0.00	384.96	0.00	0
3	E-n22-k4-s9-19	2	470.60	470.60	0.00	470.60	0.00	0	470.60	0.00	470.60	0.00	0
4	E-n22-k4-s10-14	2	371.50	371.50	0.00	371.50	0.00	0	371.50	0.00	371.50	0.00	0
5	E-n22-k4-s11-12	2	427.22	427.22	0.00	427.22	0.00	0	427.22	0.00	427.22	0.00	0
6	E-n22-k4-s12-16	2	392.78	392.78	0.00	392.78	0.00	0	392.78	0.00	392.78	0.00	0
7	E-n33-k4-s1-9	2	730.16	730.16	0.00	730.16	0.00	0	730.16	0.00	730.16	0.00	0
8	E-n33-k4-s2-13	2	714.63	714.63	0.00	714.63	0.00	0	714.63	0.00	714.63	0.00	0
9	E-n33-k4-s3-17	2	707.48	707.48	0.00	707.48	0.00	0	707.48	0.00	707.48	0.00	0
10	E-n33-k4-s4-5	2	778.74	778.74	0.00	778.74	0.00	3	778.74	0.00	778.74	0.00	**1**
11	E-n33-k4-s7-25	2	756.85	756.85	0.00	756.85	0.00	0	756.85	0.00	756.85	0.00	0
12	E-n33-k4-s14-22	2	779.05	779.05	0.00	779.05	0.00	0	779.05	0.00	779.05	0.00	0
13	E-n51-k5-s2-17	2	597.49	597.49	0.00	597.49	0.00	7	597.49	0.00	597.49	0.00	**1**
14	E-n51-k5-s4-46	2	530.76	530.76	0.00	530.76	0.00	0	530.76	0.00	530.76	0.00	0
15	E-n51-k5-s6-12	2	554.81	554.81	0.00	554.81	0.00	2	554.81	0.00	554.81	0.00	2
16	E-n51-k5-s11-19	2	581.64	581.64	0.00	581.64	0.00	6	581.64	0.00	581.64	0.00	**5**
17	E-n51-k5-s27-47	2	538.22	538.22	0.00	538.22	0.00	1	538.22	0.00	538.22	0.00	1
18	E-n51-k5-s32-37	2	552.28	552.28	0.00	552.28	0.00	1	552.28	0.00	552.28	0.00	1
19	E-n51-k5-s2-4-17-46	4	530.76	530.76	0.00	530.76	0.00	1	530.76	0.00	530.76	0.00	1
20	E-n51-k5-s6-12-32-37	4	531.92	531.92	0.00	531.92	0.00	0	531.92	0.00	531.92	0.00	*1*
21	E-n51-k5-s11-19-27-47	4	527.63	527.63	0.00	527.63	0.00	1	527.63	0.00	527.63	0.00	1
Average			565.55	565.55	0.00	565.55	0.00	1	565.55	0.00	565.55	0.00	0.67

Table 2: Computational results comparison for Set 3 for the 2E-VRP.

Number	Instance name	n_s	BKS [7]	ALNS					GRASP+VND				
				Best	% dev.	Average	% dev.	Time (s)	Best	% dev.	Average	% dev.	Time (s)
1	E-n22-k4-s13-14	2	526.15	526.15	0.00	526.15	0.00	0	526.15	0.00	526.15	0.00	0
2	E-n22-k4-s13-16	2	521.09	521.09	0.00	521.09	0.00	0	521.09	0.00	521.09	0.00	0
3	E-n22-k4-s13-17	2	496.38	496.38	0.00	496.38	0.00	0	496.38	0.00	496.38	0.00	0
4	E-n22-k4-s14-19	2	498.80	498.80	0.00	498.80	0.00	0	498.80	0.00	498.80	0.00	0
5	E-n22-k4-s17-19	2	512.81	512.81	0.00	512.81	0.00	0	512.81	0.00	512.81	0.00	0
6	E-n22-k4-s19-21	2	520.42	520.42	0.00	520.42	0.00	0	520.42	0.00	520.42	0.00	0
7	E-n33-k4-s16-22	2	672.17	672.17	0.00	672.17	0.00	3	672.17	0.00	672.17	0.00	**0**
8	E-n33-k4-s16-24	2	666.02	666.02	0.00	666.02	0.00	0	666.02	0.00	666.02	0.00	0
9	E-n33-k4-s19-26	2	680.37	680.37	0.00	680.37	0.00	0	680.37	0.00	680.37	0.00	0
10	E-n33-k4-s22-26	2	680.37	680.37	0.00	680.37	0.00	0	680.37	0.00	680.37	0.00	0
11	E-n33-k4-s24-28	2	670.43	670.43	0.00	670.43	0.00	0	670.43	0.00	670.43	0.00	0
12	E-n33-k4-s25-28	2	650.58	650.58	0.00	650.58	0.00	0	650.58	0.00	650.58	0.00	0
13	E-n51-k5-s12-18	2	690.59	690.59	0.00	690.59	0.00	4	690.59	0.00	690.59	0.00	**1**
14	E-n51-k5-s12-41	2	683.05	683.05	0.00	683.05	0.00	38	683.05	0.00	683.05	0.00	**1**
15	E-n51-k5-s12-43	2	710.41	710.41	0.00	710.41	0.00	1	710.41	0.00	710.41	0.00	1
16	E-n51-k5-s39-41	2	728.54	728.54	0.00	728.54	0.00	18	728.54	0.00	728.54	0.00	**6**
17	E-n51-k5-s40-41	2	723.75	723.75	0.00	723.75	0.00	17	723.75	0.00	723.75	0.00	**4**
18	E-n51-k5-s40-43	2	752.15	752.15	0.00	752.15	0.00	15	752.15	0.00	752.15	0.00	**12**
Average			632.45	632.45	0.00	632.45	0.00	5	632.45	0.00	632.45	0.00	**1.44**

Table 3: Computational results comparison for Set 4 for the 2E-VRP.

Number	Instance name	n_s	BKS [7]	ALNS					GRASP+VND				
				Best	% dev.	Average	% dev.	Time (s)	Best	% dev.	Average	% dev.	Time (s)
1	Instance50-s2-01	2	1569.42	1569.42	0.00	1569.42	0.00	6	1569.42	0.00	1569.42	0.00	**2**
2	Instance50-s2-02	2	1438.33	1438.33	0.00	1441.02	0.19	43	1438.33	0.00	**1438.33**	0.00	*53*
3	Instance50-s2-03	2	1570.43	1570.43	0.00	1570.43	0.00	3	1570.43	0.00	1570.43	0.00	**2**
4	Instance50-s2-04	2	1424.04	1424.04	0.00	1424.04	0.00	11	1424.04	0.00	*1429.04*	0.35	*98*
5	Instance50-s2-05	2	2193.52	2194.11	0.03	2194.11	0.03	63	**2193.52**	0.00	**2193.95**	0.02	**46**
6	Instance50-s2-06	2	1279.87	1279.87	0.00	1279.87	0.00	2	1279.87	0.00	1279.87	0.00	**1**
7	Instance50-s2-07	2	1408.57	1458.63	3.55	1458.63	3.55	6	**1408.57**	0.00	**1408.57**	0.00	*22*
8	Instance50-s2-08	2	1360.32	1360.32	0.00	1360.32	0.00	5	1360.32	0.00	1360.32	0.00	*5*
9	Instance50-s2-09	2	1403.53	1450.27	3.33	1450.27	3.33	46	**1403.53**	0.00	**1403.53**	0.00	**6**
10	Instance50-s2-10	2	1360.56	1360.56	0.00	1360.56	0.00	1	1360.56	0.00	1360.56	0.00	*2*
11	Instance50-s2-11	2	2047.46	2059.88	0.61	2059.88	0.61	101	**2059.41**	0.58	**2059.41**	0.58	**5**
12	Instance50-s2-12	2	1209.42	1209.42	0.00	1209.42	0.00	44	1209.42	0.00	1209.42	0.00	**8**
13	Instance50-s2-13	2	1450.93	1481.83	2.13	1481.83	2.13	25	**1450.93**	0.00	**1450.93**	0.00	**3**
14	Instance50-s2-14	2	1393.61	1393.61	0.00	1393.61	0.00	6	1393.61	0.00	1393.61	0.00	**2**
15	Instance50-s2-15	2	1466.83	1489.94	1.58	1489.94	1.58	9	**1466.83**	0.00	**1466.83**	0.00	**1**
16	Instance50-s2-16	2	1387.83	1387.83	0.00	1387.83	0.00	6	1387.83	0.00	1387.83	0.00	*8*
17	Instance50-s2-17	2	2088.49	2088.49	0.00	2088.49	0.00	165	2088.49	0.00	2088.49	0.00	**36**
18	Instance50-s2-18	2	1227.61	1227.61	0.00	1227.61	0.00	3	1227.61	0.00	1227.61	0.00	**2**
19	Instance50-s3-19	3	1546.28	1546.28	0.00	1546.28	0.00	25	1546.28	0.00	1546.28	0.00	*34*
20	Instance50-s3-20	3	1272.97	1272.97	0.00	1272.97	0.00	12	1272.97	0.00	1272.97	0.00	*76*
21	Instance50-s3-21	3	1577.82	1577.82	0.00	1577.82	0.00	61	1577.82	0.00	1577.82	0.00	**25**
22	Instance50-s3-22	3	1281.83	1281.83	0.00	1281.83	0.00	2	1281.83	0.00	1281.83	0.00	*37*
23	Instance50-s3-23	3	1652.98	1652.98	0.00	1652.98	0.00	5	1652.98	0.00	1652.98	0.00	**4**
24	Instance50-s3-24	3	1282.68	1282.68	0.00	1282.68	0.00	2	1282.68	0.00	1282.68	0.00	2
25	Instance50-s3-25	3	1408.57	1440.68	2.28	1440.84	2.29	53	**1408.57**	0.00	**1408.57**	0.00	**23**
26	Instance50-s3-26	3	1167.46	1167.46	0.00	1167.46	0.00	0	1167.46	0.00	1167.46	0.00	*9*
27	Instance50-s3-27	3	1444.51	1444.51	0.00	1447.79	0.23	12	1444.51	0.00	*1454.63*	0.70	*52*
28	Instance50-s3-28	3	1210.44	1210.44	0.00	1210.44	0.00	7	1210.44	0.00	1210.44	0.00	**3**
29	Instance50-s3-29	3	1552.66	1559.82	0.46	1561.81	0.59	102	**1552.66**	0.00	**1555.56**	0.19	**40**
30	Instance50-s3-30	3	1211.59	1211.59	0.00	1211.59	0.00	5	1211.59	0.00	1211.59	0.00	**2**
31	Instance50-s3-31	3	1440.86	1440.86	0.00	1440.86	0.00	37	1440.86	0.00	*1441.07*	0.01	*39*
32	Instance50-s3-32	3	1199.00	1199.00	0.00	1199.00	0.00	11	1199.00	0.00	1199.00	0.00	*13*
33	Instance50-s3-33	3	1478.86	1478.86	0.00	1478.86	0.00	16	1478.86	0.00	1478.86	0.00	*19*
34	Instance50-s3-34	3	1233.92	1233.92	0.00	1233.92	0.00	4	1233.92	0.00	1233.92	0.00	*15*
35	Instance50-s3-35	3	1570.72	1570.72	0.00	1570.80	0.01	116	1570.72	0.00	**1570.72**	0.00	**6**
36	Instance50-s3-36	3	1228.89	1228.89	0.00	1228.89	0.00	6	1228.89	0.00	1228.89	0.00	**3**
37	Instance50-s5-37	5	1528.73	1528.73	0.00	1528.81	0.01	55	1528.73	0.00	*1528.98*	0.02	*58*
38	Instance50-s5-38	5	1163.07	1163.07	0.00	1163.07	0.00	15	1163.07	0.00	1163.07	0.00	**2**
39	Instance50-s5-39	5	1520.92	1520.92	0.00	1520.92	0.00	33	1520.92	0.00	1520.92	0.00	**21**
40	Instance50-s5-40	5	1163.04	1163.04	0.00	1165.24	0.19	20	1163.04	0.00	**1163.04**	0.00	**9**
41	Instance50-s5-41	5	1652.98	1652.98	0.00	1652.98	0.00	12	1652.98	0.00	1652.98	0.00	12
42	Instance50-s5-42	5	1190.17	1190.17	0.00	1190.17	0.00	31	1190.17	0.00	1190.17	0.00	*95*
43	Instance50-s5-43	5	1406.11	1406.11	0.00	1408.95	0.20	60	1406.11	0.00	**1406.11**	0.00	**32**
44	Instance50-s5-44	5	1035.03	1035.03	0.00	1035.32	0.03	30	1035.03	0.00	**1035.03**	0.00	**9**
45	Instance50-s5-45	5	1401.87	1403.10	0.09	1406.43	0.33	104	**1402.03**	0.01	**1402.03**	0.01	**36**
46	Instance50-s5-46	5	1058.11	1058.11	0.00	1058.97	0.08	17	1058.11	0.00	**1058.11**	0.00	**9**
47	Instance50-s5-47	5	1552.66	1559.82	0.46	1564.41	0.76	103	**1552.66**	0.00	**1557.04**	0.28	**33**
48	Instance50-s5-48	5	1074.50	1074.50	0.00	1074.50	0.00	2	1074.50	0.00	1074.50	0.00	**1**
49	Instance50-s5-49	5	1434.88	1434.88	0.00	1435.28	0.03	81	1434.88	0.00	**1434.88**	0.00	**51**
50	Instance50-s5-50	5	1065.25	1065.25	0.00	1065.25	0.00	16	1065.25	0.00	1065.25	0.00	**3**
51	Instance50-s5-51	5	1387.51	1387.51	0.00	1387.72	0.02	46	1387.51	0.00	**1387.51**	0.00	**4**
52	Instance50-s5-52	5	1103.42	1103.42	0.00	1103.76	0.03	47	1103.42	0.00	**1103.42**	0.00	**30**
53	Instance50-s5-53	5	1545.73	1545.73	0.00	1545.73	0.00	37	1545.73	0.00	1545.73	0.00	**6**
54	Instance50-s5-54	5	1113.62	1113.62	0.00	1113.62	0.00	2	1113.62	0.00	1113.62	0.00	*16*
Average			1397.04	1400.96	0.28	1401.39	0.31	32	**1397.27**	**0.02**	**1397.70**	**0.05**	**21**

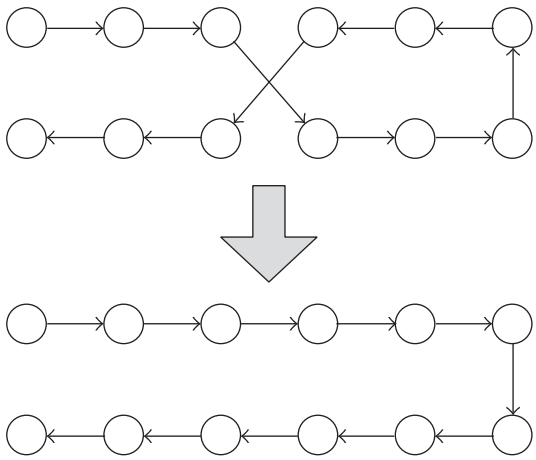

Figure 8: 2-*Opt* neighborhoods.

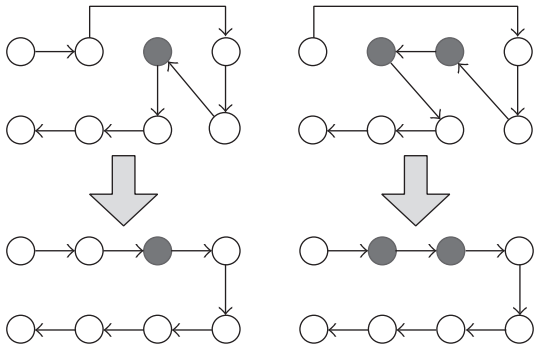

Figure 9: Two kinds of *Or-Opt* neighborhoods.

the deviations of the solutions from the best-known results, we can find that our GRASP+VND is as good as the ALNS in Set 2 and Set 3 but outperforms the ALNS in Set 4. With respect to the running times, our GRASP+VND is as fast as the ALNS in Set 2, a little faster than the ALNS in Set 3 and much faster in Set 4; besides, the running times of our GRASP+VND are limited and reasonable. Our GRASP+VND adopted 8 kinds of local search operators, while the ALNS used 8 kinds of destroy operators, 5 kinds of repair operators, and 5 kinds of local search operators; besides, our GRASP+VND used only 2 parameters, but the ALNS employed 9 parameters, so the GRASP+VND is much easier to implement and tune. From the comparisons above, we can retrieve that our GRASP+VND is both effective and efficient and outperforms the best existing heuristics for the 2E-VRP.

6. Conclusion

This paper has presented a very simple hybrid GRASP+VND heuristic to address the two-echelon vehicle routing problem (2E-VRP), a newly defined multiechelon variant of the classical vehicle routing problem (VRP). The heuristic is composed of a GRASP construction phase (embedding an extended split

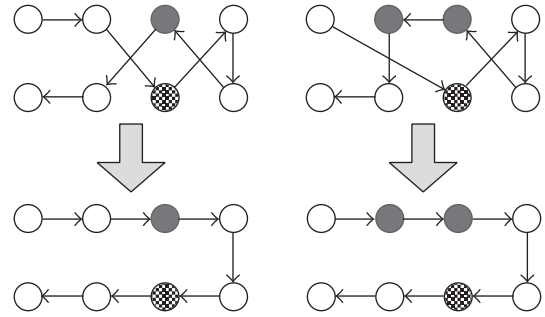

Figure 10: Two kinds of *Exchange* neighborhoods.

algorithm) to generate feasible and relatively good solutions and a VND phase to improve them.

Computational experiments on three sets of benchmark instances from the literature showed the effectiveness and efficiency of the proposed algorithm, and it outperformed the best existing heuristic methods for the 2E-VRP in both solutions quality and computing times. Moreover, the implementation of the hybrid heuristic is much easier than other heuristics. As a result, the proposed hybrid heuristic is more suitable for handling practical 2E-VRP and its relative variants arising in city logistics.

Conflict of Interests

The authors declare that there is no conflict of interests regarding the publication of this paper.

Acknowledgments

This work is supported by the National Natural Science Foundation of China under Grant no. 71090404. The authors are extremely grateful to the anonymous referees for their helpful comments.

References

[1] E. Taniguchi and R. G. Thompson, "Modeling city logistics," *Transportation Research Record*, vol. 1790, no. 1, pp. 45–51, 2002.

[2] T. G. Crainic, N. Ricciardi, and G. Storchi, "Advanced freight transportation systems for congested urban areas," *Transportation Research C: Emerging Technologies*, vol. 12, no. 2, pp. 119–137, 2004.

[3] T. G. Crainic, N. Ricciardi, and G. Storchi, "Models for evaluating and planning city logistics systems," *Transportation Science*, vol. 43, no. 4, pp. 432–454, 2009.

[4] G. Perboli, R. Tadei, and D. Vigo, "The two-echelon capacitated vehicle routing problem: models and math-based heuristics," *Transportation Science*, vol. 45, no. 3, pp. 364–380, 2011.

[5] G. Perboli and R. Tadei, "New families of valid inequalities for the two-echelon vehicle routing problem," *Electronic Notes in Discrete Mathematics*, vol. 36, pp. 639–646, 2010, Proceedings of the International Symposium on Combinatorial Optimization (ISCO '10).

[6] M. Jepsen, S. Spoorendonk, and S. Ropke, "A branch-and-cut algorithm for the symmetric two-echelon capacitated vehicle

routing problem," *Transportation Science*, vol. 47, no. 1, pp. 23–37, 2013.

[7] R. Baldacci, A. Mingozzi, R. Roberti, and R. W. Calvo, "An exact algorithm for the two-echelon capacitated vehicle routing problem," *Operations Research*, vol. 61, no. 2, pp. 298–314, 2013.

[8] T. G. Crainic, S. Mancini, G. Perboli, and R. Tadei, "Multi-start heuristics for the two-echelon vehicle routing problem," in *Evolutionary Computation in Combinatorial Optimization*, P. Merz and J. K. Hao, Eds., vol. 6622 of *Lecture Notes in Computer Science*, pp. 179–190, Springer, Berlin, Germany, 2011.

[9] W. Meihua, T. Xuhong, C. Shan, and W. Shumin, "Hybrid ant colony optimization algorithm for two echelon vehicle routing problem," *Procedia Engineering*, vol. 15, pp. 3361–3365, 2011.

[10] V. C. Hemmelmayr, J. Cordeau, and T. G. Crainic, "An adaptive large neighborhood search heuristic for two-echelon vehicle routing problems arising in city logistics," *Computers and Operations Research*, vol. 39, no. 12, pp. 3215–3228, 2012.

[11] T. G. Crainic, S. Mancini, G. Perboli, and R. Tadei, "Grasp with path relinking for the two-echelon vehicle routing problem," in *Advances in Metaheuristics*, L. D. Gaspero, A. Schaerf, and T. Stutzle, Eds., vol. 53 of *Operations Research/Computer Science Interfaces Series*, pp. 113–125, Springer, New York, NY, USA, 2013.

[12] T. A. Feo and M. G. C. Resende, "Greedy randomized adaptive search procedures," *Journal of Global Optimization*, vol. 6, no. 2, pp. 109–133, 1995.

[13] M. G. Resende and C. C. Ribeiro, "Greedy randomized adaptive search procedures: advances, hybridizations, and applications," in *Handbook of Metaheuristics*, M. Gendreau and J. Y. Potvin, Eds., vol. 146 of *International Series in Operations Research & Management Science*, pp. 283–319, Springer US, New York, NY, USA, 2nd edition, 2010.

[14] N. Mladenović and P. Hansen, "Variable neighborhood search," *Computers and Operations Research*, vol. 24, no. 11, pp. 1097–1100, 1997.

[15] P. Hansen, N. Mladenovic, J. Brimberg, and J. Perez, "Variable neighborhood search," in *Handbook of Metaheuristics*, M. Gendreau and J. Y. Potvin, Eds., pp. 61–86, Springer US, New York, NY, USA, 2nd edition, 2010.

[16] H. Hernández-Pérez, I. Rodríguez-Martín, and J. J. Salazar-González, "A hybrid GRASP/VND heuristic for the one-commodity pickup-and-delivery traveling salesman problem," *Computers and Operations Research*, vol. 36, no. 5, pp. 1639–1645, 2009.

[17] J. G. Villegas, C. Prins, C. Prodhon, A. L. Medaglia, and N. Velasco, "GRASP/VND and multi-start evolutionary local search for the single truck and trailer routing problem with satellite depots," *Engineering Applications of Artificial Intelligence*, vol. 23, no. 5, pp. 780–794, 2010.

[18] A. Salehipour, K. Sörensen, P. Goos, and O. Bräysy, "Efficient GRASP+VND and GRASP+VNS metaheuristics for the traveling repairman problem," *4OR*, vol. 9, no. 2, pp. 189–209, 2011.

[19] F. Parreño, R. Alvarez-Valdes, J. F. Oliveira, and J. M. Tamarit, "A hybrid GRASP/VND algorithm for two- and three-dimensional bin packing," *Annals of Operations Research*, vol. 179, no. 1, pp. 203–220, 2010.

[20] P. Schittekat, J. Kinable, K. Sorensen, M. Sevaux, F. Spieksma, and J. Springael, "A metaheuristic for the school bus routing problem with bus stop selection," *The European Journal of Operational Research*, vol. 229, no. 2, pp. 518–528, 2013.

[21] V. Nguyen, C. Prins, and C. Prodhon, "Solving the two-echelon location routing problem by a GRASP reinforced by a learning process and path relinking," *The European Journal of Operational Research*, vol. 216, no. 1, pp. 113–126, 2012.

[22] C. Archetti, M. G. Speranza, and A. Hertz, "A tabu search algorithm for the split delivery vehicle routing problem," *Transportation Science*, vol. 40, no. 1, pp. 64–73, 2006.

[23] G. Clarke and J. W. Wright, "Scheduling of vehicles from a central depot to a number of delivery points," *Operations Research*, vol. 12, no. 4, pp. 568–581, 1964.

[24] J. Beasley, "Route first-Cluster second methods for vehicle routing," *Omega*, vol. 11, no. 4, pp. 403–408, 1983.

[25] C. Prins, "A simple and effective evolutionary algorithm for the vehicle routing problem," *Computers and Operations Research*, vol. 31, no. 12, pp. 1985–2002, 2004.

[26] A. Subramanian, L. M. A. Drummond, C. Bentes, L. S. Ochi, and R. Farias, "A parallel heuristic for the vehicle routing problem with simultaneous pickup and delivery," *Computers and Operations Research*, vol. 37, no. 11, pp. 1899–1911, 2010.

[27] A. Subramanian, P. H. V. Penna, E. Uchoa, and L. S. Ochi, "A hybrid algorithm for the heterogeneous fleet vehicle routing problem," *The European Journal of Operational Research*, vol. 221, no. 2, pp. 285–295, 2012.

[28] A. Subramanian, P. H. V. Penna, E. Uchoa, and L. S. Ochi, "A hybrid algorithm for a class of vehicle routing problems," *The European Journal of Operational Research*, vol. 40, no. 10, pp. 2519–2531, 2013.

[29] J. Potvin and J. Rousseau, "Exchange heuristic for routeing problems with time windows," *Journal of the Operational Research Society*, vol. 46, no. 12, pp. 1433–1446, 1995.

[30] O. Bräysy and M. Gendreau, "Vehicle routing problem with time windows, part I: route construction and local search algorithms," *Transportation Science*, vol. 39, no. 1, pp. 104–118, 2005.

[31] V. P. Nguyen, C. Prins, and C. Prodhon, "A multi-start evolutionary local search for the two-echelon location routing problem," in *Hybrid Metaheuristics*, M. J. Blesa, C. Blum, G. Raidl, A. Roli, and M. Sampels, Eds., vol. 6373 of *Lecture Notes in Computer Science*, pp. 88–102, Springer, Berlin, Germany, 2010.

[32] P. Chen, H. Huang, and X. Dong, "Iterated variable neighborhood descent algorithm for the capacitated vehicle routing problem," *Expert Systems with Applications*, vol. 37, no. 2, pp. 1620–1627, 2010.

[33] T. G. Crainic, G. Perboli, S. Mancini, and R. Tadei, "Two-echelon vehicle routing problem: a satellite location analysis," *Procedia—Social and Behavioral Sciences*, vol. 2, no. 3, pp. 5944–5955, 2010, Proceedings of the 6th International Conference on City Logistics.

Hindawi Publishing Corporation
Mathematical Problems in Engineering
Volume 2014, Article ID 513606, 7 pages
http://dx.doi.org/10.1155/2014/513606

Research Article

Static and Dynamic Analysis of Railway Reinforced System with Cross-Beams

Bin Peng,[1,2] Nan Zhang,[1] and Yu Lan Gao[2]

[1] *School of Civil Engineering, Beijing Jiaotong University, Beijing 100044, China*
[2] *China Railway Engineering Consulting Group Co., Ltd., Beijing 100055, China*

Correspondence should be addressed to Nan Zhang; nzhang@bjtu.edu.cn

Received 14 November 2013; Accepted 7 March 2014; Published 9 April 2014

Academic Editor: Rui Mu

To fulfill the design requirement of railway reinforced system with cross-beams, the model for the static analysis of the railway reinforced system is optimized, the dynamic response is calculated by the vehicle-rail interaction method, the standards of both static and dynamic analysis are established, and the calculation results of many cases with different parameters are evaluated. It is found that, compared with simplified model, the optimized model simulated the conditions of construction site better, so that results are improved; the acceleration and the offloading factor of reinforced system is obtained by the dynamic analysis, whose vibration and resonance phenomenon can be simulated. The calculated result and the railway reinforcement design are safer by adopting the proposed standard in both static and dynamic analysis.

1. Introduction

Most cities in China are experiencing a rapid increase in motor ownership, which leads to a rising congestion, air pollution, and high energy consumption. The developments of public transportation systems are given priority to solve or improve these urban transportation problems [1–4]. Urban railway system is considered an effective way to improve trip structure and alleviate traffic congestion problem in metropolis due to its high capacity and efficiency. Thus, urban railway is developing fast in recent years.

However, in the cities crossed by railway, problems also exist, plane crossroads formed by railway and roads did not make traffic better, jams or even accidents are usually happen in these areas, while the appearance of frame underpass bridge alleviates the problem, it makes the traffic more fluent by separating railway and roads, which establishes interchange.

There are few frame bridge jacking constructions outside of China, the main reason is that, trains running in other countries' railway are usually not as many or frequent as in China, which makes the railway line under construction of frame bridge can be closed temporarily, while in China, railway transport ability still need to be improved even after the rapid development for many years, the railway line under construction of frame bridge can not be closed, and the trains have to pass the construction site in a certain velocity. From many methods of constructing frame underpass bridge, jacking method is a main way, which needs the railway reinforced system to ensure the safety of passing trains, therefore, cases of railway reinforced system construction are also common in China, and combined with these cases, junior design theory is formed.

However, specifications and codes nowadays seldom mention regulations about railway reinforced system, the design of railway reinforced system mostly bases on experience concluded from similar constructions, although some design work calculate with simplified model [5, 6], flaws still exist in following aspects:

(1) simplified model neglects the impact of rail, longitudinal beam, and track fastener, and applies uniform load converted from "China railway standard live loading" on transverse beam; it is supposed that the transverse beam as simply supported beam and recognized as safe. In fact, in code of "China railway standard live loading," the transverse beam right under the midwheel is obviously under the pressure of

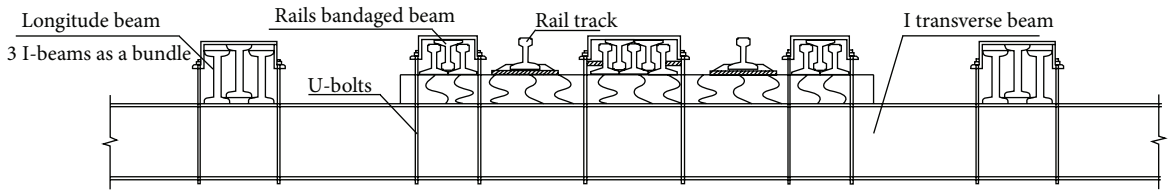

Figure 1: Section scheme of railway reinforced system with cross-beams.

lateral wheel, while longitudinal beam is the member transferring load. Also the deflection of transverse beam is measured by millimeters; the deformation of supporting ends (frame bridge and excavated soil) cannot be ignored. Therefore, longitudinal beam and supporting ends should be simulated in the model,

(2) standards of calculation results on railway reinforced system come from different sources and mainly contain regulations in the scope of railway bridge, railway track, and building structure,

(3) the vibration of railway reinforced system caused by train dynamic load is not simulated. Dynamic load of passing train will motivate vibration of the railway reinforced system; resonance phenomenon might be provoked if frequency of dynamic load and railway reinforced system is close to each other; then amplitude of reinforced system will be largely increased, so dynamic analysis should be introduced to simulate the phenomenon.

The design of railway reinforced system concerns safety of peoples' lives and fortune; therefore, improving and optimizing calculation model and introducing dynamic analysis which can simulate dynamic response and building improved research system have great significance, so that construction theory can be provided. Section scheme of railway reinforced system with cross-beams is shown in Figure 1.

In this paper, three-dimensional model with longitudinal members is established as static calculation model; the impact of frame bridge and excavated soil supporting the reinforced system is considered; the dynamic response is calculated by the vehicle-rail interaction method; the standards of both static and dynamic analysis are established and the calculation results of many cases with different parameters are evaluated. It is found that, compared with simplified model, the optimized model simulated the conditions of construction site better, so that results are improved; the acceleration and the offloading factor of reinforced system is obtained by the dynamic analysis, whose vibration and resonance phenomenon can be simulated; the calculated result and the railway reinforcement design are safer by adopting the proposed standard in both static and dynamic analysis.

2. Static Calculations

2.1. Calculation Conditions and Parameters Selection. 12 cases with different parameters of beam size, span, and velocity of train are established. Cases and parameters are listed in Table 1. Three-dimension model with railway, longitudinal beam, track-locking, some cross-beams, frame bridge, and excavated soil are established and simulated in finite element software ABAQUS; in the model, rail tracks are located in the middle of beam span; "China railway standard live loading" is applied on rail with middle wheel right above the researched beam. Other parameters of model include rail track weighing 50 kg/m, I45b longitudinal beam with 3 beams as a bundle, 3-5-3 track-locking, and I63b transverse beam; the distance of adjacent transverse beams is 0.9 m.

Table 1: Calculation conditions.

Conditions	Parameter		
	Span/m	Steel I-beamsize	Velocity/km/h
1/2/3/4	4	I45c	45/50/55/60
5/6/7/8	5	I56b	45/50/55/60
9/10/11/12	6	I63b	45/50/55/60

Table 2: Ratio of beam deflection.

Coordinate of beam	−2.7 m	−1.8 m	−0.9 m	0 m	0.9 m	1.8 m	2.7 m
Ratio of beam deflection	1	18	53	81	53	18	1

To simulate transverse beams and to ensure the calculation model is accepted by the software so that calculation process will converge, define the number of transverse beams by the following method: establishing a model including rail, longitudinal beam, and some cross-beams; applying load on rail; and simulating the midspan deflection; then cooperation work ability of transverse beams can be evaluated. As torsional stiffness of longitudinal beam restrains the bending of transverse beam, assume rotational inertia of longitudinal beam as 1. Deflection ratios of beams are listed in Table 2.

It can be concluded from calculation results above that longitudinal members coordinate the deformation of transverse beams and share train load to a certain extent; however, the deflection of transverse beam 2.7 m far from researched beam takes only 1.23% of the researched beam's deflection; therefore, only some transverse beams need to be simulated; for safety consideration, 11 transverse beams in 9-meter range are taken.

To simulate the deformation of railway reinforced system caused by supporting ends, a frame bridge model is built on the bridge side; its constitutive relation is defined as ideal elastic-plastic model without strengthening segment;

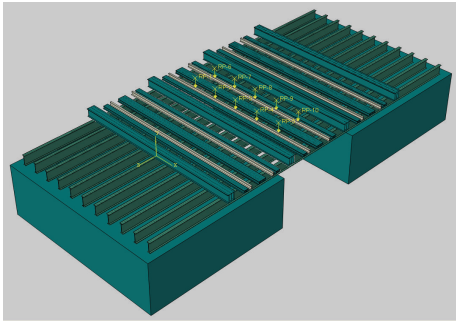

Figure 2: Calculation model.

Table 3: Unilateral wheel load under different parameters (unit: kN).

Span	Velocity			
	45 km/h	50 km/h	55 km/h	60 km/h
4 m	148.34	164.82	181.31	197.79
5 m	147.06	163.40	179.74	196.08
6 m	145.83	162.04	178.24	194.44

the contact pair is built between transverse beams and frame bridge; excavated soil model is built on the soil side, considering the transverse beams embedded in trench and supported by the fender pile at the end side; relationship of attachment is built between soil and transverse beam, whereas the roadbed of railway filled by A or B fillings or modified soil is relatively representative; excavated soil is defined as elastic; the parameters' values are taken with reference to parameters of A or B fillings or modified soil in "design guideline of ballastless track of passenger dedicated railway line." The calculation model is shown in Figure 2.

2.2. Load Calculation. Apply locomotive load of "China railway standard live loading" on railway reinforced system; for safety consideration, take 25 t as axle load. To simulate dynamic increment of train load, take axle load multiplied by dynamic coefficient, reduction coefficient, and nonuniformity coefficient as actual load; take 1.3 as nonuniformity coefficient; dynamic coefficient and reduction coefficient are functions of beam span and speed, whose calculation formulas with reference to formulas in "code for design on steel structure of railway bridge." Values of unilateral wheel's load of different cases are listed in Table 3.

2.3. Calculation Results and Evaluation. Results of cases are listed in Table 4.

In current research of static simulation on railway reinforced system with cross-beams, the evaluation of calculation results takes stress and deflection of transverse beam as indexes, while standards of indexes come from different sources; whereas railway reinforced system has characters of railway and railway bridge, regulations of both scopes should be investigated. Besides, there are correlative regulations in the "code for design of steel structures," which should be also adopted in the evaluation standard. By comparing, analyzing and concluding relevant regulations from 6 specifications or codes, we think evaluation standards of railway reinforced system with cross beams should contain indexes as follows: stress, deflection of I-beam, and deformation of rail. In consideration of safety, take the minimum number as the evaluation standard. Indexes and standards are listed in Table 5.

It can be concluded from Tables 4 and 5 that, in 12 cases, every index meets the requirement of evaluation standard.

3. Dynamic Calculation

3.1. Vehicle-Railway Coupling Analysis Theory. There are three ways to solve the vehicle-railway coupling system in the previous studies.

(1) Moving Loads. In most of early studies [7, 8], the effect of vehicle is adopted by a series of moving loads, in which the dynamic interaction between vehicle and railway is ignored. The method is fit for the cases where the vehicle and the railway have large stiffness or mass differences. Only static vehicle loads and vertical railway response are considered in these studies.

(2) Vehicle-Railway Iteration. This kind of methods was developed in the recent 20 years [9–12]. Both the vehicle and the railway are modeled in the method and two independent equations are established, which is solved by history integral. The two subsystems of vehicle and railway are linked by the predefined wheel-rail motion-force relationship. The motion status of both subsystems is fulfilled by the iteration calculation within time steps in the history integral. The method is widely used and can fit for complex and nonlinear cases.

(3) Vehicle-Railway Simultaneous Equations [13, 14]. The subsystems of vehicle and railway are combined into the global equations in kind of methods; thus the iteration between vehicle equations and railway equations is avoided [15–17]. The nondiagonal parts of the global mass, damping, and stiffness matrices are derived from the wheel-rail relation; thus the linear relationship is required in the wheel-rail motion-force.

The process of moving loads is unconditional convergent if an unconditional convergent history integral method is used; but, for a method containing 2 or more subsystems, the process is no more unconditional convergent; even unconditional convergent integral method is used, as shown in [18, 19]. Many cases are found unconvergent for the methods (2) and the methods (3) above.

In this paper, an intersystem iteration (ISI) method is used; in the method, the dynamic responses of vehicle subsystem and rail subsystem are solved separately, the iteration within time-step is avoided, the computation memory can be saved, and the programming difficulty is reduced.

In the ISI method, firstly, the subsystem of reinforced system is assumed rigid, while the vehicle motion and wheel-rail force histories are solved by the independent vehicle subsystem for the complete simulation time; then

Table 4: Calculation results.

Span/m	Beam size	Velocity/km/h	Beam deflection/mm	Rail deflection/mm	Stress/MPa
4	I45c	45	4.41	4.20	63.24
4	I45c	50	4.95	4.73	70.83
4	I45c	60	5.47	5.23	78.29
4	I45c	65	6.00	5.74	85.84
5	I56b	45	4.43	4.43	54.56
5	I56b	50	4.94	4.93	60.51
5	I56b	60	5.45	5.44	67.12
5	I56b	65	5.96	5.95	73.40
6	I63b	45	5.51	5.42	60.54
6	I63b	50	6.11	6.02	67.21
6	I63b	60	6.71	6.62	73.87
6	I63b	65	7.31	7.21	80.52

Table 5: Safety evaluation index and standard.

Regulation	Index		
	Beam span	Rail deflection	Stress
Railway track district safety regulation	l/400	—	170 MPa
Railway line repair regulation	—	10 mm	—
Code for railway track design	—	11 mm	—
Code for railway bridge verification	l/200	—	185 MPa
Code for design on steel structure of railway bridge	—	—	135 MPa
Code for design of steel structures	l/600	—	215 MPa
Evaluation standard	l/600	10 mm	135 MPa

the reinforced system motion can be obtained by applying the previously obtained wheel-rail force histories to the independent reinforced subsystem [20]. In the following, the updated reinforced system motion histories are combined with the track irregularities to form the new excitation to the vehicle subsystem for the next iteration process, until the given error threshold is satisfied.

The train is regarded as several independent vehicle elements with the same speed and interaction among the vehicle elements is ignored. Thus the vehicle-railway coupling system consists of a reinforced system subsystem and several vehicle elements.

The motion equations of the vehicle element i are expressed as

$$\mathbf{M}_{Vi}\ddot{\mathbf{X}}_{Vi} + \mathbf{C}_{Vi}\dot{\mathbf{X}}_{Vi} + \mathbf{K}_{Vi}\mathbf{X}_{Vi} = \mathbf{F}_{Vi}, \quad (1)$$

where $\mathbf{M}_{Vi}$, $\mathbf{C}_{Vi}$, $\mathbf{K}_{Vi}$, and $\mathbf{F}_{Vi}$ are the mass matrix, damping matrix, stiffness matrix, and force vector of the vehicle element i, respectively.

The motion equations of the reinforced system subsystem are expressed as

$$\mathbf{M}_B\ddot{\mathbf{X}}_B + \mathbf{C}_B\dot{\mathbf{X}}_B + \mathbf{K}_B\mathbf{X}_B = \mathbf{F}_B, \quad (2)$$

where $\mathbf{M}_B$, $\mathbf{C}_B$, $\mathbf{K}_B$, and $\mathbf{F}_B$ are the global mass, damping, and stiffness matrices and the force vector of the reinforced system subsystem, respectively. The former three ones can be obtained by the finite element method or the superposition method; the force vector $\mathbf{F}_B$ is the summing effect of the wheel-track interaction forces for all the wheelsets.

To consider the wheel-rail interaction, three assumptions are adopted.

(1) By the Kalker's Linear Theory, the lateral (Y) displacement of the wheelset is the product of the creep coefficient and the wheel-rail relative velocity.

(2) By the wheel-rail corresponding assumption, the wheelset and the rail have the same vertical (Z) and rotational (U) displacement at the wheel-rail contact point.

(3) Each car-body or bogie has 5 independent DOFs in directions Y, Z, U, V, and W; each wheelset has 1 independent DOF in direction Y and 2 dependent DOFs in directions Z and U.

From assumptions above, the wheel-rail interaction force has three components in lateral (Y), vertical (Z), and torsional (U) directions; see Figure 3.

In Figure 3, for an individual wheelset, P_1 and P_2 are the vertical interaction force between the bogie and the wheelset; P_3 and P_4 are the vertical wheel-rail interaction force; P_5 is the lateral wheel-rail interaction force; G is the static axle load.

The dynamic equilibrium equations for the vehicle-railway interaction system can be formed by the equations of the vehicle subsystem and the reinforced system subsystem.

Table 6: Results of vehicle-railway dynamic analysis.

Span	Beam size	Velocity/km/h	Acceleration/m/s^2	Max. vertical force of wheelset/kN	Min. vertical force of wheelset/kN
4 m	**63b**	**45**	**877.46**	**272.33**	**210.30**
		50	**1024.68**	**272.53**	**213.45**
		55	**1219.40**	**270.90**	**208.05**
		60	**846.97**	**271.99**	**213.56**
5 m	**63b**	**45**	**816.17**	**302.26**	**193.22**
		50	**703.85**	**295.86**	**192.78**
		55	**766.77**	**293.04**	**191.94**
		60	**904.85**	**285.10**	**185.60**
6 m	63b	45	650.14	345.29	*156.43*
		50	944.35	324.93	*153.73*
		55	748.13	327.33	*171.55*
		60	535.23	313.00	*168.10*
7 m	63b	45	487.92	333.37	*175.30*
		50	1493.48	454.60	*76.06*
		55	977.55	420.67	*103.67*
		60	581.06	387.89	*131.90*

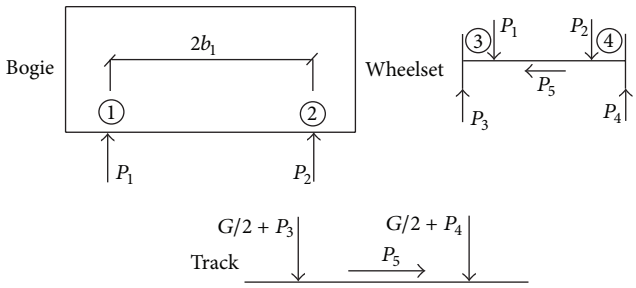

Figure 3: Wheel-rail interaction force.

When the direct stiffness method is adopted for the reinforced system, the interaction equations are

$$\begin{aligned}
&\mathbf{M}_{V1}\ddot{\mathbf{X}}_{V1} + (\mathbf{C}_{V1} + \mathbf{C}_{C1})\dot{\mathbf{X}}_{V1} + \mathbf{K}_{V1}\mathbf{X}_{V1} = \mathbf{F}_{V1},\\
&\mathbf{M}_{V2}\ddot{\mathbf{X}}_{V2} + (\mathbf{C}_{V2} + \mathbf{C}_{C2})\dot{\mathbf{X}}_{V2} + \mathbf{K}_{V2}\mathbf{X}_{V2} = \mathbf{F}_{V2},\\
&\qquad\qquad\vdots\\
&\mathbf{M}_{Vn}\ddot{\mathbf{X}}_{Vn} + (\mathbf{C}_{Vn} + \mathbf{C}_{Cn})\dot{\mathbf{X}}_{Vn} + \mathbf{K}_{Vn}\mathbf{X}_{Vn} = \mathbf{F}_{Vn},\\
&\mathbf{M}_B\ddot{\mathbf{X}}_B + \mathbf{C}_B\dot{\mathbf{X}}_B + \mathbf{K}_B\mathbf{X}_B = \mathbf{F}_B,
\end{aligned} \tag{3}$$

where n is the vehicles number of the train. The first n equations in (3) are for the vehicle subsystem, and the last equation is for the reinforced subsystem.

3.2. Model Simplification and Calculation Parameters. Dynamic simulation of railway reinforced system is calculated by vehicle-rail interaction method in the research; it aims to define lower limit of reinforced system stiffness which can ensure train's passing safe. To study dynamic characteristics of railway reinforced system safely, track irregularity must be ignored during the process of calculation; therefore, analyze the dynamic response of railway reinforced system by passing plane train model; then acceleration and wheelset load reduction can be obtained. In the process of calculating acceleration and wheelset load reduction, ignore the longitudinal members, which mean that neglecting the adjacent beam's load sharing from the beam researched is safe; then a model with transverse beams, without longitudinal members, is established. Calculate dynamic response and vertical wheel-track force of railway reinforced system when the train passes by, so that railway reinforced system's reliability can be evaluated and a suggested solution can be given.

Comparing the weight of locomotive on heavy haul railway, the van's weight per meter is greater, so apply van's weight as load in model. Distance of adjacent clasps of C80 van is 12 m; take 8.2 m as definite distance; distance of axle is 1.83 m, considering the train whose axle weighing 25 t may pass railway reinforced system; take 25 t as axle load, namely 245.15 kN, which means unilateral wheel weighs 122.575 kN. In addition, wood blocking weighs 52 kg/meter, u-bolt weighs 5 kg/meter, so there is the load of 77 kg ($52 + 5 \times 5$) on each transverse beam in total; this load is distributed on 7 points within the scope of 1.1 m, namely, 11 kg on each point.

3.3. Calculation Results and Evaluation. Settings of dynamic calculation cases and results are listed in Table 6.

Take the following case as an example: beam size is I63b; span length is 4 m; speed of train is 60 km/h; the vertical acceleration and vertical wheel-rail force history of train's first wheel are listed in Figures 4 and 5. Indexes of transverse beam varying with velocity under all conditions are listed in Figures 6, 7, and 8.

In the process of wheelset's moving on rail track, the load of one wheel or both wheels may reduce because of the impact of vibration or lateral force; there are field tests showing that wheels may derail if wheel load reduction is large. Regulations in "code for railway vehicle dynamics performance evaluation and test identification" rule the following: take rate of wheel load reduction as the limit index of wheel load reduction; therefore, use rate of wheel load reduction as control index

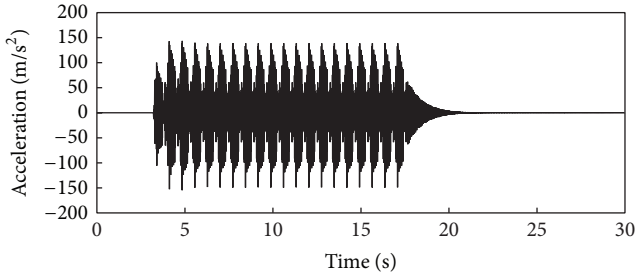

Figure 4: Vertical acceleration history of midpoint of beam.

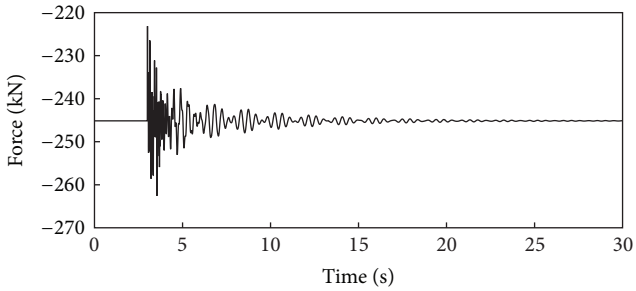

Figure 5: Vertical wheel-rail force history of train's first wheel.

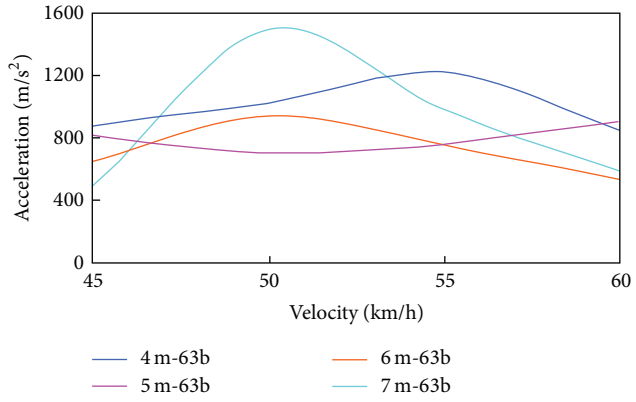

Figure 6: Vertical acceleration of midpoint of beam varying with velocity.

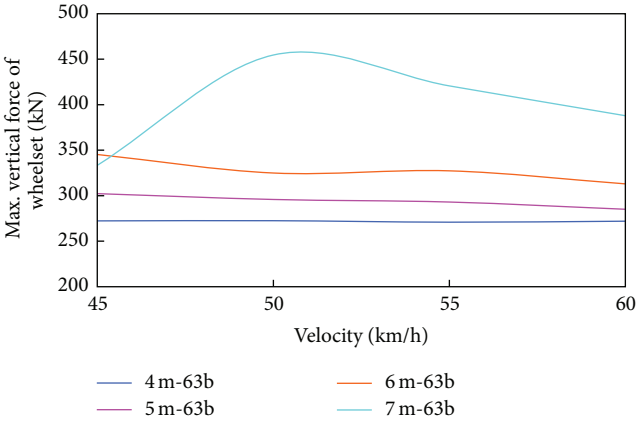

Figure 7: Max. vertical force of wheelset varying with velocity.

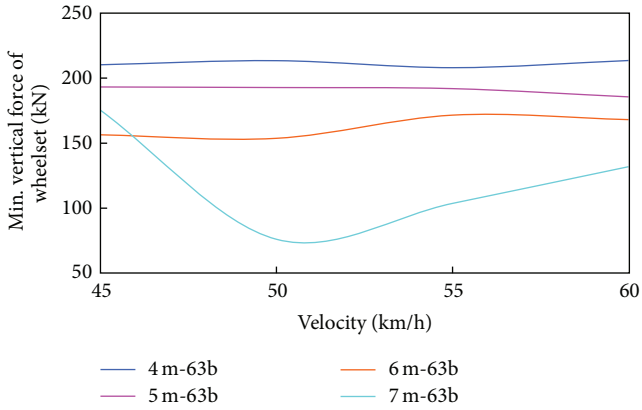

Figure 8: Min. vertical force of wheelset varying with velocity.

of dynamic calculation; and establish the standard with reference to bridge vertical rigidity limit of Shinkansen in Japan (recurring rate of wheel load reduction cannot be larger than 0.25; instantaneous rate of wheel load reduction cannot be larger than 0.375); in consideration of safety, take 0.25 as safety standard, so the safe lower limit of wheel load is 184 kN, that is 25000 kg × gravity acceleration × (1 − 0.25), which means if instantaneous vertical wheel force is less than 184 kN, there will be high risk when a train passes the railway reinforced system. Meantime, dynamic calculation can also obtain acceleration of railway reinforced system; whereas there are no relative regulations, acceleration will not be taken as evaluation index. Therefore, among the results listed in Table 6, the results whose minimum vertical load of wheelset is less than 184 kN will be evaluated as unqualified, expressed by ∗∗ aside, and conditions whose results fulfill standard under all kinds of speed are marked with bold font.

It can be seen from calculation results that, if we take I63b as transverse beam and the span length is 6 m/7 m, the value of vertical force of wheelset under all speed is less than limit value, which means there is high risk of derailment or overturn for train; if we take I63b as transverse beam and the span length is 4 m/5 m, the value of vertical force of wheelset under all speed can meet the requirement of evaluation standard. Therefore, based on dynamic calculation, the following plan of railway reinforced system is suggested: take I63b as transverse beam, ensure the length of span is less than 5 m; if length of span exceeds 5 m, supporting measures should be taken under midspan of transverse beam.

Although acceleration of rail is not taken as evaluation index, it can describe the vibration amplitude of railway reinforced system objectively. It can be seen from Figure 6 that, as indexes varying in different cases, acceleration peak appears in scope of 40~55 km/h in every case; this phenomenon is caused by resonance of vehicle and railway reinforced system. Therefore, to minimize the impact of resonance, it is suggested that a number of damper cushions should be taken in railway reinforced system.

4. Conclusions

The conditions of railway reinforced system are calculated by both static and dynamic analysis; the results are evaluated

by the proposed standard; conclusions are summarized as follows.

(1) Compared with simplified model, the optimized model simulated the conditions of construction site better, so that results are improved. The calculated result and the railway reinforcement design are safer by adopting the proposed standard in both the static and dynamic analysis.

(2) The dynamic analysis based on vehicle-railway coupling theory can simulate the dynamic response history of railway reinforced system under the moving load of train. The rail acceleration, offloading factor, the vibration, and resonance phenomenon of railway reinforced system are calculated. The mentioned items affect the safety of railway reinforced system; thus it is necessary to adopt the dynamic analysis in the designing of railway reinforced system.

(3) The evaluation standards of static and dynamic calculation should be mutual complement, so that a complete evaluation system of railway reinforced system should be formed by both the static and the dynamic calculation to evaluate the design of railway reinforced system; the plan fulfills both the static and dynamic requirement and is safe and suitable one.

Conflict of Interests

The authors declare that there is no conflict of interests regarding the publication of this paper.

Acknowledgments

The research is sponsored by the Major State Basic Research Development Program of China ("973" Program: 2013CB036203) and the Fundamental Research Funds for the Central Universities (Grant no. 2013JBM011)

References

[1] B. Yu, Z. Z. Yang, and B. Z. Yao, "Bus arrival time prediction using support vector machines," *Journal of Intelligent Transportation Systems: Technology, Planning, and Operations*, vol. 10, no. 4, pp. 151–158, 2006.

[2] B. Yu, W. H. K. Lam, and M. L. Tam, "Bus arrival time prediction at bus stop with multiple routes," *Transportation Research C: Emerging Technologies*, vol. 19, no. 6, pp. 1157–1170, 2011.

[3] B. Yu, Z. Yang, K. Chen, and B. Yu, "Hybrid model for prediction of bus arrival times at next station," *Journal of Advanced Transportation*, vol. 44, no. 3, pp. 193–204, 2010.

[4] B. Yu, Z. Z. Yang, and S. Li, "Real-time partway deadheading strategy based on transit service reliability assessment," *Transportation Research A*, vol. 46, no. 8, pp. 1265–1279, 2012.

[5] G. Q. Meng, "Analysis of reinforcement system for jack-in construction of vertical and lateral beams of frame bridge of existing railway line," *Journal of Railway Engineering Society*, vol. 106, no. 7, pp. 42–47, 2007.

[6] Y. P. Ding, Y. B. Wang, and Y. B. Qu, "Analysis of the load bearing capacity of reinforcement system with space structure for track on i-beam of frame bridge," *Journal of Railway Engineering Society*, vol. 132, no. 9, pp. 42–45, 2009.

[7] G. Diana and F. Cheli, "Dynamic interaction of railway systems with large bridges," *Vehicle System Dynamics*, vol. 18, no. 1–3, pp. 71–106, 1989.

[8] L. Frýba, *Vibration of Solids and Structures under Moving Loads*, Thomas Telford, London, UK, 1999.

[9] X. Z. Li, J. Cai, and S. Z. Qiang, "Train runability of the schemed Beijing-Shanghai high-speed railway on the Nanjing Yangtze-river bridge," *Engineering Mechanics*, no. 6, pp. 86–92, 2003 (Chinese).

[10] N. Zhang and H. Xia, "Dynamic analysis of coupled vehicle-bridge system based on inter-system iteration method," *Computers and Structures*, vol. 114, pp. 26–34, 2013.

[11] Y. B. Yang, J. D. Yau, L. C. Hsu, "Vibration of simple beams due to trains moving at high speed," *Engineering Structures*, vol. 19, no. 11, pp. 936–944, 1997.

[12] X. R. Guo, Z. M. Deng, and H. Luo, "Dynamic responses of time-dependent system of Tianxingzhou Bridge and train under wind load," in *Proceedings of the Environmental Vibrations: Prediction, Monitoring, Mitigation and Evaluation*, pp. 1208–1213, Beijing, China, 2009.

[13] P. T. Torstensson, J. C. O. Nielsen, and L. Baeza, "Dynamic train-track interaction at high vehicle speeds—modelling of wheelset dynamics and wheel rotation," *Journal of Sound and Vibration*, vol. 330, no. 22, pp. 5309–5321, 2011.

[14] J. Fayos, L. Baeza, F. D. Denia, and J. E. Tarancón, "An Eulerian coordinate-based method for analysing the structural vibrations of a solid of revolution rotating about its main axis," *Journal of Sound and Vibration*, vol. 306, no. 3–5, pp. 618–635, 2007.

[15] M. M. Gao, *Study on Train-Track-Bridge Coupling Vibration and Train Running on High-Speed Railway*, China Academy of Railway Science, Beijing, China, 2001.

[16] G. H. Li, *Stability and Vibration of Bridge Structures*, China Railway Publishing, 1996.

[17] Y. Yang and J. Yau, "Vehicle-bridge interaction element for dynamic analysis," *Journal of Structural Engineering*, vol. 123, no. 11, pp. 1512–1518, 1997.

[18] R. Clough and J. Penzien, *Dynamics of Structures*, Computers and Structures, Berkeley, Calif, USA.

[19] W. M. Zhai, *Vehicle-Track Coupling Dynamics*, China Railway Publishing, 2002.

[20] N. Zhang, Z. Fang, H. Xia, and G. J. Sun, "An inter-system iteration solution for vehicle-bridge coupling model and its application," in *Proceedings of the 1st international conference on Advances in Interaction and Multiscale Mechanics (AIMM '10)*, May 2010.

Hindawi Publishing Corporation
Mathematical Problems in Engineering
Volume 2014, Article ID 765659, 9 pages
http://dx.doi.org/10.1155/2014/765659

Research Article

Study on the Weaving Behavior of High Density Bidirectional Pedestrian Flow

Lishan Sun, Zifan Yang, Jian Rong, and Xiaoming Liu

Key Lab of Traffic Engineering, Beijing University of Technology, Beijing 100124, China

Correspondence should be addressed to Lishan Sun; lssun@bjut.edu.cn

Received 17 November 2013; Revised 2 February 2014; Accepted 3 February 2014; Published 13 March 2014

Academic Editor: Fang Zong

Weaving area may be the critical risk place in the subway transfer station. When improving service level of the weaving area, the characteristic of pedestrian weaving behavior should be systemically discussed. This paper described the mechanism of weaving behavior on high density pedestrian which was analyzed by the collection data of controlled experiment. Different weaving behaviors were contrasted due to different volumes in the bidirectional passageway. Video analysis was conducted to extract pedestrian moving behavior and calibrate the movement data with SIMI Motion. Influence of the high density weaving pedestrian was studied based on the statistical results (e.g., velocity, walking distance, and journey time). Furthermore, the quantitative method by speed analysis was announced to discriminate the conflict point. The scopes of weaving area and impact area at different pedestrian volumes were revealed to analyze the pedestrian turning angle. The paper concluded that walking pedestrians are significantly influenced by the weaving conflict and trend to turn the moving direction to avoid the conflict in weaving area; the ratio of stable weaving area and impact area is 2 to 3. The conclusions do provide a method to evaluate the transfer station safety and a facility layout guidance to improve the capacity.

1. Introduction

Transfer station is the essential node that handles over 40% of total volumes in subway transit network of Beijing, China. With the increasing volumes of transfer pedestrians, the transferring service level in urban public transfer stations is decreasing sharply due to the crowded and interweaved pedestrian flow. As the bottleneck of facilities (e.g., passageway and platform), weaving areas with different streamlines usually are critical risk places in the subway station optimization. Consequently, the pedestrian weaving behavior in high intensity weaving area should be discussed systemically in order to evaluate the weaving intensity, improve the walking comfort, and, in particular, guarantee the safety of pedestrians.

Previous research has consistently shown that the pedestrian weaving behavior in the subway station, stadium, and the evacuation or panic escape under emergency circumstance can perform as self-organization phenomena as follows. (1) Lane: pedestrians moving in opposite directions are generally organized into lanes; number of the lanes could be changed due to the pedestrian volume and speed [1]. (2) Stripe: when the intersection angle of different walking streamlines is not strictly opposite, the individual dodging behavior and overtaking behavior will occur to avoid collisions with other pedestrians in different directions [2], which reflect the behavior as the conformity phenomenon of human. (3) Arch: when the actual capacity cannot afford the volume requirement at bottlenecks of the facility, pedestrians will form a distribution like an "arch" automatically [3], and this phenomenon seriously impacts the pedestrian walking comfort and causes the physical injury. Self-organization phenomenon is the underweaving behavior which has been widely studied by the scholars around the world in the past decades, but the weaving mechanism analysis from individual pedestrian moving factors at weaving area and influence area is rarely discussed. Besides the quantitative discrimination method of the conflict point and weaving area is not mentioned in the previous research papers.

Traditional pedestrian behavior analysis method contains the investigation and pedestrian experiment. With the development of the computer technique, numerical simulation becomes widely used in the pedestrian movement studies [4–6], but the complicated parameter calibrate procedure relies

on the basic data which is collected by the investigation and experiment, and the simulation results may be inaccurately due to the limitation of the simulation model. Compared with the other two methods, the controlled experiment is more practical and accurate in analyzing the mechanism in a particular situation.

The purpose of this paper is to analysis the moving behavior of the high density weaving pedestrians in the weaving area by controlled experiment. A pedestrian experiment with different volumes was proposed to contrast the weaving behavior in high density condition. Statistical results were discussed to analyze the influence of the weaving conflict. With the efficient discrimination and division methods, turning angle of the pedestrian in weaving area was analyzed based on weaving stage division. The self-organization phenomenon is also proved through turning angle analysis.

The remainder of the paper is structured as follows. A brief review of related literature is presented in Section 2. Then an overview is given of the performed pedestrian experiment, including the experiment scene setup, participants compose and followed by a detailed description of the experiment procedure. Then, the data collection method is introduced. The next section describes the discriminant method of conflict point and division method of weaving area, followed by the characteristic analysis results and the comfort evaluation of pedestrian. Conclusions are conducted in the last section.

2. Literature Review

Crowded pedestrians' movement can be described as self-organization phenomena through various observations [3, 4]. Then a series numbers of studies show that these characteristics of pedestrian flow could emerge in different forms on macroscopic aspect. Helbing et al. [1, 2] revealed and explained that pedestrians moving in opposite directions are normally organized into lanes of which are analyzed by statistical physics and modeling framework methods; in addition he found that the lanes of the weaving pedestrians would change dynamically when the volume is changed. Hoogendoorn and Daamen [5] proposed the case of oversaturated bottlenecks or crossing pedestrian flows, pedestrians could be formed into arch. Pedestrian behavior at bottlenecks is described in detail, and different lanes are formed due to different environments [6]. For Guo and Wong's studies [7, 8], moving pedestrians with same desire directions would form a group to avoid collisions with others with different directions; moreover, different "stripe" shapes are formed due to different flows of the intersecting pedestrian flows with different angles (e.g., 45 degrees, 90 degrees, 135 degrees, and 180 degrees).

Based on the knowledge of macroscopic characteristic behaviors of the pedestrian flows, field investigations, controlled experiments, or numerical simulations were successfully applied to analyze the microscopic behaviors and mechanism of the intersection pedestrians. Helbing et al. [9] developed a model of pedestrian motion by investigating the formation of trail system in public areas, and this model can be used to predict pedestrian traveling path by evaluating typical parameter values. Yu and Song [10] found that pedestrians prefer to walk on a certain side by analyzing the walking behaviors about Chinese and Japanese with the investigations and counterflow models. Compared with field investigation methods, quantitative experiments, even to get the accurate moving data by controlling experiment environment and impact factors, would be more efficient. Ma et al. [11]discussed the moving characteristic of Chinese and French in the corridor by moving experiments; he found pedestrians always keep about 0.4 m distance to the wall. Quantified analysis about intersection pedestrians shows that people who locate on the right-forward direction does not change much, while those who locate on the left-forward direction varies with the increase of distance. Lam et al. [12] found the bidirectional pedestrian is affected by walking speed and capacity through the controlled experiment. Xie et al. [13] developed and calibrated the bidirectional pedestrian stream model with an oblique intersecting angle by the experiments. Lam et al. [14] analyzed the effect of bidirectional pedestrian flow at signalized crossing. In addition, a data collection method by video and errors process method by video are also described in his paper. With the development of computer technology, numerical simulation is widely used in the research studies of pedestrians' moving behavior to study the conditions which could not be achieved in reality [7, 15, 16].

With the theoretical and methodical analysis of pedestrian flow, the phenomena of self-organization have been scientifically studied. In recent years, the features analysis of the crowded pedestrian in weaving areas of public places (e.g., subway transfer stations, squares, shopping malls, etc.) was proposed in order to improve the capacity and walking comfort and even guarantee the safety of pedestrian. Yao et al. [17] revealed the relationship between pedestrian crowd volume, speed, and density of interweaving phenomenon by field investigation. The correlation curve proved that the weaving behavior evolved into three basic states (begin, spread and dissipated) but the threshold values of each state were not concerned in this paper. In Wu and Lu's study [18], some controlled experiments were applied to grasp the influence of walking condition on pedestrian weaving flows; the t test result shows that the speed of in weaving area is significantly lower than before and after weaving, which is decreased by 10% to 35%. Weng and Feng [19] built a simulation platform to simulate unidirection weave pedestrian from volume, density, and other feature parameters. In addition, he reported that the capacity of the weave area decreases by 20–40%; the delay of pedestrian flow turning 90 degrees is the minimum.

In order to grasp the operation status and efficiency of the weaving area in the subway station, some indexes were put forward to evaluate the comfort, service level, or safety. Wu and Lu [18] evaluated the operation of weaving area intensity, trajectory offset ratio, and distribution density factor of weaving points. Moreover, based on the three indexes, pedestrian negative utility model was established. The result shows that the pedestrian negative utility is decreased by 34.5% after improving the exit design. Homogeneity and uniformity velocity are performance indexes to measure the number of pedestrian who acts the same way with the agent and the velocities between the actor pedestrian and

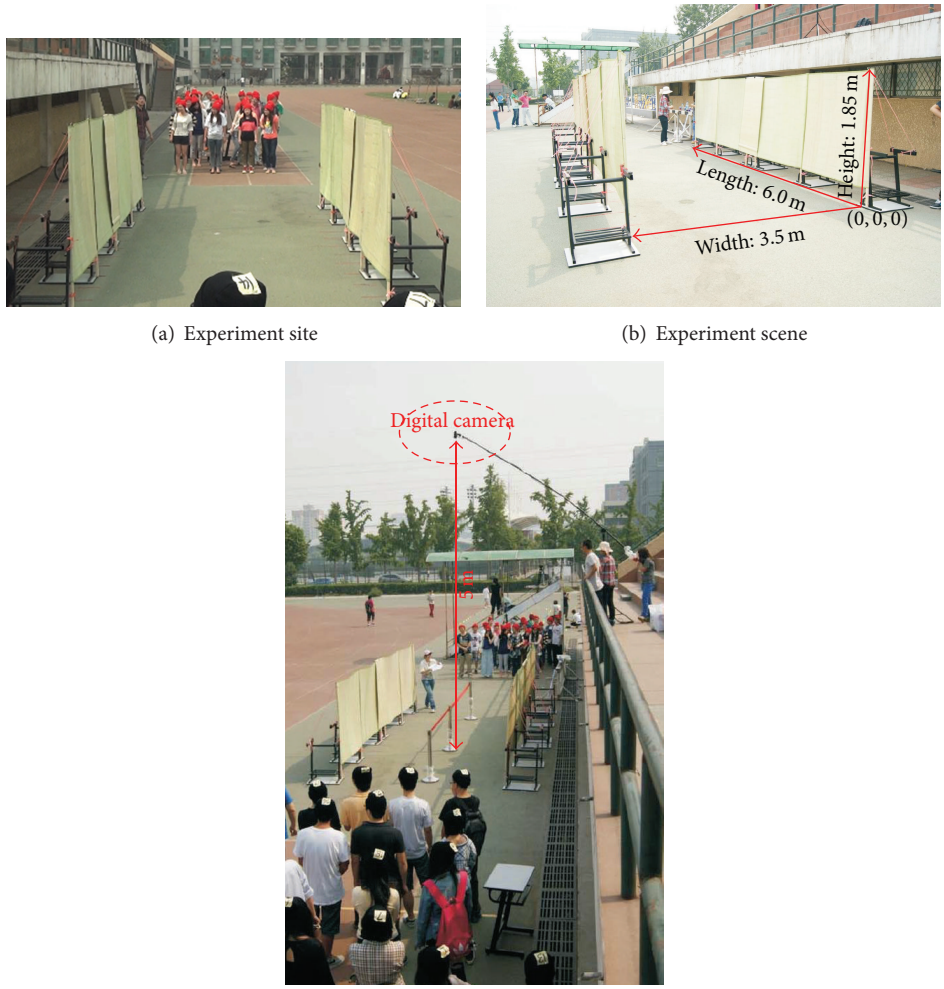

(a) Experiment site

(b) Experiment scene

(c) Experiment facility

Figure 1: Overview of the experiment.

the other pedestrians, respectively. These indexes are applied in the pedestrian simulation software which is produced by Teknomo. Besides, Teknomo et al. [20] proposed some indexes (e.g., speed, uncomfortability, delay, dissipation time, etc.) to evaluate the pedestrian on performance and sensitivity levels.

As a brief summary of the four aspects, the characteristic of self-organization phenomena has been analyzed primarily in terms of how regularly it appears to be with crowded pedestrians. The previous studies regarded the density or speed as the main research contents of the weaving pedestrians, but fewer research projects were paid on the analysis of pedestrian individual factors (e.g., acceleration and angle) under a high density situation of the passageway in subway transfer station. However, there has been no research studies that proposed a discrimination method for the conflict point, even a boundary determination method of weaving area. Furthermore, because the quantitative threshold boundary of weaving process is not mentioned in any literatures, the paper will give an effective method to describe the conflict point and weaving area on analysis of the characteristic of weaving pedestrian by experiment, and the factors difference among different sections of weaving process is also explored. Critical values of self-organization in weaving area are analyzed by the moving angle change of each time slice. The paper also discusses the weaving intensity of the each weaving stage in order to evaluate the weaving impact.

3. Pedestrian Experiment

The pedestrian experiment consists of three aspects. Scenario depicted in the first part is used for introducing the experiment conditions. And participants' information is presented later. Besides, organization and process of experiment are discussed in detail at last.

3.1. Scenario. In order to study the mechanism of weaving behavior of the high density pedestrians in the subway transfer station passageway, controlled experiments of high density counter flow have been conducted in the playground of Beijing University of Technology on May 21st, 2013 (Figure 1(a)). Two walls were located vertically to both sides

of the passageway; The wall is 1.85 meter high so that experimenters can perceive the reliability of scenarios at mental level (Figure 1(b)). A digital camera was put perpendicular in the middle above the passageway at 6 meter height in order to extract pedestrian behavior data with the fewer original errors.

3.2. Participants. Totally 50 participants of experiment were selected from the university. 25 of participants are males, while the others are females (mean age ± SD = 21 ± 1.6 years, range 19–23 years; mean height ± SD = 168.18 ± 8.12 cm, range 155–184 cm). Height of participates is strictly controlled under 1.85 meters in case of which all participants in the scenarios may be affected by the experiment environment. Other pedestrian variables with different weights, clothes, and bags are randomly selected. The population is large enough for a high density weaving behavior study in a period of time.

3.3. Experiment. According to the definition in Transit Capacity and Quality of Service Manual 2nd Edition (TCRP) Report 100 published by Transportation Research Broad (TRB) [21], the recommended capacity value of the bidirectional passageway is 4000 person/h/m. Compared with the investigation in the subway in China, this paper designs the pedestrian volumes as follows (3000 person/h/m, 4000 person/h/m, and 5000 person/h/m), and stream ratio is determined as 1 : 1. As is illustrated in the previous study [18], the passageway geometric features (passageway width and length) have no significant influence in weaving area. Thus, the passageway length and width are fixed as a 6 m ∗ 3.5 m rectangle which is similar to reality, to form high weaving intensity. Before every experiment, two group participants stand behind a red line which is 5 meters away from each side of the entrance.

The weaving experiment included three parts: (1) preparation; (2) preexperiment; (3) weaving experiments.

(1) Preparation. Two groups of these participants (25 in red hats and 25 in black hats) stood behind a start line which is 5 meters away from each side of the entrance (Figure 1(c)). The main purpose was to minimize the impact of a start delay. All participants were given the following three suggestions for taking these experiments: (1) imagining you are walking in the passageway of a subway station, two walls are located vertical to the both sides; (2) you can walk at the speed that you would like to; (3) you should begin when the walking command is released.

(2) Preexperiment. Before the weaving experiments, all participants walked through the scenario depending on their own speed twice so that they could be aware of the experiment process and experiment environment.

(3) Weaving Experiments. For the weaving experiments, participants were asked to complete the work with different pedestrian volumes. To ensure the result of experiments is close to reality, each volume is experimented for 3 times (Figure 2(a)).

4. Data Collection

During the experiment, the whole pedestrian behavior is recorded by the digital camera when participants enter the scenario. With the help of the SIMI Motion (Figure 2(b)), manual data collection method by video is used to extract the moving data accurately without errors caused by automatic data collection method. When a pedestrian enters the system, movement track data would be manually marked, so each pedestrian is marked from the time he enters the scenario until he goes out of the scenario with each time slice (0.02 seconds). In addition, all the pedestrians' moving behaviors are recorded in the database consisting of several fields, namely, as follows:

n = pedestrian number;

t = time from beginning to the end (0.02 seconds/time slice);

$length\ (t, t + \Delta t)$ = distance during each time slice of pedestrian n;

$p(n, t)$ = position (x, y) of pedestrian n at time slice t;

$v(n, x)$ = x-velocity component of pedestrian n;

$v(n, y)$ = y-velocity component of pedestrian n;

$v(n, abs)$ = instantaneous speed of pedestrian n;

$a(n, x)$ = x-acceleration component of pedestrian n;

$a(n, y)$ = y-acceleration component of pedestrian n;

$a(n, abs)$ = instantaneous acceleration of pedestrian n.

With these methods, pedestrian trajectory could be described in order to show the moving characteristic of each pedestrian in weaving area (Figures 2(c) and 2(d)).

5. Results

The purpose of this study was to analyze the pedestrian weaving behavior in high density situation. So, the analysis can be divided into three aspects.

(1) Influence of the weaving behavior: pedestrian movement can be delayed and conflict with the opposite direction pedestrians when high density flow is formed. It may impact the pedestrians who will go in and out of the weaving areas during the experiment.

(2) Discrimination of the weaving area: most of the pedestrian conflict happens in the weaving area. The weaving area is a stable zone when the different streamlines intersect together. the discrimination method is necessary for weaving pedestrian characteristic analysis.

(3) Characteristic analysis of the waving pedestrian: if pedestrians are willing to avoid the conflict with others, the turning angle will be formed. The turning angle is a necessary microscopic parameter to know the characteristic of the weaving pedestrian.

Results are presented in three parts: influence analysis, discrimination method of weaving area, and turning angle analysis.

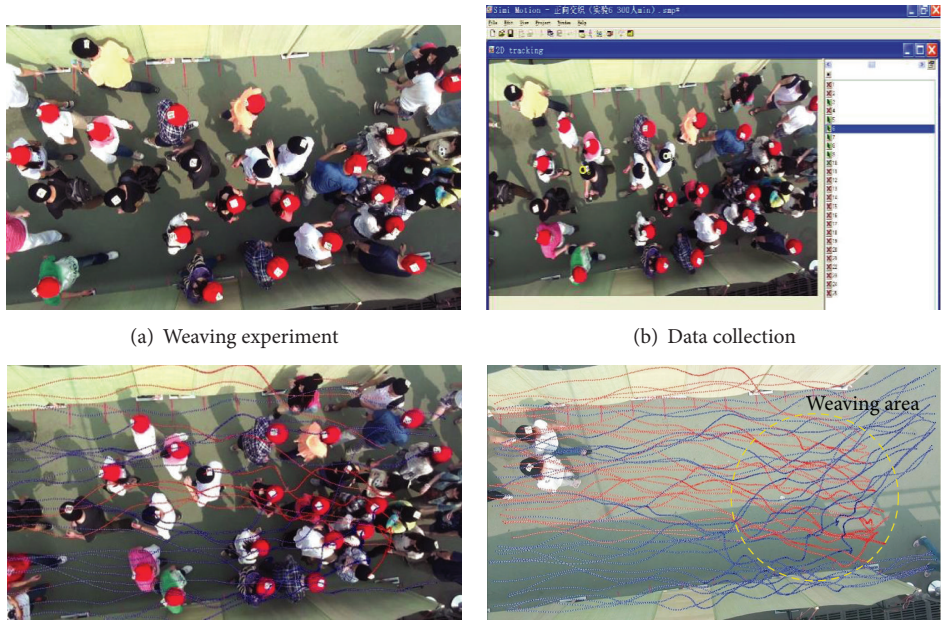

(a) Weaving experiment (b) Data collection

(c) Trajectory calibration (d) Movement trajectory

Figure 2: Data collection of the experiment.

Table 1: Statistical result for pedestrian in different volumes.

Volume/(person·h^{-1})	Index	n	Min./(m·s^{-1})	Max./(m·s^{-1})	Median/(m·s^{-1})	Mean/(m·s^{-1})	Std. deviation/(m·s^{-1})
3000	Velocity	8365	1.064	2.438	1.757	1.751	0.259
	Length	50	6.078	6.922	6.345	6.373	0.281
	Journey time	50	2	4.8	3.651	3.640	0.474
4000	Velocity	13112	0.351	2.300	1.302	1.318	0.352
	Length	50	6.436	7.298	6.789	6.786	0.192
	Journey time	50	3.2	6.6	5.2	5.149	0.674
5000	Velocity	13021	0.011	2.485	1.261	1.238	0.441
	Length	50	6.008	7.382	6.488	6.415	0.355
	Journey time	50	3.4	8.0	5.032	5.183	1.103

5.1. Influence Analysis. The statistic data used in SPSS is collected in the pedestrian weaving experiments, which aims to analyze the weaving impact on the pedestrian's moving indexes (e.g., velocity, journey time, and length). The statistical result of SPSS analysis (Table 1) can be concluded as follows.

(i) The pedestrian's speed with higher volume is much lower. The average speed at volume 5000 person/h is 1.238 m/s, which is much lower than the speed of 1.318 m/s at volume 4000 person/h and 1.751 m/s with volume 3000 person/h, respectively. The results show that the pedestrian speed is not only significantly influenced by the pedestrian flow, but also relate to the pedestrian conflict intensity. In addition, the standard deviation of higher volume is higher, which seems the pedestrian movement has been fluctuated strongly.

(ii) The pedestrian's walking length is much longer. As it is shown in the experiment description, the length of the passageway is 6-meter long. The average length of the result shows that most pedestrians have to walk long distance to avoid the conflict, which is caused by the opposite pedestrian.

(iii) The pedestrian's journey time with higher volumes is longer. According to the statistical result, the maximum value is 8 seconds which is quadruple the minimum value. It is because of that with the higher volume, lower speed, and longer walking distance, the journey time will be longer.

5.2. Discrimination Method of Weaving Area. The basic idea of weaving area discrimination is to confirm a critical value which would reflect the characteristic of the moving pedestrian. According to the research studies by Wu [22] and Sano and Shida [23], pedestrian average speed in weaving area is 10% to 30% less than that of nonweaving area. Meanwhile, the speed is one of the most important parameters in measuring the pedestrian moving behavior. By the field investigation

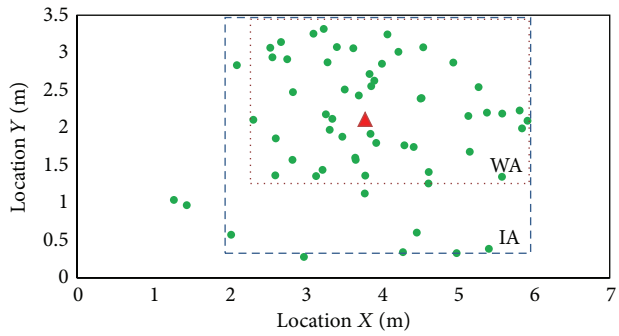

Weaving area (WA):	Impact area (IA):	Center of conflict:
x-axis: (2.10, 5.92)	x-axis: (2.03, 5.92)	$(x, y) = (3.79, 2.11)$
y-axis: (1.12, 3.31)	y-axis: (0.33, 3.31)	conflict point:
Area: 8.37 m^2	Area: 3.26 m^2	total: 60

(a) *Volume at 3000 person/h in the bidirectional passageway

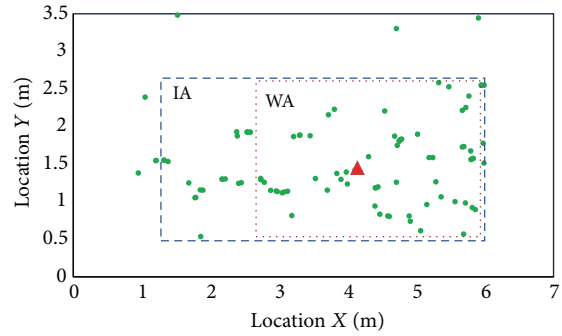

Weaving area (WA):	Impact area (IA):	Center of conflict:
x-axis: (2.78, 5.99)	x-axis: (1.38, 5.99)	$(x, y) = (4.14, 1.45)$
y-axis: (0.57, 2.58)	y-axis: (0.57, 2.58)	conflict point:
Area: 6.46 m^2	Area: 2.82 m^2	total: 102

(b) Volume at 4000 person/h in the bidirectional passageway

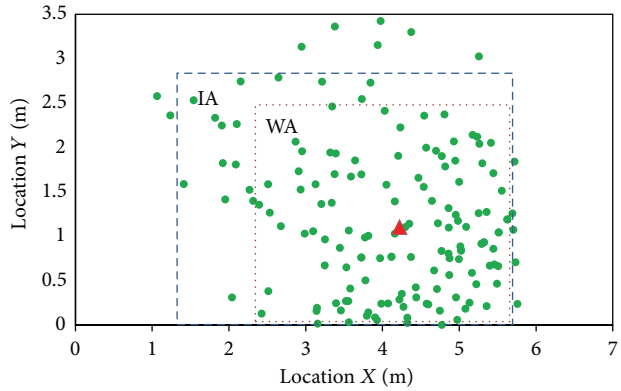

Weaving area (WA):	Impact area (IA):	Center of conflict:
x-axis: (2.32, 5.76)	x-axis: (1.41, 5.76)	$(x, y) = (4.22, 1.10)$
y-axis: (0.00, 2.46)	y-axis: (0.00, 2.79)	conflict point:
Area: 8.46 m^2	Area: 3.64 m^2	total: 159

(c) Volume at 5000 person/h in the bidirectional passageway

FIGURE 3: Weaving area, impact area, and no impact area of different volumes. Note: *impact area is the rectangle area without weaving area, and the coordinate range is also not containing.

and experiment result, we take the speed as the factor to establish the discrimination methodology, which considers the position by which speed decreased by 30% during each time slice (0.02 s) as the conflict point. Referring to the regular statistic, the concept of 85th percentage was conducted, which considers that the area contains 85% of the conflict points, as the weaving area. At the same time, the area which contains 85~95% of the conflict points is regarded as the weaving impact area. The median point in the weaving area is considered as the center of conflict. By calculating the experiment data, the scope of weaving area and impact area of different volumes is determined as follows (Figure 3).

As is depicted in Figure 3, x-axis and y-axis constitute the area of the experiment scenario which is 3.5 m $*$ 6 m equals to 21 m^2; the blue rectangle represents the impact area, which is between the blue area and brown area; the brown rectangle represents the weaving area, which is the high risk area in daily subway transfer station operation and management; the remaining area is the no impact area; it seems that pedestrians in this area are usually steady. Besides, the red triangle is the center of conflict, which represents the highest intensity position in the weaving area.

By dividing the scope of the weaving area and impact area with different volumes, it can be clearly seen that all of the experiments with high density pedestrian can form a stable weaving area; the maximum weaving area is 8.46 m^2 at volume 5000, which occupies the 40% of the scenario and the impact area occupies the 17.3%; the ratio of stable weaving area and impact area is 2.32. Compared with the volume at 5000 person/h, the weaving area of volume at 4000 person/h is the least; the impact area is 2.82 m^2, which is 2.29 times less than weaving area. The weaving area of volume 3000 is 8.37, which closes to volume 5000, but the weaving intensity is less than it; the ratio of stable weaving area and impact area is 2.56.

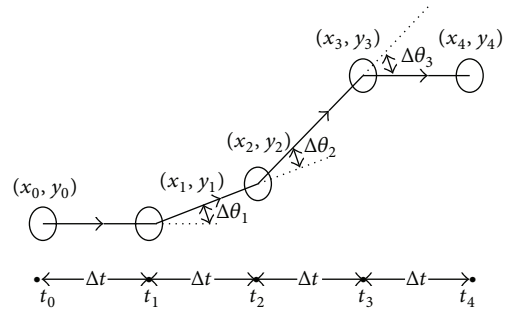

$$\Delta\theta_1 = \arctan\frac{y_2 - y_1}{x_2 - x_1} - 0$$

$$\Delta\theta_2 = \arctan\frac{y_3 - y_2}{x_3 - x_{1,2}} - \Delta\theta_1 \quad (\Delta\theta_2 > 0)$$

$$\Delta\theta_3 = \arctan\frac{y_4 - y_3}{x_4 - x_3} - \arctan\frac{y_3 - y_2}{x_3 - x_{1,2}} \quad (\Delta\theta_3 < 0)$$

Figure 4: Methodology for calculating turning angle.

Table 2: Levene's test of equality of error variances.

Dependent variable: Turing angle			
F	df1	df2	sig.
8.489	8	603	0.000

It shows that the weaving area of the high density pedestrian ranges from 6 m^2 to 9 m^2 and the ratio of stable weaving area and impact area ranges from 2 to 3, nearby 2.5. The number of conflict point is related to the volume, but the weaving area is not.

5.3. Turning Angle Analysis

5.3.1. Methodology. Macroanalysis contributes to the facility distribution, while microdata is necessary to study the characteristic of the weaving behavior of the individual pedestrian. When the pedestrians encounter another pedestrian blocking their way, they are trended to turn the moving angle to avoid the conflict in weaving area. During this process, we consider that the pedestrian will walk straightly with the shortest path unless a force changed. In order to quantify the characteristic of the weaving behavior at the microscopic aspect and analyze the pedestrian weaving intensity, turning angle is introduced, which calculate the angle difference during each time slice.

To analyze the characteristic of the weaving behavior, this research proposed a methodology to calculate the turning angle, as shown in Figure 4. Pedestrian enters the passageway at t_0; he will change the moving direction at t_1 when he avoids the encounter pedestrian, so the turning angle $\Delta\theta_1$ is the difference of angle during t_0 and t_1. Turning angle is "+", when pedestrian turns to left. Otherwise, it is "–".

5.3.2. Statistical Analysis. The pedestrian turning angles of each 0.4 s are calculated by the position data which is collected in the weaving experiment. In order to analyze whether the pedestrian volumes and weaving areas are influenced by turning angles, variance test may be the benefit methodology. But variance test could not be applied because the turning angle data was not accepted by Levene's test (Table 2), Sig. = 0.00 < 0.05. Thus, the statistical analysis is conducted by the basic data statistics (Table 3).

Table 3 shows that the turning angles increase when the volume is higher; also it is higher than other areas. At volume 3000 person/h, the statistics show that the maximum, median, and standard deviation of weaving area are higher than other areas. The reason is because the volume is low to form a relative high density in other areas. At volume 4000 person/h, the results show that the turning angle in weaving area and no impact area have no significant difference. Volume 5000 person/h result shows that all the statistical results in the weaving area are higher than the others. It means that when the volume is at 5000 person/h, the pedestrian turning angle will change significantly. It is also the highest risk area of the experiment. Besides, comparing the standard deviation in each area at the same volume, the value in no impact area is lower, which means the pedestrian walking direction changes less in this area. It is easier to form the "Lane" phenomenon such as (Figure 2(c)). The results also show that the pedestrian would like to turn right to avoid the conflict in China.

6. Conclusion

This paper describes the microscopic characteristic of pedestrian behavior in the weaving area of the subway transfer station using trajectory data from controlled experiment. By analyzing the pedestrian weaving behavior is not only to identify pedestrian behavior in the weaving condition like subway station, but also to provide a method to evaluate the transfer station safety and a facility layout guidance to improve the capacity.

To come to the microscopic characteristic, the existent research studies have been carried out in order to explore not only the data collection method, but also the parameters of the weaving pedestrians. The scope divide method of weaving area and the discrimination method to confirm the conflict point are not solved in the search. And the turning angle analysis in the weaving area is also not recommended. Thus, from the pedestrian experiment, the pedestrian parameter collection and characteristic analysis in the high density weaving area can be done systematically.

The results of the influence analysis show that the pedestrian's speed with higher volume is lower, and the standard deviation analysis is conducted to prove that the higher volume may cause the strong fluctuation. By analysis of the walking distance and journey, the conclusions show that both of two parameters are influenced by the conflict.

The paper proposed a discrimination method to confirm the conflict point, which is calculated by the speed decrease and uses the 85% statistical value to divide the scope of the weaving area and impact area. Characteristic analysis of the weaving area is provided in the further study; the results show that the ratio of stable weaving area and impact area ranges

Table 3: Turning angle with different volumes in each area not included.

Volume	Area		n	Min.	Max.	Median	Mean	Std. deviation
3000	Weaving area	+	67	0.18	35.45	9.60	11.04	8.25
		−	91					
	Impact area	+	24	0.38	28.55	9.41	10.93	7.52
		−	26					
	No impact area	+	59	0.41	23.19	7.34	8.09	5.42
		−	63					
4000	Weaving area	+	82	0.11	42.22	15.27	17.14	10.84
		−	99					
	Impact area	+	43	0.27	49.10	15.80	17.09	11.48
		−	36					
	No Impact area	+	76	0.26	38.57	11.58	11.55	9.39
		−	112					
5000	Weaving area	+	133	0.22	55.58	14.33	17.44	14.05
		−	154					
	Impact area	+	45	0.33	31.68	12.21	13.24	10.06
		−	32					
	No Impact area	+	69	0.18	43.66	12.99	15.20	10.77
		−	59					

from 2 to 3 and the number of conflict point is correlated with the pedestrian flow.

The objective of the study is to analyze the pedestrian weaving behavior with the turning angle change. The study shows that turning angles will increase when the volume is higher. Besides, by analyzing the turning angle, the results show that the turning angle will be changed dramatically when the volume is changed. The analysis of turning angle in no impact area shows that the pedestrian self-organization phenomenon occurs.

Conflict of Interests

The authors declare that there is no conflict of interests regarding the publication of this paper.

Acknowledgments

The authors wish to acknowledge the financial support for this study provided by the National Natural Science Foundation of China (nos. 51308017 and 51108028), the Beijing Municipal Natural Science Foundation (no. 8122009), Beijing Nova Program, and Specialized Research Fund for the Doctoral Program of Higher Education (no. 20121103120025).

References

[1] D. Helbing, "A stochastic behavioral model and a "microscopic" foundation of evolutionary game theory," *Theory and Decision*, vol. 40, no. 2, pp. 149–179, 1996.

[2] D. Helbing, P. Molnár, J. Farkas, and K. Bolay, "Self-organizing pedestrian movement," *Environment and Planning B: Planning and Design*, vol. 28, no. 3, pp. 361–383, 2001.

[3] L. F. Henderson, "The statistics of crowd fluids," *Nature*, vol. 229, no. 5284, pp. 381–383, 1971.

[4] L. F. Henderson and D. J. Lyons, "Sexual differences in human crowd motion," *Nature*, vol. 240, no. 5380, pp. 353–355, 1972.

[5] S. P. Hoogendoorn and W. Daamen, "Self-organization in pedestrian flow," in *Traffic and Granular Flow '03*, pp. 373–382, 2005.

[6] S. P. Hoogendoorn and W. Daamen, "Pedestrian behavior at bottlenecks," *Transportation Science*, vol. 39, no. 2, pp. 147–159, 2005.

[7] R.-Y. Guo, S. C. Wong, H.-J. Huang, P. Zhang, and W. H. K. Lam, "A microscopic pedestrian-simulation model and its application to intersecting flows," *Physica A: Statistical Mechanics and Its Applications*, vol. 389, no. 3, pp. 515–526, 2010.

[8] S. C. Wong, W. L. Leung, S. H. Chan et al., "Bidirectional pedestrian stream model with oblique intersecting angle," *Journal of Transportation Engineering*, vol. 136, no. 3, pp. 234–242, 2010.

[9] D. Helbing, J. Keltsch, and P. Molnár, "Modelling the evolution of human trail systems," *Nature*, vol. 388, no. 6637, pp. 47–50, 1997.

[10] Y. F. Yu and W. G. Song, "Effect of traffic rule breaking behavior on pedestrian counterflow in a channel with a partition line," *Physical Review E: Statistical, Nonlinear, and Soft Matter Physics*, vol. 76, no. 2, Article ID 026102, 2007.

[11] J. Ma, W.-G. Song, Z.-M. Fang, S.-M. Lo, and G.-X. Liao, "Experimental study on microscopic moving characteristics of pedestrians in built corridor based on digital image processing," *Building and Environment*, vol. 45, no. 10, pp. 2160–2169, 2010.

[12] W. H. K. Lam, J. Y. S. Lee, K. S. Chan, and P. K. Goh, "A generalised function for modeling bi-directional flow effects on indoor walkways in Hong Kong," *Transportation Research Part A: Policy and Practice*, vol. 37, no. 9, pp. 789–810, 2003.

[13] S. Xie, S. C. Wong, W. H. K. Lam, and A. Chen, "Development of a bidirectional pedestrian stream model with an oblique intersecting angle," *Journal of Transportation Engineering*, vol. 139, no. 7, pp. 678–685, 2013.

[14] W. H. K. Lam, J. Y. S. Lee, and C. Y. Cheung, "A study of the bi-directional pedestrian flow characteristics at Hong Kong signalized crosswalk facilities," *Transportation*, vol. 29, no. 2, pp. 169–192, 2002.

[15] D. R. Parisi, D. Sornette, and D. Helbing, "Financial price dynamics and pedestrian counter flows: a comparison of statistical stylized facts," *Physical Review E*, vol. 87, Article ID 012804, 2013.

[16] C. Shi, M. Zhong, X. Nong, L. He, J. Shi, and G. Feng, "Modeling and safety strategy of passenger evacuation in a metro station in China," *Safety Science*, vol. 50, no. 5, pp. 1319–1332, 2012.

[17] L. Yao, L. Sun, Z. Zhang, S. Wang, and J. Rong, "Research on the behavior characteristics of pedestrian crowd weaving flow in transport terminal," *Mathematical Problems in Engineering*, vol. 2012, Article ID 264295, 9 pages, 2012.

[18] J. Wu and S. Lu, "The features analysis and operation evaluation of pedestrian weaving area," in *Transportation Research Record Annual Meeting*, 2013.

[19] X.-X. Weng and Q.-D. Feng, "Impact analysis on pedestrian traffic flow in weave area of building," in *Proceedings of the 2nd International Conference on Mechanic Automation and Control Engineering (MACE '11)*, pp. 2215–2218, 2011.

[20] K. Teknomo, Y. Takeyama, and H. Inamura, "Microscopic pedestrian simulation model to evaluate "lane-like segregation" of pedestrian crossing," in *Proceedings of the Infrastructure Planning Conference*, vol. 24, 2001.

[21] Transit Capacity and Quality of Service Manual, 2nd Edition (TCRP) Report 100 Transportation Research Broad.

[22] W. Daamen and S. Hoogendoorn, "Calibration of pedestrian simulation model for emergency doors by pedestrian type," *Transportation Research Record*, vol. 2319, pp. 69–75, 2012.

[23] T. Sano and K. Shida, "An experiment study on pedestrian crossing conflicts by physical index," *Architecture, Planning and Environmental Engineering, Transactions of AIJ*, no. 546, pp. 127–132, 2001.

Hindawi Publishing Corporation
Mathematical Problems in Engineering
Volume 2014, Article ID 980623, 11 pages
http://dx.doi.org/10.1155/2014/980623

Research Article

An Initial Implementation of Multiagent Simulation of Travel Behavior for a Medium-Sized City in China

Chengxiang Zhuge,[1] Chunfu Shao,[1] Jian Gao,[2] Meng Meng,[1] and Weiyang Xu[3]

[1] *MOE Key Laboratory for Urban Transportation Complex Systems Theory and Technology, Beijing Jiaotong University, Beijing 100044, China*
[2] *School of Traffic and Transportation, Beijing Jiaotong University, Beijing 100044, China*
[3] *School of Economics and Management, Beijing Jiaotong University, Beijing 100044, China*

Correspondence should be addressed to Chunfu Shao; cfshao@bjtu.edu.cn

Received 7 November 2013; Revised 12 December 2013; Accepted 14 December 2013; Published 13 March 2014

Academic Editor: Baozhen Yao

Since the traditional four-step model is so simple that it cannot solve complex modern transportation problems, microsimulation is gradually applied for transportation planning and some researches indicate that it is more compatible and realistic. In this paper, a framework of agent-based simulation of travel behavior is proposed, which is realized by MATSim, a simulation tool developed for large-scale agent-based simulation. MATSim is currently developed and some of its models are under training, so a detailed introduction of simulation structure and preparation of input data will be presented. In practice, the preparation process differs from one to another in different simulation projects because the available data for simulation is various. Thus, a simulation of travel behavior under a condition of limited available survey data will be studied based on MATSim; furthermore, a medium-sized city in China will be taken as an example to check whether agent-based simulation of travel behavior can be successfully applied in China.

1. Introduction

Traffic forecasting, no matter if short-term or long-term, macroscopic or microscopic, static or dynamic, is an attractive issue in transportation planning. Four-step process, which is a famous traditional forecasting method, cannot be realistic and complex enough to solve modern transportation planning problems emerging in recent years with rapid urban development. Its shortcoming is especially expressed in two aspects [1].

(i) Static Traffic Assignment. The four-step process regards the steam flows as static (time independent), which makes it difficult or impossible to model any kind of time-dependent effects and like peak traffic spreading; congestion spillback.

(ii) Aggregate Individuals' Behavior. Transportation demand is naturally derived from performing activities at different locations which is the result of a series of decisions made by individuals. The four-step process's aggregation feature cannot solve transportation problems from the root.

In order to overcome the shortcoming above, combining the Dynamic Traffic Assignment (DTA) and Activity-Based Model (ABM) is an efficient solution. In the past decades, with the survey data for transport planning getting more detailed and complex, as well as the fact that the performance of computer hardware has been rapidly growing, a multiagent simulation, which integers the features of DTA's dynamic and ABM's individual, comes into being. By using multiagent simulation technology, each traveler is regarded as an individual agent who can make decisions according to his/her own goals, attributes, preference, resources, and so forth. Thus, different agents will make different decisions even though they stay in the same environment.

In addition, the features of the dynamic of DTA and the individual of ABM are as follows.

(i) ABM's Individual. Each agent will make independent decisions and store its decisions in a "plan" which mainly includes its activity time and location.

(ii) DTA's Dynamic. After creating agents' initial plan, a dynamic iteration of agents' route choice and time distribution will be carried out, which allows tracking persons dynamically in time; the goal of iteration is to find a dynamic balance, which is similar to Nash Equilibrium.

The agent-based microsimulation modeling technique for transportation planning is rapidly developed and is frequently applied to practice in recent years. This paper will use the MATSim as the multiagent simulation tool to simulate the travellers' behavior. MATSim which was developed by TU Berlin, ETH Zürich, and CNRS Lyon, provides a toolbox to implement large-scale agent-based transport simulations [2]. A more detailed introduction can be found in Section 3.

This paper will start with the literature review concerning the latest advancement of traffic assignment, such as DTA, ABM, and MATSim (Section 2). Then it will present the outline of the general simulation structure (Section 3) and a detailed description of the modules in MATSim. Next, we will take Baoding, one of the medium-sized cities in China, as an example, and the way to prepare the input data and to establish the scenarios is introduced (Section 4). Then the simulated results are compared with count data to validate the proposed simulation method (Section 5). Finally, it ends up with a conclusion (Section 6).

2. Literature Review

Traffic assignment plays an important role in the study of transportation problems [3–6]. The literature review below will focus on the latest advancement of traffic assignment, which will include DTA, ABM, and MATSim.

DTA is commonly used to search the best route for users in a scenario where no users can get better off by selecting another route, and the scenario is called Nash Equilibrium statement. A host of research regarding DTA has been conducted. Florian et al. described a simulation-based, iterative dynamic equilibrium traffic assignment model [7]. Bellei et al. presented a new formulation of within-day DTA, where dynamic user equilibrium is expressed as a fixed-point problem in terms of arc flow temporal profiles [8]. Muñoz and Laval studied the system optimum DTA in a network consisting of a hypothetical surface street grid and a congested freeway section [9]. Szeto et al. proposed a cell-based multiclass DTA problem that considers the random evolution of traffic states [10]. Juran et al. developed a DTA model that can evaluate the effects of moving bottlenecks on network performance in terms of both travel times and traveling paths [11]. Antoniou et al. presented an online calibration approach that jointly estimates demand and supply parameters of DTA systems and it was empirically validated through an extensive application [12]. Gentile et al. proposed a new model for the within-day DTA on road networks where the simulation of queue spillovers is explicitly addressed, and a user equilibrium is expressed as a fixed-point problem in terms of arc flow temporal profiles [13].

ABM is modeled on an individual level and successfully implemented by many models and it was employed to address variety of transportation problems [14, 15]. Davidson et al. summarized the recent successful experience in the development and application of ABM for metropolitan planning organizations in the US [16]. Hatzopoulou and Miller extended the capability of an ABM for the Greater Toronto Area to model and map traffic emissions and atmospheric dispersion [17]. Dong et al. employed the activity-based theory to model a new measure of accessibility called activity-based accessibility [18]. Recker et al. presented an estimation procedure for an ABM to estimate the relative importance of factors related to spatial and temporal interrelationships among the out-of-home activities that motivate a household's need or desire to travel [19]. Kang and Recker applied an ABM to evaluate the potential impacts of plug-in hybrid electric vehicles on energy and emissions [20]. Pendyala et al. developed a comprehensive multimodal activity-based system to predict the travel demand in Florida and the outcome of research was Florida Activity Mobility Simulator (FAMOS) [21]. Yagi and Mohammadian developed a comprehensive activity-based modeling system in the context of developing countries, providing accurate estimates which are expected to serve as better inputs for evaluation of different transportation policy scenarios [22].

There is a wide application of DTA and ABM which can be proved by the review above, but combining both theories is seldom implemented [23, 24]. MATSim, which incorporates both DTA and ABM, is an efficient tool to implement a large-scale agent-based simulation for travel behavior and traffic flow and their interactions. So far, research on MATSim has been conducted widely by many scholars, and the scope of the research mainly focuses on three aspects. (1) Basic theory for designing and implementing MATSim. At the beginning, the emphasis was placed on establishing framework of MATSim and incorporating basic models to make it run [25–27]. (2) Optimization of MATSim. At the second stage, the modes of MATSim, such as location choice [28] and mode choice [29], were enhanced and some of them were replaced with advanced ones. (3) Application of MATSim. MATSim is applied into varieties of aspects, like travel behavior [30, 31], parking behavior [32], and freight transport [33].

In conclusion, MATSim has been developed for many years and attracted a variety of researchers to apply it or optimize it, but there is still some reaming interesting work. In this paper, an external work to enrich the MATSim application will be carried out and it differs from other studies in the following aspects.

(i) MATSim will be used to simulate one of the medium-sized cities in China. A Chinese medium-sized city will be quite different from cities in foreign counties in urban development, activity type, travel behavior, and so on. In addition, a large-scale simulation of travel behavior was seldom implemented in a real city; many of the studies used numerical examples to validate simulation models of travel behavior.

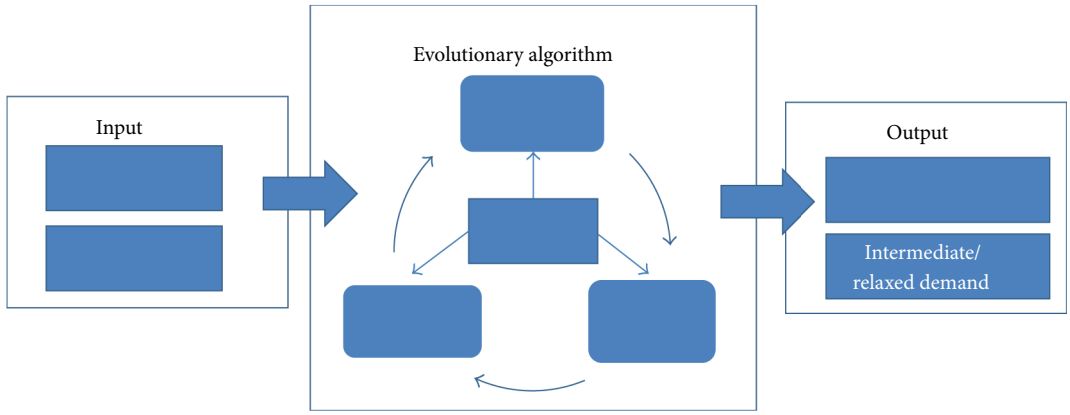

Figure 1: Schematic overview of MATSim's simulation structure.

(ii) Since different cities have different available traffic survey data, they differ in quality, spatial resolution, purpose, and so forth. An approach of how to prepare the input data with limited available information and low spatial resolution is studied in this paper.

3. Simulation Structure

3.1. A Brief Introduction of the Simulation Structure. Based on MATSim, the simulation structure of travel behavior is designed and shown in Figure 1. It mainly includes three parts: input, evolutionary algorithm (EA), and Output. Firstly, the input data (including initial demand and network) will be fed into the mobility simulation (see Section 3.2) and all agents' plans will be executed simultaneously, and then the execution results (simulated data) will tell the other modules what happened during the simulated day; secondly, every executed plan will be scored based on the simulated data on the basis of the scoring function (see Section 3.3); thirdly, according to the scoring, the replanning (including Reroute and Time Allocation Mutator, see Section 3.4) is carried out to provide the feedback which allows for the evolution of plans. Finally, after reaching the customized times of iteration, the simulation results, such as optimization statistics and analysis, intermediate plan, and relaxed plan, will be put out.

For EA is the core part of the simulation, it will be first discussed in detail in the following sections.

3.2. Execution (Mobsim). The mobility simulation (Mobsim) refers to the simulation of the physical transportation system. It creates events for every agent's action in the simulation, like entering/leaving road and departing/arriving at activity places. Then the events will be used for the scoring module. In the history of MATSim, several MobSims such as QueueSimulation, QSim, DEQSim, and JDEQSim have been developed. Some of them are still in use; others are obsolete and no longer supported today. This paper will choose Qsim which is the most commonly used Mobsim. Qsim is an external queue simulation, in which every link is regarded as a first-in first-out (FIFO) queue with three restrictions [1].

(i) Every agent has to stay on the simulated link for a certain time.

(ii) Link storage capacity is imported to limit the number of agents on the simulated link.

(iii) Flow capacity is imported to limit the number of agents that can leave the simulated link in a given period of time.

Even though the queue simulation is indeed simple, the simulated output data is enough for transportation planning.

3.3. Scoring. In order to compare different plans, a scoring function is proposed to evaluate each plan's performance. In MATSim, the utility-based approach is used. The detailed function is as follows [1].

(i) The Total Score of a Plan. It is calculated based on the following equation:

$$U_{\text{total}} = \sum_{i=1}^{n} U_{\text{perf},i} + \sum_{i=1}^{n} U_{\text{late},i} + \sum_{i=1}^{n} U_{\text{travel},i}, \tag{1}$$

where U_{total} is a total score of a given plan; n is the number of activities; $U_{\text{perf},i}$ is the utility for performing activity i; $U_{\text{late},i}$ is the utility for arriving late to activity i; and $U_{\text{travel},i}$ is the utility for travelling to activity i.

(ii) The Utility for Performing Activity. A logarithmic form is used for the utility, as follows:

$$U_{\text{perf},i}\left(t_{\text{perf},i}\right) = \max\left[0, \beta_{\text{perf}} \cdot t_i^* \left(\ln\left(\frac{\beta_{\text{perf}}}{t_i^*}\right) + \frac{\varsigma}{p \cdot t_i^*}\right)\right], \tag{2}$$

where $t_{\text{perf},i}$ is the actual performed duration of the activity i; β_{perf} is the marginal utility of an activity at its typical duration; t_i^* is the "typical" duration of an activity i; ς is a scaling constant, and p is a priority indicator.

(iii) The Utility for Arriving Late to Activity. Consider

$$U_{\text{late},i} = \beta_{\text{late}} \cdot t_{\text{late},i}, \tag{3}$$

where $\beta_{\text{late}} \leq 0$ is the marginal utility for being late; $t_{\text{late},i}$ is the number of hours being late to activity i.

(iv) The Utility for Travelling to Activity. Consider

$$U_{\text{travel},i} = \beta_{\text{travel}} \cdot t_{\text{taverl},i}, \tag{4}$$

where $\beta_{\text{travel}} \leq 0$ is the marginal utility for travelling; $t_{\text{travel},i}$ is the number of hours for travelling to activity i.

More detailed information about the scoring function can be found in the references of Balmer, 2007 [1], and Charypar and Nagel, 2005 [34].

3.4. Replanning. The replanning module is established to search for a solution space for every agent and it mainly includes two submodules: Reroute module and Time Allocation Mutator module. Reroute module allows agents adjust their route from origin to destination; Time Allocation Mutator module enables agents to modify their own departure times and activity durations or change activity locations and activity sequence. More details about the modules above are as follows [1].

3.4.1. Reroute Module. The goal of the Reroute module is to help agents find their shortest path in the network. The "shortness" is measured by travel time rather than travel distance. The most famous and most frequently used routing algorithm is Dijkstra. In MATSim, a time-dependent Dijkstra is applied. This algorithm can make the link travel time dependent by aggregating it into 15 min time bins. Link travel time is calculated based on the previous traffic flow simulation and used as the weight of the links in the network graph. With the weights plus the origin and destination of the activities, the fastest path can be calculated, which will be executed in the next mobility simulation.

3.4.2. Time Allocation Mutator. Time Allocation Mutator is a very simple random mutation module but it is very useful for agents' replanning. Being similar to Reroute module, simple modules together with a large number of iterations will obtain useful results for simulation of travel behavior.

Time Allocation Mutator mainly modifies the activities' duration time and end time (but for the first and last activity, end time is the only attribute modified). The detailed modification process is as follows: firstly, read every agent's plan; secondly, pick a random time from the uniform distribution [−30 min, +30 min]; thirdly, add the random time to the activities' duration time and end time; finally, write back the plan with time attribute modified. But pay attention to the random time as (1) any negative duration will be reset to zero; (2) any first activity end time before 00:00 AM and last activity end time after 24:00 PM will be reset to 00:00 AM and 24:00 PM, respectively.

3.5. Controller (Agent Database). Controller makes the module of execution, scoring, and replanning run successively, and the controlled content is as follows [1].

(i) Number of Plans. The number of the plans per agent will be limited to N ($N \geq 2$; usually N is 3–6). If an agent has $N + 1$ plan (the additional plan is generated in the replanning process) the $N + 1$ Plan will be stored in the agent's memory until the new plan scores. After scoring, the controller will delete the lowest-score plan.

(ii) Select Agents Performing Reroute (r%). The controller selects r% of agents to carry out the module of Reroute (see Section 3.4.1). The plans in the memory will be selected with equal probability.

(iii) Select Agents Performing Time Allocation Mutator (s%). The controller selects s% of agents to carry out the module of Time Allocation Mutator (see Section 3.4.1), however, after that, those agents will also carry out the module of Reroute. The plans in the memory will be selected with equal probability. Thus, s% of agents will carry out Time Allocation Mutator and (s% + r%) of agents will carry out Reroute.

(iv) Select Random Plan (m%). In order to re-evaluate the existing plans from time to time, the controller selects m% of agents and those agents will randomly choose a plan among all plans in their memory.

(v) Select Plans Based on the Scores ($p\% = 1 - r\% - s\% - m\%$). The controller finally selects the remained plans with the following probability:

$$p \propto e^{\beta \cdot S_j}, \tag{5}$$

where S_j is the score of the plan j; β is an empirical constant.

Note. If the controller selects an existing plan, its new score can be calculated with

$$S = (1 - \alpha) \cdot S_{\text{old}} + \alpha \cdot S_{\text{new}}, \tag{6}$$

where α is the blending factor, this will avoid agent selecting plans based on not only last iteration, but also the history scores.

The controller will make the loop run until the simulation system reach a relaxed state.

4. Input Data and Scenario

The structure of MATSim may not be complex, but preparing the input data and constructing a simulation scenario are much more sophisticated. In practice, there is a large variety of input data which can differ in quality, spatial resolution, purpose, and so forth. So it will generally take months, even years, to prepare the correct data for simulation. In order to run a simulation, the lowest requirement includes an initial plan, a road network, and a simulation configuration. The detailed process of preparing the above data will be presented as follows.

```
<person id="682" age="30" employed="yes">
<plan selected="yes">
    <act type="h9" facility="1593" x="365401.69341762" y="4300664.48060939" end_time="09:39:27" />
    <leg mode="car" dep_time="09:39:27">
    </leg>
    <act type="w3" facility="313" x="365843.21376734" y="4306032.0981801" end_time="13:52:24" />
    <leg mode="car" dep_time="13:52:24">
    </leg>
    <act type="h1" facility="1593" x="365401.69341762" y="4300664.48060939" end_time="15:21:30" />
    <leg mode="car" dep_time="15:21:30">
    </leg>
    <act type="w3" facility="313" x="365843.21376734" y="4306032.0981801" end_time="17:41:27" />
    <leg mode="car" dep_time="17:41:27">
    </leg>
    <act type="h9" facility="1593" x="365401.69341762" y="4300664.48060939" />
</plan>
</person>
```

Algorithm 1: An example of a typical initial plan.

4.1. Scenario Description

4.1.1. A Brief Introduction of Baoding. This paper will take Baoding as an example to simulate a medium-sized city in China. Baoding, which is located in Hebei Province, is made up of one main urban area and four counties (Mancheng County, Xushi County, Anxin County, and Qingyuan County). This paper will only simulate the travel behavior of inhabitants in the main urban area. The main urban area of Baoding has a population of 1.06 million.

4.1.2. Activity Chains and Their Distribution. In this paper, only the resident driving private car is simulated. Based on the census 2007 of Baoding, the activity is classified into five types: home, work, shop, education, and leisure. The analysis results show that home-work-home and home-work-home-work-home are the most common patterns, and the average length of the activity chains is close to 3.

4.1.3. Network Preparation. The simulation network of Baoding is prepared through OpenMapStreet and it includes 502 nodes and 1474 links. The link attributes contain length, capacity, free speed, lanes, modes, and so forth. The road network is showed by Figure 2.

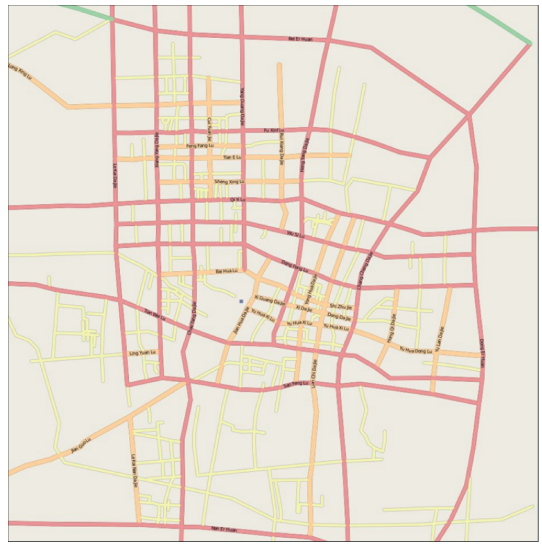

Figure 2: Road network of Baoding.

4.2. Initial Demand Preparation.

The modeling of the initial demand can be split up into several steps depending on the available raw data and the planner's needs. But an initial plan should at least include the following information.

(i) Activity location which is given as a set of coordinates.

(ii) Assigned departure times and arrival times for every activity.

(iii) A travel leg among two activities; in this paper, the mode is set as car.

Algorithm 1 shows a typical initial plan. It includes attributes of the person and his initial plan. The attributes are made up of ID, age, and employment statues. The initial plan is made up of 5 activities, and they are home, work, home, work, and home in sequence, which are set as variable of act type. Take the first activity, for example; the activity location is in the facility with ID of 1593 and its coordinate is represented by variables of x and y, and, besides, the end time of the activity is represented by variable of end_time. The leg mode and dep_time are used to describe the mode the person chooses and time the people leaving the facility.

Different available data need different processes to prepare an initial data. Figure 3 shows a detailed preparing process based on the available data of Baoding. The process is mainly made up of three parts.

Part 1: List All the Available Data for Simulation. Part 1 only contains one step, namely step 1. To check all the available

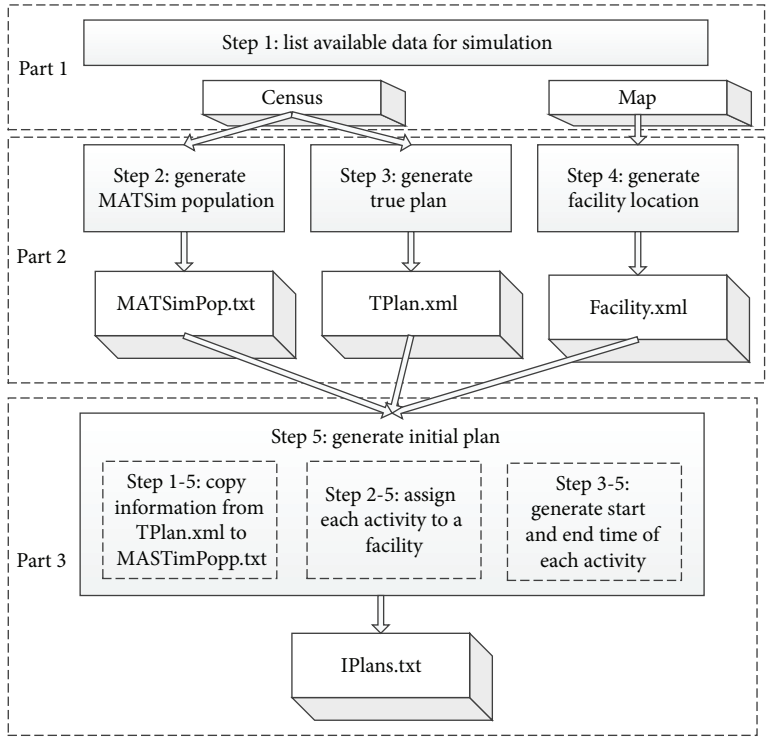

Figure 3: The process of preparing the initial data.

data and make better use of them is a vital step in the simulation. Take Baoding, for example; the available data are the census 2007 of Baoding and the map of Baoding in 2007. The census sample includes 2267 persons' daily plan, but the number of persons whose travel mode is car is 93, which is extremely small. Each daily plan includes trip origin, trip destination, starting time, ending time, activity type, and travelling leg. But unfortunately, the data of trip origin and destination are in traffic zone level, which cannot be directly applied to agent-based simulation and should be adjusted. The map of Baoding in 2007 comprises the available facilities for performing activities, such as shopping, leisure, and work.

Part 2: Prepare Data for Generating Initial Plan. Part 2 is made up of step 2, step 3, and step 4.

In step 2, since the survey sample is really small, the MATSim population is synthesized on the basis of census. MTSim population includes a few persons (agents) whose information only includes age, home location, and work location and all the above information is stored in MATSim-Pop.txt, which will be used for generating initial plan.

In step 3, generate a true plan file (TPlan.xml) which contains a handful of plans whose travel mode was car based on the census 2007 of Baoding. The following information is included: person ID, trip ID, origin coordinates, destination coordinates, activity duration, and activity type. Note that the trip origin and destination are in traffic zone level, so a random assigning method was used for selecting a location for performing activities.

In step 4, prepare the available facilities for performing activities, that is, getting the exact location, type, and attributes of facilities. All the information was saved in Factilities.xml. There were five facility types corresponding to five activity types. The numbers of facilities for shopping, education, leisure, work, and home are 256, 51, 478, 912, and 1321, respectively. In addition, before the facilities location is determined, the coordination transform should be discussed. WGS84-coordinates are widely used, like GPS data, OpenStreetMap data, and Google earth data. For the distance calculation in WGS84-coordinates (or any spherical coordinates) is rather complex, in MATSim, the coordinates should be converted into another coordinate reference system (CRS). This paper chooses the UTM (Universal Transverse Mercartor Grid System) as the coordinate used in MATSim. According to the UTM global zoning, Baoding is located in the zone 50N and its EPSG code is 32650.

Part 3: Generating Initial Plan. After preparing the required data (MATSimPop.txt, TPlan.xml, and Factilities.xml) in Part 2, generating initial plan would be conducted.

Step 5-1, copy all the information from a true plan, which is stored in TPlan.xml, to the plan of each agent who made up the MATSim population, except for the location of each activity.

Step 5-2, randomly assign each activity to a facility based on nearby searching method; thus the location of each activity can be generated. The detailed searching method is described with an example as follows. Assume that an agent ends its previous activity and goes shopping next, the controller of the MATSim will define a circle around the previous activity location with a certain radius (the radius is represented as R), and the agent will randomly choose a facility for shopping. In

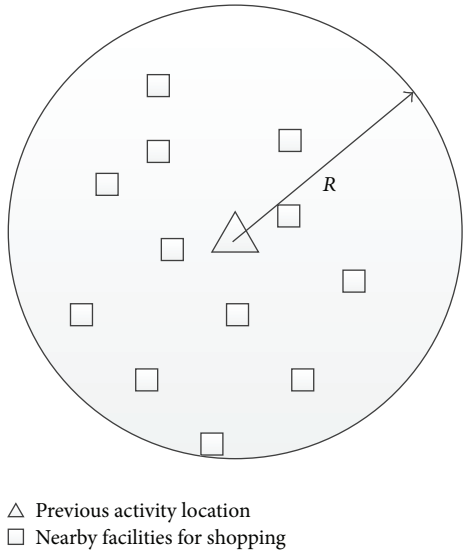

Figure 4: Schematic diagram of randomly assigning each activity to a facility.

real life, inhabitants will tend to choose a nearer school for education, choose a nearer shop/market for shopping, and so on. So the concept of the searching method seems to be realistic. The R was set to 3 km, according to Baoding's size, population and so on. The schematic diagram is showed in Figure 4.

Step 5-3, generate the start and end time of each activity on the basis of activity duration. For example, the end time of the previous activity is P_{endtime}, and the duration of the next performed activity is T_{duration}; then the Gaussian function is used to generate the next activity's end time, and the equation is as follows:

$$T_{\text{endtime}} = P_{\text{endtime}} + T_{\text{duration}} + \text{Gaussian} \cdot 3600, \quad (7)$$

where T_{endtime} is the end time of the next activity. Gaussian represents the rand number generated based on Gaussian distribution whose mean is 0 and the standard deviation is 1.

When all the above steps are completed, the initial plan is finally created.

4.3. Count Data. Inputting count data to MATSim is a typical way to check whether the simulation of travel behavior is realistic. In this paper, six count stations' data will be used. The count data is obtained by an artificial method. The survey time is at May 10, 2007, from 7:00 AM to 9:00 AM.

4.4. Simulation Configuration. In this paper, two different simulation scenarios will be built up.

(i) Scenario 1: 10% of all agents carry out Reroute.

(ii) Scenario 2: 10% of all agents will carry out Time Allocation Mutator, but these agents will also carry out Reroute after time changes.

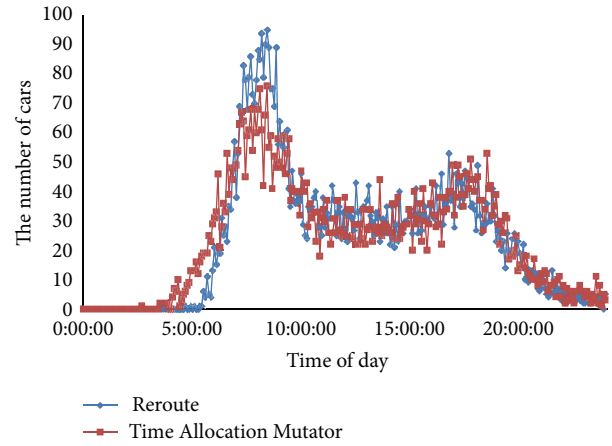

Figure 5: Comparison of the number of departures of cars between two scenarios.

Other simulation configurations of the above three scenarios are the same.

(i) The number of the plans stored in each agent's memory is limited to 5.

(ii) 10% of all agents will randomly select an existing plan.

(iii) The remaining 70% of all agents will select an existing plan based on the plan scores.

(iv) The number of iterations will be set to 50.

(v) The "QSim" module will be used for mobility simulation.

5. Results and Discussion

Simulation results of the two different scenarios will be discussed in the following aspects.

(i) Comparison of the Number of Departures and Arrivals of Cars between Two Scenarios. Figures 5 and 6 show the number of departures and arrivals of cars between the two scenarios, respectively. Both figures have the same trend which has two peaks. The two peaks occur around 8:00 and 18:00, respectively. In addition, in terms of Figure 4, the first peak of Scenario 2 (Time Allocation Mutator) is lower than Scenario 1 (Reroute) and the number of cars of Scenario 2 is higher than Scenario 1 from 5:00 AM to 8:00 AM, which indicates that some agents advance their departure time to avoid high traffic volume during the peak time. Figure 5 has the same trend as Figure 4 due to the same reason.

(ii) Comparison of the Evolution of the Average Best Score and Average Executed Score for the Two Scenarios. Figures 7 and 8 demonstrate the average executed score and average best score of two scenarios, respectively, and they also have the same trend. The score of Scenario 1, which only carries out Reroute, keeps invariant from iteration 0 and iteration 50 in both figures, while the score of Scenario 2, which carries out Time Allocation Mutator, has an increasing trend in both

Table 1: Bias and error of two scenarios.

Time period	Bias/error	Scenario 1 (Reroute)	Scenario 2 (Time Allocation Mutator)
7:00-8:00 AM	Mean absolute bias	−24	−147
	Mean absolute error	158	204
	Mean relative bias	−0.75%	−24.04%
	Mean relative error	32.09%	37.91%
8:00-9:00 AM	Mean absolute bias	−45	−222
	Mean absolute error	252	281
	Mean relative bias	6.41%	−25.57%
	Mean relative error	44.00%	41.29%
7:00–9:00 AM	Mean absolute bias	−35	−185
	Mean absolute error	205	243
	Mean relative bias	2.83%	−24.80%
	Mean relative error	38.05%	39.60%

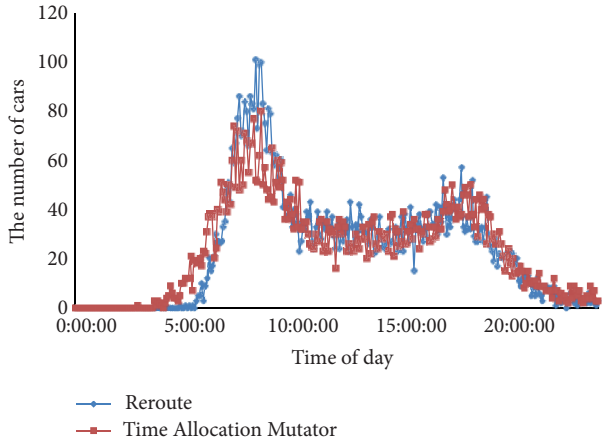

Figure 6: Comparison of the number of arrivals of cars between two scenarios.

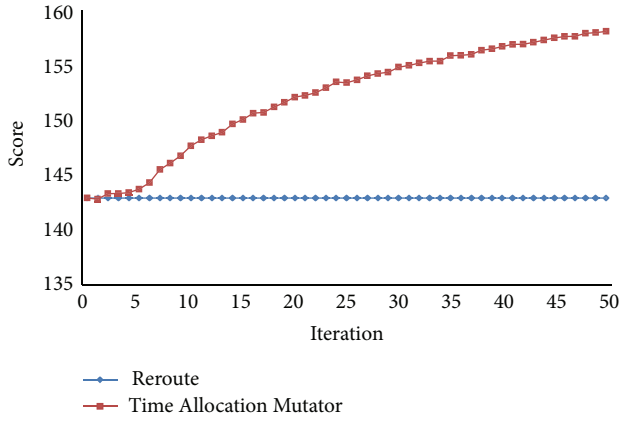

Figure 7: Comparison of the evolution of the average executed score for the two scenarios.

figures. According to the trend mentioned above, we can conclude that Reroute does not improve the agents' performance, while Time Allocation Mutator has a significantly beneficial influence on the performance of agents. The reason why score

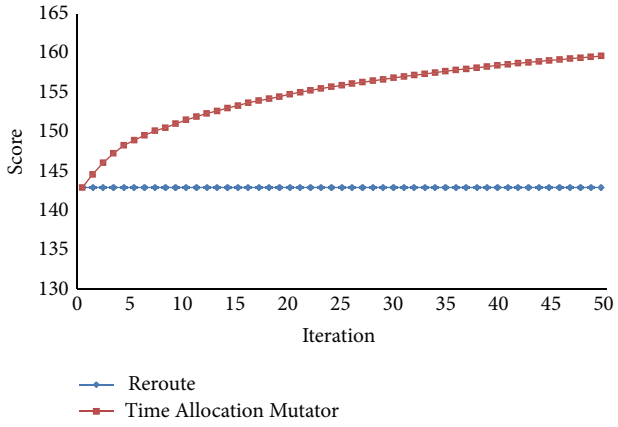

Figure 8: Comparison of the evolution of the average best score for the two scenarios.

of Scenario 1 remains the same is that agents cannot improve their performance through changing their routes.

(iii) Comparison of the Simulated Data and the Count Data of the Two Scenarios. The comparison between the simulated data and count data of the two scenarios is presented in Figure 9. Figures 9(a), 9(b), 9(c), and 9(d) demonstrate the comparison in Scenario 1 at 7-8 AM, in Scenario 2 at 7:00-8:00 AM, in Scenario 1 at 8:00-9:00 AM, and in Scenario 2 at 8:00-9:00 AM, respectively. The bias and error of the simulation results are summarized in Table 1. The mean absolute bias, mean absolute error, mean relative bias, and mean relative error are jointly used to check the simulation results. The equations to calculate the above indicators are as follows:

(i) mean absolute bias:

$$E = \frac{1}{n} \sum \left(q_{\text{simulated}} - q_{\text{counted}} \right), \tag{8}$$

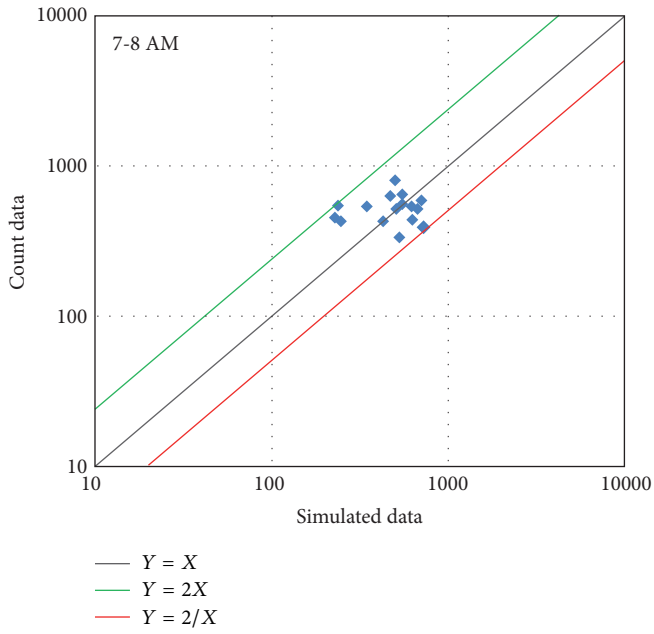

(a) Simulated data versus count data at 7:00-8:00 AM (Simulation with Reroute only)

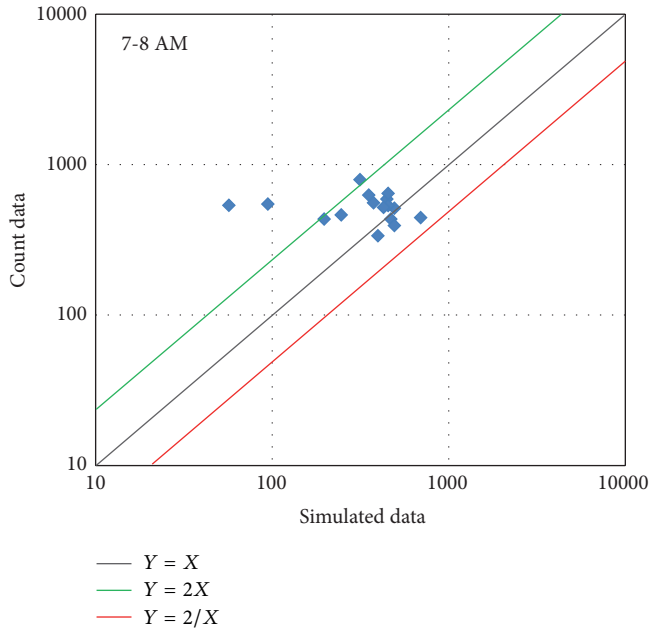

(b) Simulated data versus count data at 7:00-8:00 AM (Simulation with Time Allocation Mutator)

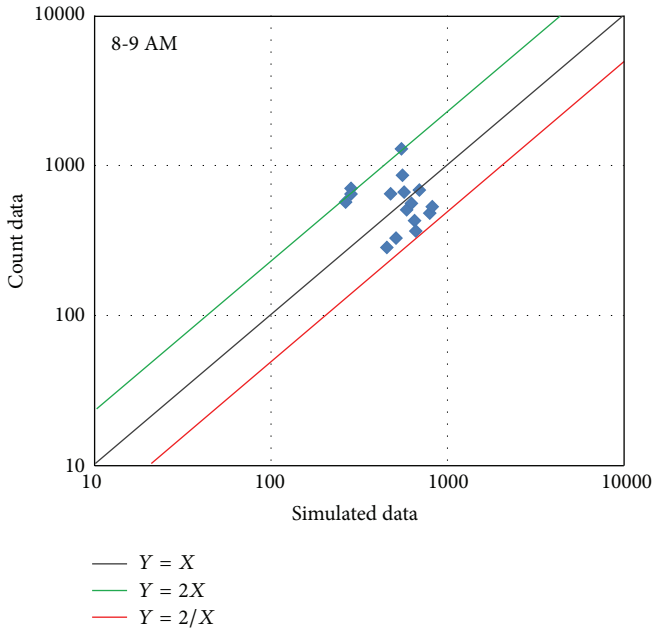

(c) Simulated data versus count data at 8:00-9:00 AM (Simulation with Reroute only)

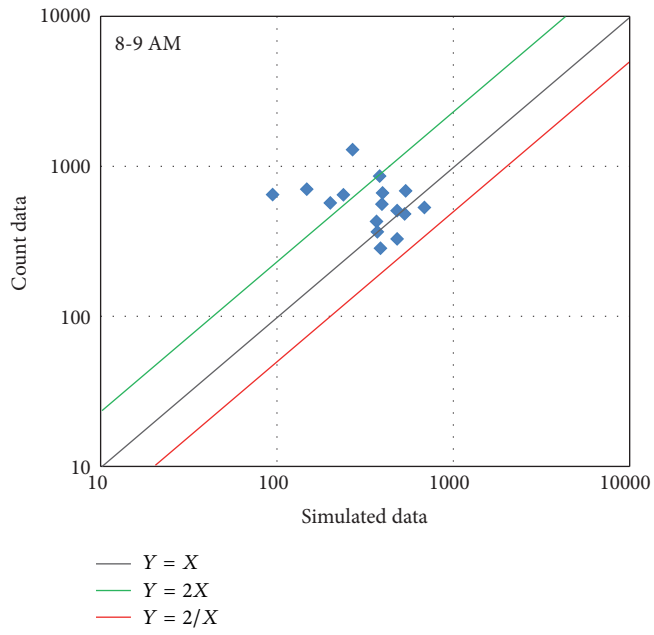

(d) Simulated data versus count data at 8:00-9:00 AM (Simulation with Time Allocation Mutator)

Figure 9: Comparison between simulated data and count data.

(ii) mean absolute error:

$$|E| = \frac{1}{n} \sum \left(\left| q_{\text{simulated}} - q_{\text{counted}} \right| \right), \tag{9}$$

(iii) mean relative bias

$$e = \frac{1}{n} \sum \left(\frac{q_{\text{simulated}} - q_{\text{counted}}}{q_{\text{counted}}} \right), \tag{10}$$

(iv) mean relative error

$$|e| = \frac{1}{n} \sum \left(\left| \frac{q_{\text{simulated}} - q_{\text{counted}}}{q_{\text{counted}}} \right| \right). \tag{11}$$

In terms of mean relative error, which is commonly used for validating the accuracy of simulation, the accuracy of Scenario 1 (38.05%) is close to Scenario 2 (39.60%) at 7:00–9:00 AM. In addition, from 7:00 AM to 8:00 AM, the mean

relative error of Scenario 1 (32.09%) is lower than Scenario 2 (37.91%), while the mean relative error of Scenario 1 (44%) is higher than Scenario 2 (41.29%) from 8:00 AM to 9:00 AM; thus Time Allocation Mutator does not perform better than Reroute in terms of simulation accuracy.

6. Conclusions

This paper implements the agent-based simulation of travel behavior in a medium-sized city in China, and the main achievements of this paper are as follows:

(i) A detailed simulation structure, which includes a variety of modules, is introduced.

(ii) Successfully realizing the simulation of travel behavior under a condition of limited survey data, besides, a framework of preparing the input data, is presented.

(iii) Simulating the travel behavior of residents in a medium-sized city in China by MATSim was seldom done in previous studies.

However, the above achievement is only a basic simulation work. In the near future, the related work below will be carried out.

(i) This paper only simulates the travel behavior of resident whose travel mode is car, so other modes will be added to the simulation scenario to check whether agent-based simulation results are still realistic.

(ii) A large-scale agent-based simulation will be carried out in a Chinese metropolis, such as Beijing, Shanghai, on Guangzhou.

(iii) Optimize the modules in MATSim to improve its simulation precision and computing time.

Conflict of Interests

The authors declare that there is no conflict of interests regarding the publication of this paper.

Acknowledgments

This research was supported by the National Basic Research Program of China (no. 2012CB725403), the National Natural Science Foundation of China (nos. 51338008, 71210001, 51178032), and the Fundamental Research Funds for the Central Universities (no. 2012YJS069).

References

[1] M. Balmer, *Travel demand modeling for multi-agent traffic simulations: algorithms and systems [M.S. thesis]*, ETH Zürich, Zürich, Switzerland, 2007.

[2] B. Raney, N. Cetin, A. Völlmy et al., "An agent-based microsimulation model of Swiss travel: first results," *Networks and Spatial Economics*, vol. 3, no. 1, pp. 23–41, 2003.

[3] B. Yu and Z. Z. Yang, "An ant colony optimization model: the period vehicle routing problem with time windows," *Transportation Research E*, vol. 47, no. 2, pp. 166–181, 2011.

[4] B. Yu, Z. Yang, K. Chen, and B. Yu, "Hybrid model for prediction of bus arrival times at next station," *Journal of Advanced Transportation*, vol. 44, no. 3, pp. 193–204, 2010.

[5] Y. Bin, Y. Zhongzhen, and Y. Baozhen, "Bus arrival time prediction using support vector machines," *Journal of Intelligent Transportation Systems*, vol. 10, no. 4, pp. 151–158, 2006.

[6] B. Yao, P. Hu, M. Zhang et al., "Artificial bee colony algorithm with scanning strategy for periodic vehicle routing problem," *Simulation*, vol. 89, no. 6, pp. 762–770, 2013.

[7] M. Florian, M. Mahut, and N. Tremblay, "Application of a simulation-based dynamic traffic assignment model," *European Journal of Operational Research*, vol. 189, no. 3, pp. 1381–1392, 2008.

[8] G. Bellei, G. Gentile, and N. Papola, "A within-day dynamic traffic assignment model for urban road networks," *Transportation Research B*, vol. 39, no. 1, pp. 1–29, 2005.

[9] J. C. Muñoz and J. A. Laval, "System optimum dynamic traffic assignment graphical solution method for a congested freeway and one destination," *Transportation Research B*, vol. 40, no. 1, pp. 1–15, 2006.

[10] W. Y. Szeto, Y. Jiang, and A. Sumalee, "A cell-based model for multi-class doubly stochastic dynamic traffic assignment," *Computer-Aided Civil and Infrastructure Engineering*, vol. 26, no. 8, pp. 595–611, 2011.

[11] I. Juran, J. N. Prashker, S. Bekhor, and I. Ishai, "A dynamic traffic assignment model for the assessment of moving bottlenecks," *Transportation Research C*, vol. 17, no. 3, pp. 240–258, 2009.

[12] C. Antoniou, M. Ben-Akiva, and H. N. Koutsopoulos, "Nonlinear Kalman filtering algorithms for on-line calibration of dynamic traffic assignment models," *IEEE Transactions on Intelligent Transportation Systems*, vol. 8, no. 4, pp. 661–670, 2007.

[13] G. Gentile, L. Meschini, and N. Papola, "Spillback congestion in dynamic traffic assignment: a macroscopic flow model with time-varying bottlenecks," *Transportation Research B*, vol. 41, no. 10, pp. 1114–1138, 2007.

[14] B. Yao, C. Yang, J. Hu, J. Yao, and J. Sun, "An improved ant colony optimization for flexible job shop scheduling problems," *Advanced Science Letters*, vol. 4, no. 6-7, pp. 2127–2131, 2011.

[15] B. Yu, Z. Yang, and S. Li, "Real-time partway deadheading strategy based on transit service reliability assessment," *Transportation Research A*, vol. 46, no. 8, pp. 1265–1279, 2012.

[16] W. Davidson, R. Donnelly, P. Vovsha et al., "Synthesis of first practices and operational research approaches in activity-based travel demand modeling," *Transportation Research A*, vol. 41, no. 5, pp. 464–488, 2007.

[17] M. Hatzopoulou and E. J. Miller, "Linking an activity-based travel demand model with traffic emission and dispersion models: transport's contribution to air pollution in Toronto," *Transportation Research D*, vol. 15, no. 6, pp. 315–325, 2010.

[18] X. Dong, M. E. Ben-Akiva, J. L. Bowman, and J. L. Walker, "Moving from trip-based to activity-based measures of accessibility," *Transportation Research A*, vol. 40, no. 2, pp. 163–180, 2006.

[19] W. Recker, J. Duan, and H. Wang, "Development of an estimation procedure for an activity-based travel demand model," *Computer-Aided Civil and Infrastructure Engineering*, vol. 23, no. 7, pp. 483–501, 2008.

[20] J. E. Kang and W. W. Recker, "An activity-based assessment of the potential impacts of plug-in hybrid electric vehicles on energy and emissions using 1-day travel data," *Transportation Research D*, vol. 14, no. 8, pp. 541–556, 2009.

[21] R. M. Pendyala, R. Kitamura, A. Kikuchi, T. Yamamoto, and S. Fujii, "Florida activity mobility simulator overview and preliminary validation results," *Transportation Research Record*, no. 1921, pp. 123–130, 2005.

[22] S. Yagi and A. K. Mohammadian, "An activity-based microsimulation model of travel demand in the Jakarta Metropolitan area," *Journal of Choice Modelling*, vol. 3, no. 1, pp. 32–57, 2010.

[23] B. Yu, W. H. K. Lam, and M. L. Tam, "Bus arrival time prediction at bus stop with multiple routes," *Transportation Research C*, vol. 19, no. 6, pp. 1157–1170, 2011.

[24] B. Yu, Z. Yang, and B. Yao, "An improved ant colony optimization for vehicle routing problem," *European Journal of Operational Research*, vol. 196, no. 1, pp. 171–176, 2009.

[25] M. Rieser, K. Nagel, U. Beuck, M. Balmer, and J. Rümenapp, "Agent-oriented coupling of activity-based demand generation with multiagent traffic simulation," *Transportation Research Record*, vol. 2021, no. 1, pp. 10–17, 2007.

[26] M. Balmer, K. Meister, M. Rieser, K. Nagel, and K. W. Axhausen, "Agent-based simulation of travel demand: structure and computational performance of MATSim-T," in *Proceedings of the 2nd TRB Conference on Innovations in Travel Modeling*, IVT Institut für Verkehrsplanung und Transportsysteme, Portland, Ore, USA, June 2008.

[27] M. Balmer, M. Rieser, K. Meister et al., "Matsim-T: architecture and simulation times," in *Multi-Agent Systems for Traffic and Transportation Engineering*, pp. 57–78, 2009.

[28] A. Horni, D. M. Scott, M. Balmer, and K. W. Axhausen, "Location choice modeling for shopping and leisure activities with MATSim: combining microsimulation and time geography," *Transportation Research Record*, no. 2135, pp. 87–95, 2009.

[29] D. Grether, Y. Chen, M. Rieser et al., "Effects of a simple mode choice model in a large-scale agent-based transport simulation," in *Complexity and Spatial Networks*, pp. 167–186, Springer, Berlin, Germany, 2009.

[30] W. Gao, M. Balmer, and E. J. Miller, "Comparison of MATSim and EMME/2 on greater toronto and hamilton area network, Canada," *Transportation Research Record*, no. 2197, pp. 118–128, 2010.

[31] T. W. Nicolai, L. Wang, K. Nagel et al., "Coupling an urban simulation model with a travel model-a first sensitivity test," in *Proceedings of the Computers in Urban Planning and Urban Management (CUPUM '11)*, pp. 11–07, Also VSP WP, Lake Louise, Canada, 2011.

[32] R. A. Waraich and K. W. Axhausen, "Agent-based parking choice model," *Transportation Research Record*, vol. 2319, no. 1, pp. 39–46, 2012.

[33] J. W. Joubert, P. J. Fourie, and K. W. Axhausen, "Large-scale agent-based combined traffic simulation of private cars and commercial vehicles," *Transportation Research Record*, no. 2168, pp. 24–32, 2010.

[34] D. Charypar and K. Nagel, "Generating complete all-day activity plans with genetic algorithms," *Transportation*, vol. 32, no. 4, pp. 369–397, 2005.

Hindawi Publishing Corporation
Mathematical Problems in Engineering
Volume 2014, Article ID 781395, 9 pages
http://dx.doi.org/10.1155/2014/781395

Research Article

The Effect of Travel Information on Travelers' Choice of Travel Modes and Routes: A Case Study of the Travel between the Campuses

Linjie Gao,[1] Zhicai Juan,[2] Anning Ni,[1] and Peng Jing[2]

[1] *School of Naval Architecture, Ocean & Civil Engineering, Shanghai Jiao Tong University, Shanghai 200240, China*
[2] *Antai College of Economics & Management, Shanghai Jiao Tong University, Shanghai 200052, China*

Correspondence should be addressed to Linjie Gao; ljgao@sjtu.edu.cn

Received 18 November 2013; Revised 25 January 2014; Accepted 27 January 2014; Published 10 March 2014

Academic Editor: Baozhen Yao

The traffic state of the urban road network is determined by travelers' choices of travel modes and routes. With the development of science and technology, people tend to have more travel choices and their distinctive temperaments often lead to different choices even in the same situation. Therefore, a study of different factors that may affect people's travel choices plays a crucial role in the optimization of the traffic system. Focusing on the four major travel modes between Minhang campus and Xuhui campus of Shanghai Jiao Tong University (SJTU) in Shanghai, China, this paper tries to gather the information of the factors that affect travel choices and the extent of such effects both in general cases and when prior information is given by means of questionnaires. Based on data processing, the paper draws pie charts on the travel choices under different circumstances and makes a qualitative analysis of the influential factors. Then, a quantitative analysis is made by using the models of utility function and linear programming. Finally, in contrast with the results, the paper finds out the extent of the effect of travel information on the choice of travel modes and routes of the travelers with different temperaments.

1. Introduction

In everyday life, our travel is faced with the choices of travel modes and routes. Since every traveler expects to spend the shortest time arriving at the destination at the least cost, they must make the choice according to the comparison and contrast of the available information. Therefore, the effect of the travel information on the travelers' choice behavior remains the focus of research scholars in the world. With a clear understanding of such a choosing process and its influential factors, we can promote the research and optimization of the travel behavior and the thorough traffic network.

The combination of fare, time, stability, comfort, convenience, and other factors will affect travelers' choice of travel modes and routes in different ways. As we know, travel information has an effect on travelers' expectation of the utility of the travel plan which is closely related to travelers' temperament. That is to say, travelers with different temperaments will make different choices when confronted with the same information. Consequently, it is significant to study the effect of travelers' temperament on the travel choice.

This paper mainly focuses on how the variables of the factors that determine the utility expectation affect the choice of travel modes and routes of the travelers with different temperaments facing various travel information. Also, the paper aims to analyze the effect of the travel information on the travel behavior.

The paper consists of five sections as follows. Section 2 is literature review, concerning the focus of research. Section 3 relates the research thought and the research methods. Section 4 dwells upon the data collection and the modeling analysis. And the last section is about the research conclusion and the future research directions.

Table 1: Characteristics of travel modes.

Travel modes	Fare	Time	Frequency	Convenience	Stability	Comfort
School bus	¥4	40–45 min	10 times a day from Mon to Fri; 4 times a day on weekends	5-to-20-minute walk to school bus stop; wait in line 15 minutes in advance for students	8	8
Bus and metro	¥5	60–70 min	Once every 5 to 10 minutes	15-to-20-minute walk to bus stop; 0-to-10-minute wait; 0-to-5 minutes for transfer	10	6
Regular bus	¥2	70–80 min	Once every 15 minutes	20-minute walk to bus stop; 0-to-15-minute wait	8	5
Taxi	over ¥80	40–50 min	Anytime	Less-than-15-minute walk to entrance	6	9

Notes: stability scale 1 to 10: the least stable to the most stable;
comfort scale 1 to 10: the least comfortable to the most comfortable.

2. Literature Review

With the development of information and communication technology, travelers are increasingly concerned about travel information before and during the travel and accordingly make their travel choices. Since the effect of travel information on travelers' choice during the actual travel is hard to obtain and analyze, most researchers focus more on the collection of the stated preference data and the analysis of the effect of travel information on travel decision behavior and traffic system under experimental and virtual circumstances. Since the 1990s, the scholars, represented by Hani Mahmassani at University of Texas in the USA and Yasunori Iida at Kyoto University in Japan, have made a lot of advancements in the field. By setting up the traffic simulation platform and constructing the two-route network or simple network with single origin and destination, they studied the effect of travelers' behavior on traffic system with the available travel information in the experimental and analytical methods and analyzed the effect of travel information and its reliability on travel behaviors [1–4]. Later, Koutsopulos et al. made further studies in this direction [5–11]. Ewing et al. examined the relationship between mode of travel to school and the full range of factors that might affect mode choice [12]. Shu-Sen et al. classified travel into rigid travel and flexible travel. Shu-Sen et al. held that travelers also take fare, comfort, safety, and other factors of various travel modes into account, besides travel properties as travel distance and destination [13]. Wei-Guo and Si-Ji made a study of travelers' choice of travel modes in the simulation method rather than in the traditional mathematical and sampling method [14]. de Palma and Picard studied on route choice decision based on the ordered probit analysis and econometric estimates under travel time uncertainty [15]. Khattak et al. analyzed travelers' willingness to pay for better quality information received from a traveler information system [16]. Besides, Chorus et al. made route choice and mode choice studies based on simulation [17–19].

All the researchers have made abundant studies of travelers' choice of travel modes or routes, or the combined choice of both. In their studies, the factors that affect travelers' choice mainly focus on time, fare, stability, comfort, and convenience. The research methods of theirs are either qualitative, by posing the influential factors, or comparison and contrast of the results in the simulation or experimental methods, or by means of actual sampling. However, seldom did they make a quantitative analysis of all the factors. This paper will make a study of the extent of the effect of the variables of the factors on the choice of travel modes and routes of travelers with different temperaments, in the combined qualitative and quantitative methods.

3. Research Thought and Methodology

In the recent 15 years, almost every university has several campuses due to the large-scale consolidation of universities and colleges in China. Commuting between campuses is increasingly becoming representative of urban travel. Therefore, this paper makes a study of the commuting system of Minhang campus and Xuhui campus of Shanghai Jiao Tong University (SJTU) in China, choosing students as the respondents. With a distance of 25 kilometers between the two campuses, the optional travel modes consist of school buses, the transfer from buses to metro (bus and metro), regular buses, and taxis. The characteristics of the four travel modes are shown in Table 1.

First of all, travelers are divided into four types according to the four temperaments from Galen [20]:

(i) sanguine (Type A travelers): excited-pleasant and shallow-broad,

(ii) choleric (Type B travelers): exited-unpleasant and deep-broad,

(iii) phlegmatic (Type C travelers): calm-pleasant and shallow-narrow,

(iv) melancholic (Type D travelers): calm-unpleasant and deep-narrow.

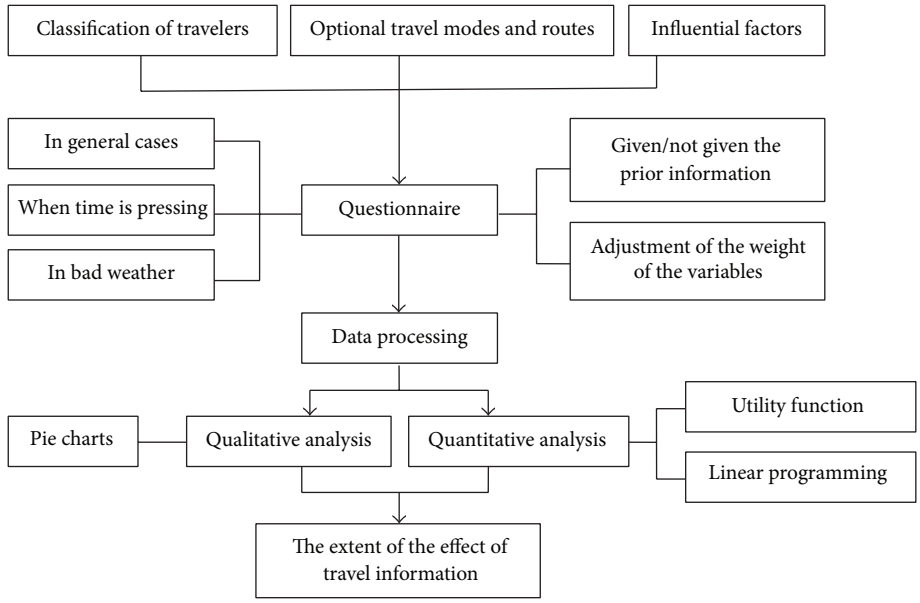

Figure 1: Framework of research.

Thereafter, we design the questionnaire with the subject of the effect of travel information on the travelers' choice of travel modes and routes.

Second, we study the choosing behavior of the travelers with the four temperaments under the following three circumstances by means of paper questionnaires and online survey.

(A) Given (or not given) the prior information of various travel modes, how travelers choose the available travel modes and routes.

(B) Under different preconditions, how travelers choose the travel modes and routes.

(C) How travelers change their former decisions with the change of the variables of the travel modes (fare, schedule, comfort, routes, etc.).

Finally, by screening the collected questionnaires, we take in the valuable data, make a quantitative analysis of the priority of choosing travel modes by means of utility function and make a contrast with the actual research results; then, by making adjustments to the weight of the variables (fare, time, stability, comfort, and convenience) by way of linear programming, we make the results of utility function approaching the actual results and arrive at the extent of the effect of the variables on the choice of travel modes.

The framework of the research is shown in Figure 1.

4. Data Collection and Modeling Analysis

4.1. Data Collection. A total of 597 questionnaires had been issued to students, 420 in paper version and 177 sent online. At the end of the survey, 459 questionnaires were collected, 282 in paper version and 177 received online. Through the initial screening, there are 204 valid questionnaires excluding 255 invalid questionnaires (which cannot be used in the qualitative analysis).

4.2. Qualitative Analysis of the Influential Factors

4.2.1. Time Outweighs Comfort (concerning the Extent of Their Effect). As we know, taxis take priority among the four travel modes, when time and comfort are concerned. From Figures 2(a), 2(b), and 2(c), we can see that there is a drastic rise in the percentage of choosing taxis as the travel mode when time is pressing and in bad weather. The 1% in general cases increases to 33% when time is pressing and to 25% in bad weather. There are more respondents who tend to give priority to time (by taking taxis) when time is pressing than those who tend to give priority to comfort (by taking taxis) in bad weather.

4.2.2. Comfort Outweighs Stability (concerning the Extent of Their Effect). From Figure 2(d), we can see, concerning commuting with a frequency of five days a week, only a small proportion of respondents choose regular buses and taxis; comparatively, the percentage of choosing the transfer from buses to metro decreases from 44% to 27%; however, the percentage of choosing school buses increases from 46% to 67%. That is to say, under such circumstances, school buses occupy a predominant position. As we see, when the transfer from buses to metro and school buses are concerned, they bear similarities in time, fare, and convenience but differ in comfort and stability which may affect travelers' choice. Due to the limit of capacity, school buses cannot allow all the students to wait in line on board. Therefore, school buses are more comfortable while the transfer from buses to metro tend to be more stable. On average, comfort outweighs

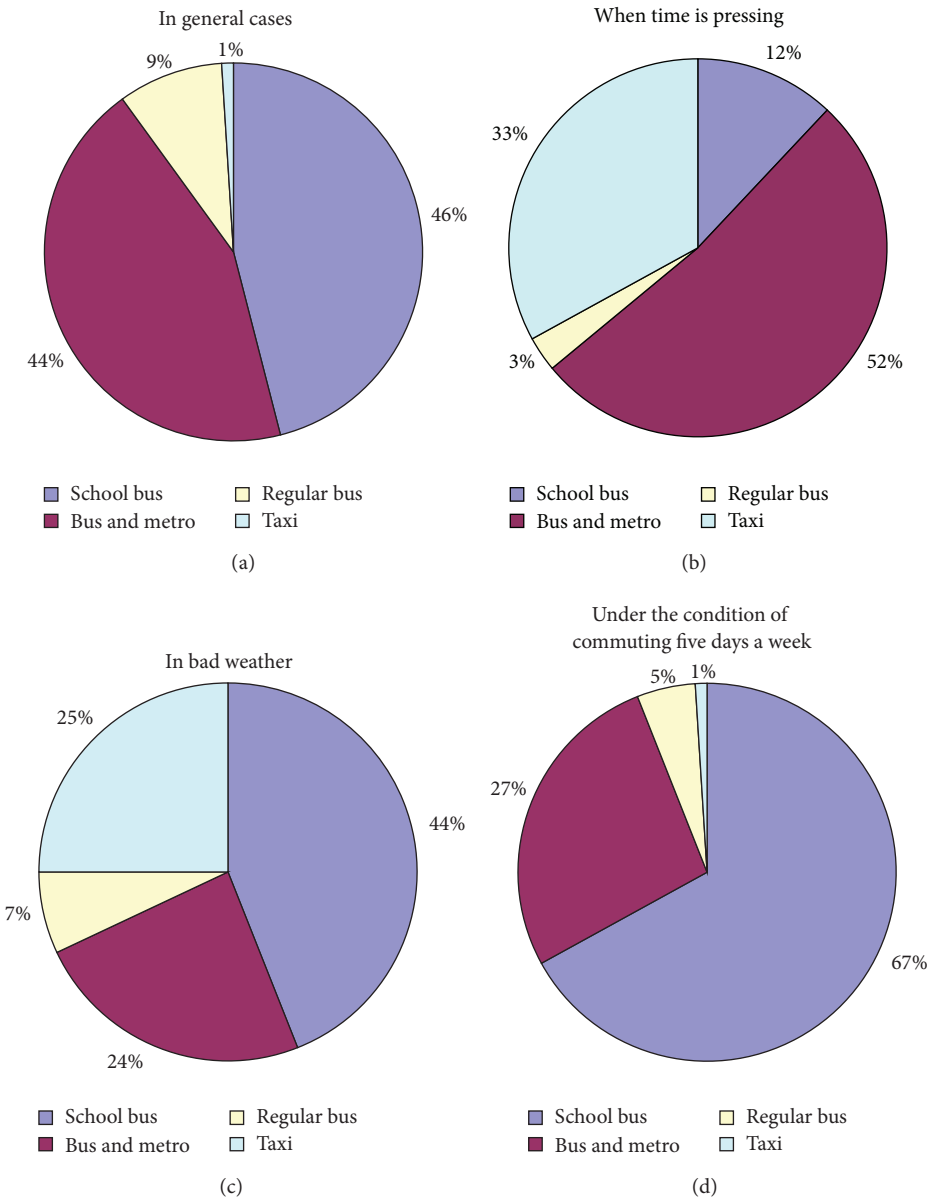

Figure 2: The proportion of the choices of travel modes under different circumstances.

stability among the five factors that influence the travelers' choice.

4.2.3. The Extent of the Effect of Stability on Travelers' Choice Rises with the Extent of the Travelers' Introversion. In general cases, if given prior information (the estimated time, fare, and route of various travel modes), the choices of travelers with different temperaments are shown in Figure 3.

The transfer from buses to metro is characteristic of stability. As is seen from Figure 3, the percentage of travelers' choosing the transfer from buses to metro is changing with their different temperaments. For those extroverted travelers, the percentage is 25% for sanguine (Type A travelers) and 27% for choleric (Type B travelers); while for those introverted travelers, the percentage rises to 31% for phlegmatic (Type C travelers) and 53% for melancholic (Type D travelers). Therefore, we think the introverted travelers tend to choose the travel modes of strong stability and the extent of the effect of stability on travelers' choice rises with the extent of the travelers' introversion.

4.2.4. The Effect of Fare Is Evident, Especially Greater on Introverted Travelers. We see from Figure 4, only 16% of respondents are willing to choose school buses as the travel

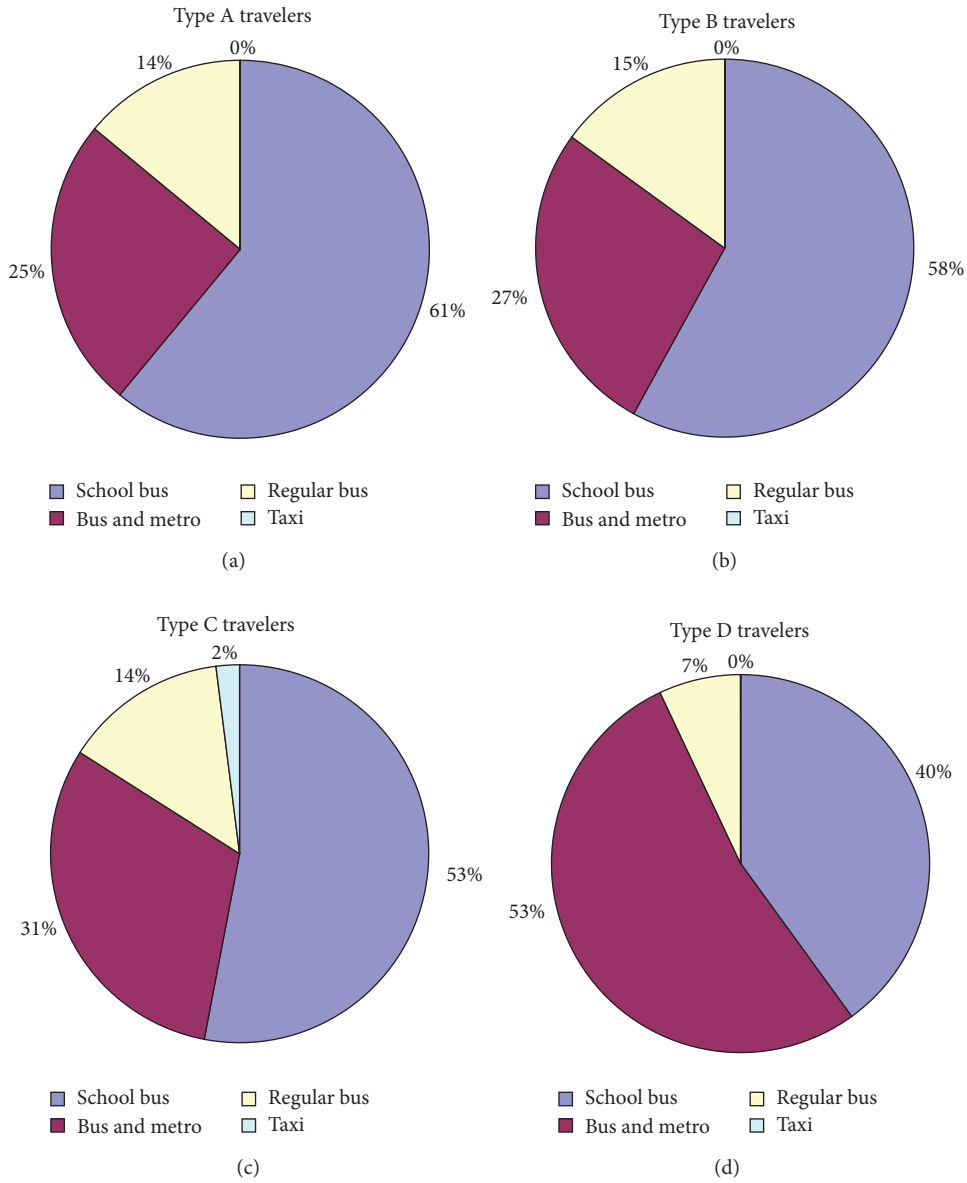

Figure 3: The proportion of the choices of travel modes of travelers with different temperaments.

mode, when the fare rises from ¥4 to ¥8. It is easy to see that travelers are greatly affected by the factor of fare.

From Figure 5, we can see that 19% of Type A students, 26% of Type B students, 10% of Type C students, and 6% of Type D students keep choosing school buses, even when there is a rise of fare from ¥4 to ¥8. Therefore, we consider introverted travelers to be more affected by the change of fare. In another word, the effect of fare is greater on introverted travelers than extroverted ones.

4.3. The Quantitative Analysis of the Factors

4.3.1. Quantitative Evaluation of the Factors. According to the data from the questionnaire of the factors that affect the choice of travel modes, we average the evaluation data from travelers with different temperaments and the travelers on the whole, as is seen in Table 2.

4.3.2. Quantitative Evaluation of the Travel Modes. We average the data of overall evaluation of all travel modes chosen by different types of respondents in the survey, as is seen in Table 3.

4.3.3. Linear Programming. Due to the few samples of Type D travelers, we failed to make a quantitative analysis. The frequently chosen travel modes between two campuses are school buses and the transfer from buses to metro, rather than regular buses and taxis. According to the observation of the data, travelers' evaluation of the regular buses does

Table 2: The evaluation utility of the factors that affect the travel mode choice.

Types of travelers	Travel modes	Fare	Time	Stability	Comfort	Convenience
Type A travelers	School Bus	2.58	2.47	2.05	1.84	2.05
	Bus and Metro	1.32	1.37	2.00	1.37	1.37
	Regular Bus	1.95	0.37	0.74	0.32	0.42
	Taxi	0.16	1.79	1.21	2.47	2.16
Type B travelers	School Bus	2.76	2.48	1.52	1.81	1.76
	Bus and Metro	1.24	1.62	2.38	1.33	1.67
	Regular Bus	2.00	0.10	0.90	0.38	0.38
	Taxi	0.00	1.81	1.19	2.48	2.19
Type C travelers	School Bus	2.58	2.08	1.58	2.08	1.75
	Bus and Metro	1.50	1.75	2.50	1.33	1.67
	Regular Bus	1.92	0.29	0.83	0.38	0.75
	Taxi	0.00	1.88	1.08	2.21	1.83
Type D travelers	School Bus	3.00	0.80	1.00	1.00	1.00
	Bus and Metro	1.60	2.00	2.20	1.60	1.80
	Regular Bus	1.40	0.80	0.80	1.20	1.20
	Taxi	0.00	2.40	2.00	2.20	2.00
Type A travelers	School Bus	2.67	2.22	1.65	1.86	1.78
	Bus and Metro	1.38	1.62	2.30	1.36	1.59
	Regular Bus	1.91	0.29	0.83	0.42	0.58
	Taxi	0.04	1.87	1.22	2.36	2.04

Table 3: The overall evaluation utility of the travel modes.

Types of travelers	School bus	Bus and metro	Regular bus	Taxi
Type A travelers	2.53	2.21	1.05	0.21
Type B travelers	2.10	2.48	1.10	0.33
Type C travelers	2.17	2.43	1.13	0.60
Type D travelers	0.00	2.80	1.60	1.60

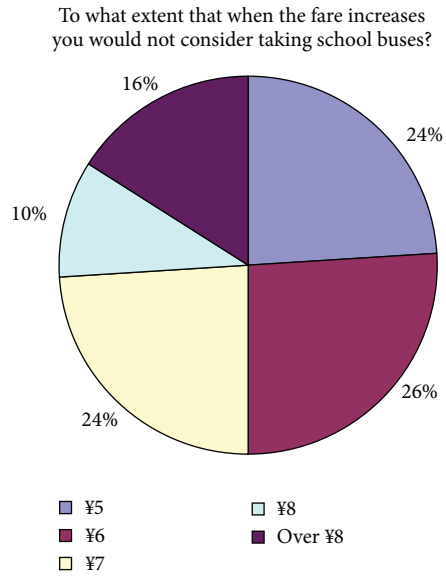

Figure 4: The analysis of the effect of fare on the choice of school buses.

not agree with the real condition. Therefore, disregarding the regular buses, the analysis is only made of the other three travel modes: school buses, the transfer from buses to metro, and taxis.

Consider the following.

Assume that X, Y, Z, P, and Q represent the variables of the five factors: fare, time, stability, comfort, and convenience.

Assume that a, b, c, d, and e represent the weight of the five factors: fare, time, stability, comfort, and convenience.

Assume that $S = a + b + c + d + e$, and $0 \leqslant S \leqslant 1$.

We get the evaluation of all the travel modes.

School buses:

$$S1 = a * X11 + b * Y12 + c * Z13 + d * P14 + e * Q15. \quad (1)$$

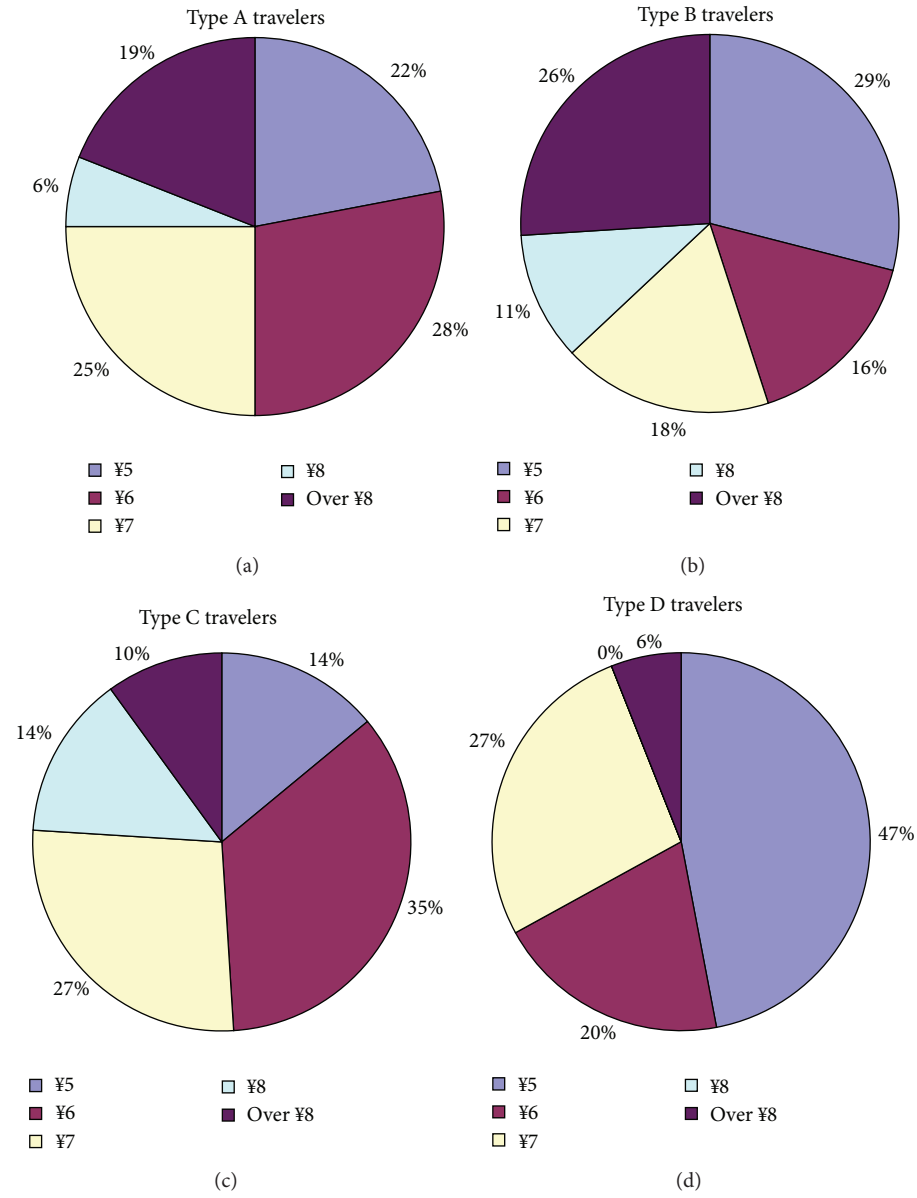

Figure 5: The analysis of the effect of fare on different types of travelers' choice of school buses.

Transfer from buses to metro:

$$S2 = a * X21 + b * Y22 + c * Z23 + d * P24 + e * Q25. \quad (2)$$

Taxis:

$$S4 = a * X41 + b * Y42 + c * Z43 + d * P44 + e * Q45. \quad (3)$$

According to the data in Table 3, we can see the relation among $S1, S2$, and $S4$ for the three types of travelers as follows:

for Type A travelers, $S1 > S2 > S4$;

for Type B travelers, $S2 > S1 > S4$;

for Type C travelers, $S2 > S1 > S4$.

According to linear programming macro command, we set target function as MIN $(1 - S)$, with the constraints as follows:

(1) $S \leq 1,\ a > 0,\ b > 0,\ c > 0,\ d > 0,\ e > 0$;

(2) Type A travelers: $S1 > S2 > S4$;

Type B travelers: $S2 > S1 > S4$;

Type C travelers: $S2 > S1 > S4$;

(3) setting constraints on the upper and lower limits of the weight a, b, c, d, and e in various cases, as is shown in Table 4.

The processing results of linear programming are shown in Table 5. (/ represents that there are no results that agree with the condition.)

Table 4: The range of the weight of the factors.

Upper limit	0.5	0.5	0.5	0.45	0.45	0.45	0.4	0.4	0.4
Lower limit	0.05	0.1	0.15	0.05	0.1	0.15	0.05	0.1	0.15

Table 5: The extent of importance of the factors.

Types of travelers	Upper limit	Lower limit	Fare	Time	Stability	Comfort	Convenience	Optimized results
Type A travelers	0.50	0.05	0.48	0.05	0.05	0.37	0.05	0.00
	0.50	0.10	0.42	0.10	0.10	0.28	0.10	0.00
	0.50	0.15	0.35	0.15	0.15	0.20	0.15	0.00
	0.45	0.05	0.45	0.05	0.09	0.36	0.05	0.00
	0.45	0.10	0.42	0.10	0.10	0.28	0.10	0.00
	0.45	0.15	0.35	0.15	0.15	0.20	0.15	0.00
	0.40	0.05	0.40	0.05	0.15	0.35	0.05	0.00
	0.40	0.10	0.40	0.10	0.12	0.28	0.10	0.00
	0.40	0.15	0.35	0.15	0.15	0.20	0.15	0.00
	Total		**3.62**	**0.90**	**1.05**	**2.53**	**0.90**	
Type B travelers	0.5	0.05	0.05	0.15	0.50	0.05	0.25	0.00
	0.5	0.1/0.15	/	/	/	/	/	/
	0.45	0.05	0.05	0.09	0.45	0.05	0.36	0.00
	0.45	0.1/0.15	/	/	/	/	/	/
	0.4	0.05	0.06	0.05	0.40	0.05	0.34	0.10
	0.4	0.1/0.15	/	/	/	/	/	/
	Total		**0.16**	**0.29**	**1.35**	**0.15**	**0.96**	
Type C travelers	0.5	0.05	0.05	0.15	0.50	0.05	0.25	0.00
	0.5	0.1/0.15	/	/	/	/	/	/
	0.45	0.05	0.05	0.09	0.45	0.05	0.36	0.00
	0.45	0.1/0.15	/	/	/	/	/	/
	0.4	0.05	0.06	0.05	0.40	0.05	0.34	0.10
	0.4	0.1/0.15	/	/	/	/	/	/
	Total		**0.16**	**0.29**	**1.35**	**0.15**	**0.96**	
Overall travelers	0.50	0.05	0.05	0.05	0.50	0.05	0.24	0.11
	0.50	0.1/0.15	/	/	/	/	/	/
	0.45	0.05	0.05	0.05	0.45	0.05	0.18	0.22
	0.45	0.1/0.15	/	/	/	/	/	/
	0.40	0.05	0.05	0.05	0.40	0.05	0.11	0.34
	0.40	0.1/0.15	/	/	/	/	/	/
	Total		**0.15**	**0.15**	**1.35**	**0.15**	**0.53**	

Notes: the column of optimized results represents the weight that cannot be classified into a certain category after linear programming.

4.3.4. The Analysis of the Results. From Table 5, we can see that for Type A travelers, the ranking of the factors that affect the choice of travel modes and routes is fare > comfort > stability > time and convenience. For Types B and C travelers, the ranking is stability > convenience > time > comfort > fare. For all the travelers, the ranking is stability > convenience > fare, time, and comfort.

Therefore, we can see that the prior information consisting of all the influential factors has a different effect on the choice of travel modes and routes of the travelers with different temperaments. The overall analysis of the travelers conceals the effect of temperaments on travel behaviors. From the figures of the optimized results in the quantitative analysis of all the travelers, we can also see that there is a bigger error if the analysis of travel behaviors excludes the distinction of temperaments.

5. Conclusion

This paper has classified travelers into four types according to the temperaments and collected the evaluation data of the factors that affect their choice of travel modes and routes under three different circumstances. We have made a detailed study of the extent of the importance of the effect of the five factors on the different types of travelers' choice of travel modes and routes in general cases and with prior information, by means of the qualitative and quantitative analysis. We can discover the important effect of

temperaments on travelers' choice of travel modes and routes. For Type A travelers (sanguine) and Type B/C travelers (choleric/phlegmatic), the ranking of the factors that affect their choices of travel modes and routes is inconsistent.

The future study should be directed to the expansion of samples to travelers with different occupations and the collection of data by more advanced means of smartphones, travel logs, and so forth. Through the deep analysis of a large quantity of data, the study should also be made of the interaction of all the factors affecting travel choice behaviors so as to have a more profound understanding of the process of travel choice behaviors and provide the foundation for the policymaking of transportation demand management.

Conflict of Interests

The authors declare that there is no conflict of interests regarding the publication of this paper.

Acknowledgment

This research is supported by the National Natural Science Foundation of China (50808123).

References

[1] H. S. Mahmassani and P. S. T. Chen, "An investigation of the reliability of real-time information for route choice decisions in a congested traffic system," *Transportation*, vol. 20, no. 2, pp. 157–178, 1993.

[2] H. S. Mahmassani and Y. H. Liu, "Dynamics of commuting decision behaviour under advanced traveller information systems," *Transportation Research C*, vol. 7, no. 2-3, pp. 91–107, 1999.

[3] Y. Iida, T. Akiyama, and T. Uchida, "Experimental analysis of dynamic route choice behavior," *Transportation Research B*, vol. 26, no. 1, pp. 17–32, 1992.

[4] B. Z. Yao, P. Hu, X. H. Lu, J. J. Gao, and M. H. Zhang, "Transit network design based on travel time reliability," *Transportation Research C*, 2014.

[5] H. N. Koutsopoulos, A. Polydoropoulou, and M. Ben-Akiva, "Travel simulators for data collection on driver behavior in the presence of information," *Transportation Research C*, vol. 3, no. 3, pp. 143–159, 1995.

[6] S. Peeta and J. W. Yu, "A hybrid model for driver route choice incorporating en-route attributes and real-time information effects," *Networks and Spatial Economics*, vol. 5, no. 1, pp. 21–40, 2005.

[7] J. W. Yu and S. Peeta, "Experimental analysis of a hybrid route choice model to capture dynamic behavioral phenomena under advanced information systems," *KSCE Journal of Civil Engineering*, vol. 15, no. 1, pp. 175–185, 2011.

[8] C. G. Chorus, T. A. Arentze, and H. J. P. Timmermans, "Information impact on quality of multimodal travel choices: conceptualizations and empirical analyses," *Transportation*, vol. 34, no. 6, pp. 625–645, 2007.

[9] C. G. Chorus, J. L. Walker, and M. E. Ben-Akiva, "A joint model of travel information acquisition and response to received messages," *Transportation Research C*, vol. 26, no. 1, pp. 61–77, 2013.

[10] C. G. Chorus, J. L. Walker, and M. E. Ben-Akiva", "Traveler decision making under conditions of knowledge limitations and information provision," in *Proceedings of the 86th Annual Meeting of the Transportation Research Board*, Washington, DC, USA, 2007.

[11] B. Z. Yao, P. Hu, M. H. Zhang, and S. Wang, "Artificial bee colony algorithm with scanning strategy for periodic vehicle routing problem," *Simulation*, vol. 89, no. 6, pp. 762–770, 2013.

[12] R. Ewing, W. Schroeer, and W. Greene, "School location and student travel: analysis of factors affecting mode choice," *Transportation Research Record*, no. 1895, pp. 55–63, 2004.

[13] H. Shu-Sen, S. Rui, and T. Yuan, "Behavior of urban residents travel mode choosing and influencing factors—taking Beijing as an example," *Communications Standardization*, vol. 9, pp. 124–127, 2008.

[14] L. Wei-Guo and H. Si-Ji, "Simulation method for the research of the passengers' traffic mode choice behavior," *Journal of System Simulation*, vol. 14, no. 1, pp. 47–50, 2002.

[15] A. de Palma and N. Picard, "Route choice decision under travel time uncertainty," *Transportation Research A*, vol. 39, no. 4, pp. 295–324, 2005.

[16] A. J. Khattak, Y. Yim, and L. S. Prokopy, "Willingness to pay for travel information," *Transportation Research C*, vol. 11, no. 2, pp. 137–159, 2003.

[17] C. G. Chorus, T. A. Arentze, and H. J. P. Timmermans, "Information impact on quality of travel choices: analysis of data from a multimodal travel simulator," in *Proceedings of the 86th Annual Meeting of the Transportation Research Board*, Washington, DC, USA.

[18] L. Gao, Z. Juan, and A. Ni, "Model and algorithm of dynamic routing based on simulation," in *Proceedings of the 10th International Conference of Chinese Transportation Professionals (ICCTP '10)*, pp. 2397–2407, ASCE, August 2010.

[19] J. Wahle, A. L. C. Bazzan, F. Klügl, and M. Schreckenberg, "The impact of real-time information in a two-route scenario using agent-based simulation," *Transportation Research C*, vol. 10, no. 5-6, pp. 399–417, 2002.

[20] D. Lester, "Galen's four temperaments and four-factor theories of personality: a comment on 'toward a four-factor theory of temperament and/or personality'," *Journal of Personality Assessment*, vol. 54, no. 1-2, pp. 423–426, 1990.

Hindawi Publishing Corporation
Mathematical Problems in Engineering
Volume 2014, Article ID 728107, 10 pages
http://dx.doi.org/10.1155/2014/728107

Research Article

Deterioration Prediction of Urban Bridges on Network Level Using Markov-Chain Model

Li Li,[1,2] Lijun Sun,[1] and Guobao Ning[3]

[1] *Key Laboratory of Road and Traffic Engineering of the Ministry of Education, Tongji University, Shanghai 201804, China*
[2] *Jiangxi Ganyue Expressway Co., Ltd. Nanchang 330025, China*
[3] *School of Automotive Studies, Tongji University, Shanghai 201804, China*

Correspondence should be addressed to Guobao Ning; guobao.ning@tongji.edu.cn

Received 28 November 2013; Accepted 20 January 2014; Published 2 March 2014

Academic Editor: Baozhen Yao

Bridges play an important role in urban transportation network. However, it is hard to predict the bridge deterioration precisely in Shanghai, because records of various bridge types with different maintenance status coexist in the same database and the bridge age span is also large. Therefore a Markov-chain model capable of considering maintenance factors is proposed in this study. Three deterioration circumstances are modeled including natural decay, conventional recoverable decay, and enhanced recoverable decay. Three components as well as the whole bridge are predicted including bridge deck system, superstructure, and substructure. The Markov-chain model proposed can predict not only the distribution of the percentage of different condition rating (CR) grades on network level in any year but also the deterioration tendency of single bridge with any state. Bridge data records of ten years were used to verify the model and also to find the deterioration tendency of urban bridges in Shanghai. The results show that the bridge conditions would drop rapidly if no recoverable repair treatments were conducted. Proper repair could slow down the deterioration speed. The enhanced recoverable repair could significantly mitigate the deterioration process and even raise the CR grades after several years of maintenance and repair.

1. Introduction

An urban bridge management system (BMS) has been put into use in Shanghai since 2002 and become steady since 2004. More than ten years of bridge condition records have been accumulated up to now. Most of the records are about small and medium bridges which also belong to categories II to V (Table 1) according to Chinese technical code of urban bridges management CJJ 99–2003 [1]. Many types of bridges are included in this BMS database including concrete girder bridges, arch bridges, and steel bridges, where the concrete girder bridges take the majority of the entire data records (more than 80%). The bridge maintenance efforts are also in various forms including routine maintenance, minor repair, medium repair, major repair, and even reconstruction. New bridges and old bridges coexist in the same database and the age of some bridges is even over 100 years. The basic condition of the bridges in Shanghai BMS is so complicated that a prediction approach capable of considering a variety of factors should be used to forecast the urban bridge deterioration process.

Two categories of methods can be used to develop bridge deterioration models, deterministic and stochastic methods. The deterministic model assumes that the bridge deterioration tendency is certain, so regression analysis is commonly used to determine the decay rate [2–4]. These models are often relatively convenient to use but fail to consider uncertainty and randomness of the bridge deterioration process [5]. Stochastic models are better in such aspects. Engineering experience can be used to describe the uncertain factors [6]. Discrete probabilistic models based on state and time are effective in predicting the infrastructure facility deterioration [7]. The discrete probability models are represented by Markov process, which is based on the concept of probabilistic cumulative damage [8] and now commonly used in performance prediction of infrastructure facilities [9]. It is believed that Markov process has three advantages [10]. Firstly, it is able to reflect uncertainties of

Table 1: Urban bridge management system in China.

Category	Significance
I	Super large bridges and bridges with special structures
II	Bridges on freeways
III	Bridges on arterial roads
IV	Bridges on sub arterial roads
V	Bridges on bypass

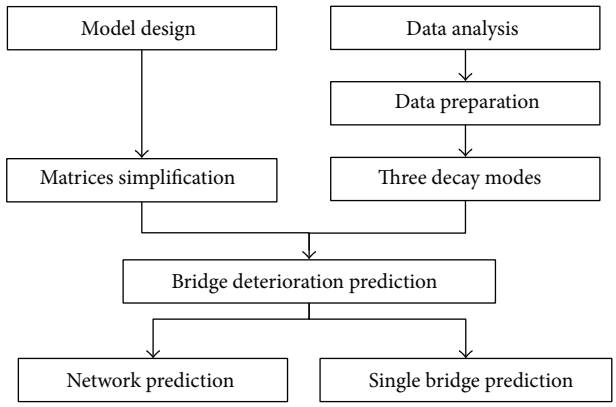

Figure 1: The organization of this study.

various aspects [11]. Secondly, the prediction of future state is based on the present state so the model is incremental [7]. And lastly, it can be applied on network level with many facilities involved which requires calculation efficiency [12]. Some bridge management systems have adopted Markov model to predict the performance of bridges such as Pontis and BRIDGIT [13, 14].

Although the Markov process has been widely used in bridge performance prediction, most applications only focus on some bridge component such as deck or directly consider the bridge as a whole. Besides, the sample size is small in most applications [15]. Actually every bridge component as well as the whole bridge has different deterioration characteristics and the maintenance status usually has varying degrees of impact on different bridge components. Therefore it is necessary to develop a Markov model based on large sample to predict the deterioration tendency of different components of urban bridges, which is also the objective of this study.

The study is organized as shown in Figure 1 and the paper can be divided into six sections. Section 2 presents the basic form of the Markov-chain model used for bridge deterioration prediction. Section 3 provides details of data records in Shanghai BMS and the data processing principles under two circumstances as well as the corresponding processing results. The calculation of Markov transition probability matrices is in Section 4 and the bridge deterioration prediction using these transition probability matrices is discussed in Section 5. Lastly, the conclusions are presented in Section 6.

2. Markov-Chain Model

A Markov process describes a system that can be in one of several states. Each state can pass to another at each time step according to fixed probabilities. Markov-chain model is a special case of the Markov process whose time and state parameters are both discrete. A Markov chain can be treated as a series of state transitions based on certain probabilities. A stochastic process whose transition probability of a future state depends only on the present state is defined as a first-order Markov process [16]. For a stochastic process $\{X(t),\ t \in T\}$, if the conditional probability can be expressed as follows, $\{X(t),\ t \in T\}$ is a Markov chain with discrete parameters:

$$P\left(X_{t+1} = i_{t+1} \mid X_0 = i_0, X_1 = i_1, \ldots, X_t = i_t\right) = P\left(X_{t+1} = i_{t+1} \mid X_t = i_t\right), \tag{1}$$

where, i_t is the process state at time t, and P is the conditional probability of a future event. There are two assumptions about Markov chains. First, the future state of a stochastic process depends only on the present state and has nothing to do with the past. Second, the transition probability between two states should be constant. So the time step needs to be determined properly to keep simple state transition.

Bridge condition decays with time (year) and can be considered as discrete condition states at certain time intervals. Thus Markov chains could be the proper tool to model the bridge deterioration process. As the bridge condition is usually evaluated through several rating levels, the transition probabilities should be expressed as a matrix, called the transition probability matrix. A typical transition probability matrix P is shown in

$$P = \left[\begin{pmatrix} p_{11} & \cdots & p_{1n} \\ \vdots & \ddots & \vdots \\ p_{n1} & \cdots & p_{nn} \end{pmatrix}\right], \quad p_{ij} \geq 0 \quad i, j \in I, \quad \sum_{j \in I} p_{ij} = 1 \quad i \in I, \tag{2}$$

where, n is the number of bridge condition states; matrix element p_{ij} represents the probability that the bridge condition will pass from state i to state j during a certain time step. Therefore, if the initial bridge condition is known, the future condition after t time intervals can be obtained by (3), where C is the condition vector [17]:

$$C(t) = C(0) \times P^t. \tag{3}$$

The transition probability matrix is the key of the Markov-chain model and is commonly obtained by statistical data of bridge conditions. Two methods can be used to calculate transition probability matrix, the regression method based on nonlinear optimization [15, 18] and the percentage method [19]. The regression method is affected significantly by the prior maintenance actions, whose records may not be readily

available, while the percentage method requires at least two consecutive condition records without any maintenance interventions [10], and it will generally increase the difficulty of data processing. However, the requirement of the percentage method is comparatively easy to achieve, so it will be used in this paper.

3. Condition Data on Urban Bridges

3.1. Data Profiles. An urban bridge management system (BMS) has been put into use in Shanghai since 2002 and become steady since 2004, which means the process of bridge data collection has been standardized and thus the data reliability is improved. Bridge detection is conducted once a year. Therefore there are ten years of bridge condition records available in the BMS up to now. The number of detected bridges increases year by year in most cases with the expansion of detection range. However, quantity decrease may happen occasionally due to bridge demolition, repair, and management change.

Urban bridges are divided into five categories in China according to their significance in the road system [1] as shown in Table 1. Shanghai BMS includes bridges from category II to V and the bridges of type I are usually under the management of specialized agencies. Thus bridges in Shanghai BMS are almost small and medium bridges, and the concrete girder bridges take the majority of the entire database. Data profiles of bridge records in Shanghai BMS from 2004 to 2013 can be found in Table 2. For bridge deterioration prediction on network level, all types of bridges should be taken into account, so bridge categories will not be considered when calculating the transition probability matrix. But it should be noted that the deterioration tendency predicted in this paper may actually be more meaningful for concrete girder bridges because of the large proportion of such bridge type in BMS records.

3.2. Data Preparation. The bridge condition in Shanghai BMS can be evaluated into five grades as shown in Table 3. On the circumstance of routine maintenance and minor repair, the condition rating (CR) of a bridge should maintain the original grade or decay to the next grade between two consecutive years. In other words CR grade cannot decay beyond one grade on such circumstance. However, in the cases of medium or major repair and reconstruction, the bridge condition may be improved and thus the CR grade can be raised to any level according to the repair efforts. Besides, there might be some detection errors in the BMS which lead to unreasonable CR grades. All these situations coexist in the BMS database which make the deterioration prediction complicated and inaccurate. Therefore the bridge condition data needs to be preprocessed to calculate the transition probability matrix.

Two kinds of deterioration process can be modeled using Shanghai BMS database, natural decay under routine maintenance or minor repair and conventional recoverable decay with medium or major repair as well as reconstruction. So the data processing methods should be different for each circumstance as follows.

(i) Natural decay: CR grades A to D cannot decay beyond one grade between two consecutive years, while grade E should not change because the bridge condition cannot be even worse. Data records which do not meet the conditions above should be excluded from the BMS database.

(ii) Conventional recoverable decay: CR grades A to C cannot decay beyond one grade between two consecutive years, because only routine maintenance and minor repair will be applied on such bridges. However, CR grades D and E have the chances of being improved because of the repair. So only data records with grades A to C need to be processed.

The bridge structure consists of three parts, bridge deck system, superstructure, and substructure. Each part can be evaluated separately and the CR grade for the whole bridge can be obtained by summing the weighted grades of all three parts [1]. Thus a single bridge actually has four data records and all these records should be preprocessed according to the principles above. The result of data preparation is shown in Table 4. Quantity of the valid data records for bridge deck system is the smallest, which is probably because the deck system detection based on visual observation is with the greatest variability. On the contrary, the detection for substructure is comparatively the steadiest, which means the decay of the substructure is slow or the components are hard to detect.

4. Calculation of Markov Transition Probability Matrices

4.1. Model Assumption and Matrices Simplification. The CR in Shanghai BMS has five grades which can generate the state vector space of Markov-chain model. For ease of calculation, the state vector should be transformed from [A, B, C, D, E] to [5, 4, 3, 2, 1], and elements of the state vector are called status value. As urban bridges in Shanghai are detected once a year, a one-year transition probability could be determined to help simplify the transition probability matrix. Therefore, the probabilities for two (or more) state jumps in two years should be negligible. Besides, the rows of the transition matrix must sum up to one.

It follows that only five transition probabilities are needed to fully define a particular transition matrix in the circumstance of natural decay. The case of the conventional recoverable decay is a little more complicated, but for grades A to C (also 5 to 3) only three transition probabilities are needed. The simplified transition probability matrices are shown in (4), where P_{nat} is the transition probability matrix

Table 2: Data profiles of bridge records in Shanghai BMS (2004–2013).

Year	Bridge quantity						
	Concrete girder	Arch	Steel	Truss	Combined system	Others	Total
2004	894	129	23	19	26	0	1091
2005	1139	140	9	14	13	42	1357
2006	1241	138	8	10	11	39	1447
2007	1274	142	8	10	11	41	1486
2008	1404	152	4	9	10	29	1608
2009	1381	145	10	9	9	36	1590
2010	1476	142	9	11	9	39	1686
2011	1521	136	8	11	9	44	1729
2012	1571	121	7	9	0	48	1756
2013	1639	86	10	9	0	57	1801

Table 3: Definition of bridge condition ratings.

Grade	Definition	Maintenance recommendations
A	Intact	Routine maintenance
B	Good	Routine maintenance and minor repair
C	Up to standard	Minor repair
D	Bad	Medium or major repair
E	Dangerous	Major repair or reconstruction

under natural decay and P_{rec} is under the conventional recoverable decay:

$$P_{\text{nat}} = \begin{bmatrix} p_{55} & 1-p_{55} & & & & \\ & p_{44} & 1-p_{44} & & & \\ & & p_{33} & 1-p_{33} & & \\ & & & p_{22} & 1-p_{22} & \\ & & & & 1 \end{bmatrix},$$
$$P_{\text{rec}} = \begin{bmatrix} p_{55} & 1-p_{55} & & & \\ & p_{44} & 1-p_{44} & & \\ & & p_{33} & 1-p_{33} & \\ p_{25} & p_{24} & p_{23} & p_{22} & p_{21} \\ p_{15} & p_{14} & p_{13} & p_{12} & p_{11} \end{bmatrix}. \quad (4)$$

4.2. Transition Probability Matrices Calculation. Valid CR grades of urban bridge records in Shanghai BMS during 2004 to 2013 are used to calculate the transition probability matrix, which have been preprocessed in Section 3.2.

In the circumstance of natural decay, only five transition probabilities are needed for each part of the bridge as well as the whole bridge. The calculation results can be found in Tables 5, 6, 7, and 8. Every two consecutive years have a group of transition probabilities. However, the final transition probability matrix under natural decay should be only one for each part of the bridge as well as the whole bridge. Therefore the calculation results need to be further processed.

As shown by Table 5 to Table 8, the distribution of transition probabilities for each grade is not uniform. Thus the average value and standard deviation can be used to analyze these data. The transition probabilities that exceed the valid range should be excluded, and the final transition probabilities are the average value of the valid values, as shown in

$$R_i = \overline{p}_{ii} \pm s_i \quad p_{ii} = \overline{p_{ii}^{\text{valid}}} \quad p_{ii}^{\text{valid}} \in R_i \quad i \in [5, 4, 3, 2], \quad (5)$$

where, R_i is the valid range of transition probabilities for each grade i; $\overline{p}_{ii}$ and s_i are the average value and standard deviation of transition probabilities through all years for each grade i; p_{ii} is the final transition probabilities for each grade i; p_{ii}^{valid} is the valid probabilities for each grade i. The data processing results can be found in Table 9.

The case for the conventional recoverable decay is a little more complicated because the probabilities of CR grades D and E for two (or more) state jumps in two years should be taken into consideration. The actual data in Shanghai BMS are used so the transition probabilities of grades D and E are based on the real situation of urban bridges in Shanghai. The transition probabilities for grades A to C are the same as the probabilities under natural decay. The results of grades D and E are shown in Table 10, where the final probabilities are the average value of the transition probabilities through all years because the assumption that the rows of the transition matrix must sum up to one needs to be satisfied.

5. Deterioration Prediction Using Markov Chains

5.1. Condition Rating Prediction on Network Level. With the Markov transition probability matrices and present status of urban bridges, the future status of bridge conditions at any year can be predicted. The transition matrix under natural decay represents the developing tendency that only routine maintenance and minor repair are conducted, while the transition matrix under conventional recoverable decay means all the maintenance and repair treatments are taken into account, which is also the actual situation of urban bridge management situation in Shanghai. But in the light of the technical regulation for urban bridge management [1], all the bridges with CR grade E should be repaired and bridges with CR grade D should be partly repaired according

Table 4: Number of valid data records.

Decay process	Bridge components	Time interval								
		2004 2005	2005 2006	2006 2007	2007 2008	2008 2009	2009 2010	2010 2011	2011 2012	2012 2013
Decay 1	Deck system	627	859	879	1058	1227	1161	1153	1276	1366
	Superstructure	785	1094	1149	1227	1359	1386	1393	1410	1361
	Substructure	866	1133	1185	1309	1391	1480	1449	1499	1565
Decay 2	Deck system	700	1036	973	1140	1252	1199	1224	1311	1461
	Superstructure	834	1132	1186	1275	1375	1397	1414	1442	1396
	Substructure	877	1144	1191	1313	1392	1481	1456	1502	1567

Decay 1: natural decay; Decay 2: conventional recoverable decay.

Table 5: Transition probabilities for bridge deck system under natural decay.

Year	p_{55}	p_{44}	p_{33}	p_{22}
2004-2005	0.782	0.563	0.614	0.755
2005-2006	0.886	0.699	0.799	0.905
2006-2007	0.884	0.687	0.710	0.805
2007-2008	0.861	0.662	0.857	0.828
2008-2009	0.843	0.593	0.712	0.963
2009-2010	0.820	0.667	0.847	0.902
2010-2011	0.902	0.676	0.861	0.920
2011-2012	0.901	0.660	0.808	0.919
2012-2013	0.763	0.640	0.765	0.667

Table 6: Transition probabilities for superstructure under natural decay.

Year	p_{55}	p_{44}	p_{33}	p_{22}
2004-2005	0.949	0.828	0.727	0.857
2005-2006	0.964	0.872	0.818	0.813
2006-2007	0.921	0.730	0.750	0.818
2007-2008	0.938	0.896	1.000	0.846
2008-2009	0.952	0.842	0.786	1.000
2009-2010	0.961	0.712	0.789	0.909
2010-2011	0.927	0.698	0.500	0.647
2011-2012	0.955	0.778	0.952	0.833
2012-2013	0.854	0.702	0.849	0.692

Table 7: Transition probabilities for substructure under natural decay.

Year	p_{55}	p_{44}	p_{33}	p_{22}
2004-2005	0.931	0.803	0.692	1.000
2005-2006	0.957	0.899	1.000	1.000
2006-2007	0.936	0.841	1.000	1.000
2007-2008	0.932	0.922	1.000	1.000
2008-2009	0.966	0.890	1.000	1.000
2009-2010	0.947	0.936	0.875	1.000
2010-2011	0.951	0.895	0.750	0.000
2011-2012	0.949	0.909	1.000	0.500
2012-2013	0.881	0.904	0.786	1.000

Table 8: Transition probabilities for whole bridge under natural decay.

Year	p_{55}	p_{44}	p_{33}	p_{22}
2004-2005	0.887	0.855	0.944	0.905
2005-2006	0.947	0.876	0.903	0.929
2006-2007	0.921	0.859	0.815	0.958
2007-2008	0.918	0.921	0.889	1.000
2008-2009	0.949	0.954	1.000	1.000
2009-2010	0.929	0.883	0.909	0.909
2010-2011	0.909	0.836	0.750	1.000
2011-2012	0.912	0.917	0.911	0.867
2012-2013	0.796	0.835	0.951	0.889

to their damage degree. However, these requirements are hardly fully realized in actual practice due to the budget and manpower limits. In this study an ideal status called "enhanced recoverable repair" assumes that all "E bridges" (bridges with CR grade E) and most of the "D bridges" are repaired. Furthermore most of the repaired bridges can recover to the top level. This assumption is mainly based on the technical regulation for urban bridge management [1] and the current management status of urban bridges in Shanghai. According to the regulation [1], all "E bridges" and parts of "D bridges" need to be repaired, but neither the maintenance level nor the maintenance proportion are clearly defined. Besides, based on the current technical capacity, financial resources, and management mechanism of the urban bridge management in Shanghai, only parts of the "D and E bridges" can be effectively repaired, and the maintenance level is also uncertain. Therefore, the ideal maintenance status should fully comply with the requirement of the regulation and be provided with enough budget and technical support. As a result of such assumption, all "E bridges" and at least half of the "D bridges" should be repaired to the top CR level. The probabilities for "D bridges" of maintaining the original state and being degraded refer to the current practical status of "D bridges." The transition probabilities under such status are shown in Table 10, and all bridges components as well as the whole bridge are assumed to have the same transition probabilities for "D and E bridges."

Table 9: Final transition probabilities under natural decay.

Category	Element	Average value	Standard deviation	Final probability
Bride deck system	p_{55}	0.849	0.048	0.859
	p_{44}	0.650	0.042	0.665
	p_{33}	0.775	0.079	0.773
	p_{22}	0.851	0.090	0.880
Superstructure	p_{55}	0.936	0.032	0.946
	p_{44}	0.784	0.073	0.778
	p_{33}	0.797	0.135	0.787
	p_{22}	0.824	0.099	0.846
Substructure	p_{55}	0.939	0.023	0.943
	p_{44}	0.889	0.039	0.903
	p_{33}	0.900	0.120	0.952
	p_{22}	0.833	0.333	0.938
Whole bridge	p_{55}	0.907	0.043	0.921
	p_{44}	0.882	0.039	0.878
	p_{33}	0.897	0.070	0.918
	p_{22}	0.940	0.049	0.925

Table 10: Final transition probabilities under conventional recoverable decay.

Element	Bridge deck system	Superstructure	Substructure	Whole bridge	Enhanced recoverable decay
p_{25}	0.216	0.178	0.155	0.303	0.500
p_{24}	0.122	0.090	0.104	0.074	0
p_{23}	0.253	0.273	0.275	0.102	0
p_{22}	0.355	0.374	0.415	0.488	0.400
p_{21}	0.055	0.085	0.051	0.034	0.100
p_{15}	0.131	0.280	0.278	0.474	1
p_{14}	0.087	0.066	0.037	0.032	0
p_{13}	0.145	0.124	0.167	0.032	0
p_{12}	0.268	0.164	0.148	0.111	0
p_{11}	0.370	0.365	0.370	0.351	0

Taking the bridge condition in 2013 as the present status $C(0)$, the status vector is as shown in (6). The bridge condition during next five years $C(t)$ can be predicted through (7), where P_{cir} is the Markov transition probability matrix under certain circumstance:

$$C(0) = [0.565, 0.235, 0.154, 0.036, 0.010], \quad (6)$$

$$C(t) = C(0) \times (P_{\text{cir}})^t, \quad t = 1, 2, 3, 4, 5. \quad (7)$$

The prediction results under three circumstances are displayed by Figures 2, 3, 4, and 5. The results show that the bridge condition will deteriorate rapidly under natural decay circumstance. The condition of the bridge deck system has the fastest decline while the decay rate of the substructure is lowest. It is mainly because the substructure is with the lowest probability of being damaged in urban environment. However, other factors may also lead to this situation such as bridge detection. The substructure is relatively harder to detect because most parts are underwater. At the end of the next five years (2018) the percentage of "A bridges" of deck system will be less than 30%, while the percentage of "E bridges" will be up to 7.8%, which means the number of bridges in danger status will exceed 140. The minor and major repair can mitigate the bridge condition deterioration significantly as shown in the prediction results under conventional recover decay circumstance. It also represents the actual situation of bridge management in Shanghai. Still taking the deck system for example, the percentage of "A bridges" in this situation will be close to 50% in 2018, and the "E bridges" will drop to 0.9%. Of course, the results under enhanced recoverable decay are even better. The percentage of "A bridges" will be up to 58%, while the "E bridges" will be reduced to 0.6%, which is even better than the present situation (2013). Although the conditions of bridge deck system and superstructure can be improved under the circumstance of enhanced recoverable decay, as shown in Figures 2(c) and 3(c), it has limited effect on the conditions of substructure and the whole bridge as shown in Figures 4(c) and 5(c) compared to the circumstance of conventional recoverable decay.

5.2. Single Bridge Prediction versus Age. Markov-chain model can also be used to predict the condition deterioration versus

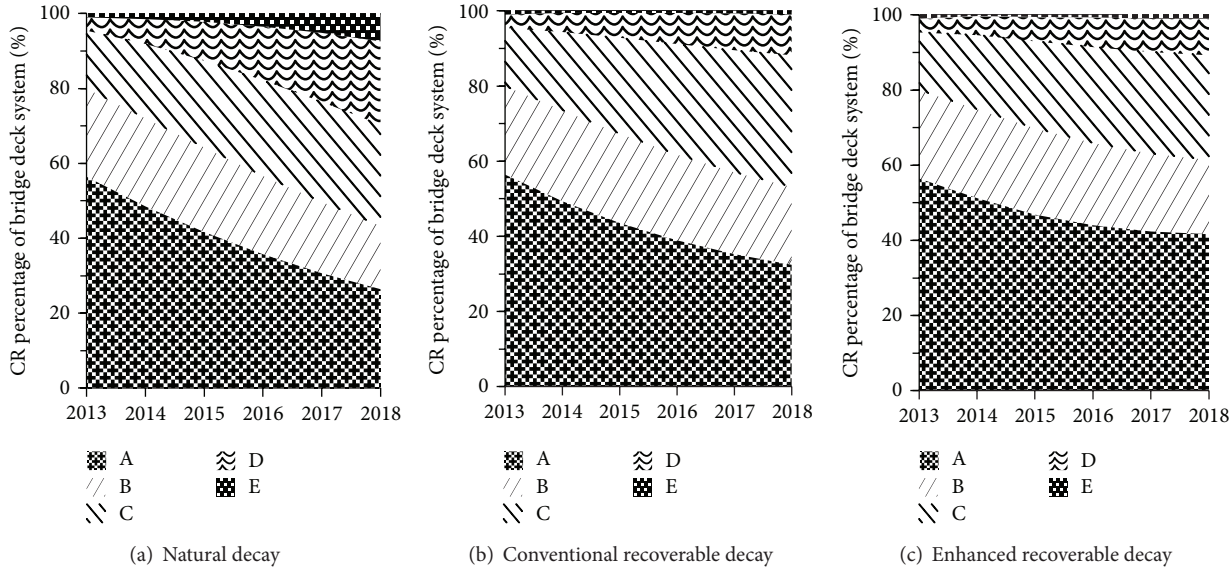

(a) Natural decay (b) Conventional recoverable decay (c) Enhanced recoverable decay

Figure 2: Bridge deck system prediction on network level in next five years.

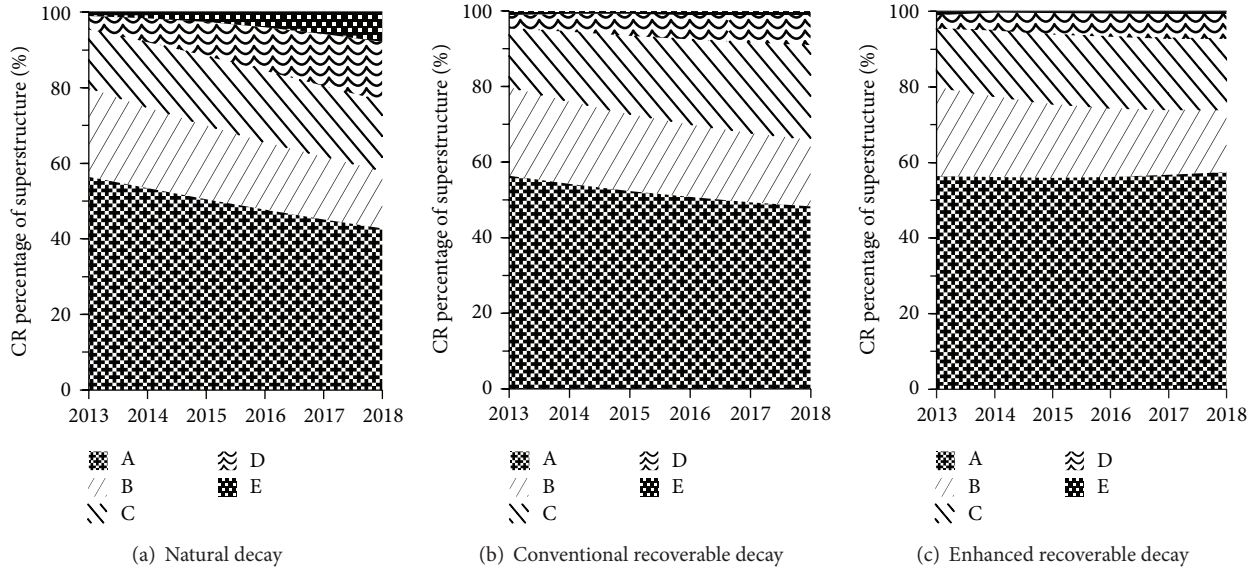

(a) Natural decay (b) Conventional recoverable decay (c) Enhanced recoverable decay

Figure 3: Superstructure prediction on network level in next five years.

age of a single bridge under different circumstances. The expected condition can be found in (8), where $C(t)^*$ is the condition rating (status value) of single bridge after t years; $C(0)^*$ is the status vector of the initial condition of single bridge; P_{cir} is the transition probability matrix under certain circumstance; and CR is the bridge condition rating vector, which is constant vector. In this study, CR = [5; 4; 3; 2; 1]. Consider

$$C(t)^* = C(0)^* \times (P_{\text{cir}})^t \times \text{CR}. \tag{8}$$

It is assumed that a bridge deteriorates from the intact state and the forecast period is 20 years. Then the initial status vector $C(0)^*$ should be [1, 0, 0, 0, 0]. The bridge condition deterioration tendency for different components as well as the whole bridge can be found in Figure 6, where the ordinate scales 5 to 1 are equal to CR grades A to E. It is shown that the condition of bridge deck system declines fastest and the CR grade will be below D after 20 years if no recoverable treatments are conducted. Medium and major repair can slow down the deterioration tendency of all bridge components as well as the whole bridge, but it has the greatest effect on the bridge deck system. Enhanced repair has some good influence on the deterioration process, especially in the case of deck system and superstructure, but for the substructure

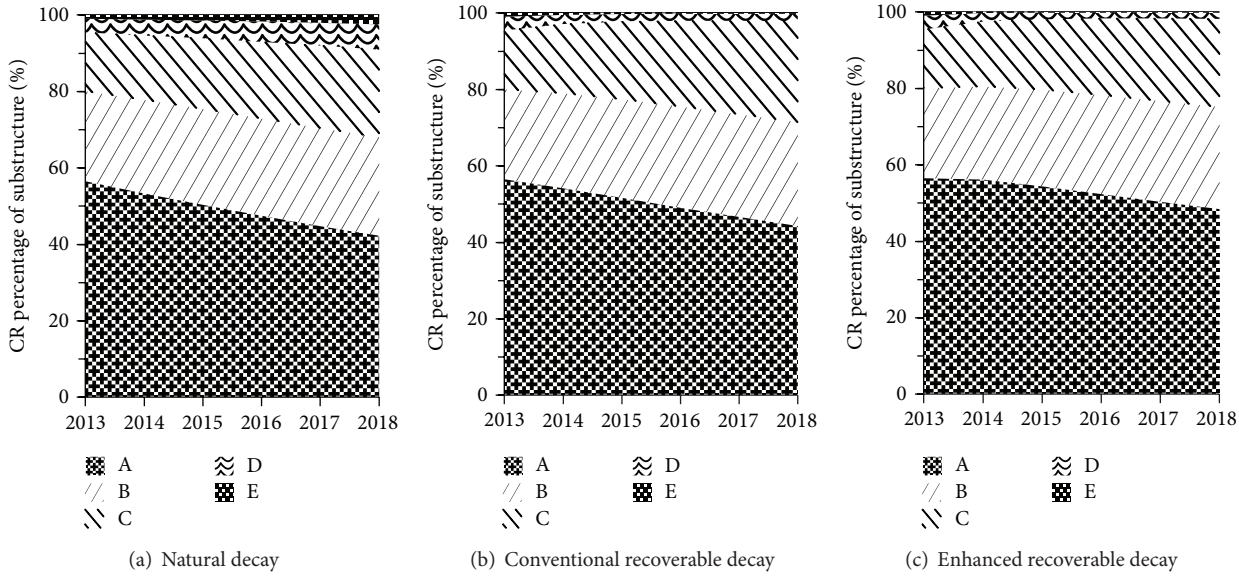

(a) Natural decay (b) Conventional recoverable decay (c) Enhanced recoverable decay

Figure 4: Substructure prediction on network level in next five years.

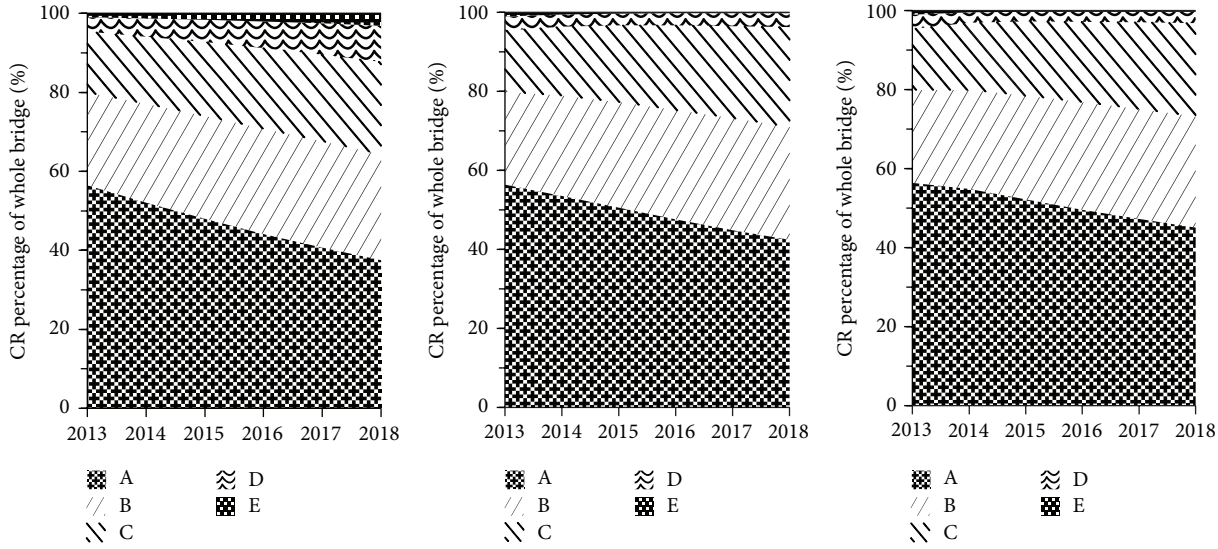

(a) Natural decay (b) Conventional recoverable decay (c) Enhanced recoverable decay

Figure 5: Whole bridge prediction on network level in next five years.

and the whole bridge, effect of the enhanced repair is quite little, which means that the present management strategy for urban bridges in Shanghai is reasonable.

6. Conclusion

The urban bridge BMS in Shanghai has successfully operated for more than ten years. Thousands of bridge condition data records can be used to predict the deterioration tendency of urban bridges to provide advice for bridge management. However, the basic condition of the data records is complicated because all kinds of bridge status coexist in the same database including bridges without any repair and bridges with different degrees of repair efforts such as routine maintenance, minor, medium and major repair, and even reconstruction. It follows that a prediction model capable of considering a variety of factors should be used to forecast the bridge deterioration process. Therefore a Markov-chain model was proposed in this study. A group of bridge condition data about ten years were used to verify the model and also to find the deterioration tendency of urban bridges in Shanghai.

The CR grades of bridges were used to generate the state vector space and the time step was set to one year because the bridge detection was conducted once a year, which also helped to simplify the form of Markov transition probability

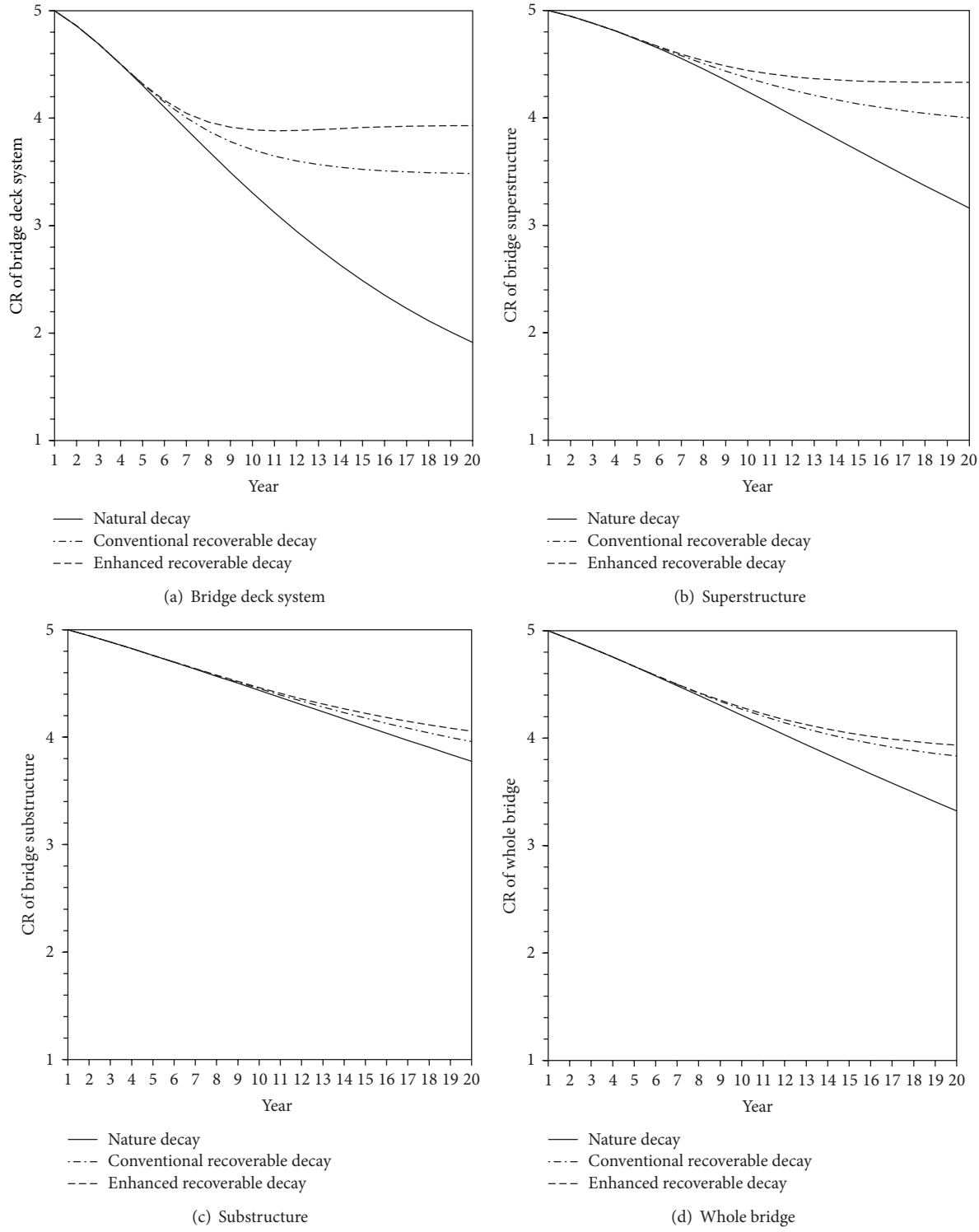

Figure 6: CR deterioration of single bridge.

matrix. The Markov-chain mode can model not only the distribution of the percentage of different CR grades in a transportation network in any year but also the deterioration tendency of a single bridge from any state.

Three decay circumstances were considered in this study, natural decay, conventional recoverable decay, and enhanced recoverable decay. The conventional recoverable decay represents the actual situation of urban bridge management in Shanghai at present, under which only "D and E bridges" need to be repaired to recover to better conditions, while other bridges are under routine maintenance and minor repair so the CR grade cannot be raised. The natural decay is the status

without any effective maintenance and repair, and CR grades of all bridges in this status cannot be improved. The circumstance of enhanced recoverable decay is an ideal status which fully complies with the Chinese technical regulations of urban bridge management [1], which requires that all "E bridges" and most of "D bridges" should be repaired. Three types of bridge components as well as the whole bridge were predicted by Markov-chain model under the three circumstances mentioned above. The results showed that the bridge conditions would drop rapidly if there were no recoverable repair treatments conducted, especially for the bridge deck system and the superstructure. Proper repair could slow down the deterioration speed of all kinds of bridge components. The effect was most obvious on the bridge deck system and the superstructure came second. The enhanced repair could significantly mitigate the deterioration process and even raise the CR grades after several years of maintenance and repair in the case of the bridge deck system and the superstructure. However other components as well as the whole bridge were not so sensitive to enhanced repair. It seemed the conventional repair was proper enough for the bridges in Shanghai at present and the management strategy applied now was quite reasonable.

Conflict of Interests

The authors declare that there is no conflict of interests regarding the publication of this paper.

Acknowledgment

This work was supported by the Postdoctoral Foundation of Jiangxi province in China (2012RC17 and 2013KY32).

References

[1] "Technical code of maintenance for city bridges," China, CJJ 99-2003.

[2] Z. Chen, *Research on technology structure of transportation infrastructure management system [Ph.D. thesis]*, Tongji University, Shanghai, China, 2005.

[3] D. Veshosky, C. R. Beildleman, and G. W. Buetow, "Comparative analysis of bridge superstructure deterioration," *Journal of Structural Engineering*, vol. 120, no. 7, pp. 2123–2136, 1994.

[4] B. Yanev and X. Chen, "Life-cycle performance of New York City bridges," Transportation Research Record 1389, 1993.

[5] S. Ranjith, S. Setunge, R. Gravina, and S. Venkatesan, "Deterioration prediction of timber bridge elements using the Markov chain," *Journal of Performance of Constructed Facilities*, vol. 27, no. 3, pp. 319–325, 2013.

[6] D. S. Wang, M. Zhu, and J. R. Zhong, "Aided seismic damage prediction system for bridges using statistical analysis methods," *World Earthquake Engineering*, vol. 19, no. 3, pp. 117–122, 2003.

[7] S. Madanat, R. Mishalani, and W. H. W. Ibrahim, "Estimation of infrastructure transition probabilities from condition rating data," *Journal of Infrastructure Systems*, vol. 1, no. 2, pp. 120–125, 1995.

[8] J. L. Bogdanoff, "A new cumulative damage model—part I," *Journal of Applied Mechanics*, vol. 45, no. 2, pp. 246–250, 1978.

[9] T. Micevski, G. Kuczera, and P. Coombes, "Markov model for storm water pipe deterioration," *Journal of Infrastructure Systems*, vol. 8, no. 2, pp. 49–56, 2002.

[10] G. Morcous, "Performance prediction of bridge deck systems using markov chains," *Journal of Performance of Constructed Facilities*, vol. 20, no. 2, pp. 146–155, 2006.

[11] Z. Lounis, "Reliability-based life prediction of aging concrete bridge decks," in *Proceedings of the International RILEM Workshop on Life Prediction and Aging Management of Concrete Structures*, pp. 229–238, Cannes, France, 2000.

[12] G. Morcous and H. Rivard, "Computer assistance in managing the maintenance of low-slope roofs," *Journal of Computing in Civil Engineering*, vol. 17, no. 4, pp. 230–242, 2003.

[13] K. Golabi and R. Shepard, "Pontis: a system for maintenance optimization and improvement of US bridge networks," *Interfaces*, vol. 27, no. 1, pp. 71–88, 1997.

[14] H. Hawk and E. P. Small, "The BRIDGIT bridge management system," *Structural Engineering International*, vol. 8, no. 4, pp. 309–314, 1998.

[15] M. Cesare, C. Santamarina, C. Turkstra, and E. Vanmarcke, "Modeling bridge deterioration with Markov chains," *Journal of Transportation Engineering*, vol. 118, no. 6, pp. 820–833, 1992.

[16] E. Parzen, *Stochastic Processes*, Holden-Day Series in Probability and Statistics, Holden-Day, San Francisco, Calif, USA, 1962.

[17] L. Collins, *An Introduction to Markov Chain Analysis*, Concepts and Techniques in Modern Geography, Geo Abstracts, 1975.

[18] A. A. Butt, M. Y. Shahin, K. J. Feighan, and S. H. Carpenter, "Pavement performance prediction model using the Markov process," *Transportation Research Record*, pp. 12–19, 1987.

[19] J. Yi, M. Saito, and K. C. Sinha, "Bridge performance prediction model using the Markov chain," *Transportation Research Record*, no. 1180, pp. 25–32, 1988.

Hindawi Publishing Corporation
Mathematical Problems in Engineering
Volume 2014, Article ID 206024, 6 pages
http://dx.doi.org/10.1155/2014/206024

Research Article

The Best Path Analysis in Military Highway Transport Based on DEA and Multiobjective Fuzzy Decision-Making

Wu Juan,[1,2] Lu Huapu,[1] Sun Xu,[1] Liu Xianfeng,[2] and Yang Huijun[2]

[1] *Institute of Transportation Engineering, Tsinghua University, Beijing 100084, China*
[2] *Academy of Military Transportation, Tianjin 300161, China*

Correspondence should be addressed to Wu Juan; wujuan_qh@yahoo.cn

Received 1 November 2013; Revised 6 January 2014; Accepted 8 January 2014; Published 20 February 2014

Academic Editor: Gang Chen

Military transport path selection directly affects the transport speed, efficiency, and safety. To a certain degree, the results of the path selection determine success or failure of the war situation. The purpose of this paper is to propose a model based on DEA (data envelopment analysis) and multiobjective fuzzy decision-making for path selection. The path decision set is established according to a search algorithm based on overlapping section punishment. Considering the influence of various fuzzy factors, the model of optimal path is constructed based on DEA and multitarget fuzzy decision-making theory, where travel time, transport risk, quick response capability, and transport cost constitute the evaluation target set. A reasonable path set can be calculated and sorted according to the comprehensive scores of the paths. The numerical results show that the model and the related algorithms are effective for path selection of military transport.

1. Introduction

During the hi-tech local war, the mission of the military supplies support is very heavy, so the status of the military transport has become increasingly prominent [1]. Due to the characteristics of high flexibility and adaptability, military highway transport is still a significant mode of military transport [2]. Transport by car is an important means of conducting operational and tactical maneuver and supplies support [3, 4].

With the increasing uncertainty in occurrence and the quick decision of modern war, military transport needs more reliability and higher speed, so path optimization has become an important part of the military transport system. A good path selection plays an important role in completing the whole transport task on time, improving the efficiency of the transport, and enhancing logistic support capability.

There are many successful applications about routing optimization and selection in literatures [5–14]. However, in response to the antagonism and instability characteristics of modern war, to guarantee the stability and efficiency of the logistics, the wartime military highway transportation path selection should meet the following principles.

(1) Path must be feasible and better controlled traffic roads are required to be chosen in the first place to ensure that troops and supplies can reach the destination on time and safely.

(2) Try to select the path with short travel time, high safety, high economic benefit, and the least number of transfers as much as possible.

(3) The emergency transport plans are required to deal with various potential damage states to ensure that alternate routes may be selected flexibly after the enemy fire.

In view of the peculiarity of military highway transport in war, various factors should be comprehensively considered in path selection, such as the mileage of the path, speed, travel time, reliability, security, fuel consumption, transport loss, and supporting capability [1–4]. Some of these factors are fuzzy, uncertain, and difficult to quantify. Nowadays, most of the algorithms of path selection in military highway transport are based on the optimization of urban traffic, without considering the specific requirements of the military maneuvers and the fuzziness of these factors [15]. In this

paper, to solve the path selection problem under the influence of various fuzzy factors in military transport, a model based on DEA and multiobjective fuzzy decision-making method is proposed.

2. Path Decision Set Establishment

For military transport path selection, sections that do not conform to the requirements of the transport task should be removed from the existing road network. After that, considering the particularity of military transportation, we also want to choose paths with high dissimilarity so as to equally distribute the risk as much as possible [16, 17].

To meet needs of warfare, transport task needs to be accomplished within the prescribed period of time. So in this paper, dissimilar paths [18–20] that are in accord with the time constraints are chosen as path optimization decision set.

Given a graph $G = (N, A, T)$, where $N = \{1, 2, ..., n\}$, A is the set of directed links (arcs) and T is the set of time cost of each arc. Each arc(i, j) in the graph has a time cost t_{ij}.

The problem of searching the dissimilar path set R_0 from the source node to the sink node could be stated as follows:

$$R_0 = \{R \mid T(R) \le T_{\max}\} \quad \text{s.t.} \tag{1}$$

$$T(R) = \sum_{(i,j)\in A} t_{ij} x_{ij} \tag{2}$$

$$x_{ij} = \begin{cases} 1 & \text{if } (i, j) \text{ is in path } R; \\ 0 & \text{otherwise,} \end{cases}$$

where $T_{\max}$ is the acceptable longest time to complete transport task; $T(R)$ is travel time of path R from the source node to the sink node.

Using the dissimilar path algorithm based on overlapping punishment, the dissimilar path set R_0 consisting of M paths that is in accord with the time constraints is obtained. The search algorithm consists of the following steps.

Step 1 (initialization). Consider

$$m = 0, \qquad i = 1, \qquad R_0 = \emptyset. \tag{3}$$

Step 2. Using the Dijkstra algorithm [21] to search the shortest path R_i from starting point to end point based on time cost weight, travel time on path R_i is T_i.

Step 3. If $T_i \le T_{\max}$ and $m < M$, go to the next step. Otherwise calculation stops.

Step 4. If $R_i \notin R_0$, update $m = m + 1$ and $R_0 = R_0 \cup \{R_i\}$; go to the next step.

Step 5. Update $i = i + 1$. Update travel time on each section as follows:

$$t_e^i = \left(1 + \frac{\alpha}{T_{\min}}\right)^n t_e^0, \tag{4}$$

where t_e^0 is the initial time weight of section e, t_e^i is the time weight of section e at i loop, α is overlapping penalty coefficient, and n is the used times of section e. Return to Step 2.

Using this algorithm, path decision set is obtained and arranged in order to increase travel time on each path:

$$R_0 = \{R_1, R_2, \ldots, R_M\}. \tag{5}$$

3. Military Path Analysis Based on DEA and Multiobjective Fuzzy Decision-Making

In the path selection of military transport, considering the influence of various fuzzy factors, multiobjective fuzzy decision-making method is an effective way [22–25].

3.1. Objective Factors of Path Selection. In wartime path selection, the decision-maker often considers simultaneously multiple conflicting objectives [26]. In this paper, travel time, transport risks, rapid response capability, and transport costs are selected as the objective factors.

(1) Travel Time. In the process of troops maneuvering, especially long-range maneuvering, most of the time was spent in transport. In order to shorten the whole troops maneuvering time, the travel time is an important factor to measure the vehicle turn-round efficiency.

(2) Transport Risk. During the war, supply lines and transportation facilities are often the prime targets of enemy fire. To ensure personnel and supplies reach their destination safely, transport risk will be an important factor to consider in path selection.

(3) Rapid Response Capability. In order to ensure the reliability and stability of military transport system after enemy attack, rapid response capability is required in wartime transport. There are various methods to enhance rapid response capabilities before the war, such as perfecting defense system of the critical traffic facilities in advance and putting forward the emergency transport plans to deal with various potential damage states. With these methods, alternate routes may be selected flexibly after the enemy fire.

(4) Transport Cost. When meeting the requirements of military demands, much more economic benefits could be pursued in path optimization. In the military transport, transport cost includes two aspects: one is traditional fuel cost, vehicle depreciation cost, and so forth; the other is the integrated support costs such as oil support and alert support.

3.2. Membership Functions for Objective Factors

3.2.1. Membership Functions for Travel Time. The purpose of transport time evaluation is only to compare the relative length of travel time on different routes. Therefore,

the difference between travel time on each route and the shortest travel time is used as the evaluation criteria. Consider

$$\Delta T = T - T_{\min}, \tag{6}$$

where $T_{\min}$ is the shortest travel time on routes in R_0 and ΔT is travel time difference with the shortest travel time of each route. The smaller the value of ΔT is, the better this route is.

$$\begin{aligned} &\text{Define travel time remark set: } V_t \\ &= \{\text{excellent, good, medium, poor}\}. \end{aligned} \tag{7}$$

According to the experience of military transport, in general, for ΔT, a value within the range $\{0 \sim 0.15T_{\min}\}$ can be considered excellent; a larger value within the range $\{0.15T_{\min} \sim 0.35T_{\min}\}$ is good and one within $\{0.35T_{\min} \sim 0.65T_{\min}\}$ is medium; a value over 0.65 is always considered poor.

The common forms of membership functions include triangle, trapezoid, Gaussian, and clock form. Here, triangular fuzzy function is used to determine the membership degree of travel time. Then, membership functions of travel time difference ΔT on route k are defined as follows [27]:

$$U_{1k}^{t}(\Delta t) = \begin{cases} 1 - \dfrac{10\Delta T}{(3T_{\min})} & 0 \le \dfrac{\Delta T}{T_{\min}} < 0.15 \\ 0 & \dfrac{\Delta T}{T_{\min}} \ge 0.15, \end{cases} \tag{8}$$

$$U_{2k}^{t}(\Delta t) = \begin{cases} \dfrac{10\Delta T}{(3T_{\min})} & 0 \le \dfrac{\Delta T}{T_{\min}} < 0.15 \\ 1.75 - \dfrac{5\Delta T}{T_{\min}} & 0.15 \le \dfrac{\Delta T}{T_{\min}} < 0.35 \\ 0 & \dfrac{\Delta T}{T_{\min}} \ge 0.35, \end{cases} \tag{9}$$

$$U_{3k}^{t}(\Delta t) = \begin{cases} 0 & 0 \le \dfrac{\Delta T}{T_{\min}} < 0.15 \\ -0.75 + \dfrac{5\Delta T}{T_{\min}} & 0.15 \le \dfrac{\Delta T}{T_{\min}} < 0.35 \\ 2.25 - \dfrac{10\Delta T}{(3T_{\min})} & 0.35 \le \dfrac{\Delta T}{T_{\min}} < 0.65 \\ 0 & \dfrac{\Delta T}{T_{\min}} \ge 0.65, \end{cases} \tag{10}$$

$$U_{4k}^{t}(\Delta t) = \begin{cases} 0 & 0 \le \dfrac{\Delta T}{T_{\min}} < 0.35 \\ -1.25 + \dfrac{10\Delta T}{(3T_{\min})} & 0.35 \le \dfrac{\Delta T}{T_{\min}} < 0.65 \\ 1 & \dfrac{\Delta T}{T_{\min}} \ge 0.65. \end{cases} \tag{11}$$

So membership vector of travel time difference ΔT of route k is

$$U_k^t = \left(U_{1k}^{t}(\Delta t), U_{2k}^{t}(\Delta t), U_{3k}^{t}(\Delta t), U_{4k}^{t}(\Delta t)\right)^T. \tag{12}$$

3.2.2. Membership Functions for Transport Risk, Rapid Response Capability, and Transport Cost. The three factors are of great fuzziness and difficult to quantify, and their membership functions are difficult to be defined directly. In this paper, comprehensive weighted statistics method is used to establish these membership functions.

(1) Define Remark Set for the Three Factors. Consider

$$\begin{aligned} V_s &= \{\text{excellent, good, medium, poor}\}, \\ V_r &= \{\text{excellent, good, medium, poor}\}, \\ V_c &= \{\text{excellent, good, medium, poor}\}, \end{aligned} \tag{13}$$

where V_s, V_r, and V_c are the remark sets of transport risk, rapid response capability, and transport cost.

(2) Determine Evaluation Personnel and the Weight of Each Type of Personnel. Based on the experience, evaluation personnel were selected from combat commanders, combat service staff officers, and transport professionals.

The weight of each type of personnel for transport risks assessment is

$$R^s = \left(r_1^s, r_2^s, r_3^s\right)^T, \quad \text{where } \sum_{i=1}^{3} r_i^s = 1,\ r_i^s > 0. \tag{14}$$

The weight of each type of personnel for rapid response capability assessment is

$$R^r = \left(r_1^r, r_2^r, r_3^r\right)^T, \quad \text{where } \sum_{i=1}^{3} r_i^r = 1,\ r_i^r > 0. \tag{15}$$

The weight of each type of personnel for transport costs assessment is

$$R^c = \left(r_1^c, r_2^c, r_3^c\right)^T, \quad \text{where } \sum_{i=1}^{3} r_i^c = 1,\ r_i^c > 0. \tag{16}$$

(3) Membership Degree Calculation. Suppose type i personnel have n_i individuals, of whom m_{jik} individuals agree that route k belongs to remark. Then, the evaluation results are as follows:

$$A_{jik}^s = \frac{m_{jik}^s}{n_i}, \qquad A_{jik}^r = \frac{m_{jik}^r}{n_i}, \qquad A_{jik}^c = \frac{m_{jik}^c}{n_i}. \tag{17}$$

Then, membership degree of each objective factor is as follows:

$$\begin{aligned} U_{jk}^s &= \left(A_{j1k}^s, A_{j2k}^s, A_{j3k}^s\right) \times R^s, \\ U_{jk}^r &= \left(A_{j1k}^r, A_{j2k}^r, A_{j3k}^r\right) \times R^r, \\ U_{jk}^c &= \left(A_{j1k}^c, A_{j2k}^c, A_{j3k}^c\right) \times R^c, \end{aligned} \tag{18}$$

where $i = 1, 2, 3$; $j = 1, 2, 3, 4$; $k = 1, 2, 3, \ldots, M$.

Then, the evaluation vector of route k was obtained as follows:

$$\begin{aligned} U_k^s &= \left(U_{1k}^s, U_{2k}^s, U_{3k}^s, U_{4k}^s\right)^T, \\ U_k^r &= \left(U_{1k}^r, U_{2k}^r, U_{3k}^r, U_{4k}^r\right)^T, \\ U_k^c &= \left(U_{1k}^c, U_{2k}^c, U_{3k}^c, U_{4k}^c\right)^T. \end{aligned} \tag{19}$$

Then, the evaluation matrix of route set R_0 was obtained as follows:

$$U^s = \left(U_1^s, U_2^s, U_3^s, U_4^s\right)^T,$$
$$U^r = \left(U_1^r, U_2^r, U_3^r, U_4^r\right)^T, \quad (20)$$
$$U^c = \left(U_1^c, U_2^c, U_3^c, U_4^c\right)^T.$$

3.3. DEA Model for Evaluation. DEA method [28–30] is a sort of evaluating method used to evaluate the relative validity of decision-making unit with multiple inputs and outputs. In DEA method, C^2R model is the earliest one and most widely used now. So the following evaluation is mainly according to C^2R model.

(1) Using path from path decision set as decision-making unit and using membership degree as input and output indicators, for each path, the score value of each remark grade on each objective factor is calculated.

In this paper, $V = \{\text{excellent, good, medium, poor}\}$; the corresponding membership degree of "medium" and "poor" is used as input and the corresponding membership degree of "excellent" and "good" is used as output.

The weight vectors of input and output are given as the variable vectors as follows:

$$\vec{v} = \left(v_1, \ldots, v_m\right)^T, \qquad \vec{u} = \left(u_1, \ldots, u_s\right)^T. \quad (21)$$

For route k, the score value vector on each objective factor can be calculated as follows:

$$h_k = \frac{\vec{u}^T \overrightarrow{y}_k}{\vec{v}^T \overrightarrow{x}_k} = \frac{\sum_{i=1}^{s} u_i y_{ik}}{\sum_{j=1}^{m} v_j x_{jk}}, \quad k = 1, \ldots, M. \quad (22)$$

By choosing appropriate weight vector $\vec{\mu}$ and $\vec{v}$ to maximize the value of h_k, the optimal score of route k on this objective factor can be obtained. For example, for route k_0, C^2R model is proposed as follows:

$$\begin{aligned} \max \quad & h_{k0} = \frac{\sum_{i=1}^{s} u_i y_{ik0}}{\sum_{j=1}^{m} v_j x_{jk0}} \\ \text{s.t.} \quad & \frac{\sum_{i=1}^{s} u_i y_{ik}}{\sum_{j=1}^{m} v_j x_{jk}} \le 1 \quad k = 1, \ldots, M, \\ & u_i \ge 0, \quad i = 1, \ldots, s, \\ & v_j \ge 0, \quad j = 1, \ldots, m. \end{aligned} \quad (23)$$

This model is fractional program and can be converted into linear program to solve by using the Charnes-Cooper transformation.

Taking membership degree of route k into the model, the score value θ_{ki} on each objective factor can be calculated.

(2) Using path from path decision set as decision-making unit and using θ_{ki} as input and output indicators, the final score of each path can be calculated. The path with the highest score is the optimal one.

Table 1: Road section travel time.

Section	1-2	1-3	1-4	2-3	2-5	2-6	3-4	4-6	5-6	5-7	6-7
Travel time (h)	1	2	1	1	5	6	3	5	4	4	5

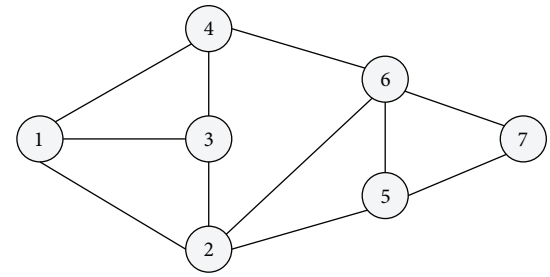

Figure 1: The road networks.

4. Case Studies

To meet the demand of the combat replenishment, a batch of military supplies need to be moved from node 1 to node 7 in time. Figure 1 shows the layout of the road network. Travel time on each road section is shown in Table 1. According to the requirements of the combat process, this transport task is required to be completed within 15 h and 5 alternative paths need to be selected for safety reasons.

(1) Dissimilar Path Set Calculation. Using the Dijkstra algorithm to search the shortest path R_1 based on time weight, travel time on path R_1 is T_1. The other four paths are obtained by using the dissimilar path algorithm based on overlapping punishment. Suppose that overlapping penalty coefficient is 0.5; the results are:

$$R_1 = \{1, 2, 5, 7\}, \quad R_2 = \{1, 4, 6, 7\}, \quad R_3 = \{1, 3, 2, 5, 7\},$$
$$R_4 = \{1, 2, 6, 7\}, \quad R_5 = \{1, 4, 6, 5, 7\}. \quad (24)$$

Path decision set is $R_0 = \{R_1, R_2, R_3, R_4, R_5\}$ and the corresponding travel time set is $T_0 = \{10, 11, 12, 12, 14\}$. The shortest travel time $T_{\min} = 10$.

(2) Membership Degree Calculation. Evaluation personnel consist of 5 battle commanders, 10 combat service staff officers, and 15 transportation professionals.

The weight of each type of personnel for transport risk assessment is $R_s = (0.45, 0.35, 0.2)^T$.

The weight of each type of personnel for rapid response capability is $R_r = (0.4, 0.35, 0.25)^T$.

The weight of each type of personnel for transport cost is $R_c = (0.2, 0.3, 0.5)^T$.

The evaluation results for path decision set by the evaluation personnel are shown in Table 2. Each element of the evaluation vector represents the number of each type of evaluation personnel who agree with this grade.

The difference between travel time on each route and the shortest travel time is shown in Table 3.

Table 2: Evaluation results by evaluation personnel.

	Path	R_1	R_2	R_3	R_4	R_5
Transport risk	Excellent	(0, 2, 4)	(1, 3, 5)	(2, 5, 7)	(3, 6, 8)	(3, 4, 7)
	Good	(2, 3, 5)	(2, 4, 5)	(2, 4, 5)	(2, 3, 5)	(2, 4, 6)
	Medium	(2, 4, 5)	(2, 2, 4)	(1, 1, 3)	(0, 1, 2)	(0, 2, 2)
	Poor	(1, 1, 1)	(0, 1, 1)	(0, 0, 0)	(0, 0, 0)	(0, 0, 0)
Rapid response capability	Excellent	(2, 3, 5)	(2, 4, 5)	(1, 4, 5)	(2, 4, 6)	(1, 3, 5)
	Good	(2, 4, 5)	(1, 2, 4)	(2, 5, 6)	(2, 3, 4)	(3, 6, 4)
	Medium	(1, 2, 3)	(2, 3, 5)	(1, 1, 3)	(1, 2, 3)	(1, 1, 4)
	Poor	(0, 1, 2)	(0, 1, 1)	(1, 0, 1)	(0, 1, 2)	(0, 0, 2)
Transport costs	Excellent	(3, 5, 7)	(2, 4, 7)	(1, 4, 6)	(2, 5, 6)	(1, 3, 4)
	Good	(2, 4, 5)	(2, 3, 5)	(2, 4, 5)	(2, 3, 7)	(1, 2, 4)
	Medium	(0, 1, 3)	(1, 3, 2)	(2, 1, 3)	(1, 2, 1)	(2, 3, 4)
	Poor	(0, 0, 0)	(0, 0, 1)	(0, 1, 1)	(0, 0, 1)	(1, 2, 3)

Table 3: Travel time difference of each route.

Path	R_1	R_2	R_3	R_4	R_5
Travel time difference	0	1	2	2	4

Table 4: Membership degree.

	Route	R_1	R_2	R_3	R_4	R_5
Travel time	Excellent	1	0.667	0	0	0
	Good	0	0.333	0.75	0.75	0
	Medium	0	0	0.25	0.25	0.917
	Poor	0	0	0	0	0.083
Transport risk	Excellent	0.123	0.262	0.448	0.587	0.503
	Good	0.352	0.387	0.387	0.352	0.400
	Medium	0.387	0.303	0.165	0.061	0.097
	Poor	0.138	0.048	0.0	0.0	0.0
Rapid response capability	Excellent	0.348	0.384	0.304	0.400	0.268
	Good	0.384	0.217	0.435	0.332	0.517
	Medium	0.200	0.348	0.165	0.200	0.182
	Poor	0.068	0.051	0.096	0.068	0.033
Transport costs	Excellent	0.503	0.433	0.360	0.430	0.263
	Good	0.367	0.337	0.367	0.404	0.234
	Medium	0.130	0.197	0.210	0.133	0.303
	Poor	0.0	0.033	0.063	0.033	0.200

Table 5: Score value of each route on each remark grade.

Remark grade	R_1	R_2	R_3	R_4	R_5
Excellent	0.551	0.462	0.245	0.313	0.232
Good	0.238	0.324	0.519	0.498	0.250
Medium	0.163	0.185	0.204	0.169	0.442
Poor	0.048	0.029	0.032	0.020	0.076

Table 6: Final score of each path.

Route	R_1	R_2	R_3	R_4	R_5
Final score	0.393	0.371	0.312	0.340	0.250

Membership degree is calculated in Table 4.

(3) Comprehensive Evaluation. Taking membership degree of route k into DEA model (8), the score value θ_{ki} on each objective factor can be calculated as shown in Table 5.

Using θ_{ki} as input and output indicators, the final score of each path can be calculated as shown in Table 6.

So, the calculation results are sorted in a descending order: $R_1 > R_2 > R_4 > R_3 > R_5$.

5. Conclusions

In this paper, path selection problem considering the influence of various fuzzy factors in military transport is investigated. Based on overlapping section punishment search algorithm, the path decision set is established. Then, a path selection decision model is presented based on DEA and multiobjective fuzzy decision-making method, where the evaluation target set consists of travel time, transport risk, quick response capability, and transport cost. For factors of great fuzziness and difficult to quantify, comprehensive weighted statistics method is used to establish the membership functions. Using path as decision-making unit, the comprehensive evaluation by DEA model can sort the path set, where the path with the higher comprehensive score indicates the much better one. Finally, the calculation results show the validity and effectiveness of the proposed method.

Conflict of Interests

The authors declare that there is no conflict of interests regarding the publication of this paper.

Acknowledgment

This work is partly supported by Science and Technology Program of Beijing, China (Grant no. Z121100000312101).

References

[1] X. D. Sun, *Military Logistics*, PLA Publishing Press, Beijing, China, 2002.

[2] Z. R. Chen and P. X. Bao, *Military Transportation*, PLA Publishing Press, Beijing, China, 2001.

[3] X. D. Luo, *Combat Power Projection*, Military Science Press, Beijing, China, 2003.

[4] S. S. Yu and G. H. Yu, *Force Projection*, National Defense University, Beijing, China, 2003.

[5] B. Y. Chen, W. H. K. Lam, A. Sumalee, and Z.-L. Li, "Reliable shortest path finding in stochastic networks with spatial correlated link travel times," *International Journal of Geographical Information Science*, vol. 26, no. 2, pp. 365–386, 2012.

[6] B. Y. Chen, W. H. K. Lam, A. Sumalee, Q. Q. Li, H. Shao, and Z. X. Fang, "Finding reliable shortest paths in road networks under

uncertainty," *Networks & Spatial Economics*, vol. 13, pp. 123–148, 2013.

[7] B. Y. Chen, W. H. K. Lam, Q. Q. Li, A. Sumalee, and K. Yan, "Shortest path finding problem in stochastic time-dependent road networks with stochastic first-in-first-out property," *IEEE Transactions on Intelligent Transportation Systems*, vol. 14, no. 4, pp. 1907–1917, 2013.

[8] B. Z. Yao, P. Hu, M. H. Zhang, and S. Wang, "Artificial bee colony algorithm with scanning strategy for periodic vehicle routing problem," *SIMULATION*, vol. 89, no. 6, pp. 762–770, 2013.

[9] B. Yu, W. H. K. Lam, and M. L. Tam, "Bus arrival time prediction at bus stop with multiple routes," *Transportation Research C*, vol. 19, no. 6, pp. 1157–1170, 2011.

[10] B. Yu and Z. Z. Yang, "An ant colony optimization model: the period vehicle routing problem with time windows," *Transportation Research E*, vol. 47, no. 2, pp. 166–181, 2011.

[11] B. Yu, Z. Z. Yang, and L. I. S, "Real-time partway deadheading strategy based on transit service reliability assessment," *Transportation Research A*, vol. 46, no. 8, pp. 1265–1279, 2012.

[12] B. Yu, Z.-Z. Yang, and J.-X. Xie, "A parallel improved ant colony optimization for multi-depot vehicle routing problem," *Journal of the Operational Research Society*, vol. 62, no. 1, pp. 183–188, 2011.

[13] B. Yu, Z.-Z. Yang, and B. Yao, "An improved ant colony optimization for vehicle routing problem," *European Journal of Operational Research*, vol. 196, no. 1, pp. 171–176, 2009.

[14] B. Z. Yao, P. Hu, X. H. Lu, J. J. Gao, and M. H. Zhang, "Transit network design based on travel time reliability," *Transportation Research C*. In press.

[15] Y. F. Shi, *Optimizing transportation route with uncertain factor in war [Ph.D. thesis]*, Southeast Jiaotong University, 2005.

[16] I. Akgün and B. Ç. Tansel, "Optimization of transportation requirements in the deployment of military units," *Computers and Operations Research*, vol. 34, no. 4, pp. 1158–1176, 2007.

[17] K. McKinzie and J. W. Barnes, "A review of strategic mobility models supporting the defense transportation system," *Mathematical and Computer Modelling*, vol. 39, no. 6–8, pp. 839–868, 2004.

[18] V. Akgün, E. Erkut, and R. Batta, "On finding dissimilar paths," *European Journal of Operational Research*, vol. 121, no. 2, pp. 232–246, 2000.

[19] P. Dell'Olmo, M. Gentili, and A. Scozzari, "On finding dissimilar Pareto-optimal paths," *European Journal of Operational Research*, vol. 22, no. 12, pp. 106–109, 2005.

[20] M. Caramia, S. Giordani, and A. Iovanella, "On the selection of k routes in multiobjective hazmat route planning," *IMA Journal Management Mathematics*, vol. 21, no. 3, pp. 239–251, 2010.

[21] S. D. Gu, *Operational Research*, Tsinghua University Press, Beijing, China, 2005.

[22] A. Quattrone and A. Vitetta, "Random and fuzzy utility models for road route choice," *Transportation Research E*, vol. 47, no. 6, pp. 1126–1139, 2011.

[23] Y. J. Liu and K. F. Yan, "Fuzzy multi-criteria decision-making method in planning of transport hub," *Journal of Wuhan Urban Construction Institute*, vol. 23, no. 2, pp. 63–66, 2006.

[24] W. K. M. Brauers, E. K. Zavadskas, F. Peldschus, and Z. Turskis, "Multi-objective decision-making for road design," *Transport*, vol. 23, no. 3, pp. 183–193, 2008.

[25] D. D. Wu, Y. Zhang, D. Wu, and D. L. Olson, "Fuzzy multi-objective programming for supplier selection and risk modeling: a possibility approach," *European Journal of Operational Research*, vol. 200, no. 3, pp. 774–787, 2010.

[26] Y. Liu, M. P. Yun, and G. X. Peng, "A multi-objective programming model of route choice of emergency vehicles before travel," *Journal of Highway and Transportation Research and Development*, vol. 26, no. 8, pp. 135–139, 2009.

[27] Q. C. Wu, T. Z. Chen, and Y. Su, "The best path analysis based on multi-target fuzzy decision-making," *Journal of Computer Simulation*, vol. 32, no. 18, pp. 156–160, 2010.

[28] F. H. Lotfi, G. R. Jahanshahloo, M. Khodabakhshi, M. Rostamy-Malkhlifeh, Z. Moghaddas, and M. Vaez-Ghasemi, "A review of ranking models in data envelopment analysis," *Journal of Applied Mathematics*, vol. 2013, Article ID 492421, 20 pages, 2013.

[29] W.-W. Fu and W.-Z. Jin, "Fuzzy comprehensive evaluation of urban public transport system based on DEA model," *Journal of Wuhan University of Technology*, vol. 32, no. 18, pp. 156–160, 2010.

[30] M. Zerafat Angiz L., A. Emrouznejad, and A. Mustafa, "Fuzzy assessment of performance of a decision making units using DEA: a non-radial approach," *Expert Systems with Applications*, vol. 37, no. 7, pp. 5153–5157, 2010.

Hindawi Publishing Corporation
Mathematical Problems in Engineering
Volume 2014, Article ID 914689, 9 pages
http://dx.doi.org/10.1155/2014/914689

Research Article

Multiobjective Optimization Based Vessel Collision Avoidance Strategy Optimization

Qingyang Xu,[1] Chuang Zhang,[2] and Ning Wang[2]

[1] *Shandong University, Weihai, China*
[2] *Dalian Maritime University, Dalian, China*

Correspondence should be addressed to Qingyang Xu; xuqy1981@163.com

Received 9 November 2013; Revised 23 December 2013; Accepted 25 December 2013; Published 6 February 2014

Academic Editor: Baozhen Yao

The vessel collision accidents cause a great loss of lives and property. In order to reduce the human fault and greatly improve the safety of marine traffic, collision avoidance strategy optimization is proposed to achieve this. In the paper, a multiobjective optimization algorithm NSGA-II is adopted to search for the optimal collision avoidance strategy considering the safety as well as economy elements of collision avoidance. Ship domain and Arena are used to evaluate the collision risk in the simulation. Based on the optimization, an optimal rudder angle is recommended to navigator for collision avoidance. In the simulation example, a crossing encounter situation is simulated, and the NSGA-II searches for the optimal collision avoidance operation under the Convention on the International Regulations for Preventing Collisions at Sea (COLREGS). The simulation studies exhibit the validity of the method.

1. Introduction

With the appearance of larger, specialized, and faster vessel, the environment of marine traffic becomes more and more sophisticated. Therefore, the collision accidents occur frequently, even though some advanced auxiliary vessel collision avoidance equipment is widely used aboard. The vessel collision accidents cause a great loss of lives and property. Navigational collision is a major safety concern at sea. According to the investigation of Li et al. [1], 80% of collision accidents are caused by human factor, including wrong decision or careless. Therefore, the subject of how to provide reasonable navigational information for navigators has been studied.

In early navigation, vessel collision avoidance depended on the experience of navigators due to lack of advanced equipment. Recently, Automatic Radar Plotting Aid (ARPA) appears and is widely installed on most merchant vessels [2]. The data handling and graphic display of equipment enhance the collision avoidance efficiency, and the decision is more and more objective [3]. ARPA provides an interface for navigators to evaluate the validity of a collision avoidance strategy by the predicted values of two important parameters of target vessels-Distance at Closest Point of Approach (DCPA) and Time to Closest Point of Approach (TCPA) [4]. The navigator can make a decision according to result of ARPA. However, the ARPA only can assess the movement of vessels according to a certain speed and course, and it cannot evaluate the economic characteristic of the different operations. Therefore, the navigator's decision is always suboptimal, and sometimes the wrong judgment is rendered.

With the appearance and development of new navigation equipment like AIS [5, 6], advanced computer technology, and so forth, the application of intelligent optimization algorithm has been used for collision avoidance strategy searching. Genetic algorithm (GA) is a popular heuristic algorithm, which has been used for many subjects, such as system identification [7, 8], supply chain [9], and scheduling problem [10]. Śmierzchalski and Michalewicz [11], Szlapczynski [12], and Szlapczynski and Szlapczynska [13] first made use of genetic algorithm to plan the route of vessel in static or dynamic environment in order to avoid obstacles. Similar heuristic optimization algorithms have been used by other

researchers: GA is used to find the optimal path and manoeuvres in collision avoidance [14–16]. Cheng and Liu made use of genetic algorithm to optimize the collision avoidance route of urban river [17, 18]. There are also other related approaches used to vessel collision avoidance and route planning, such as ant colony algorithm [19–21] and expert system [22]. The collision avoidance optimization problem is to find a reasonable way to make the vessel avoid the obstacles with minimal wastage and maximum safety. It is a multiobjective optimization problem. The above-mentioned collision avoidance problems are generally considered to have been solved form the scientific point of view, even if some solutions have not been applied yet. Moreover, in most of above-mentioned researches, the problems are always defined as a single-objective problem or transformed to a single-objective problem by the weights allocation. However, the parameters of weight are always experiential, which are difficult to set.

Recently, the number of multiobjective evolutionary algorithms increases drastically due to their popularity and capability of successfully solving multiobjective optimization problems [23, 24]. In this paper, we adopt a multiobjective optimization algorithm (NSGA-II) instead of a single-objective optimization algorithm to optimize the collision avoidance strategy. The NSGA proposed by Srinivas and Deb [25] has been successfully applied to solving many problems. An improved version of NSGA, which they called NSGA-II, overcome some disadvantages of NSGA, such as high computational complexity of nondominated sorting, lack of elitism, and need a sharing parameter. NSGA-II is considered as the state-of-the-art multiobjective evolutionary algorithm [26, 27]. The collision avoidance operation of vessel is selected as the optimized variables instead of the path that is constructed of coordinates set. Thus, the navigators can get the rudder angle for collision avoidance by the optimization of NSGA-II.

This paper is organized as follows. The problem of vessel collision avoidance optimization is presented firstly in Section 2, and then the multiobjective optimization algorithms (NSGA-II) for collision avoidance strategy optimization are discussed in Section 3. Finally, a of crossover encounter situation is simulated, and the optimization process and results are discussed in Section 4.

2. Vessel Collision Avoidance Optimization Problems

2.1. Multiobjective Optimization Problem. A multiobjective optimization problem is defined by a set of D parameters (decision variables), a set of N objective functions, and a set of m constraints. The objective functions and the constraints are functions of the decision variables. The aim of the optimization is to

$$\begin{aligned} &\text{minimize (and maximize)} \quad y = f(x) \\ &\qquad = [f_1(x), f_2(x), \ldots, f_M] \\ &\text{s.t.} \qquad x = [x_1, x_2, \ldots, x_d, \ldots, x_D] \\ &\qquad x_{d_{\min}} \le x_d \le x_{d_{\max}} \\ &\qquad \times (d = 1, 2, \ldots, D), \end{aligned} \tag{1}$$

where x is the vector of decision variables, f are the objective functions, M is the objective number, and $x_{d\_\min}$ and $x_{d\_\max}$ are the bound of decision variables.

Considering a minimization problem for each objective, it is said that a decision vector X_a dominates another vector X_b ($X_a > X_b$) if and only if

$$\forall i = 1, 2 \ldots k, \quad f_i(X_a) \ge f_i(X_b) \quad \text{or} \quad f_i(X_a) > f_i(X_b). \tag{2}$$

We can say that a vector of decision variables X is a Pareto-optimal solution or nondominated solution. Therefore, the Pareto-optimal set is the set of all Pareto-optimal solutions. The aim of an optimization algorithm is to find a set of Pareto-optimal solutions approximating the true Pareto-optimal front.

2.2. Collision Avoidance Strategy Optimization Problem. The goal of the collision avoidance strategy optimization is to find an optimal collision avoidance operation, which has the minimal time loss or way loss spending on maneuvering, while fulfilling some COLREGS rules [28]. Therefore, the individual evaluation is consolidated of security and economic factors [29]. The evaluation function includes three elements. The first part is the security assessment of the strategy, and it is a very important part of the evaluation function, namely, risk of collision. The safety of the strategy is mainly reflected by the collision risk between local vessel and target vessel. After generating the initial strategy, the Nomoto model is used to simulate the vessel and the collision risk is evaluated according to the information of the vessels. Different collision avoidance strategies lead to different collision risks. The second factor is the economic factors [12], such as the sailing time and distance. The third one is the smoothness factor, namely, the rudder angle changing or course changing.

Therefore, the collision avoidance strategy optimization based multiobjective is composed of three objectives as follows:

$$\text{minimize } y = f(x) = [f_1, f_2, f_3]. \tag{3}$$

The fitness can be calculated by the simulation data, and the primary optimized variable is the rudder angle that navigator or autopilot should be adopted in the collision avoidance.

2.2.1. Safety Evaluation. In the navigation, safety is the primary problem. In the paper, the minimum distance of the two vessels in the collision avoidance is adopted to evaluate the security. The evaluation function is shown as follows:

$$f_1^i = \text{safety}_i = F - \min\left(D^i\right), \tag{4}$$

where safety_i is the safety evaluation of ith strategy, D is the distance of passing close, F is a big value to make sure that the safety_i is positive, and function min() is minimum function. In the process of navigation, the routing is not a line, but a track belt. According to Yang's literature [30], the distance between two vessels should be maintained more than $(L_0 + L_t)\pi/18$ to prevent vessel collision caused by suction. If the distance between the two vessels is less than $(L_0+L_t)\pi/18$ in the simulation, the two vessels have a collision and the fitness is zero.

COLREGS rules should be considered except for f_1^i, which is an international rule at sea. Some rules are about the collision avoidance as follows.

(1) None of the ship domains are violated, that means every vessel having its own zone, which cannot be violated by other vessels.

(2) Speed alterations are not to be applied unless necessary (collision cannot be avoided by a configured maximum course alteration value). In vessel collision avoidance, the speed is always constant except that the collision avoidance cannot be achieved by course turning.

(3) COLREGS rules are not violated (especially rules 13 to 17).

   (a) Rule 13: "an overtaking vessel must keep well clear of the vessel being overtaken" in overtaking situations.

   (b) Rule 14: "when two power-driven vessels are meeting head-on, both must alter course to starboard, so that they pass on the port side of the other" in head-on situations.

   (c) Rule 15: "when two power-driven vessels are crossing, the vessel, which has the other on the starboard side, must give way" in crossing situations.

   (d) Rule 16: "the give-way vessel must take early and substantial action to keep well clear."

   (e) Rule 17: "the stand-on vessel may take action to avoid collision if it becomes clear that the give-way vessel is not taking appropriate action."

According to rules 13–17, the local vessel and target vessel have different responsibility in different encounter situation. For example, the overtaking vessel cannot affect the navigation of overtaken vessel in overtaking situation; in head-on situation, the two vessels must adopt collision avoidance measures separately; crossing situation is a complex situation, the given-way vessel must adopt collision avoidance measures, and the stand-on vessel must stay the speed and course. The COLREGS rules can be considered as the constraints of the fitness evaluation. Although there are some constraints, we have considered it at the generation of population and do not integrate into the fitness function.

2.2.2. Economy Evaluation. Energy conservation is very important. The second part of evaluation is the economical evaluation of the strategy. Economy is mainly reflected by the time and voyage consumption. Since the speed of vessel is constant in the process of collision avoidance, there is a linear relation with the distance and time of vessels. Therefore, only voyage consumption is considered in the evaluation function. The evaluation function is as follows:

$$f_2^i = \text{economy}_i = \sum_k^n \sqrt{(x_k - x_{k-1})^2 + (y_k - y_{k-1})^2}, \quad (5)$$

where economy_i is the economical evaluation of ith strategy, k is the simulation steps, n is the steps length of collision avoidance, and (x, y) is the coordinate of vessel.

2.2.3. Smoothness Evaluation. The third part is the smoothness evaluation. Excessive smoothness of the routing is not conducive to realize collision avoidance or does not meet the actual manipulation habit. Conversely, an unduly large turning angle will cause a longer voyage with excessive energy and time consumption. In the paper, rudder angle changing is used to evaluate the smoothness of strategy:

$$f_3^i = \text{smooth}_i = \Delta\delta_i, \quad (6)$$

where smooth_i is the smoothness evaluation of ith strategy and δ_i is the rudder angle.

3. Multiobjective Based Collision Avoidance Strategy Optimization

3.1. The NSGA-II Algorithm. The NSGA-II [31] is one of the most famous multiobjective optimization algorithm. The NSGA [25] first is presented in 1994; then another improved one NSGA-II was proposed in 2002. According to Section 2, the rudder angle is the primary optimization variables. The individual is evaluated by the nondominated sorting method. The flow of the algorithm is shown as in Algorithm 1.

NSGA-II is based on Pareto solutions, measuring individual fitness according to their dominance property. The non-dominated individuals in the population are regarded as the fittest, and the dominated individuals are assigned lower fitness values, such as the steps (12)–(17) of the Algorithm 1. By this way, the number of dominated individuals will be counted as the fitness values instead of the value of objective function. To maintain the diversity in the Pareto solutions, NSGA-II introduced a measure of individual's density respect to other individuals in the objective space, such as the steps (34)–(38) of the Algorithm 1 and had an elitism mechanism and crowed comparison operator to preserve the diversity of population. In step (39) of the Algorithm 1, an arithmetic crossover and Gaussian mutation operation will be adopted. In the simulation of this paper, the crossover ratio is 1.2, and the scale and shrink of Gaussian mutation are 0.1 and 0.5.

3.2. The Flow of Collision Avoidance Strategy Optimization. The vessel collision avoidance strategy optimization is a complex system, which has many procedures. Figure 1 is the flow of collision avoidance strategy optimization. In order to evaluate the fitness of strategies, we adopt a mathematical

```
(1)  Pop = InitPop(N)
(2)  InitRank()
(3)  Pop1 = select(Pop)
(4)  Popt = crossover(Pop)
(5)  Pop2 = mutation(Popt)
(6)  while terminal_condition
(7)        Pop(n) = Pop1(n) ∪ Pop2(n)
(8)        for p in Pop(n):
(9)              pdomq = [ ]
(10)               np = 0
(11)               for q in Pop(n)
(12)                     if p dominate q
(13)                           pdomq.add(q)
(14)                     else if p is dominated by q
(15)                           np = np + 1
(16)                     if np is the first rank of Pareto
(17)                     p_rank = 1
(18)         F1.add(p)
(19)         F.add(F1)
(20)         while F[i]
(21)               for p in F[i]
(22)                     for q in pdomq
(23)                           if nq is dominated by other individual
(24)                                 q_rank = i + 1
(25)                                 Q.add(q)
(26)               F.add(Q)
(27)               i = i + 1
(28)         Pop(n + 1) = []
(29)         while len(Pop(n + 1) + len(F[i]) < N
(30)         nLen = len(F[i])
(31)         for i in F[i]
(32)               init i.distance = 0
(33)         for objFun in M objective function
(34)               F[i] = sort(F[i], objFun)
(35)               for i in xrange(1, len(I) − 2):
(37)                     F[i][i].distance = F[i][i].distance + (objFun(F[i][i + 1] − objFun(F[i][i − 1])))/(Max(objFun()) − Min(objFun()))
(38)               Pop1(n + 1) = [Pop(n + 1); F[i]]
(39)         Pop2(n + 1) = generate new pop
(40)               i+ = i + 1
             n = n + 1
```

Algorithm 1

model of vessel of simulate the vessels. The vessel must assess the encounter situation all the time and collision avoidance will be carried out according to the encounter situation. The safe and economic collision avoidance strategy comes from numerous collision avoidance strategies that follows the requirement of International Regulations for Preventing Collisions at Sea (COLREGS) with highest fitness.

Collision risk evaluation is a very important part. There are many ways to evaluate the collision risk of vessels, including collision risk models [32] and ship domains [33]. In this paper, ship domain and ship Arena which are based on human praxiology and psychology are selected as the collision risk evaluation way. Fujii and Yamanouchi [34] proposed the concept of ship domain firstly. The domain is an ellipse, of which the geometrical centre is identical to the position of ship center, the major semi-axis is along the fore and aft of ship, and the minor semi-axis isalong the bear abeam of ship. Then, it is introduced to England in 1971. Goodwin [35] confirmed the existence of ship domain and established the model of ship domain according to the traffic investigation of south of the North Sea in open sea. It was derived from statistic methods from large number of record and simulator data. The definition of domain made by Goodwin [35] is "the surrounding effective waters that the navigator of a ship wants to keep clear of other ships or fixed objects." The domain is divided into three sectors. The domain is shown in Figure 2. Goodwin's model has shown that the navigator's actions is influenced by the COLREGS. The starboard side is larger than port side, and astern side is the smallest part. Different sectors of Goodwin's ship domain is not continual or convenient to carry out traffic simulation on computer. So Davis et al. [36] smoothed Goodwin's

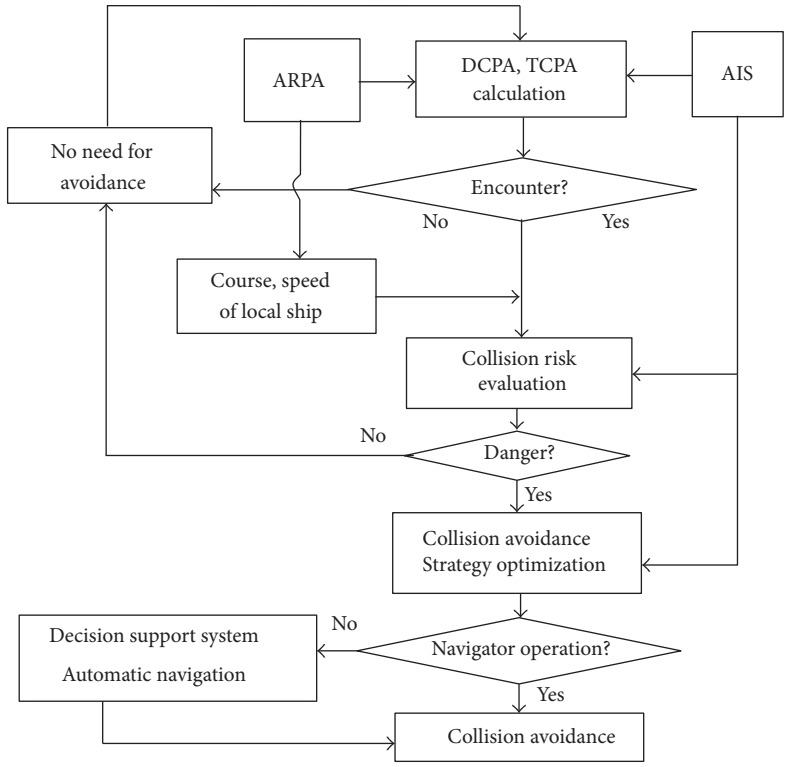

Figure 1: The flow of collision avoidance strategy optimization.

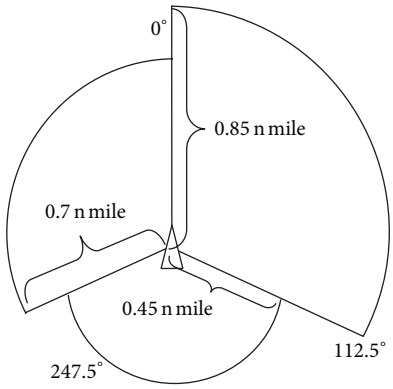

Figure 2: Ship domain at open sea.

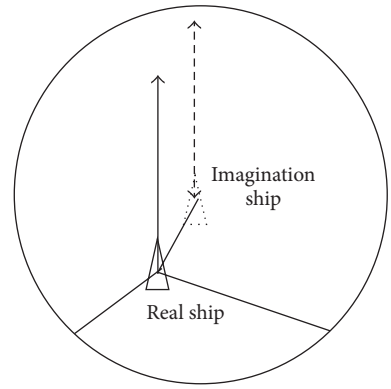

Figure 3: Ship domain of Davis.

domain boundary. He made use of a circle whose area is equal to the sum area of the three sectors to Goodwin's domain. The ship shifted to bottom-left corner in the Davis's ship domain to keep the characteristic of Goodwin's. It is advantage for computer simulation as in Figure 3. The numerical model is shown as follows:

$$F = X^2 + Y^2 - r^2,$$

$$X = (x - x_I)\cos\varphi - (y - y_I)\sin\varphi,$$

$$Y = (x - x_I)\sin\varphi - (y - y_I)\cos\varphi,$$

$$x_I = x_R + d\sin(\varphi + 19^\circ),$$

$$y_I = y_R + d\cos(\varphi + 19^\circ), \quad (7)$$

where F is the distance to domain. If the ship is outside of the domain, $F < 0$. φ is the course of ship. x_I, y_I are the coordination of imagination ship center. x_R, y_R are the coordination of real ship center. r is the radius of domain. d is the distance from real ship to imagination ship.

The ship Arena is used for navigators to determine the time of taking collision avoidance actions [37]. If any, we needed to keep our own ship domain unviolated. It is a bigger area than ship domain. The parameters are shown in Figure 4.

Arena is a bigger area that navigator can adopt action or not when the target vessel is in the Arena. If the target vessel violates our domain in future, the navigator will adopt

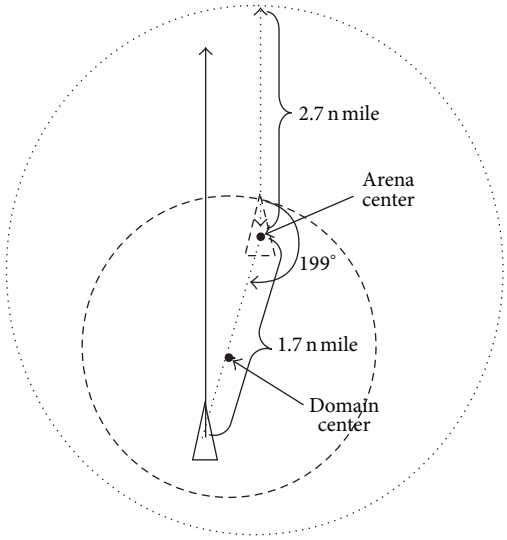

Figure 4: The comparison diagram of ship domain and Arena.

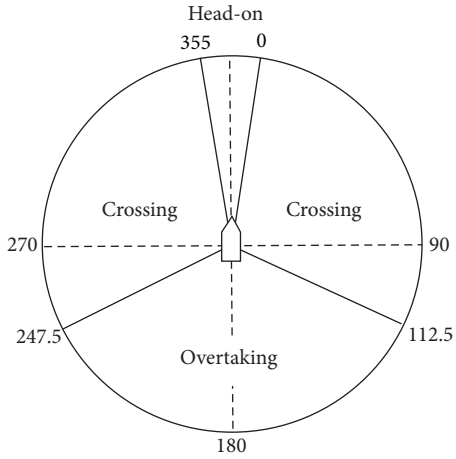

Figure 5: Encounter situation.

action to avoid this. In that period and in the following years or so, many scholars modified the ship domain and carried out practical researches. Since then, the ship domain has been widely used in ships' collision avoidance, marine traffic simulation, calculation of encounter rates, appraisal of collision risk, VTS design, and so forth.

4. Simulations

The encounter statuses of vessels are divided into head-on, crossing, and overtaking situations when two vessels have an encounter with a good visibility, the encounter statuses of vessels are divided into head-on, crossing, and overtaking situations [19]. Figure 5 is the three encounter situations. In the collision avoidance decision-making supporting system, we need to judge the encounter situation according to the status of two vessels, so as to determine the collision avoidance strategy [38].

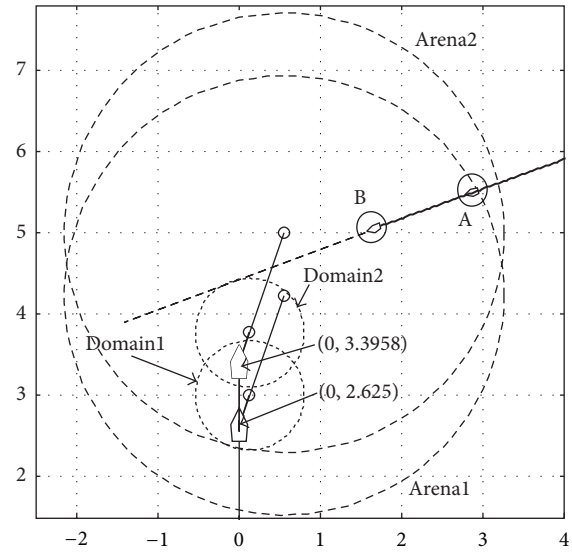

Figure 6: The encounter status of two vessels.

In the simulations, the parameters of target vessel are that the vessel moves with a speed V_t = 25 kn, the course is C_t = 250°, the starting coordinates is (7, 5.5), and the length of the vessel is 110 m. The parameters of local vessel are that the vessel moves with a speed V_0 = 15 kn, the course is C_0 = 0°, the starting coordinates is (0, 0), the length of vessel is 250 m, and the indexing of KT are K = 0.193, T = 34.119. In the simulations, the speed of vessels is constant, and there is no wind and waves. For NSGA-II, the ratio of intermediate crossover is 1.2 and the scale and shrink of Gaussian mutatin are 0.1 and 0.5.

According to status of two vessels, there is no collision risk at the beginning according ship Arena and domain. The two vessels will have a crossing encounter situation, and local vessel is the give-way vessel and the target vessel is stand-on vessel according to the collision liability division. With the navigation of the vessels, the target vessel will violate the Arena of local vessel, which is shown in Figure 6. The target vessel violates Arena1 of local vessel at point A but does not violate the Domain1 of local vessel. Therefore, the local vessel does not need to adopt collision operation. However, the target violates the Domain2 of local when his position is point B, and we should adopt collision avoidance operations to avoid danger. Otherwise, the two vessels will have a collision in future, which is shown in Figure 7.

In order to reduce the evaluation amount of unnecessary individuals, the individuals are generated in the feasible region according to the COLREGS. In order to facilitate a clear description of the process of collision avoidance optimization, the population size of NSGA-II is set to 30. In Figure 8, it is the collision avoidance effect of population of infantile iteration. In Figure 9, it is the collision avoidance effect of population of later optimization. From Figure 9 we can know that the individuals are convergent to a certain area.

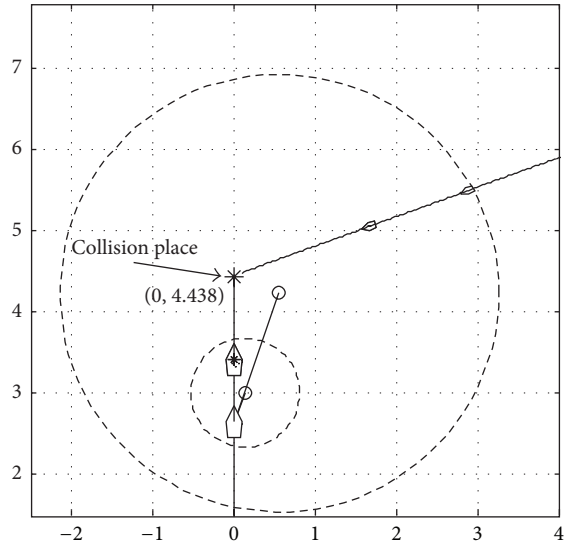

Figure 7: The two vessels have a collision.

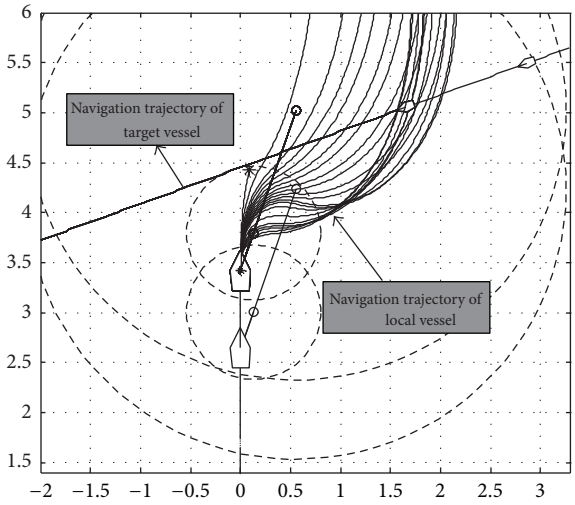

Figure 8: The collision avoidance effect of population of infantile iteration.

According to the final optimization result, an optimal collision avoidance strategy is selected when the rudder angle is 11 degrees, according to the fitness priority. The changes of DCPA, TCPA, and RT (distance of vessels) are shown in Figure 10. From the figure, we can see that the distance of two vessels is smaller and smaller with the navigation. If there is not collision avoidance operation, the two vessels will have collision before Time 200. The DCPA and TCPA have a jump from Time 200 when the collision avoidance operation is adopted. After collision avoidance, RT becomes bigger.

In Figure 11, it is the comparison diagram of DCPA, TCPA, and RT when rudder angle is 6, 11, and 20 degrees.

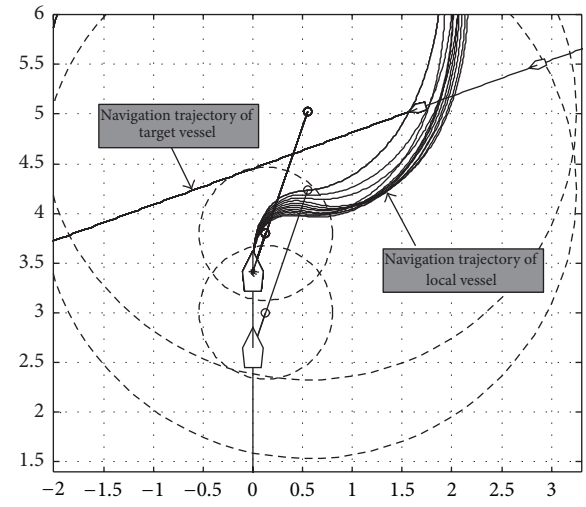

Figure 9: The collision avoidance effect of population of later optimization.

The DCPA change of rudder angle = 11 is bigger than rudder angle = 6 and smaller than rudder angle = 20. The minimal RT of rudder angle = 11 is bigger than rudder angle = 6 and smaller than rudder angle = 20.

From Figure 11, we can see that there is a bigger DCPA for a longer time when the rudder angle has a value of 11°. At about time 175, the collision avoidance is carried out, then the distance of two vessels has an inflection point at time 200 and RT becomes bigger subsequently. However, different operations have different effects. Although a bigger rudder angle, like 20°, can obtain well safety fitness, other fitness will be suboptimal. Therefore, we can get an optimal collision strategy (11° of rudder angle) by the optimization of NSGA-II.

5. Conclusions

The environment of maritime traffic becomes more and more hostile. Therefore, the subject of how to provide reasonable collision avoidance information for navigators aboard has been studied. In this paper, we make use of the advanced navigational equipment and multiobjective optimization algorithm to obtain an optimal collision avoidance strategy. The optimization result is a safe and economical operation instruction considering COLREGS. The simulation results exhibit the validity of the method. After that the optimal collision avoidance operation is carried out, and the vessel will be out of danger. Then, the vessel can resume to the original route. Although the results are promising, we only discussed the optimization mechanisms of the collision avoidance system. The optimization is based on the navigational information of local vessel and target vessel. The corresponding sensors are required on actual vessel, and there will be a complex sea conditions in practical.

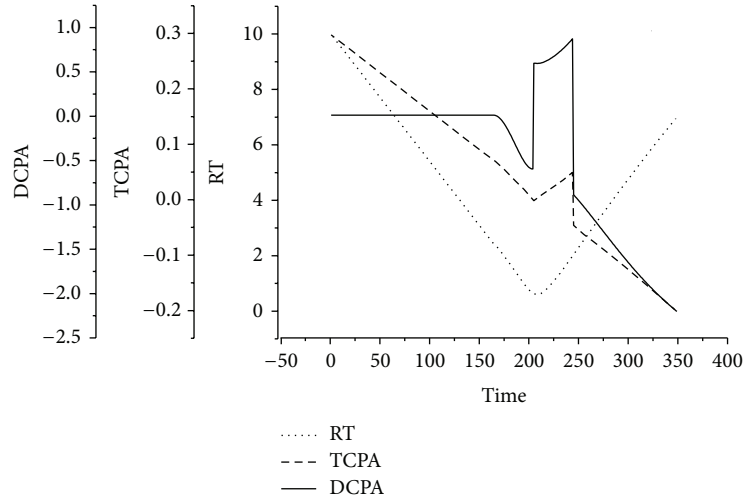

Figure 10: The changes of DCPA, TCPA, and RT when rudder angle is 11 degrees.

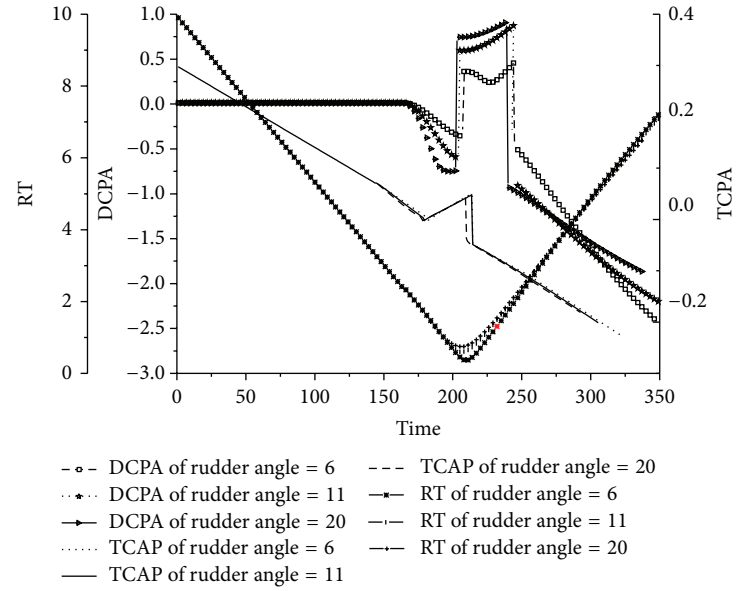

Figure 11: The changes of DCPA, TCPA, and RT when rudder angle is 6, 11, and 20 degree.

Conflict of Interests

The authors declare that there is no conflict of interests regarding the publication of this paper.

Acknowledgments

The author thanks the reviewers for their careful reading and helpful comments that have improved the paper. This work is supported by the National Natural Science Foundation of China (under Grant 51009017), Applied Basic Research Funds from Ministry of Transport of P. R. China (under Grant 2012-329-225-060), China Postdoctoral Science Foundation (under Grant 2012M520629), and Fundamental Research Funds for the Central Universities of China (under Grants 2009QN025, 2011JC002, and 3132013025).

References

[1] L. Li, S. Yang, B. Cao, and Z. Li, "A summary of studies on the automation of ship collision avoidance intelligence," *Journal of Jimei University (Natural Science)*, vol. 11, no. 2, pp. 188–192, 2006.

[2] T. Statheros, G. Howells, and K. McDonald-Maier, "Autonomous ship collision avoidance navigation concepts, technologies and techniques," *Journal of Navigation*, vol. 61, no. 1, pp. 129–142, 2008.

[3] X. Zeng, M. Ito, and E. Shimizu, "Collision avoidance of moving obstacles for ship with genetic algorithm," in *Proceedings of the 6th International Workshop on Advanced Motion Control*, pp. 513–518, Nagoya, Japan, 2000.

[4] H. C. Chin and A. K. Debnath, "Modeling perceived collision risk in port water navigation," *Safety Science*, vol. 47, no. 10, pp. 1410–1416, 2009.

[5] H.-Z. Hsu, N. A. Witt, J. B. Hooper, and A. P. Mcdermott, "The AIS-Assisted collision avoidance," *Journal of Navigation*, vol. 62, no. 4, pp. 657–670, 2009.

[6] J. M. Mou, C. van der Tak, and H. Ligteringen, "Study on collision avoidance in busy waterways by using AIS data," *Ocean Engineering*, vol. 37, no. 5-6, pp. 483–490, 2010.

[7] R. D. Al-Dabbagh, A. Kinsheel, M. S. Bin Baba, and S. Mekhilef, "An integration of compact Genetic algorithm and local search method for optimizing ARMA (1,1) model of likelihood estimator," in *Proceedings of the 2nd International Conference on Computer Science and Computational Mathematics*, pp. 60–67, Melaka, Malaysia, 2013.

[8] R. D. Al-Dabbagh, M. S. Baba, S. Mekhilef, and A. Kinsheel, "The compact Genetic Algorithm for likelihood estimator of first order moving average model," in *Proceedings of the 2nd International Conference on Digital Information and Communication Technology and it's Applications*, pp. 474–481, 2012.

[9] B. Yu, Z. Yang, and C. Cheng, "Optimizing the distribution of shopping centers with parallel genetic algorithm," *Engineering Applications of Artificial Intelligence*, vol. 20, no. 2, pp. 215–223, 2007.

[10] B. Yu, Z.-Z. Yang, and B. Yao, "An improved ant colony optimization for vehicle routing problem," *European Journal of Operational Research*, vol. 196, no. 1, pp. 171–176, 2009.

[11] R. Śmierzchalski and Z. Michalewicz, "Modeling of ship trajectory in collision situations by an evolutionary algorithm," *IEEE Transactions on Evolutionary Computation*, vol. 4, no. 3, pp. 227–241, 2000.

[12] R. Szlapczynski, "Evolutionary sets of safe ship trajectories: a new approach to collision avoidance," *Journal of Navigation*, vol. 64, no. 1, pp. 169–181, 2011.

[13] R. Szlapczynski and J. Szlapczynska, "On evolutionary computing in multi-ship trajectory planning," *Applied Intelligence*, vol. 37, pp. 155–174, 2012.

[14] M. Ito, F. Zhang, and N. Yoshida, "Collision avoidance control of ship with genetic algorithm," in *Proceedings of the IEEE International Conference on Control Applications and IEEE International Symposium on Computer Aided Control System Design*, pp. 1791–1796, Kohala Coast, Hawaii, USA, August 1999.

[15] X. Zeng, "Evolution of the safe path for ship navigation," *Applied Artificial Intelligence*, vol. 17, no. 2, pp. 87–104, 2003.

[16] M.-C. Tsou, S.-L. Kao, and C.-M. Su, "Decision support from genetic algorithms for ship collision avoidance route planning and alerts," *Journal of Navigation*, vol. 63, no. 1, pp. 167–182, 2010.

[17] X. Cheng and Z. Liu, "Study on ship collision avoidance trajectory optimization in inland waterways with genetic algorithm," *Navigation of China*, vol. 67, no. 2, pp. 38–46, 2006.

[18] X. Cheng and Z. Liu, "Trajectory optimization for ship collision avoidance in three fork sea-route of inland waterway," *Ship & Ocean Engineering*, vol. 37, no. 4, pp. 74–76, 2008.

[19] M.-C. Tsou and C.-K. Hsueh, "The study of ship collision avoidance route planning by ant colony algorithm," *Journal of Marine Science and Technology*, vol. 18, no. 5, pp. 746–756, 2010.

[20] J. B. Escario, J. F. Jimenez, and J. M. Giron-Sierra, "Optimisation of autonomous ship manoeuvres applying Ant Colony Optimisation metaheuristic," *Expert Systems with Applications*, vol. 39, no. 11, pp. 10120–10139, 2012.

[21] B. Yu and Z. Z. Yang, "An ant colony optimization model: the period vehicle routing problem with time windows," *Transportation Research E*, vol. 47, no. 2, pp. 166–181, 2011.

[22] T. Tran, *Avoidance Navigation Totally Integrated System*, Universtiy of Southamton, Southampton, UK, 2001.

[23] N. Belgasmi, L. B. Said, and K. Ghedira, "Greedy local improvement of SPEA2 algorithm to solve the multiobjective capacitated transshipment problem," in *Learning and Intelligent Optimization*, pp. 364–378, Springer, Berlin, Germany, 2011.

[24] N. Belgasmi, L. B. Saïd, and K. Ghédira, "Evolutionary multiobjective optimization of the multi-location transshipment problem," *Operational Research*, vol. 8, no. 2, pp. 167–183, 2008.

[25] N. Srinivas and K. Deb, "Muiltiobjective optimization using nondominated sorting in genetic algorithms," *Evolutionary Computation*, vol. 2, no. 3, pp. 221–248, 1994.

[26] M. R. Rani, H. Selamat, H. Zamzuri, and Z. Ibrahim, "Multiobjective optimization for PID controller tuning using the global ranking genetic algorithm," *International Journal of Innovative Computing, Information and Control*, vol. 8, no. 1, pp. 269–284, 2012.

[27] S. Bechikh, N. Belgasmi, L. B. Said, and K. Ghédira, "PHC-NSGA-II: a novel multi-objective memetic algorithm for continuous optimization," in *Proceedings of the 20th IEEE International Conference on Tools with Artificial Intelligence (ICTAI '08)*, pp. 180–189, November 2008.

[28] R. Szlapczynski, "Evolutionary sets of safe ship trajectories within traffic separation schemes," *Journal of Navigation*, vol. 66, no. 1, pp. 65–81, 2013.

[29] Y. Yavin, C. Frangos, T. Miloh, and G. Zilman, "Collision avoidance by a ship with a moving obstacle: computation of feasible command strategies," *Journal of Optimization Theory and Applications*, vol. 93, no. 1, pp. 53–66, 1997.

[30] S. Yang, *Decision-Making Support System for Ship Anti-Collision Based on Multi-Agent*, Shanghai Maritime University, Shanghai, China, 2008.

[31] K. Deb, A. Pratap, S. Agarwal, and T. Meyarivan, "A fast and elitist multiobjective genetic algorithm: NSGA-II," *IEEE Transactions on Evolutionary Computation*, vol. 6, no. 2, pp. 182–197, 2002.

[32] Q. Y. Xu, X. Y. Meng, and N. Wang, "Intelligent evaluation system of ship management," *International Journal on Marine Navigation and Safety of Sea Transportation*, vol. 4, no. 4, pp. 479–482, 2010.

[33] N. Wang, X. Meng, Q. Xu, and Z. Wang, "A unified analytical framework for ship domains," *Journal of Navigation*, vol. 62, no. 4, pp. 643–655, 2009.

[34] Y. Fujii and H. Yamanouchi, "The distribution of collisions in Japan and methods of estimating collision damage," *Journal of Navigation*, vol. 26, no. 1, pp. 108–113, 1973.

[35] E. M. Goodwin, "A statistical study of ship domains," *Journal of Navigation*, vol. 28, no. 3, pp. 328–344, 1975.

[36] P. V. Davis, M. J. Dove, and C. J. Stockel, "A computer simulation of multi-ship encounters," *Journal of Navigation*, vol. 35, no. 2, pp. 347–352, 1982.

[37] P. V. Davis, M. J. Dove, and C. T. Stockel, "A computer simulation of marine traffic using domains and arenas," *The Journal of Navigation*, vol. 33, no. 1, pp. 215–222, 1980.

[38] Z. Zheng, *Research on Automatic Decision-Making System of Vessel Collision Avoidance*, Dalian Maritime University, Dalian, China, 2000.

Hindawi Publishing Corporation
Mathematical Problems in Engineering
Volume 2014, Article ID 478573, 9 pages
http://dx.doi.org/10.1155/2014/478573

Research Article

Lane Changing Trajectory Planning and Tracking Controller Design for Intelligent Vehicle Running on Curved Road

Lie Guo,[1] Ping-Shu Ge,[2] Ming Yue,[1] and Yi-Bing Zhao[1]

[1] *School of Automotive Engineering, State Key Laboratory of Structural Analysis for Industrial Equipment, Dalian University of Technology, Dalian 116024, China*
[2] *College of Electromechanical & Information Engineering, Dalian Nationalities University, Dalian 116600, China*

Correspondence should be addressed to Ping-Shu Ge; gps@dlnu.edu.cn

Received 29 October 2013; Accepted 18 December 2013; Published 9 January 2014;

Academic Editor: Rui Mu

To enhance the active safety and realize the autonomy of intelligent vehicle on highway curved road, a lane changing trajectory is planned and tracked for lane changing maneuver on curved road. The kinematics model of the intelligent vehicle with nonholonomic constraint feature and the tracking error model are established firstly. The longitudinal and lateral coupling and the difference of curvature radius between the outside and inside lane are taken into account, which is helpful to enhance the authenticity of desired lane changing trajectory on curved road. Then the trajectory tracking controller of closed-loop control structure is derived using integral backstepping method to construct a new virtual variable. The Lyapunov theory is applied to analyze the stability of the proposed tracking controller. Simulation results demonstrate that this controller can guarantee the convergences of both the relative position tracking errors and the position tracking synchronization.

1. Introduction

Intelligent vehicle has become a hot topic worldwide in recent years. So far, several national and international research programs have been initiated, such as advanced safety vehicle (ASV), intelligent vehicle highway system (IVHS), or the partners for advanced transit and highways (PATH) program, whose main goals are to increase the safety and efficiency in normal traffic environments [1]. An intelligent vehicle should possess the following three abilities simultaneously. The first ability is to recognize the driving environments like the driver does using different types of sensors, such as lane detection and obstacle detection [2]. The second is to realize its longitudinal control so as to keep in the longitudinal direction [3]. The third ability is to steer so as to guide the vehicle along reference trajectories at all possible speeds even in the presence of disturbances [4, 5]. Therein, the lane changing maneuver is one of the extensive investigated automatic driving operations for intelligent vehicles once the optimized trajectory is planned [6]. This paper focuses on the safety of lane changing for intelligent vehicle on curved roads by tracking the planned trajectory.

The lane changing maneuver is carried out by planning the reference trajectory according to the vehicle states and road information, and then the control laws are designed using onboard sensors to track this virtual trajectory [7]. The trapezoidal acceleration profile resultant trajectory has been known as generating the least possible lateral acceleration on the vehicle [8]. To meet the restriction of the various curvature and change rate for lane changing on curved road, this paper utilizes the trajectory planning method based on trapezoidal acceleration profile. Once the virtual trajectory is planned, the lane changing controller is designed to track this trajectory [9]. For example, Hatipoglu et al. [10] reported the design of an automated lane changing controller with a two-layer hierarchical architecture. Ammoun et al. [11] drew an area of the virtual desire lane changing trajectory by adding speed or acceleration constraints. Lee et al. [12] proposed an integrated lane change driver model and used

closed-loop simulation of the ESC system to control lane changing and lane following maneuvers.

However, the lane changing controllers introduced above depend on the fact that lane changing maneuvers mainly take place on straight road segment. While on curved road, the situation is different with straight road. Toledo-Moreo and Zamora-Izquierdo [13] proposed an interactive multiple model-based method for predicting lane changes in highways. Inspired by the observation that any change in the road curvature affects the vehicle lateral dynamics, Ho et al. [14] realized the lane keeping and lane changing control by using the same controller. Their algorithm incorporates the curvature of a virtual road, the actual steering angle, and the vehicle lateral model to estimate the vehicle position. Ren et al. [7] planned the lane changing trajectory of vehicle on a circular curved road considering the curvature difference between inside and outside lanes. Then the reference yaw angle, yaw rate, and yaw angle acceleration were derived, and the yaw-rate-tracking controller was designed to realize the lane changing maneuvers by applying nonsingular terminal sliding mode technology.

Most of those lane changing maneuvers researched above ignore the influence of lane curvature change and the vehicle longitudinal velocity on lane changing trajectory. This paper aims at the study of the automated lane changing on curved road, where the curvatures of the outside and inside lane are not zero, nor equal. The main contributions of this paper are as follows: (1) a trajectory planning method suitable for curved road is proposed based on trapezoidal acceleration profile; (2) the coupled function of the vehicle's longitudinal and lateral motion on lane changing trajectory is taken into account, namely, the curvature radius of which is a vector in lane changing maneuver; (3) on this basis, the trajectory tracking control algorithm is designed using integral backstepping with Lyapunov theory.

The remainder of this paper is organized as follows. The lane change trajectory is planned in Section 2. Section 3 builds the vehicle kinematics and tracking error model and then designs the trajectory tracking controller. Simulation and discussion are given in Section 4. Section 5 concludes this paper.

2. Trajectory Planning for Lane Changing

Lane change reference trajectories play a crucial role in the lane change maneuver. Currently, the commonly used trajectories for lane changing are isokinetic migration lane changing trajectory, arc lane changing trajectory, trapezoidal acceleration lane changing trajectory, sine function lane changing trajectory, and so forth [15]. The trapezoidal acceleration profile resultant trajectory has been known as generating the least possible lateral acceleration on the vehicle. The time requirement for changing lane and the vehicle dynamics can be combined to choose the desired lateral acceleration [7, 16]. This paper utilizes the trajectory planning method based on trapezoidal acceleration profile to meet the restriction of the various curvatures and change

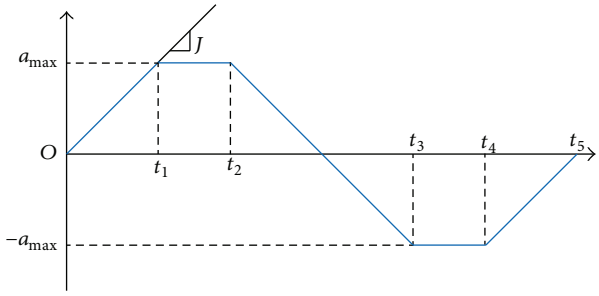

Figure 1: Schematic diagram of trapezoidal acceleration profile.

rate for lane changing on curved road. This method regards that the acceleration profile consists of two opposite ladders with the same size, as Figure 1. The lateral acceleration rate is defined as

$$\begin{aligned}\ddot{y}_d(t) = {} & J_{\max}(t-t_0)\cdot u(t-t_0) - J_{\max}(t-t_1)\cdot u(t-t_1) \\ & - J_{\max}(t-t_2)\cdot u(t-t_2) + J_{\max}(t-t_3)\cdot u(t-t_3) \\ & + J_{\max}(t-t_4)\cdot u(t-t_4) - J_{\max}(t-t_5)\cdot u(t-t_5),\end{aligned} \tag{1}$$

where $\ddot{y}_d(t)$ is the desired vehicle lateral acceleration and $J_{\max}$ denotes the maximum of lateral acceleration rate. $u(t)$ is a unit step function and t is the elapse time of the lane changing maneuver. t_0 denotes the starting time for this maneuver and t_5 denotes the finishing time.

The key times for the lane changing maneuver satisfy the following constraints:

$$\begin{aligned} t_1 &= \frac{a_{\max}}{J_{\max}}, \\ t_2 &= -\frac{a_{\max}}{2J_{\max}} + \frac{\sqrt{\left(a_{\max}/J_{\max}\right)^2 + 4d_\omega/a_{\max}}}{2}, \\ t_3 &= 2t_1 + t_2, \\ t_4 &= t_1 + 2t_2, \qquad t_5 = 2t_1 + 2t_2, \end{aligned} \tag{2}$$

where d_w is defined as the distance between the outside and inside lane. It is obvious that each time is the function of lateral acceleration and lateral acceleration rate. Once the vehicle lateral acceleration and lateral acceleration rate are determined, the trajectory for lane changing can be planned.

The lane changing trajectory on curved road is planned based on research results for lane changing on straight road segment, assuming that the outside and the inside lane have the same instantaneous center O_R, and the curvature radius R of the outside lane is a constant.

The vehicle's motion state during lane changing on curved road is shown in Figure 2. The inertial coordinate system is established, where O denotes the starting position of vehicle during lane changing. The x-axis is along the tangent of outside lane centerline, while y-axis is in the direction of

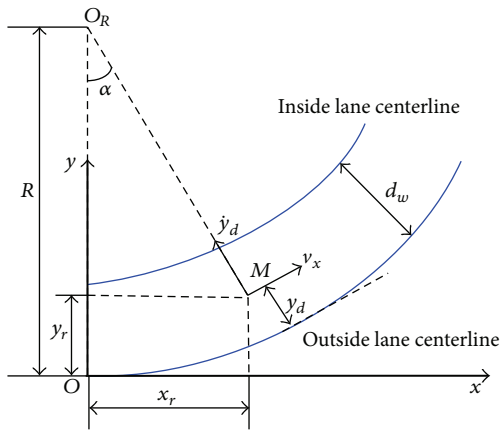

Figure 2: Schematic diagram of lane changing trajectory.

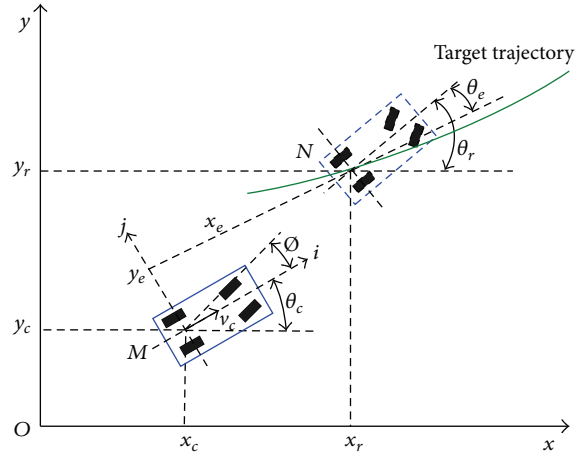

Figure 3: Vehicle real posture and the reference posture in world coordinate system.

instantaneous center O_R. v_x represents the vehicle longitudinal velocity.

The desired lateral velocity and lateral displacement are represented by $\dot{y}_d(t)$ and $y_d(t)$, respectively, and the desired longitudinal velocity of vehicle is denoted by $v_d(t)$. Among that, the longitudinal acceleration $\dot{v}_d(t)$ during lane changing maneuver is shown as follows:

$$\dot{v}_d(t) = \begin{cases} 0 & 0 < t \le t_1 \\ 0.4(t - t_1) & t_1 < t \le t_2 \\ 0.2 & t_2 < t \le t_3 \\ -0.4(t - t_4) & t_3 < t \le t_4 \\ 0 & t_4 < t \le t_5. \end{cases} \tag{3}$$

Assuming that the starting time t_0 is zero, then at time t during lane changing procedure, the displacement from the starting lane to the target lane is denoted by $y_d(t)$, so the instantaneous radius of the vehicle's center M yields $R - y_d(t)$, and the angular velocity of M around the instantaneous center O_R is obtained as $v_d(t)/[R - y_d(t)]$. Hence, at time t, the rotated angle of the vehicle around O_R can be calculated by the integral operation as

$$\alpha = \int_0^t \frac{v_d(t)}{R - y_d(t)}. \tag{4}$$

Here the values of vehicle's desired motion states at the time t during lane changing maneuver can be derived. Along the x-axis, the desired displacement, velocity, and acceleration can be calculated as

$$\begin{aligned} x_r(t) &= [R - y_d(t)] \sin\alpha, \\ \dot{x}_r(t) &= v_d(t) \cos\alpha - \dot{y}_d(t) \sin\alpha, \\ \ddot{x}_r(t) &= \left[\dot{v}_d(t) - \frac{v_d(t)\,\dot{y}_d(t)}{R - y_d(t)}\right] \cos\alpha \\ &\quad + \left[\ddot{y}_d(t) + \frac{v_d^2(t)}{R - y_d(t)}\right] \sin\alpha. \end{aligned} \tag{5}$$

Along the y-axis, the desired displacement, velocity, and acceleration can be calculated as

$$\begin{aligned} y_r(t) &= R - [R - y_d(t)] \cos\alpha, \\ \dot{y}_r(t) &= v_d(t) \sin\alpha + \dot{y}_d(t) \cos\alpha, \\ \ddot{y}_r(t) &= \left[\dot{v}_d(t) - \frac{v_d(t)\,\dot{y}_d(t)}{R - y_d(t)}\right] \sin\alpha \\ &\quad + \left[\ddot{y}_d(t) + \frac{v_d^2(t)}{R - y_d(t)}\right] \cos\alpha \end{aligned} \tag{6}$$

and the reference yaw angle and yaw angular velocity can be determined as

$$\begin{aligned} \theta_r(t) &= \arctan\frac{\dot{y}_r(t)}{\dot{x}_r(t)}, \\ \dot{\theta}_r(t) &= \frac{\ddot{y}_r(t)\,\dot{x}_r(t) - \dot{y}_r(t)\,\ddot{x}_r(t)}{\dot{x}_r^2(t) + \dot{y}_r^2(t)}. \end{aligned} \tag{7}$$

3. Trajectory Tracking Controller Design

3.1. Vehicle Kinematics and Tracking Error Model. Due to the directionality of the vehicle motion, the vehicle's position and orientation are described by two independent coordinates, which are world coordinate system Oxy and local coordinate system Mij. This paper takes the center of the vehicle driving wheels as the origin of Mij. The position and orientation, namely, the posture of an intelligent vehicle, are shown in Figure 3.

The kinematics model of the vehicle is the starting point to model the kinematics of the lateral and orientation errors. The vehicle model is approximated by the popular Ackerman model [17], regarding the vehicle as rigid body and assuming that the two front wheels turn slightly differentially. Thus, the instantaneous rotation center can be purely computed by

kinematic means. The nonlinear vehicle kinematics model can be described as [18]

$$\dot{p}_c = \begin{bmatrix} \dot{x}_c \\ \dot{y}_c \\ \dot{\theta}_c \end{bmatrix} = \begin{bmatrix} \cos\theta_c & 0 \\ \sin\theta_c & 0 \\ 0 & 1 \end{bmatrix} \begin{bmatrix} v_c \\ \omega_c \end{bmatrix} = Ju_c, \tag{8}$$

where $p_c = [x_c \ \ y_c \ \ \theta_c]^T \in R^3$ is the vehicle's current posture. $M(x_c \ \ y_c)$ is the vehicle's current position in Oxy. θ_c is the vehicle's current moving orientation along x-axis anticlockwise; namely, it is the angle between the coordinate system of Oxy and Mij. Assuming that the control vector $u_c = [v_c \ \ \omega_c]^T \in R^2$, $v_c > 0$, u_c is a function of time t. Here, $v_c \in R$ denotes the linear velocity of the midpoint of the vehicle rear axle, denoted as control point. $\omega_c \in R$ indicts the angular velocity of the intelligent vehicle. Both of them are input variables in the kinematics model. J denotes the velocity Jacobian matrix of the vehicle.

As shown in Figure 1, assuming that $p_r = [x_r \ \ y_r \ \ \theta_r]^T \in R^3$ is the vehicle's reference posture, $N(x_r \ \ y_r)$ indicts the vehicle's reference position, and θ_r denotes its reference moving orientation. It is necessary to define a suitable representation for the vehicle trajectory tracking error. This step is all the more important that an adequate choice significantly facilitates the control design [19]. In order to track a given trajectory smoothly, a path must be computed from a given initial location and heading to some target point on the desired trajectory. A tracking error function is generally defined by a vector between the predictive reference vector and a controlled vehicle traveling vector. The error functions are a velocity equation that is calculated by current posture, which is derived from the velocity equation [20]. Therefore, the relationship between control vector and the posture error should be explained. To achieve the tracking performance of $p_c \to p_r$ when $t \to \infty$, the tracking error vector $p_e = [x_e \ \ y_e \ \ \theta_e]^T \in R^3$ in Mij can be explained as follows:

$$p_e = \begin{bmatrix} x_e \\ y_e \\ \theta_e \end{bmatrix}_{(Mij)} = \begin{bmatrix} \cos\theta_c & \sin\theta_c & 0 \\ -\sin\theta_c & \cos\theta_c & 0 \\ 0 & 0 & 1 \end{bmatrix} \begin{bmatrix} x_r - x_c \\ y_r - y_c \\ \theta_r - \theta_c \end{bmatrix}_{(Oxy)} = J_1 (p_r - p_c)_{(Oxy)}, \tag{9}$$

where (x_e, y_e) is the phasor coordinate of MN in Mij and J_1 denotes the posture error transfer matrix, which transfers the posture error from Oxy to Mij. Obviously, the tracking error vector $(x_e, y_e, \theta_e) = 0$ if and only if $(x_c, y_c, \theta_c) = (x_r, y_r, \theta_r)$.

Differentiating the previous tracking error (9) and substituting $\dot{p}_c$ by (8), differential equation of vehicle posture error can be derived as

$$\dot{p}_e = \begin{bmatrix} \dot{x}_e \\ \dot{y}_e \\ \dot{\theta}_e \end{bmatrix} = \begin{bmatrix} \omega_c y_e - v_c + v_r \cos\theta_e \\ -\omega_c x_e + v_r \sin\theta_e \\ \omega_r - \omega_c \end{bmatrix}, \tag{10}$$

where v_r, ω_r are reference linear velocity and angular velocity of vehicle, respectively.

3.2. Controller Design. The intelligent vehicle has the nature of nonholonomic constraint feature because the number of system inputs is less than the number of system outputs or system states. Lots of control methods are applied to control the nonholonomic systems, for example, linear feedback [21], fuzzy logic [22], variable structure [23], neural network [24], and so on [25]. There have no absolutely more predominant scheme than the others to resolve the nonholonomic problems presently though each of the control methods has advantages and disadvantages. Since the higher-dimensional and nonlinear characteristics of nonholonomic constraints, integral backstepping technology is often used to derive the controller of the intelligent vehicle.

In this paper, the complex nonlinear system is split into several subsystems whose number is less than system rank. Then the Lyapunov functions are constructed and the virtual controller of each subsystem is designed. Finally, the controller which is uniformly and ultimately bounded could be achieved by integrator recession and gradual correction. Therefore, the issue of trajectory tracking for lane changing on curved road based on system kinematics model could be transformed to find an appropriated control input $u_c = [v_c \ \ \omega_c]^T$ under any initial error; then to track reference posture $p_r = [x_r \ \ y_r \ \ \theta_r]^T$ and input $u_r = [v_r \ \ \omega_r]^T$, such that the tracking error space $p_e = [x_e \ \ y_e \ \ \theta_e]^T$ is abounded and satisfies that

$$\lim_{t \to \infty} \left[|x_e(t)| + |y_e(t)| + |\theta_e(t)| \right] = 0. \tag{11}$$

In the tracking error model (10), the lateral position error y_e cannot be directly controlled. To overcome this difficulty, this paper defines a new virtual variable $\overline{x}_e$ by using integral backstepping [26], which is as follows:

$$\overline{x}_e = x_e - k_1 \frac{2n_1\omega_c}{1+\omega_c^2} y_e, \tag{12}$$

where k_1 and n_1 are positive constants and $k_1(2n_1\omega_c/(1+\omega_c^2))y_e$ is virtual feedback parameter.

Differentiating (12) yields

$$\dot{\overline{x}}_e = \dot{x}_e - k_1 \frac{2n_1 - 2n_1\omega_c^2}{\omega_c^4 + 2\omega_c^2 + 1} \dot{\omega}_c y_e - k_1 \frac{2n_1\omega_c}{1+\omega_c^2} \dot{y}_e. \tag{13}$$

In this case, when $x_e \to k_1(2n_1\omega_c/(1+\omega_c^2))y_e$ and $\theta_e \to 0$, according to system (3), it obtains that

$$\dot{y}_e = -x_e\omega_c = -k_1 \frac{2n_1\omega_c^2}{1+\omega_c^2} y_e. \tag{14}$$

Suppose a Lyapunov function $V_y = (1/2)y_e^2$; note that differentiating this Lyapunov function is

$$\dot{V}_y = y_e\dot{y}_e = -k_1 \frac{2n_1\omega_c^2}{1+\omega_c^2} y_e^2. \tag{15}$$

Obviously, $\forall t \in (0, +\infty)$, $\dot{V}_y \le 0$, and then system (14) will be asymptotically stabilized as $t \to 0$. According to the proposed preliminary, the trajectory controller can be given as

$$u_c = \begin{bmatrix} v_c \\ \omega_c \end{bmatrix} = \begin{bmatrix} v_r \cos\theta_e - k_1 \dfrac{2n_1 - 2n_1\omega_c^2}{\omega_c^4 + 2\omega_c^2 + 1}\dot{\omega}_c y_e + k_1 \dfrac{2n_1\omega_c^2}{1+\omega_c^2} x_e - k_1 v_r \dfrac{2n_1\omega_c}{1+\omega_c^2}\sin\theta_e + k_2 x_e - k_1 k_2 \dfrac{2n_1\omega_c}{1+\omega_c^2} y_e \\ \omega_r + 2k_3 v_r y_e \cos\dfrac{\theta_e}{2} + k_4 \sin\dfrac{\theta_e}{2} \end{bmatrix}, \tag{16}$$

where k_1,k_2,k_3, and k_4 are all positive constants whose value could determine the control directly.

3.3. Stability Analysis. According to the above analysis, a candidate Lyapunov function is defined as follows:

$$V = \frac{1}{2}\overline{x}_e^2 + \frac{1}{2}y_e^2 + \frac{2}{k_3}\left(1 - \cos\frac{\theta_e}{2}\right), \tag{17}$$

with $k_3 > 0$ and $\overline{x}_e$ given by (12). As can be directly verified; V is a positive-definite and lower bounded function. Differentiating (17) yields

$$\begin{aligned} \dot{V} &= \overline{x}_e\dot{\overline{x}}_e + y_e\dot{y}_e + \frac{1}{k_3}\sin\frac{\theta_e}{2}\dot{\theta}_e \\ &= \overline{x}_e\left(\dot{x}_e - k_1\frac{2n_1 - 2n_1\omega_c^2}{\omega_c^4 + 2\omega_c^2 + 1}\dot{\omega}_c y_e - k_1\frac{2n_1\omega_c}{1+\omega_c^2}\dot{y}_e\right) \\ &\quad + y_e\left(-\omega_c x_e + v_r\sin\theta_e\right) + \frac{1}{k_3}\sin\frac{\theta_e}{2}\left(\omega_r - \omega_c\right) \\ &= \overline{x}_e\left[\left(\omega_c y_e - v_c + v_r\cos\theta_e\right) - k_1\frac{2n_1 - 2n_1\omega_c^2}{\omega_c^4 + 2\omega_c^2 + 1}\dot{\omega}_c y_e\right. \\ &\qquad \left. - k_1\frac{2n_1\omega_c}{1+\omega_c^2}\left(-\omega_c x_e + v_r\sin\theta_e\right)\right] \\ &\quad + y_e\left[\left(-\omega_c\left(\overline{x}_e + k_1\frac{2n_1\omega_c}{1+\omega_c^2}y_e\right) + v_r\sin\theta_e\right)\right] \\ &\quad + \frac{1}{k_3}\sin\frac{\theta_e}{2}\left(\omega_r - \omega_c\right) \\ &= \overline{x}_e\left[v_r\cos\theta_e - v_c - k_1\frac{2n_1 - 2n_1\omega_c^2}{\omega_c^4 + 2\omega_c^2 + 1}\dot{\omega}_c y_e\right. \\ &\qquad \left. - k_1\frac{2n_1\omega_c}{1+\omega_c^2}\left(-\omega_c x_e + v_r\sin\theta_e\right)\right] \\ &\quad - k_1\frac{2n_1\omega_c^2}{1+\omega_c^2}y_e^2 \\ &\quad + \frac{1}{k_3}\sin\frac{\theta_e}{2}\left[\left(\omega_r - \omega_c\right) + 2k_3 v_r y_e\cos\frac{\theta_e}{2}\right]. \end{aligned} \tag{18}$$

Substituting (16) into (18) yields

$$\dot{V} = -k_2\overline{x}_e^2 - k_1\frac{2n_1\omega_c^2}{1+\omega_c^2}y_e^2 - \frac{k_4}{k_3}\sin^2\frac{\theta_e}{2}. \tag{19}$$

Note that k_1, k_2, k_3, and k_4 are all positive constants and $2n_1\omega_c^2/(1+\omega_c^2) > 0$, obviously, $\dot{V} \le 0$ for $\forall t \in (0, +\infty)$ according to (19). V is a class of function which has the characteristic of being continuously differentiable, positive definite, and bounded, so $\dot{V}$ is a negative semidefinite and uniformly continuous function.

Barbalat's lemma plays a key role in Lyapunov stability theory. Its basic theory is as follows. If a function $F(t,x)$ satisfies the following conditions: $F(t,x)$ is lower bounded and $\dot{F}(t,x)$ is negative semidefinite and uniformly continuous in time, then $\dot{F}(t,x) \to 0$ as $t \to \infty$. According to Barbalat's lemma, if $\dot{V} \to 0$ with $t \to \infty$, which is equivalent to that

$$\begin{aligned} &\overline{x}_e^2 \longrightarrow 0, \qquad y_e^2(t) \longrightarrow 0, \\ &\frac{2n_1\omega_c}{1+\omega_c^2}y_e(t) \longrightarrow 0, \qquad \sin^2\frac{\theta_e}{2} \longrightarrow 0. \end{aligned} \tag{20}$$

If $\sin^2(\theta_e/2) \to 0$, then

$$\lim_{t\to\infty}\theta_e \longrightarrow 0 \quad \left(\theta_e \in [-\pi, \pi)\right), \tag{21}$$

while $\lim_{t\to\infty}\overline{x}_e = 0$, that is to say,

$$x_e \longrightarrow k_1\frac{2n_1\omega_c}{1+\omega_c^2}y_e(t). \tag{22}$$

For the reason that v_r and ω_r are equal to zero with asynchronism, while ω_c is not identically zero and $k_1(2n_1\omega_c/(1+\omega_c^2))y_e(t) \to 0$ based on the control law, so $y_e \to \infty$.

Analyses above indicate that $x_e \to \infty$. $\theta_e \in [-\pi, \pi)$ is equivalent to $\theta_e \in [0, +\infty)$ because θ_e is a periodic function. Obviously, according to Barbara's lemma and Russell's invariant principle, it can be concluded that tracking errors $p_e = \begin{bmatrix} x_e & y_e & \theta_e \end{bmatrix}^T$ is globally, uniformly, and ultimately bounded. Therefore, with the controller (16), we can get $\lim_{t\to\infty}[|x_e(t)| + |y_e(t)| + |\theta_e(t)|] = 0$. That is to say, the designed trajectory tracking controller for the above lane changing maneuver has characteristics of global stability.

4. Simulation and Discussion

This paper performs a computer simulation on the intelligent vehicle by using the designed controller to tracking the predefined lane changing trajectory on curved roads. A brief diagram for this controller can be described by Figure 4.

According to the standard of roadway designing manual when design the highway alignment, it is necessary to establish the proper relation between design speed and curvature. The minimum radii of curves are important control values

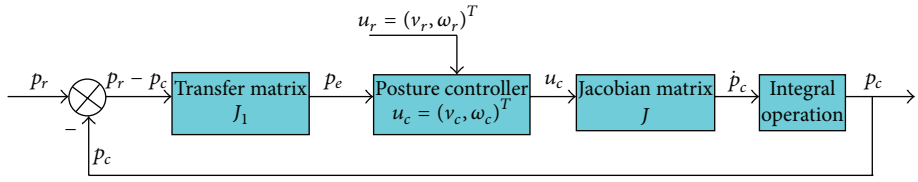

Figure 4: Schematic diagram of vehicle's control system structure.

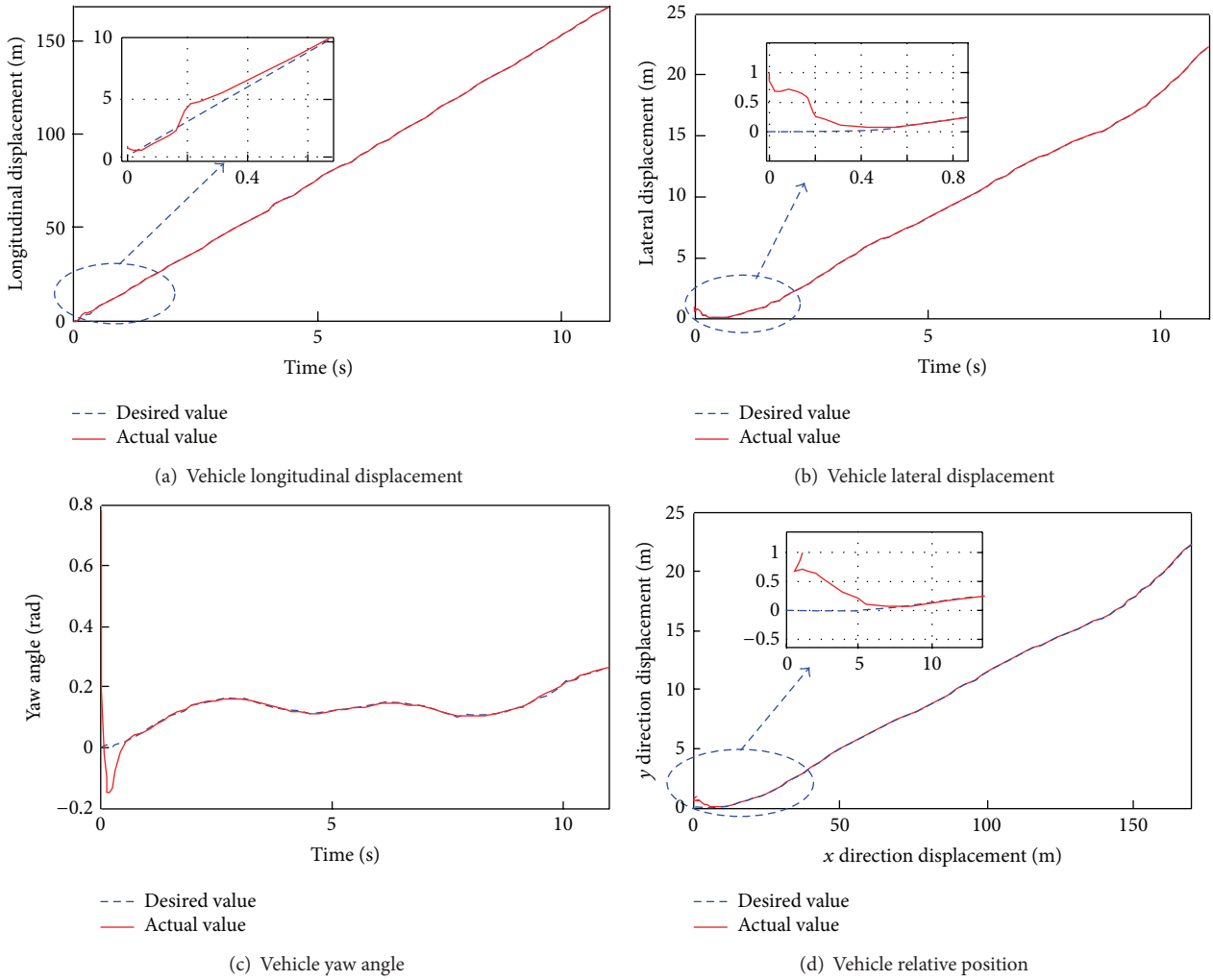

Figure 5: Trajectory tracking simulation results for lane changing.

in designing for safe operation. For example, when the design speed of road is higher than 100 km/h, then the usual minimum radius of curve must be longer than 650 m. The common width of the lane on highway is 3.75 m. The target of this paper is to guarantee the safety of intelligent vehicle on highway curved roads with high speed. Therefore, the parameters for the simulation scenarios are set considering the above specifications.

The curvature radius of the outside lane R is set to be 650 m, the space between the outside and inside lane d_w is 3.75 m, and the maximum of the desired lateral jerk $J_{\max}$ is 0.1 g/s. We can get that $t_1 = 1$ s, $t_2 = 1.5$ s from (2), so the time needed for lane changing is $t_5 = 5$ s. Here, the gravity acceleration $g = 10\,\text{m/s}^2$. In the simulation, the initial values of the desired longitudinal displacement and longitudinal velocity are 0 and 15 m/s, respectively, the longitudinal acceleration $\dot{v}_d(t)$ is described as (3), and the initial tracking error $[x_e \;\; y_e \;\; \theta_e]^T = [-1 \; -1 \; -\pi/4]^T$.

As a report from National Highway Traffic Safety Administration indicates, most lane changes are with a mean duration of over 11 s. Besides, to reflect the influence of radius difference between the outside and inside lane on lane changing trajectory, the process of the lane changing maneuver was divided into three steps. Step 1 conducts the action from the outside to the inside lane duration from 1–5 s. During step 2, the vehicle runs along the inside lane so as

Table 1: Parameters of the controller.

Symbol	k_1	k_2	k_3	k_4	n_1
Value	1.5	2	2	2.5	1

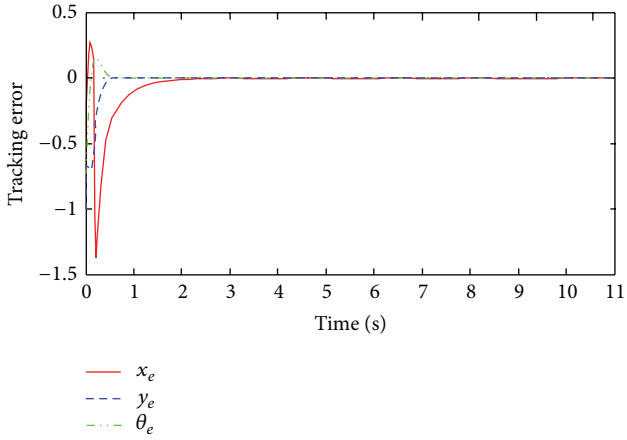

Figure 6: Trajectory tracking error for lane changing.

to avoid continuous lane changing maneuver. Step 3 conducts the action from the inside to the outside lane duration from 6–11 s. Therefore, the simulation time of the lane changing maneuver was set to be 11 s. The control parameters of the simulation are shown in Table 1.

The corresponding simulation results are given in Figures 5 and 6. Figure 5 is shown as the trajectory tracking simulation curves of lane changing, where the dotted lines are the desired states of lane changing and the solid lines denote the actual states.

Figures 5(a), 5(b), and 5(c) denote changes of the longitudinal displacement, the lateral displacement, and the yaw angle with process time t for lane changing on curved road, respectively. As can be seen from the figures above, these 3 actual states can all realize the tracking of corresponding desired state at about 0.6 s. Figure 5(d) is the x-y trajectory tracking curve, which describes the lane changing trajectory on curved road in Oxy; from the local enlarging graphs of this figure, we can get that the desired lane changing trajectory could be tracked effectively after longitudinal driving about 10 m.

The change of tracking error x_e, y_e, and θ_e with process time t is shown in Figure 6.

As shown in Figure 6, these 3 tracking errors described intelligent vehicle system all converge to zero asymptotically under the function of trajectory tracking controller. Simulation results demonstrate that the controller has characteristics of quick convergence and global stability, and it can realize ideal tracking of lane changing trajectory on curved road. Figure 7 displays the steering angle of the vehicle during the lane change maneuver.

Figure 8 shows the system control inputs, where (a) denotes the linear velocity input and (b) indicates the angular velocity input. The control input $u_c = [v_c \ \omega_c]^T$ tends to be stable at about 0.6 s in lane changing maneuver, and the intelligent vehicle system is globally stable. Additionally, from

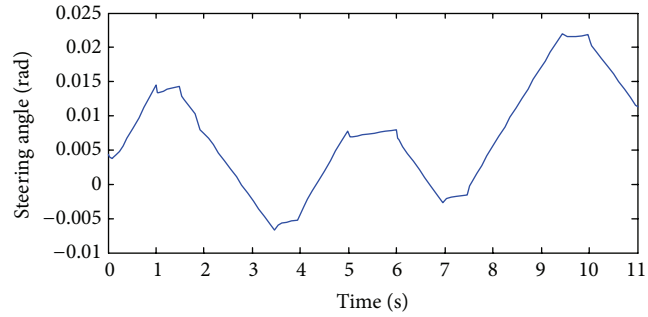

Figure 7: The steering angle of the intelligent vehicle.

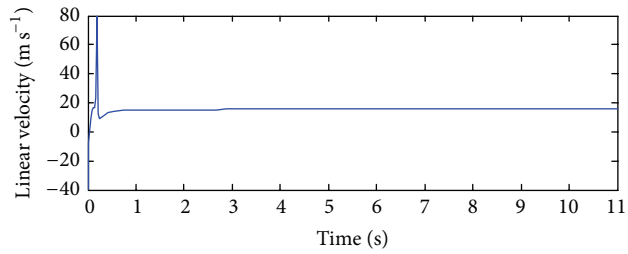

(a) Controller input of linear velocity u_c

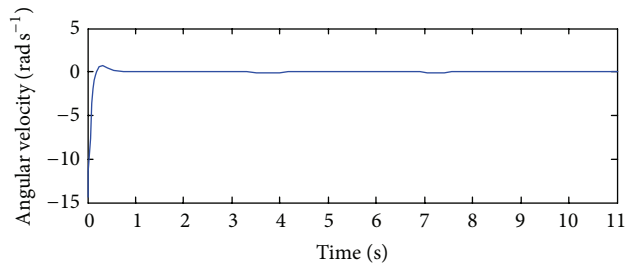

(b) Controller input of angular velocity ω_c

Figure 8: Inputs curves of the tracking controller.

(a) and (b), it can be seen that $|u_c|_{\max} = 16$ m/s and $|\omega_c|_{\max} = 0.08$ rad/s, which makes the control smoothing in vehicle's lane changing maneuver. Meanwhile, the linear velocity when driving along the inside lane is 15.5 m/s and the angular velocity is 0.02 rad/s.

5. Conclusions

In this paper, a lane changing trajectory is planned and tracked for lane changing of an intelligent vehicle on curved road. From the development in the previous sections and the simulation results above, we have the following conclusions.

(1) Taking into account the difference of curvature radius between the outside and inside lane, this paper utilizes the trajectory planning method based on trapezoidal acceleration profile to meet the restriction of the various curvatures and change rate for lane changing on curved road. Then it considers the coupled function of the vehicle's longitudinal and lateral motion on lane changing trajectory, namely, the curvature radius of which is a vector in lane changing maneuver. In order to track smoothly to a given trajectory,

the tracking error function is generated by a vector between the predictive reference vector and the vehicle real posture, which is derived from the velocity equation.

(2) Aiming to figure out the nonholonomic constraints of the tracking model and the strong coupling between vehicle's longitudinal and lateral motion, the trajectory tracking control algorithm is designed using integral backstepping with intermediate virtual controllers, which is devoted to the research of trajectory tracking for lane changing on curved road. Simulation results demonstrate that this controller can guarantee the convergences of both the relative position tracking errors and the position tracking synchronization.

Simulations have been carried out to demonstrate the effectiveness of the proposed control methods, but relevant tracking experiments on the intelligent vehicle prototype should be performed on the intelligent vehicle. Next step, we will concentrate on that to test and verify simulation results.

Conflict of Interests

The authors declare that there is no conflict of interests regarding the publication of this paper.

Acknowledgments

This research was financed by the National Natural Science Foundation of China (51305065 and 61175101), the Urumqi City Science and Technology Project (G121310001) and the Fundamental Research Funds for the Central Universities (DUT13JS02 and DUT13JS14).

References

[1] R. Gregor, M. Lützeler, M. Pellkofer, K.-H. Siedersberger, and E. D. Dickmanns, "EMS-vision: a perceptual system for intelligent vehicles," *IEEE Transactions on Intelligent Transportation Systems*, vol. 3, no. 1, pp. 48–59, 2002.

[2] K. Choi, S. Park, S. Kim et al., "Methods to detect road features for video-based in-vehicle navigation systems," *Journal of Intelligent Transportation Systems*, vol. 14, no. 1, pp. 13–26, 2010.

[3] R. Sengupta, S. Rezaei, S. E. Shladover, D. Cody, S. Dickey, and H. Krishnan, "Cooperative collision warning systems: concept definition and experimental implementation," *Journal of Intelligent Transportation Systems*, vol. 11, no. 3, pp. 143–155, 2007.

[4] L. Cai, A. B. Rad, and W. Chan, "An intelligent longitudinal controller for application in semiautonomous vehicles," *IEEE Transactions on Industrial Electronics*, vol. 57, no. 4, pp. 1487–1497, 2010.

[5] B. Yu, Z. Z. Yang, and L. I. S, "Real-time partway deadheading strategy based on transit service reliability assessment," *Transportation Research A*, vol. 46, no. 8, pp. 1265–1279, 2012.

[6] J. E. Naranjo, C. González, R. García, and T. de Pedro, "Lane-change fuzzy control in autonomous vehicles for the overtaking maneuver," *IEEE Transactions on Intelligent Transportation Systems*, vol. 9, no. 3, pp. 438–450, 2008.

[7] D. B. Ren, J. Y. Zhang, J. M. Zhang, and S. M. Cui, "Trajectory planning and yaw rate tracking control for lane changing of intelligent vehicle on curved road," *Science China Technological Sciences*, vol. 54, no. 3, pp. 630–642, 2011.

[8] D. Soudbakhsh, A. Eskandarian, and D. Chichka, "Vehicle steering maneuvers with direct trajectory optimization," in *Proceedings of the IEEE Intelligent Vehicles Symposium (IV '10)*, pp. 449–453, San Diego, Calif, USA, June 2010.

[9] C. S. Yang, Z. Yang, X. N. Huang, S. B. Li, and Q. Zhang, "Modeling and robust trajectory tracking control for a novel six-rotor unmanned aerial vehicle," *Mathematical Problems in Engineering*, vol. 2013, Article ID 673525, 13 pages, 2013.

[10] C. Hatipoglu, Ü. Özguner, and K. A. Redmill, "Automated lane change controller design," *IEEE Transactions on Intelligent Transportation Systems*, vol. 4, no. 1, pp. 13–22, 2003.

[11] S. Ammoun, F. Nashashibi, and C. Laurgeau, "An analysis of the lane changing manoeuvre on roads: the contribution of inter-vehicle cooperation via communication," in *Proceedings of the IEEE Intelligent Vehicles Symposium (IV '07)*, pp. 1095–1100, Istanbul, Turkey, June 2007.

[12] T. Lee, B. Kim, K. Yi, and C. Jeong, "Development of lane change driver model for closed-loop simulation of the active safety system," in *Proceedings of the 14th IEEE International Intelligent Transportation Systems Conference (ITSC '11)*, pp. 56–61, Washington, DC, USA, October 2011.

[13] R. Toledo-Moreo and M. A. Zamora-Izquierdo, "IMM-based lane-change prediction in highways with low-cost GPS/INS," *IEEE Transactions on Intelligent Transportation Systems*, vol. 10, no. 1, pp. 180–185, 2009.

[14] M. L. Ho, P. T. Chan, and A. B. Rad, "Lane change algorithm for autonomous vehicles via virtual curvature method," *Journal of Advanced Transportation*, vol. 43, no. 1, pp. 47–70, 2009.

[15] F. You, R. Wang, R. Zhang, and W. Xiong, "Lane changing and overtaking control method for intelligent vehicle based on backstepping algorithm," *Transactions of the Chinese Society of Agricultural Machinery*, vol. 39, no. 6, pp. 42–45, 2008.

[16] B. Z. Yao, P. Hu, M. H. Zhang, and S. Wang, "Artificial bee colony algorithm with scanning strategy for periodic vehicle routing problem," *SIMULATION*, vol. 89, no. 6, pp. 762–770, 2013.

[17] J. Ackermann, J. Guldner, W. Sienel, R. Steinhauser, and V. I. Utkin, "Linear and nonlinear controller design for robust automatic steering," *IEEE Transactions on Control Systems Technology*, vol. 3, no. 1, pp. 132–143, 1995.

[18] M. A. Sotelo, E. Naranjo, R. García, T. D. Pedro, and C. González, "Comparative study of chained systems theory and fuzzy logic as a solution for the nonlinear lateral control of a road vehicle," *Nonlinear Dynamics*, vol. 49, no. 4, pp. 463–474, 2007.

[19] R. Rajamani, H. Tan, B. K. Law, and W. Zhang, "Demonstration of integrated longitudinal and lateral control for the operation of automated vehicles in platoons," *IEEE Transactions on Control Systems Technology*, vol. 8, no. 4, pp. 695–708, 2000.

[20] J. Lee and W. Yoo, "An improved model-based predictive control of vehicle trajectory by using nonlinear function," *Journal of Mechanical Science and Technology*, vol. 23, no. 4, pp. 918–922, 2009.

[21] Z. Li, S. S. Ge, M. Adams, and W. S. Wijesoma, "Robust adaptive control of uncertain force/motion constrained nonholonomic mobile manipulators," *Automatica*, vol. 44, no. 3, pp. 776–784, 2008.

[22] D. Chwa, "Sliding-mode tracking control of nonholonomic wheeled mobile robots in polar coordinates," *IEEE Transactions on Control Systems Technology*, vol. 12, no. 4, pp. 637–644, 2004.

[23] T. Das and I. N. Kar, "Design and implementation of an adaptive fuzzy logic-based controller for wheeled mobile robots," *IEEE Transactions on Control Systems Technology*, vol. 14, no. 3, pp. 501–510, 2006.

[24] C. X. Ding, W. H. Wang, X. Wang, and M. Baumann, "A neural network model for driver's lane-changing trajectory prediction in urban traffic flow," *Mathematical Problems in Engineering*, vol. 2013, Article ID 967358, 8 pages, 2013.

[25] B. Yao, C. Yang, J. Yao, and J. Sun, "Tunnel surrounding rock displacement prediction using support vector machine," *International Journal of Computational Intelligence Systems*, vol. 3, no. 6, pp. 843–852, 2010.

[26] A. Rantzer, "A dual to Lyapunov's stability theorem," *Systems and Control Letters*, vol. 42, no. 3, pp. 161–168, 2001.

Hindawi Publishing Corporation
Mathematical Problems in Engineering
Volume 2014, Article ID 850141, 8 pages
http://dx.doi.org/10.1155/2014/850141

Research Article

Beam Structure Damage Identification Based on BP Neural Network and Support Vector Machine

Bo Yan,[1] Yao Cui,[1] Lin Zhang,[1] Chao Zhang,[1] Yongzhi Yang,[1] Zhenming Bao,[2] and Guobao Ning[3]

[1] *Transportation Management College, Dalian Maritime University, Dalian 116026, China*
[2] *School of Naval Architecture Engineering, Dalian University of Technology, Dalian 116024, China*
[3] *School of Automotive Studies, Tongji University, Shanghai 201804, China*

Correspondence should be addressed to Guobao Ning; guobao_tj@163.com

Received 10 November 2013; Revised 29 November 2013; Accepted 30 November 2013; Published 6 January 2014

Academic Editor: Rui Mu

It is not easy to find marine cracks of structures by directly manual testing. When the cracks of important components are extended under extreme offshore environment, the whole structure would lose efficacy, endanger the staff's safety, and course a significant economic loss and marine environment pollution. Thus, early discovery of structure cracks is very important. In this paper, a beam structure damage identification model based on intelligent algorithm is firstly proposed to identify partial cracks in supported beams on ocean platform. In order to obtain the replacement mode and strain mode of the beams, the paper takes simple supported beam with single crack and double cracks as an example. The results show that the difference curves of strain mode change drastically only on the injured part and different degrees of injury would result in different mutation degrees of difference curve more or less. While the model based on support vector machine (SVM) and BP neural network can identify cracks of supported beam intelligently, the methods can discern injured degrees of sound condition, single crack, and double cracks. Furthermore, the two methods are compared. The results show that the two methods presented in the paper have a preferable identification precision and adaptation. And damage identification based on support vector machine (SVM) has smaller error results.

1. Introduction

The designed life of an offshore platform is usually in 15~20 years. The maintenance cost of it is extremely expensive, but compared with its purchasing expense, it seems to be acceptable. As a result, from economic angle, it is important to evaluate the new platform, estimate residual life of existing platform, and prolong the life time of jacket platform for insuring production safety and improving production efficiency, extending lifespan and saving maintenance cost. Thus, it is necessary to provide an effective beam structure damage identification model to timely detect damage, evaluate damage degree, then verify and improve the design method of current platform, and provide references for future structure residual life assessment.

There are many literatures about the damage identification problem. Kim and Melhem [1] summarized the applications of the wavelet analysis method in system damage checking and health monitoring in mechanical and other structures. Sun and Chang [2] utilized wavelet packet transform to analyze the signal of structure measurement; besides damage index based on wavelet packet is given and combined with neural network to identify the damage. In the 1970s, Cawley and Adams [3] proposed that using vibration test data into analog neural network is a method that could be applied to detect and research material damage. Elkordy et al. [4] did structural damage detection by BP network. The research is based on the experimental data of a shaker and a simulated data of a finite element to carry out the network training. And then the paper used network after training to identify

structural damage. Pandey and Barai [5] took the replacement under static load as multilayer perceptron model's input to test and recognize the damages of steel bridge. Kirkegaard and Rytter [6] took advantage of the frequency change before and after the injury and used the BP neural network to locate the damage and identify the damage degree of steel beam. Vakil-Baghmisheh et al. [7] proposed an alternative method of material structural damage identification based on genetic algorithm. An analysis model of a cantilever beam with crack was applied to obtain the frequency of structure by numerical simulation. Chou and Ghaboussi [8] thought of the damage problem as optimization problem and solved the problem with genetic algorithms. Several freedom of static was used to measure the displacement to determine the cross-sectional area and the changes of structural elastic modulus. Other successful applications can be found in literatures [9, 10].

This paper attempts to propose a beam structure damage identification model based on intelligent algorithm to identify the crack of noncracked beam, since BP neural network and SVM have been successfully applied in solving these kinds of complex problems [11–19]. Thus, BP neural network and SVM are also applied to identify the damage degree of the beam with crack intelligently in the conditions of good, single, and double cracks.

This paper introduces beam structure damage identification models based on BP neural network and SVM, respectively. Therefore, the remainder of this paper is organized as follows. Section 2 describes beam structure damage identification models based on BP neural network and SVM, respectively. Section 3 attempted to determinate the input parameters. In Section 4, an empirical example was used to examine the effectiveness of the beam structure damage identification models. Conclusions are displayed in Section 5.

2. Beam Structure Damage Identification Model

2.1. Artificial Neural Network. Artificial network, a computer artificial intelligence, based on neural structure and physiology simulates human thinking. Modern computers specialize in calculation and quick information processing. But for the capacity of dealing with complexity (schema awareness, pattern recognition and making final decision in complex environment), modern computers are nowhere near as human. Modern computers can only implement some form of the stored-program architecture according to program edited in advance and do not have the capacity to adapt to complex environment and study in the environment. The differences between the way human brain works and the functions of computer system are great. Brain is a highly complex, nonlinear, and parallel processing system which is formed from a jumble of interconnected basic units. Though the reaction speed of brain single neuron is lower than the speed of general computer's basic unit (logic gate), about 5 orders of magnitude, the number of neuron is huge, and every single neuron can connect with thousands or more other neurons. The brain's speed of processing complex problems is far more quick than computer.

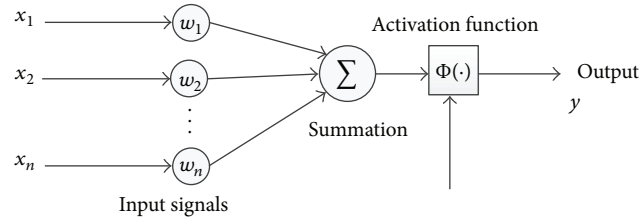

Figure 1: Model of the neuron.

Therefore, human takes advantage of the characteristics of brain's operating mechanism and organizational structure, from the perspective of emulating the brain intelligence, looking for a better way to storage and handle information. Ultimately, a new integrated information system based on new intelligent computer is constructed which is closer to human intelligence and can be used for processing complex information. In this paper, artificial neural network is used to identify the degree of damage of beam structural.

2.1.1. Neural Model. The model of neuron is shown in Figure 1. The basic unit of ANN and the basic elements are as follows.

(1) A group of related connection. The connection strength is represented by the weight given on the connection line. It is in the active state if the weight value is positive and in the suppressive state if the weight value is negative.

(2) Summation unit. It is used to require the weighted sum of a number of input signals.

(3) Nonlinear activation function. It plays the role of the nonlinear mapping and limits the output amplitude variation range of neuron. The common activation function includes segmented linear function, the threshold value function, sigmoid function, and so on.

2.1.2. BP Neural Network. BP neural network is mostly used in the beam structure damage identification. BP network algorithm consists of reverse and forward propagation. It contains hidden layer, output layer, and input layer, in which the states of neurons in each layer can only influence the neurons under them. Initially, through the process of forward propagation, the signal is transmitted from the input layer to hidden layer and calculated in the hidden layer. The results calculated in hidden layer are transmitted to output layer and outputted. The results are compared with the expected value, and the error will be corrected through the reverse propagation, that is, backtrack. The function in the hidden layer used in the process is called activation function. This process will be repeated. The weight will be changed according to the results in last layer during every reverse calculation to reduce the error. When the error meets the requirement, stop the calculation.

The change of BP network connection weights has a high level of confidence. However, this algorithm is a method of

gradient descent search, so it has some inherent characteristics which are shown as follows.

(1) Slower Convergence. In dealing with complex issues, BP algorithm may need training in repetition to achieve convergence. And when the whole network reaches a certain level after training, the convergence speed of BP network will slow down to a very low level and occupy the machine for a long time.

(2) Easy to Fall into the Local Minima of Error Function. As the BP algorithm uses a gradient descent method to solve problems, the training results gradually approach the minimum of error along the curve surface of the error function. However, when training for a complex problem, its error function is always high-dimensional space surface. The training results are easy to fall into the local minimum rather than the global minimum. Therefore, although the network weights under the BP algorithm converge to a unique value, it is difficult to ensure that the error surface obtained is a global minimum solution.

(3) The Instability of System Training. The change of weight is determined by each learning rate. If the learning rate is large, it can cause the system to become unstable. In the initial training of the network, larger learning rate can obtain faster convergence rate and better error decreases. But it is limited to the early stage of training. When training reaches later period, the high-speed learning efficiency may make the correction rate of network weight too large. So in the processing of error correction, the error beyond the minimum and the system fall into the situation of never converge, making the whole system unstable.

In the classic BP algorithm, the learning rate is often set to be a constant, which largely determines the performance of the algorithm. High learning rate can improve the efficiency of the algorithm effectively but often causes excessive fluctuations in weight and makes the system not stable. Low learning rate will elongate learning time and occupy too much machine. To solve this problem, related researchers proposed a variety of adaptive learning rate methods. In this paper, competitive learning method is used to fix the entire BP neural network.

2.2. Basic Theory of Support Vector Machine. Many traditional statistical methods based on law of large numbers require large amounts of sample data to be the theoretical basis, which often do not fit with the reality. Because, in practice, the situation where the sample number is shortage is very common. The use of these methods makes it difficult to obtain satisfactory results. Thus, in the last century, Vapnik, and so forth, studied the statistical learning theory (SLT) deeply, which is a specialized method to study how to use limited number of samples for machine. The statistical inference rules of the theory only consider the asymptotic properties and can find the optimal solution under the conditions of limited information. In mid-1990s, the machine learning theory under the conditions of the limited sample was developed and applied gradually. And ultimately, a relatively complete theoretical system is formed [20].

Support vector machine (SVM) was proposed by Vapnik [21–23], which is a statistical-based learning method. SVM is based on a limited sample data and balances the reasoning ability and complexity of the model to achieve optimal results. This approach has its unique advantages in solving high-dimensional pattern recognition, nonlinear, and small sample event and can also be used in the regression analysis and so on [24].

2.2.1. The Feature of SVM. The basic features of SVM for classifying and regressing problems are as follows [25].

(1) SVM is specific for the case of limited samples. The calculated objective is to obtain the optimal solution under the existing data rather than when the samples are infinity.

(2) When the data is linear inseparability, the linearly nonseparable data in low-dimensional vector space is transited to high-dimensional vector space by nonlinear transformation to make it linearly separable. The data is analyzed and calculated according to the characteristics of nonlinear part in high-dimensional vector space.

(3) To minimize the risk experience, confidence interval, and optimization of the overall results of learning machine, according to the theory of structural risk minimization, an optimal separating hyperplane must be obtained in space.

2.2.2. Principle of SVM. Generalized optimal separating hyperplane. Assume that the training data

$$(x_1, y_1), \ldots, (x_l, y_l) \quad x \in R^n, \ y \in (+1, -1) \tag{1}$$

can be separated by a hyperplane

$$(\omega \cdot x) - b = 0 \tag{2}$$

without error. When the distance between the hyperplane and its nearest training point is maximum, the hyperplane is optimal hyperplane.

To describe the hyperplane, the following forms are used

$$\begin{aligned} (\omega \cdot x_i) - b \geq 1, &\quad \text{if } y_i = 1, \\ (\omega \cdot x_i) - b \leq -1, &\quad \text{if } y_i = -1. \end{aligned} \tag{3}$$

Use the compact form of these inequalities

$$y_i \left[(\omega \cdot x_i) - b \right] \geq 1, \quad i = 1, \ldots, l. \tag{4}$$

It is easy to verify that the optimal hyperplane satisfies condition formula (3) and attains the following:

$$\phi(\omega) = \|\omega\|^2 \tag{5}$$

minimum.

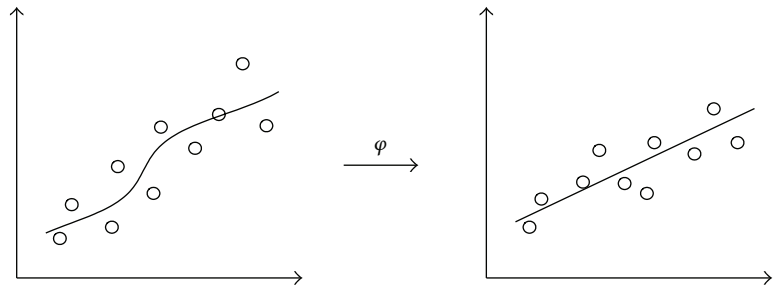

Figure 2: The mapping from the original space to feature space.

For a hyperplane,

$$(\omega^* \cdot x) - b = 0, \qquad \|\omega^*\| = 1 \tag{6}$$

if vector x is classified according to the following form:

$$y = \begin{cases} 1 & \text{if } (\omega^* \cdot x) - b \geq \Delta \\ -1 & \text{if } (\omega^* \cdot x) - b \geq \Delta. \end{cases} \tag{7}$$

It is called Δ interval separating hyperplane and has the following information about Δ collection interval separating hyperplane of VC dimension theorem.

Nonlinear problems change from low-dimensional feature space to high-dimensional feature space and the optimal linear hyperplane can be obtained in this space. Similarly, with regard to the linearly inseparable problem, by the transformation of nonlinear mapping function, the input data in the low-dimensional space is converted into the high-dimensional space, so as to achieve the purpose of solving the problem. To solve the above problem in the high-dimensional feature space, it only needs to make inner product operation to kernel function $K(x_i, x_j) = \varnothing(x_i)\varnothing(x_j)$ in original space. This is determined by the fact that there are no other operations expecting the inner product operation among the training samples of classification function and optimization functions.

Therefore, most of the nonlinear problems in original space can be transformed into a linear separable problem after space conversion, as shown in Figure 2.

However, the difficulty of transforming the nonlinear problem into a high-dimensional space is that the nonlinear mapping in this process may be very complex. According to functional theory, as long as the kernel function $K(x_i, x_j)$ satisfies Mercer conditions, it must correspond to the inner product of one space. For such conversion, it is not necessary to have a specific transformation process. In order to avoid complex calculations in such high-dimensional space, the kernel function $K(x, x')$ is used to replace the dot product of optimal separating hyperplane and the problem can be solved. However, this method is based on the fact that the linear classification function does not include any other operations expecting support vector inner product of the training sample and the sample to be classified. At the same time, in the solution process, this function only takes the inner product operation to training samples. The classification function of this method in the sample space can be written as

$$f(x) = \operatorname{sgn}\left(\sum_{i=1}^{n} \alpha_i^* y_i K(x_i, y_i)\right) + b. \tag{8}$$

The choice of kernel function needs to meet Mercer conditions, and different forms of kernel functions can produce different support vector machines (see Table 1).

Table 1: Common kernel function.

Kernel function	Expression	Parameter
Liner kernel function	$K(x_i, x_j) = x_i \cdot x_j$	
Polynomial kernel function	$K(x_i, x_j) = (x_i \cdot x_j + 1)^d$	d
Radial basis function (RBF) kernel function	$K(x_i, x_j) = \exp\left(-\gamma \|x_i - x_j\|^2\right)$	$\gamma > 0$
Sigmoid kernel function	$K(x_i, x_j) = \tanh\left(b(x_i, x_j) + c\right)$	b, c

3. Input Parameter Determination

In the process of damage identification, when training the sample data is based on the parameters of displacement vibration models or their derivatives, whether it is artificial neural network or support vector machine, the final recognition results may produce great error and sometimes even produce disorder phenomenon, so the parameter settings must be paid attention to. Strain mode is a very sensitive parameter to injury. It has advantages of high accuracy, being easy to test, mature analytical methods, and many others. In fact, when the artificial neural network is used to train, if the accuracy of the input parameters is ensured to be high enough, the results of the degree of damage recognition must be accurate and efficient. On the contrary, if the precision is lacking, the recognition results can not be guaranteed. Therefore, it is reasonable to select the strain mode difference parameter as the input data of support vector machine model and the neural network in this chapter. The flowchart of the two smart methods of beam structure damage identification is in Figure 3.

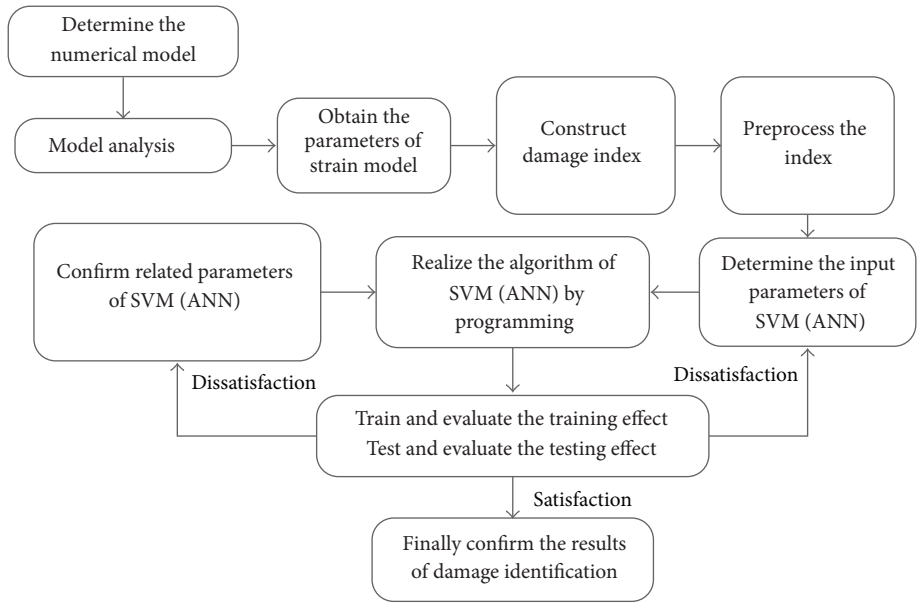

Figure 3: Flowchart of damage identification for beam structure.

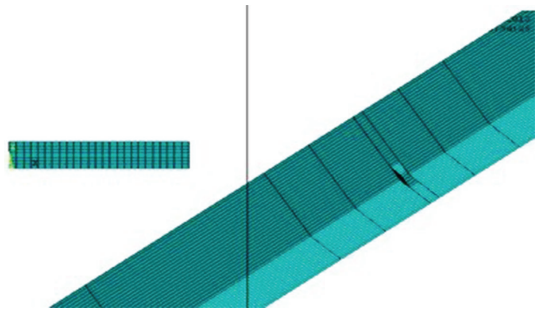

Figure 4: FEM model of a supported beam with local damage.

Table 2: The damage identification results of single quarter crack with 1% noise level.

Working condition number	Damage element number	Ideal result of SVM	Actual result of SVM
No. 1	10	3.125%	3.150%
No. 2	10	6.250%	6.300%
No. 3	10	12.500%	12.520%
No. 4	10	15.625%	15.650%

4. Empirical Example

A simple supported beam with localized damage is shown in Figure 4. The geometric dimensions are that the length is 400 mm, the width is 10 mm, and the height is 2 mm. The beam is used to simulate the conditions, the fourth quarter single crack across, the fourth quarter double cracks across and so on. The crack length is 1/5 of the beam width, and the crack depth is 3.125%, 6.250%, 12.500%, and 15.625% of the effective section height. The crack width is 2 mm. The modulus is 211 GPa and density is 7850 Kg/m^3. The Poisson's ratio is set to be 0.33. Eight-node SOLID45 solid element of ANSYS finite element analysis software is applied to model. Grid is divided into 25 equal parts in horizon, 16 equal parts vertically and 40 equal parts in length.

4.1. Intelligent Recognition with BP Neural Network. The training samples of BP neural network should choose continuous third strain mode difference of beam. Thus, input vector of network training is three-dimensional and the output vector is one-dimensional. They represent the damage degree of one unit. So, in order to build a three-tier network, three input layer neurons and output layer neurons are needed. Through repeated trials, when the neurons in hidden layer are 6 in the final, the training effect is optimal (speed and accuracy of training). Assuming the damage degree of beam was 3.125%, 6.250%, 12.500%, and 15.625%, the samples whose damage degree is 20% are used as test samples to verify the damage identification capability of the neural network. At the same time, the effects of noise are taken into account. Thus, random noise is added into the strain model when the damage cases were calculated. The added noise levels are 1% and 3%. The test results of the network are shown in Tables 2 and 3.

It can be seen from Table 2, when the level of noise is 1%, the effect of identification is good, while the identification errors of each unit are all small. The largest error is only 0.8% which occurred in the case 3. The recognition effect is still good when the level of noise is 3%, but the biggest error is slightly larger, reaching 1.12% which appeared in the case 3. Therefore, when the noise level is 1%, the recognition results of damage are more excellent which can be seen in Tables 4 and 5.

Table 3: The damage identification results of single quarter crack with 3% noise level.

Working condition number	Damage element number	Ideal result of SVM	Actual result of SVM
No. 1	10	3.125%	3.160%
No. 2	10	6.250%	6.310%
No. 3	10	12.500%	12.540%
No. 4	10	15.625%	15.680%

Table 4: The damage identification results of double cracks with 1% noise level.

Working condition number	Damage element number	Ideal result of SVM	Actual result of SVM
No. 1	10	3.125%	3.180%
	20	3.125%	3.150%
No. 2	10	6.250%	6.320%
	20	6.250%	6.300%
No. 3	10	12.500%	12.490%
	20	12.500%	12.460%
No. 4	10	15.625%	15.660%
	20	15.625%	15.640%

Table 5: The damage identification results of double cracks with 3% noise level.

Working condition number	Damage element number	Ideal result of SVM	Actual result of SVM
No. 1	10	3.125%	3.190%
	20	3.125%	3.170%
No. 2	10	6.250%	6.350%
	20	6.250%	6.330%
No. 3	10	12.500%	12.460%
	20	12.500%	12.470%
No. 4	10	15.625%	15.690%
	20	15.625%	15.670%

4.2. Intelligent Recognition with Support Vector Machine. Assuming that the damage extent of beam is 3.125%, 6.250%, 12.500%, and 15.625%, these samples are taken as the training samples. The samples whose damage extent is 20% are used as test samples to verify the damage identification capability of this neural network. The input parameters are the strain modes difference of the first 3 structural orders. The damage recognition results are shown in Tables 6 and 7.

4.3. The Comparison of Recognition Performance between BP Neural Networks and Support Vector Machine

(1) The Comparison of Run Time. It needs at least 37 times of iterations on average that the BP neural network can achieve the specified error, while the average running time is 3 minutes and 12 seconds. The SVM requires only one minute time to achieve the results. This showed that the learning convergence speed of SVM is quick and can approximate any nonlinear function.

Table 6: Damage degree recognition results of single crack in support vector machine.

Working condition number	Damage element number	Ideal result of SVM	Actual result of SVM
No. 1	10	3.125%	3.200%
No. 2	10	6.250%	6.290%
No. 3	10	12.500%	12.510%
No. 4	10	15.625%	15.640%

Table 7: Damage degree recognition results of double cracks in support vector machine.

Working condition number	Damage element number	Ideal result of SVM	Actual result of SVM
No. 1	10	3.125%	3.140%
	20	3.125%	3.130%
No. 2	10	6.250%	6.290%
	20	6.250%	6.280%
No. 3	10	12.500%	12.470%
	20	12.500%	12.450%
No. 4	10	15.625%	15.650%
	20	15.625%	15.630%

(2) The Contrast of Recognition Results. The difference of prediction error between SVM model and BP neural network model is less. The error has been very small in some units and did not affect the discrimination of damage elements. Through the errors of the two methods, support vector machine is slightly better than BP neural network model. This is because the support vector machine is built on the VC dimension theory and structural risk minimization principle. Its generalization ability is stronger and can effectively avoid the overlearning problems. So SVM can ensure finding the global optimal solution. Therefore, support vector machine algorithm is more accurate for solving the damage position problem of beam structural. The accuracy of recognition results for single crack and double cracks with the SVM is better than the results of BP neural network. So it is a better approach to identify the degree of injury. The average recognition accuracy of structural damage degree of the two methods is shown in Table 8.

4.4. Performance Analysis of the Identification Models Based on BP Neural Networks and SVM. The results of SVM and BP neural network are significantly better than the results of ordinary SVM or BP neural network model. Due to continuous interactive analysis and improvement, the results of the improved model are obtained from smart model. This

Table 8: Damage degree determination accuracy of the two methods.

Type	Working condition number	Recognition efficiency of BP neural network	Recognition efficiency of SVM
Single crack	1	99.9%	100%
Double cracks	2	99.6%	99.9%

suggests that support vector machine model or BP neural network model can effectively remove outliers to ensure higher prediction accuracy. The computing inspiration of BP neural network is from the structure and function of biological neural network. The neurons of BP neural network are interconnected to form a group, which handles the calculation method of link information. In most cases, BP neural network is an adaptive system. Compared with BP neural network model, BP neural network algorithm is difficult to achieve satisfactory results. SVM model can identify beam structure damage better. The computational complexity of SVM depends on the number of support vectors. Support vector machines can reach the global optimum, while the BP neural network tends to fall into a local optimal solution. So support vector machine is a powerful tool to identify the degree of structural damage.

5. Conclusions

The paper expounds the basic theories of neural network and support vector machine. Using the two methods damages in local damaged beams structure is located. And the strain model differences are selected to be input parameters. In the example of a simple supported beam, the strain model differentials of sound condition, a quarter of single cracked condition, a quarter of double cracked condition, and double cracked midspan condition, are imported. The crack depths of these conditions are 3.125%, 6.250%, 12.500%, and 15.625%, respectively. The samples are taken as training samples, and 20% damage degree samples served as testing samples that verified the capacities of damage identification of support vector machine and BP neural network. Considering noise effect, the noise levels of BP neural network are added into 1% and 3%. In this paper, both of the two methods could gain a preferable identification precision and adaptation under the conditions of single crack and double cracks. And the beam structure damage identification model base on SVM is of smaller error, less operation time, and better veracity.

Thus, the main contributions of this paper to the literature can be summarized as follows. Firstly, it attempts to develop the models to identify the beam structure damage. It is expected to help to efficiently make reasonable and effective measures to reduce the harm of damage. Secondly, in order to improve the identification accuracy, the beam structure damage identification model based on support vector machine and BP neural network is used to identify the damage level. The performance of the proposed model can provide some valuable insight for researchers as well as practitioners.

Conflict of Interests

The authors declare that there is no conflict of interests regarding the publication of the paper.

Acknowledgment

This work was supported by Grants from the Fundamental Research Funds for the Central Universities nos. 3132013337-4-5 and 3132013079.

References

[1] H. Kim and H. Melhem, "Damage detection of structures by wavelet analysis," *Engineering Structures*, vol. 26, no. 3, pp. 347–362, 2004.

[2] Z. Sun and C. C. Chang, "Structural damage assessment based on wavelet packet transform," *Journal of Structural Engineering*, vol. 128, no. 10, pp. 1354–1361, 2002.

[3] P. Cawley and R. D. Adams, "Improved frequency resolution from transient tests with short record lengths," *Journal of Sound and Vibration*, vol. 64, no. 1, pp. 123–132, 1979.

[4] M. F. Elkordy, K. C. Chang, and G. C. Lee, "Neural networks trained by analytically simulated damage states," *Journal of Computing in Civil Engineering*, vol. 7, no. 2, pp. 130–145, 1993.

[5] P. C. Pandey and S. V. Barai, "Multilayer perceptron in damage detection of bridge structures," *Computers and Structures*, vol. 54, no. 4, pp. 597–608, 1995.

[6] P. H. Kirkegaard and A. Rytter, "The use of neural networks for damage detection and location in a steel member," in *Neural Networks and Combinatorial Optimization in Civil and Structural Engineering*, pp. 1–9, Civil-Comp Press, Edinburgh, UK, 1993.

[7] M.-T. Vakil-Baghmisheh, M. Peimani, M. H. Sadeghi, and M. M. Ettefagh, "Crack detection in beam-like structures using genetic algorithms," *Applied Soft Computing Journal*, vol. 8, no. 2, pp. 1150–1160, 2008.

[8] J.-H. Chou and J. Ghaboussi, "Genetic algorithm in structural damage detection," *Computers and Structures*, vol. 79, no. 14, pp. 1335–1353, 2001.

[9] W. J. Yi and X. Liu, "Damage diagnosis of structures by genetic algorithms," *Engineering Mechanics*, vol. 18, no. 2, pp. 64–71, 2001.

[10] Y. Y. Lee and K. W. Liew, "Detection of damage location in a beam using the wavelet analysis," *International Journal of Structural Stability and Dynamics*, vol. 1, no. 3, pp. 455–465, 2001.

[11] B.-Z. Yao, C.-Y. Yang, J.-B. Yao, and J. Sun, "Tunnel surrounding rock displacement prediction using support vector machine," *International Journal of Computational Intelligence Systems*, vol. 3, no. 6, pp. 843–852, 2010.

[12] B. Yao, C. Yang, J. Hu, J. Yao, and J. Sun, "An improved ant colony optimization for flexible job shop scheduling problems," *Advanced Science Letters*, vol. 4, no. 6-7, pp. 2127–2131, 2011.

[13] B. Z. Yao, P. Hu, M. H. Zhang, and S. Wang, "Artificial bee colony algorithm with scanning strategy for periodic vehicle routing problem," *SIMULATION*, vol. 89, no. 6, pp. 762–770, 2013.

[14] B. Yu, W. H. K. Lam, and M. L. Tam, "Bus arrival time prediction at bus stop with multiple routes," *Transportation Research C*, vol. 19, no. 6, pp. 1157–1170, 2011.

[15] B. Yu and Z. Z. Yang, "An ant colony optimization model: the period vehicle routing problem with time windows," *Transportation Research E*, vol. 47, no. 2, pp. 166–181, 2011.

[16] B. Yu, Z. Z. Yang, and S. Li, "Real-time partway deadheading strategy based on transit service reliability assessment," *Transportation Research A*, vol. 46, no. 8, pp. 1265–1279, 2012.

[17] Y. Bin, Y. Zhongzhen, and Y. Baozhen, "Bus arrival time prediction using support vector machines," *Journal of Intelligent Transportation Systems*, vol. 10, no. 4, pp. 151–158, 2006.

[18] B. Yu, Z.-Z. Yang, and B. Yao, "An improved ant colony optimization for vehicle routing problem," *European Journal of Operational Research*, vol. 196, no. 1, pp. 171–176, 2009.

[19] H. Zhou, W. Li, C. Zhang, and J. Liu, "Ice breakup forecast in the reach of the Yellow River: the support vector machines approach," *Hydrology and Earth System Sciences Discussions*, vol. 6, no. 2, pp. 3175–3198, 2009.

[20] M. K. Mayer, "A network parallel genetic algorithm for the one machine sequencing problem," *Computers & Mathematics with Applications*, vol. 37, no. 3, pp. 71–78, 1999.

[21] V. N. Vapnik, *The Nature of Statistical Learning Theory*, Springer, New York, NY, USA, 1995.

[22] V. N. Vapnik, "An overview of statistical learning theory," *IEEE Transactions on Neural Networks*, vol. 10, no. 5, pp. 988–999, 1999.

[23] V. N. Vapnik, *The Nature of Statistical Learning Theory*, Springer, New York, NY, USA, 2000.

[24] B. Dengiz, F. Altiparmak, and A. E. Smith, "Local search genetic algorithm for optimal design of reliable networks," *IEEE Transactions on Evolutionary Computation*, vol. 1, no. 3, pp. 179–188, 1997.

[25] M. L. M. Beckers, E. P. P. A. Derks, W. J. Melssen, and L. M. C. Buydens, "Parallel processing of chemical information in a local area network—III. Using genetic algorithms for conformational analysis of biomacromolecules," *Computers and Chemistry*, vol. 20, no. 4, pp. 449–457, 1996.

Hindawi Publishing Corporation
Mathematical Problems in Engineering
Volume 2013, Article ID 101483, 9 pages
http://dx.doi.org/10.1155/2013/101483

Research Article

Structural Damage Identification of Pipe Based on GA and SCE-UA Algorithm

Yaojin Bao,[1] He Xia,[1] Zhenming Bao,[2] Shuiping Ke,[3] and Yahui Li[4]

[1] *College of Civil Engineering, Beijing Jiaotong University, Beijing 100044, China*
[2] *School of Naval Architecture Engineering, Dalian University of Technology, Dalian 116024, China*
[3] *College of Management and Economics, Tianjin University, Tianjin 300072, China*
[4] *Transportation Management College, Dalian Maritime University, Dalian 116026, China*

Correspondence should be addressed to Shuiping Ke; ksppp2003@163.com

Received 1 November 2013; Revised 8 November 2013; Accepted 10 November 2013

Academic Editor: Bin Yu

Structure of offshore platform is very huge, which is easy to be with crack caused by a variety of environmental factors including winds, waves, and ice and threatened by some unexpected factors such as earthquake, typhoon, tsunami, and ship collision. Thus, as a main part of the jacket offshore platform, pipe is often with crack. However, it is difficult to detect the crack due to its unknown location. Genetic algorithm (GA) and SCE-UA algorithm are used to detect crack in this paper, respectively. In the experiment, five damages of the pipe in the platform model can be intelligently identified by genetic algorithm (GA) and SCE-UA. The network inputs are the differences between the strain mode shapes. The results of the two algorithms for structural damage diagnosis show that both of the two algorithms have high identification accuracy and good adaptability. Furthermore, the error of SCE-UA algorithm is smaller. The results also suggest that the structural damage of pipe can be identified by intelligent algorithm.

1. Introduction

Nondestructive testing of fault diagnosis can detect whether the construction has flaws under the condition that the construction is not assembled and destroyed, because of properties of material changing with the flaws. General nondestructive testing such as impact-echo method, infrared method, and ultrasonic method is all local damage detection technology that need check damaged points of the constructions first. Although these technologies do not need many instruments and their consequences are accurate, they spend long time and high cost to detect structural damage. In addition, they are hard to detect and evaluate some invisible components about some large-scale complicated structures completely and accurately. Heuristic algorithm is often a first choice to solve complicated problem [1–4]. Thus, this paper attempts to identify the structural damage for pipe with intelligent algorithm.

One of the most important problems of damage identification is to determine damage signature. The damage index of strain is more sensitive than the displacement damage index; therefore, the application fields of strain modal are more widely. Hillary and Ewins [5] proposed the concept of strain modal and applied the strain transfer function to the identification of exciting force. Staker [6] utilized the strain transfer function to estimate the fatigue lifetime. Bernasconi and Ewins [7] and Yam et al. [8] deduced and discussed the theory of strain modal by using displacement modal differential operation method. Tsang [9] used element format to verify the correlation theory of strain modal that was verified by numerical simulation and experiment. Hong et al. [10] used the property of Wavelet Transform which could forecast the Lipshitz index and combined the Wavelet Transform with Lipshitz index to estimate damage. Ren et al. [11] applied Wavelet Transform and Lipshitz index to locate the damage and identify the degree of the damage under the moving load. Kirkegaard and Rytter [12] took advantage of the frequency change before and after damage, applying BP neural networks to locate and identify the damage of steel beam. Mitsuru et al. [13] took relative displacement and relative speed between structure layers as input of the whole network and took the recovery ability between layers as output, using the steel

structure data of seven layers before and after repair to verify the effectiveness of the proposed method. Ruotolo and Surace [14] put BP neural networks into use to diagnose the damage of slab construction. Masri et al. [15] proved that BP neural network is a powerful tool to dissolve the typical structural dynamic system identification problem. Chiang and Lai [16] did relative researches about construe damage identification using GA: first, approximate location of a structural damage is estimated by using modal residual force; then, the possibility of non unique recognition results will be reduced by using GA; at last, possible damage location will be determined by using optimization method. Chou and Ghaboussi [17] regarded a damage problem as an optimization problem and adopted GA to solve it. Cross-sectional area and change of structure modulus of elasticity could be estimated by measuring the freedom to the static displacement. Different from other algorithms, GA confirms the optimum value of objective function by searching a lot of points. It is found that GA can identify the structural damage even with little information. Yi and Liu [18] employed the weighted combination of vibration mode errors and frequency errors to do some numerical simulation about damage of fixed beam, five-span continuous beams, and three spans ten layer framework. They considered that global search ability of GA is useful to identify the structural damage. Zhu and Xiao [19] defined the relative error summation of stress test and stress analysis of all point in the structure as objective function and imposed inequality constraint condition and penalty function. They identified the damage of the Zhaobaoshan bridge.

The effectiveness of construal damage identification based on GA dependeds on the stability of the objective function and algorithm. Considering that GA can perform optimization search based on multiparameter, the objective function based on multiple information can enhance the accuracy of damage identification on some degree. This paper adopted the intelligent algorithm based on strain modal to identify the damage of the nonpenetrative platform pipe crack. Selecting five damages of the platform as an example, this paper used GA and SCE-UA algorithm with better parallel effect to obtain the signal damage degree output of the platform model. At the same time, two methods were evaluated by using the same data.

2. Improved GA for Pipe Structure Damage Identification

2.1. Coarse-Grained Strategies. GA has disadvantages such as precocity and low search efficiency in a practical application. Therefore, the eventual result is local optimal solution, not global optimal solution. For this reason, this paper drew upon predecessors and introduced genetic algorithm to prevent the breeding between relatives. Coarse-grain genetic algorithm is also known as MIMD or distributed genetic algorithm. Individuals are exchanged between the islands, which is called the migration. The division of population and the migration strategy are the pivotal issues of the coarse-grain genetic algorithm.

If the terminal conditions are the same, serial genetic algorithm and coarse-grain genetic algorithm have different iteration time and number of times. That is because that the genetic operators of serial genetic algorithm are operated in the local environment. At present, coarse-grain genetic algorithm has some difficulties, the most important one of which is how to determine the right migration policies.

2.2. Parallel Strategy

Step 1 (Migration Operation). To improve the path diversity, new paths need to be exploited so that better solutions could be obtained. Thus, migration operation is introduced, which means that some excellent individuals are migrated to other subgroups in search of more optimal paths [20]. When external individuals immigrated into a stable new local environment, some individual of the original subgroup will be stimulated by the environment and make the leap of progress, which is very similar to nature.

Step 2 (Convergence Judgment). If the operation reaches the maximum number of iterations or satisfies the convergence condition, then exit sub. Otherwise go to Step 2. The specific flow chart is as in Figure 1.

2.3. GA Parameters Determination for Damage Identification

(1) Design Variable. The damage degree of cell α_i (i is on behalf of cell number) is treated as design variable. If $\alpha_i = 0$, this cell has no damage. The number of design variable should be equal to the number of possible damage cells.

(2) Fitness Function. Due to the fact that it is a minimization problem, GA does the selective operation according to individual fitness value. The bigger the fitness value is, the greater the probability chosen into the next generation was. Therefore, a fitness function should be used to transform the individual objective function values. After transforming, the fitness value will be larger if the objective function value is smaller. The fitness function is as follows:

$$\text{fitness} = \frac{1}{1 + \sum_{i=1}^{N} \sum_{j=1}^{M} \left| u_{ij}^{m} - u_{ij}^{a} \right|}. \quad (1)$$

(3) Genetic Manipulation. This example uses real coding to describe the individuals, and the value of genes of chromosome is viewed as the damage degree of corresponding cell. Assume that there is a line with a certain length; each parent corresponds to the part of the line according to the fitness value with the ratio. The algorithm moves along the line in the same size of the step. Every step of the algorithm determines the location of the parent based on landing position, and the value of the first step is uniform random value of a less step. Then, mutation and crossover operation should be fulfilled by creating a new binary vector. If one digit of the vector is 1, the gene comes from the first generation, and if it is 0, the gene is generated by the second generation and these genes should be merged to form a new individual.

(4) Parallel Strategies. First, the individual similarity of the current population ought to be calculated. It is shown that

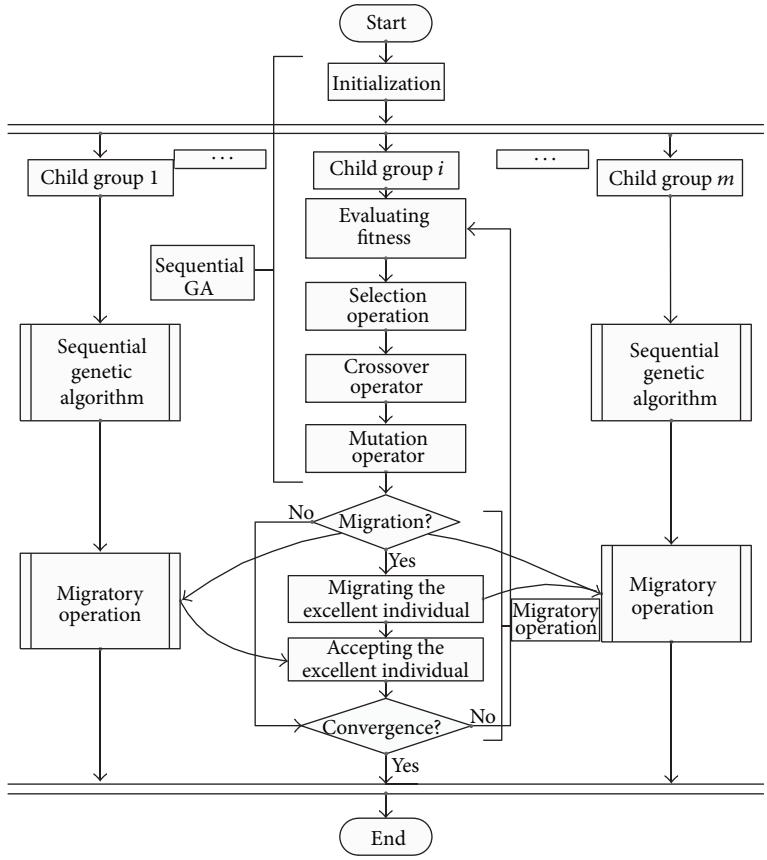

Figure 1: Flow chart of coarse-grained parallel genetic algorithm.

all the differences are small and value of the population is closed to the global optimal target value if the individual similarity of the current population is less than the minimum. For increasing the diversity of population, the current population should accept an individual of other population with maximum similarity to the current one. On the other hand, when the individual similarity is bigger than the maximum, the differences between individuals are great, meaning that the individual is far from the global optimal value. So the individual can accept an optimal individual from other population to hasten convergence. This migration strategy could save the optimal individual of population directly to the next generation.

3. SCE-UA Algorithm for Damage Identification of Pipe Structure

3.1. Principle and Description of SCE-UA Algorithm. SCE-UA algorithm is a global optimization algorithm, which integrates the advantages of random search algorithm simplex method, clustering analysis and biological evolution method, and so on. It can effectively deal with the objective function with rough reflecting surface, not sensitive area [21]. Moreover, the algorithm is not interfered from the local minimum point [22]. It combines the complex search technology based on the deterministic with the biological competition principle of evolution in nature, and its key point is CCE. In CCE algorithm, each compound vertex is potential parent and could be involved in the calculation of producing the next generation. In the process of building, the child compound is selected by random, which leads to the search in the feasible region more thorough.

3.2. Parallel Strategy. SCE-UA algorithm has high intrinsic parallelism. Its process conforms to the Master-Slave pattern, so it is paralleled easily without changing any structure. In Master-Slave pattern, Master process performs the operation including sample space, initialization, compound sorting, and other global mixing operations; Slave process does the evolutionary operation. The figure of SCE-UA algorithm based on the Master-Slave is as in Figure 2.

First, the Master program performs the initialization operation, inputs the data of the model, and generates s samples randomly in the sample space. Then, the samples are sorted according to the new objective function. Finally, the compound types divided are delivered to the Slave process. If the number of processor $n > p$, a processor is assigned to process a Slave; otherwise, a processor will be assigned to process more than a Slave. After that, a Slave process will be divided to some child compound types that generates next generation. When the evolutionary operation is completed, slave process will transfer the results to Master process for performing the mixing process. Then, the above processes are performed continuously, until the results are converged.

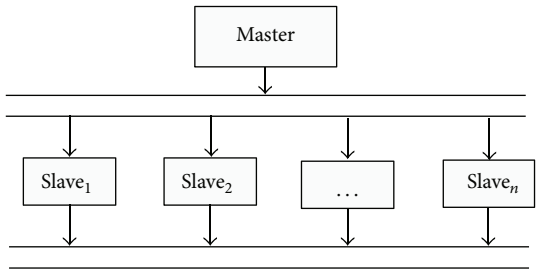

Figure 2: Parallel SCE-UA algorithm based on Master-Slave strategies.

4. Applying GA and SCE-UA Algorithm for Damage Identification of Pipe Structure

4.1. Input Parameters of the Algorithms. GA and SCE-UA algorithm must constitute an objective function when they are applied to damage identification of pipe structure. At present, the structural modal parameters are widely adopted (vibration mode and frequency), but strain modal can achieve high accuracy [8], so this paper chooses strain modal as input parameter.

Displacement modal calculated by finite element could be transferred to strain modal which is very accurate. The objective function of GA and SCE-UA algorithm is the difference value of strain modal between the intact and damage structure.

4.2. Damage Degree Identification and Evaluation of Pipe Structure. Generally, damage could reduce structural stiffness. Then, assuming that there are R variables, the descripiton of structural damage follows:

$$\alpha_i \in (0,1), \quad i = 1 \sim R, \tag{2}$$

where α_i is the damage degree of cell i, so stiffness matrix of cell i is shown as (4)

$$K_{ei}^{d} = \alpha_i K_{ei}^{0}, \tag{3}$$

where K_{ei}^{0} stands for a stiffness matrix generated in an undamaged condition and K_{ei}^{d} stands for a stiffness matrix generated in a damaged condition. Then, global stiffness matrix in damaged condition is as follows:

$$K^{d}(\alpha_1, \alpha_2, \ldots, \alpha_R) = \sum_{i=1}^{R} K_{ei}^{d}. \tag{4}$$

This paper calculated the strain modal in N different damage cases, collected M displacement data in each working condition, and obtained the corresponding strain modal. u_{ij}^{a} denotes the strain modal j under damage case i; u_{ij}^{m} means corresponding strain modal in undamaged condition. By adjusting damage variable α_i ($i = 1 \sim R$), u_{ij}^{a} will be approached to u_{ij}^{m}:

$$\min \sum_{i=1}^{N} \sum_{j=1}^{M} \left| u_{ij}^{m} - u_{ij}^{a} \right|, \quad 0 < \alpha_i < 1. \tag{5}$$

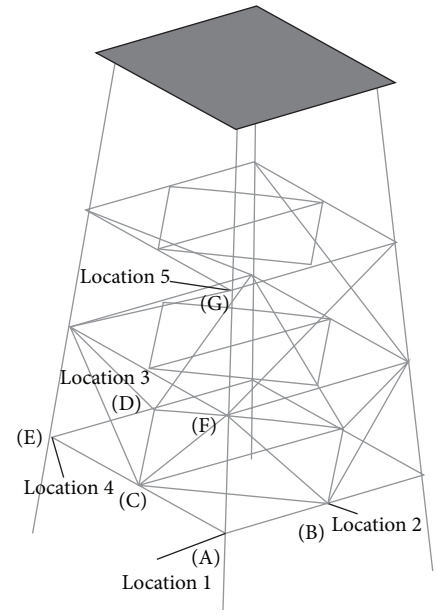

Figure 3: The structure of jacket offshore platform.

Table 1: The list of damage cases.

The label of damage cases	Damage degree (%)
1	10
2	20
3	30
4	40

Thus, the problem is transferred to the mentioned objective function (5). As a result, GA and SCE-UA algorithm with powerful searching ability are applied for structural damage identification.

5. Case Studies

There is a jacket offshore platform, which can be seen in Figure 3. The platform is made of Q235 steel pipe. There are seven points selected for damage identification, which are noted as A, B, C, D, E, F, and G. Their locations can be seen in Figure 3. This paper considered five locations under 4 different damage cases. Damage cases are shown in Table 1.

(1) Location 1: damage is in Point A at Platform jacket leg.

(2) Location 2: damage is in Point B at horizontal pipe BC.

(3) Location 3: damage is in Point D at inclined pipe DG.

(4) Location 4: damage is in Point C at horizontal pipe AE.

(5) Location 5: damage is in Point G of the second layer jacket FG.

5.1. Damage Identification of Horizontal Pipe Structure. GA and SCE-UA algorithm are used to identify the structural

Table 2: The damage degree table of Point A at platform jacket leg in genetic algorithm.

Cell number	1–304	305	306–21600
Case 1			
Design value of damage degree	0.000	0.100	0.000
Identification value of damage degree	0.000	0.098	0.000
Case 2			
Design value of damage degree	0.000	0.200	0.000
Identification value of damage degree	0.000	0.187	0.000
Case 3			
Design value of damage degree	0.000	0.300	0.000
Identification value of damage degree	0.000	0.291	0.000
Case 4			
Design value of damage degree	0.000	0.400	0.000
Identification value of damage degree	0.000	0.383	0.000

Table 3: The damage degree table of Point A at platform jacket leg in SCE-UA algorithm.

Cell number	1–304	305	306–21600
Case 1			
Design value of damage degree	0.000	0.100	0.000
Identification value of damage degree	0.000	0.098	0.000
Case 2			
Design value of damage degree	0.000	0.200	0.000
Identification value of damage degree	0.000	0.189	0.000
Case 3			
Design value of damage degree	0.000	0.300	0.000
Identification value of damage degree	0.000	0.293	0.000
Case 4			
Design value of damage degree	0.000	0.400	0.000
Identification value of damage degree	0.000	0.391	0.000

Table 4: The damage degree table of Point B at horizontal pipe BC in genetic algorithm.

Cell number	1–8754	8755	8756–21600
Case 1			
Design value of damage degree	0.000	0.100	0.000
Identification value of damage degree	0.000	0.089	0.000
Case 2			
Design value of damage degree	0.000	0.200	0.000
Identification value of damage degree	0.000	0.191	0.000
Case 3			
Design value of damage degree	0.000	0.300	0.000
Identification value of damage degree	0.000	0.271	0.000
Case 4			
Design value of damage degree	0.000	0.400	0.000
Identification value of damage degree	0.000	0.387	0.000

damage of spud leg FG, horizontal pipe AE, and inclined pipe BC. Strain modal data were input to GA and SCE-UA algorithm, the number of groups is 50, and the iterations are 1000. Specific damage degree of two methods is shown as in Tables 2 and 3.

5.2. Analysis of Results. It is indicated that both GA and SCE-UA algorithm have accurate identification results from Tables 3, 4, 5, 6, 7, 8, 9, 10, and 11. Although some identification values are not the same as the design values, the errors are very small. By comparing the two algorithms in Table 12, it is found that the results of SCE-UA are more exact. SCE-UA algorithm obtained better identification accuracy than GA did, which proves that SCE-UA is a powerful approach for damage identification of signal crack.

5.3. Comparison of Algorithms. The parameters of this paper are shown as in Table 13, and we compared the evolution results of two algorithms as in Figure 4.

Table 5: The damage degree table of Point B at horizontal pipe BC in SCE-UA algorithm.

Cell number	1–8754	8755	8756–21600
Case 1			
Design value of damage degree	0.000	0.100	0.000
Identification value of damage degree	0.000	0.091	0.000
Case 2			
Design value of damage degree	0.000	0.200	0.000
Identification value of damage degree	0.000	0.193	0.000
Case 3			
Design value of damage degree	0.000	0.300	0.000
Identification value of damage degree	0.000	0.284	0.000
Case 4			
Design value of damage degree	0.000	0.400	0.000
Identification value of damage degree	0.000	0.393	0.000

Table 6: The degree damage table of Point D at inclined pipe DG in genetic algorithm.

Cell number	1–15	16	17–3300
Case 1			
Design value of damage degree	0.000	0.100	0.000
Identification value of damage degree	0.000	0.092	0.000
Case 2			
Design value of damage degree	0.000	0.200	0.000
Identification value of damage degree	0.000	0.189	0.000
Case 3			
Design value of damage degree	0.000	0.300	0.000
Identification value of damage degree	0.000	0.281	0.000
Case 4			
Design value of damage degree	0.000	0.400	0.000
Identification value of damage degree	0.000	0.387	0.000

Table 7: The damage degree table of Point D at inclined pipe DG in SCE-UA algorithm.

Cell number	1–15	16	17–3300
Case 1			
Design value of damage degree	0.000	0.100	0.000
Identification value of damage degree	0.000	0.097	0.000
Case 2			
Design value of damage degree	0.000	0.200	0.000
Identification value of damage degree	0.000	0.192	0.000
Case 3			
Design value of damage degree	0.000	0.300	0.000
Identification value of damage degree	0.000	0.286	0.000
Case 4			
Design value of damage degree	0.000	0.400	0.000
Identification value of damage degree	0.000	0.392	0.000

We can find that operation time of SCE-UA algorithm is less under the same population size and evolutional generation. Although two algorithms almost did not change afterwards, SCE-UA has better convergence and higher robustness [23]. The fitness of SCE-UA did not change after 800th. The fitness of GA increased rapidly before 500th generation, but it changed smoothly after 500th generation. GA had good convergence rate only in the initial stage of evolution, but when the distance is close to the optimal solution, GA was unable to search the optimal solution of this area quickly.

Table 8: The damage degree table of Point C at horizontal pipe AE in genetic algorithm.

Cell number	1–26695	26696	26697–56400
Case 1			
Design value of damage degree	0.000	0.100	0.000
Identification value of damage degree	0.000	0.086	0.000
Case 2			
Design value of damage degree	0.000	0.200	0.000
Identification value of damage degree	0.000	0.191	0.000
Case 3			
Design value of damage degree	0.000	0.300	0.000
Identification value of damage degree	0.000	0.286	0.000
Case 4			
Design value of damage degree	0.000	0.400	0.000
Identification value of damage degree	0.000	0.391	0.000

Table 9: The damage degree table of Point C at horizontal pipe AE in SCE-UA algorithm.

Cell number	1–26695	26696	26697–56400
Case 1			
Design value of damage degree	0.000	0.100	0.000
Identification value of damage degree	0.000	0.093	0.000
Case 2			
Design value of damage degree	0.000	0.200	0.000
Identification value of damage degree	0.000	0.192	0.000
Case 3			
Design value of damage degree	0.000	0.300	0.000
Identification value of damage degree	0.000	0.286	0.000
Case 4			
Design value of damage degree	0.000	0.400	0.000
Identification value of damage degree	0.000	0.394	0.000

Table 10: The damage degree table of Point G of the second layer jacket FG in genetic algorithm.

Cell number	1–22004	22005	22006–56400
Case 1			
Design value of damage degree	0.000	0.100	0.000
Identification value of damage degree	0.000	0.083	0.000
Case 2			
Design value of damage degree	0.000	0.200	0.000
Identification value of damage degree	0.000	0.197	0.000
Case 3			
Design value of damage degree	0.000	0.300	0.000
Identification value of damage degree	0.000	0.274	0.000
Case 4			
Design value of damage degree	0.000	0.400	0.000
Identification value of damage degree	0.000	0.388	0.000

6. Conclusions

Pipe structure of offshore platform is very huge, which was suffered by a variety of environmental factors. Thus, the jacket offshore platform was often caused with crack. It is an important task to identify the structural damage of pipe. However, it is difficult to detect the crack due to its unknown location. Thus, the damage identification problem is a large-scale complicated problem. Heuristic algorithm is often a first choice to solve this kind of complicated problem. This paper firstly overviewed the basic theory of GA and SCE-UA algorithm and expounded the flow of the two algorithms. The process of applying GA and SCE-UA to identify the structural damage degree of platform is introduced. We selected strain

Table 11: The damage degree table of Point G of the second layer jacket FG in genetic algorithm.

Cell number	1–22004	22005	22006–56400
Case 1			
Design value of damage degree	0.000	0.100	0.000
Identification value of damage degree	0.000	0.082	0.000
Case 2			
Design value of damage degree	0.000	0.200	0.000
Identification value of damage degree	0.000	0.199	0.000
Case 3			
Design value of damage degree	0.000	0.300	0.000
Identification value of damage degree	0.000	0.281	0.000
Case 4			
Design value of damage degree	0.000	0.400	0.000
Identification value of damage degree	0.000	0.394	0.000

Table 12: Damage determination analysis of the two methods.

Type	Damage degree (%)	Accuracy of GA	Accuracy of SCE-UA
Single crack	10	100%	100%
	20	99.8%	99.9%
	30	100%	100%
	40	99.9%	100%

Table 13: Parameters in GA and SCE-UA.

Algorithm	Population size	Evolutional generation	Computation time
GA	50	1000	293.7
SCE-UA	50	1000	231.2

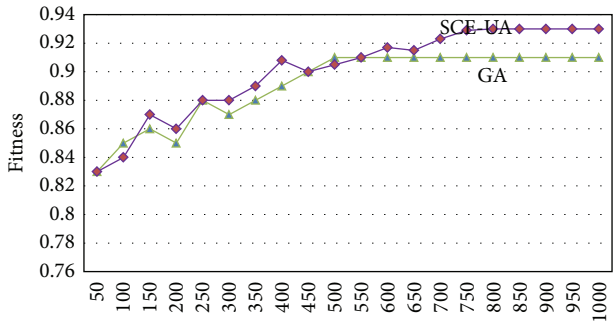

Figure 4: Fitness of each calculation.

modal difference as the input parameter owing to its accuracy and took 5 damages of a platform as an example to identify structural damage. The results showed that GA and SCE-UA algorithm can achieve higher recognition accuracy and have good adaptabilities. The errors of SCE-UA algorithm are smaller, the computation time is less, and convergence is better. SCE-UA is a powerful tool for identifying structural damage of a platform pipe. In addition, the results also suggest that intelligent algorithm is a feasible method for structural damage identification.

Acknowledgment

The research is sponsored by the Major State Basic Research Development Program of China ("973" Program 2013CB036203), the Program for New Century Excellent Talents in the university (NCET-10-0219).

References

[1] B. Z. Yao, P. Hu, M. H. Zhang, and S. Wang, "Artificial bee colony algorithm with scanning strategy for the periodic vehicle routing problem," *Simulation*, vol. 89, no. 6, pp. 762–770, 2013.

[2] B. Z. Yao, C. Y. Yang, J. Hu, J. B. Yao, and J. Sun, "An improved ant colony optimization for flexible job shop scheduling problems," *Advanced Science Letters*, vol. 4, no. 6-7, pp. 2127–2131, 2011.

[3] B. Yu and Z. Z. Yang, "An ant colony optimization model: the period vehicle routing problem with time windows," *Transportation Research Part E*, vol. 47, no. 2, pp. 166–181, 2011.

[4] B. Yu, Z. Z. Yang, and B. Z. Yao, "An improved ant colony optimization for vehicle routing problem," *European Journal of Operational Research*, vol. 196, no. 1, pp. 171–176, 2009.

[5] B. Hillary and D. J. Ewins, "The use of strain gauges in force determination and frequency response function measurements," in *Proceedings of the 2nd International Modal Analysis Conference (IMAC '84)*, pp. 627–634, Orlando, Fla, USA, 1984.

[6] C. H. Staker, "Modal analysis efficiency improved via strain frequency response functions," in *Proceedings of the 3rd International Modal Analysis Conference (IMAC '85)*, pp. 612–617, 1985.

[7] O. Bernasconi and D. J. Ewins, "Application of strain modal testing to real structures," in *Proceedings of the 7th International Modal Analysis Conference(IMAC '89)*, pp. 1453–1464, Los Angeles, Calif, USA, 1989.

[8] L. H. Yam, T. P. Leung, D. B. Li, and K. Z. Xue, "Theoretical and experimental study of modal strain analysis," *Journal of Sound and Vibration*, vol. 191, no. 2, pp. 251–260, 1996.

[9] W. F. Tsang, "Use of dynamic strain measurements for the modeling of structures," in *Proceedings of the 8th International Modal Analysis Conference (IMAC '90)*, pp. 1246–1251, 1990.

[10] J.-C. Hong, Y. Y. Kim, H. C. Lee, and Y. W. Lee, "Damage detection using the Lipschitz exponent estimated by the wavelet transform: applications to vibration modes of a beam," *International Journal of Solids and Structures*, vol. 39, no. 7, pp. 1803–1816, 2002.

[11] Y. C. Ren, S. C. Ma, and L. Lin, "Beam fracture identification under moving load of the wavelet study," *Journal of Vibration and Shock*, vol. 23, no. 2, pp. 82–85, 2004.

[12] P. H. Kirkegaard and A. Rytter, "The use of neural networks for damage detection and location in a steel member," in *Neural Networks and Combinatorial Optimization in Civil and Structural Engineering*, pp. 1–9, Civil-Comp, Edinburgh, UK, 1993.

[13] N. Mitsuru, S. F. Masrisami, A. G. Chassiakos, and T. K. Caughey, "A method for non-parametric damage detection through the use of neural networks," *Earthquake Engineering and Structural Dynamics*, vol. 27, no. 9, pp. 997–1010, 1998.

[14] R. Ruotolo and C. Surace, "Damage assessment of multiple cracked beams: numerical results and experimental validation," *Journal of Sound and Vibration*, vol. 206, no. 4, pp. 567–588, 1997.

[15] S. F. Masri, A. W. Smyth, A. G. Chassiakos, T. K. Caughey, and N. F. Hunter, "Application of neural networks for detection of changes in nonlinear systems," *Journal of Engineering Mechanics*, vol. 126, no. 7, pp. 666–676, 2000.

[16] D.-Y. Chiang and W.-Y. Lai, "Structural damage detection using the simulated evolution method," *AIAA journal*, vol. 37, no. 10, pp. 1331–1333, 1999.

[17] J.-H. Chou and J. Ghaboussi, "Genetic algorithm in structural damage detection," *Computers and Structures*, vol. 79, no. 14, pp. 1335–1353, 2001.

[18] J. W. Yi and X. Liu, "Structural damage detection based on genetic algorithm," *Engineering Mechanics*, vol. 18, no. 2, pp. 64–71, 2001.

[19] J. S. Zhu and R. C. Xiao, "Large span cable-stayed bridge damage identification based on the regular testing and genetic algorithm," *China Civil Engineering Journal*, vol. 39, no. 5, pp. 85–89, 2006.

[20] T. Matsumura, M. Nakamura, J. Okech, and K. Onagat, "A parallel and distributed genetic algorithm on loosely-coupled multiprocessor systems," *IEICE Transactions on Fundamentals of Electronics, Communications and Computer Sciences*, vol. E81-A, no. 4, pp. 540–546, 1998.

[21] Q. Y. Duan, V. K. Gupta, and S. Sorooshian, "Shuffled complex evolution approach for effective and efficient global minimization," *Journal of Optimization Theory and Applications*, vol. 76, no. 3, pp. 501–521, 1993.

[22] G. Kuczera, "Efficient subspace probabilistic parameter optimization for catchment models," *Water Resources Research*, vol. 33, no. 1, pp. 177–185, 1997.

[23] D. E. Goldberg, *Genetic Algorithms in Search, Optimization and Machine Learning*, Addison-Wesley, Reading, Mass, USA, 1st edition, 1989.

Hindawi Publishing Corporation
Mathematical Problems in Engineering
Volume 2013, Article ID 594187, 12 pages
http://dx.doi.org/10.1155/2013/594187

Research Article

Bayesian Network Assessment Method for Civil Aviation Safety Based on Flight Delays

Huawei Wang[1] and Jun Gao[2]

[1] *College of Civil Aviation, Nanjing University of Aeronautics and Astronautics, Nanjing 210016, China*
[2] *Department of Management, Shijiazhuang Mechanical Engineering College, Shijiazhuang 050003, China*

Correspondence should be addressed to Huawei Wang; huawei678@163.com

Received 27 October 2013; Revised 28 November 2013; Accepted 29 November 2013

Academic Editor: Fang Zong

Flight delays and safety are the principal contradictions in the sound development of civil aviation. Flight delays often come up and induce civil aviation safety risk simultaneously. Based on flight delays, the random characteristics of civil aviation safety risk are analyzed. Flight delays have been deemed to a potential safety hazard. The change rules and characteristics of civil aviation safety risk based on flight delays have been analyzed. Bayesian networks (BN) have been used to build the aviation operation safety assessment model based on flight delay. The structure and parameters learning of the model have been researched. By using BN model, some airline in China has been selected to assess safety risk of civil aviation. The civil aviation safety risk of BN model has been assessed by GeNIe software. The research results show that flight delay, which increases the safety risk of civil aviation, can be seen as incremental safety risk. The effectiveness and correctness of the model have been tested and verified.

1. Introduction

The rapid increase of flight delays has already become a prominent problem in the development of civil aviation in China. It not only affects the service quality and economic benefit of civil aviation, but also reduces the civil aviation safety level. The flight delays have attracted public attention and become one of the key factors in impeding the development of civil aviation in China.

The close relationship between flight delays and safety risk is the two principal contradictions, which seriously affects the development of civil aviation in China. The complicated relation is principally due to the following reasons. Firstly, the operation and management subject of flight regularity and civil aviation safety are coincident. Secondly, the factors, such as resource shortage and operation management behavior, can give rise to the flight delays and safety operation simultaneously. Thirdly, the environmental factors, such as severe weather and human disturbance, result in not only flight delays but also safety risk. At the same time, flight delays cannot only result in potential safety risk of civil aviation but also come up simultaneously. Some specialists in civil aviation have realized that flight delays are an important potential risk in the management of civil aviation safety. If the safety risk, which is concurrent and induced, is not controlled in time, the aviation accident and grievous potential accident will take place under certain conditions. The aviation accident will bring about heavy losses.

The civil aviation safety level in China is in the state of steady improvement. Now China has already become one of the countries, who have high civil aviation safety level in the world. However, the number of delay flights in China is always very high. In 2012, there were 2,502,000 scheduled flights, which include 1,872,000 regular flights and 630,000 irregular flights, and the average flight punctuality rate is 75.69%. The flight delays are caused 38.5% by airlines, 25.0% by flow control, and 21.6% by weather, so it is very severe in the development of civil aviation. The main reason that can affect civil aviation safety and flight delays is that the attributes of flight delays are subject to dominant indicators and the attributes of civil safety are subject to potential indicators. Potential safety risk exists and is in the high state, which will pose a threat to the safety of civil aviation. It may lead to the fluctuation of safety level of civil aviation and even

worse the situation of civil aviation. Therefore, it is necessary to analyze the effect of flight delays on the safety of civil aviation in detail, assess the safety level of civil aviation based on flight delays, and provide measures and suggestions for the collaborative management of flight delays and the civil aviation safety.

Some scholars had already researched the related problems on flight delays and civil aviation safety. Airline maintenance operation affects not only flight delays but also civil aviation safety. Sachon and Paté-Cornell [1] built a probabilistic risk analysis model, represented by an influence diagram, to quantify the effect of airline's maintenance policy on flight delay, cancellation, and in-flight safety. McCrea et al. [2] made a novel severe-model paradigm to be applied for the context of a large scale in specified probability threshold when encountering severe weather, subject to collision safety, airline equity, and sector workload considerations. More research is to study flight delay and the aviation safety problem, respectively. In the respect of flight delay, Zheng et al. [3] calculated the time series of after-affect delay spread time using delay time distribution of the flights assigned gate in airport and random delay in flights. Wong and Tsai [4] used coproportional hazards model to build departure and arrival delay models that show how flight delay propagation can be formulated through repeated chain effects in aircraft rotations. Yan and Tang [5] developed a heuristic approach embedded in a framework designed to help the airport authorities make airport gate assignments that are sensitive to stochastic flight delays. Pyrgiotis et al. [6] developed an analytical queuing and network decomposition model to study the complex phenomenon of the propagation of delays within a large network of major airports, which has been used to compute the delay due to local congestion at individual airports and captures the "ripple effect" that leads to propagation of these delays. Santos and Robin [7] found that four significant variables in explaining delays at European airports were market concentration, slot coordination, hub airports, and hub airlines using flight data for the period 2000–2004. Using longitudinal data from a major airline and conditional difference-in-differences technique, Ferrer et al. [8] analyzed the effects of flight delay on passengers' future purchasing behavior. To develop a decision-support tool for air traffic control, presented an algorithm for optimal arrival flight sequencing and spacing in near-terminal, which used discrete delay times as optimization variables.

In the field of civil aviation safety, some scholars utilized data on both accident and safety indicators. Shyur [9] presented a specified proportional hazard model considering the baseline hazard function as a quadratic spline function, which had investigated and demonstrated its applicability in aviation risk assessment. Janic [10] described the main cause of aircraft accident, proposed a methodology for quantifying risk and safety, and offered an assessment of risk and safety in civil aviation. Chen et al. [11] ranked the significant threats and human errors affecting aviation safety and used the analytical hierarchy process to calculate the weigh for each criterion which were than ranked in order of importance. Marais and Robichaud [12] investigated and quantified the contribution of maintenance, both in terms of frequency and severity, to passenger airline risk by analyzing three different sources of data from 1999 to 2008. Brooker [13] examined the ability of Bayesian belief network-based techniques to make accurate aviation risk predictions. Hadjimichael [14] developed a flight operation risk assessment system (FORAS), which was a risk modeling methodology representing risk factors and their interrelationships as a fuzzy expert system. A FORAS risk model provided a quantitative risk index representing an estimate of cumulative effects of potential hazards on a single flight operation. Lee [15] developed a quantitative model for assessing aviation risk factors as a means of increasing the effectiveness of safety risk management system by integrating the fuzzy linguistic scale method, failure mode, effects and criticality analysis principle, and as low as reasonably practicable approach. Rose [16] studied the limitations and problems of trying to measure safety and operational risk and presented useful metrics from incident reporting data. Oster Jr. et al. [17] brought forward that the next generation of safety challenge now required development and understanding of new forms of data to improve safety in other segments of commercial aviation, moving from a reactive, incident-based approach toward a more proactive, predictive, and system-based approach.

From the above research literature, we understand that there is little study in the systematic analysis of flight delays, which have an effect on civil aviation safety and safety assessment.

The complexity of civil aviation safety risk assessment based on flight delays shows in the following aspects.

(i) There are many factors that affect flight delays and civil aviation safety risk. Coupling with the interaction between flight delays and civil aviation increases the difficulty of analysis.

(ii) The mechanism of flight delays, which can erupt simultaneously and induce civil aviation safety, remains to be further analyzed in detail.

(iii) The rate of civil aviation accident is low. But the increase of potential safety hazard and the deviation of safety state may not arise in the shape of accident, accident threat, or unsafe event immediately.

(iv) It is difficult to collect the direct statistics of the relevant factors. So, it is often completed with the help of subjective information by experts' experience.

Therefore, the difference between aviation safety risk based on flight delays and general aviation risk assessment can be concluded.

(i) Change of Assessment Elements. The general civil aviation safety assessment only focuses on the elements of safety itself. The safety assessment of civil aviation based on flight delays is one of the assessment elements, which not only reflects the value change of safety elements, but also embodies the relationships between the civil aviation safety system and flight delay system.

(ii) The Difference of Definition the Analysis Scope. Because both the flight delays system and civil aviation safety system

are big systems, it is difficult or insoluble for civil aviation safety assessment based on flight delays if all the elements of flight delay system and civil aviation system are considered. So, emphasis is given to civil aviation safety elements associated with flight delays, which is different from general civil aviation safety assessment.

(iii) The Difference of Risk Evolution. The elements of flight delay system are dynamic, which is real-time change. The risk elements of civil aviation safety system are relatively stable. So, the civil aviation safety assessment based on flight delays is dynamic, while the general civil aviation safety assessment is relatively stable.

The main contribution of the paper can be concluded as follows.

(i) The composition of civil safety risk based on flight delays has been analyzed systematically, which includes the aggregation and the transmission of civil aviation safety risk;

(ii) The change rules of civil aviation safety risk based on flight delays have been analyzed, which include the increase of potential safety risks leading to civil aviation safety risk, the common causes of safety risk and flight delays leading to aviation safety risk, and flight delays leading to the increase in civil aviation safety risk degree as an inducement;

(iii) The safety assessment model of civil aviation by BN, which considered the composition of civil safety risk based on flight delays, the randomness of civil aviation safety risk variation, the change rules of civil aviation safety risk based on flight delays.

Therefore, according to the characteristics of civil aviation, the paper presents an assessment model of civil aviation safety risk based on flight delays. The remaining part of the paper is organized as follows. Section 2 introduces the frame structure of algorithm. Section 3 analyzes the characteristics and change regulation of civil aviation safety risk based on flight delay. Section 4 builds an assessment model of civil aviation operation safety risk by the Bayesian network. Section 5 uses example to validate the effectiveness of the proposed method. Finally, some concluding remarks are made.

2. The Risk Assessment Framework of Civil Aviation Safety Based on Flight Delays

There are three criteria in building risk assessment framework of civil aviation safety in the paper.

(i) Considering the concurrence of subjective and objective data in risk assessment of civil aviation safety, the mechanism of action and dynamic change reflected by some factors in civil aviation system operation should be considered in building the model.

(ii) Flights delay should be seen as an incremental risk and be analyzed based on the risk analysis of civil aviation safety.

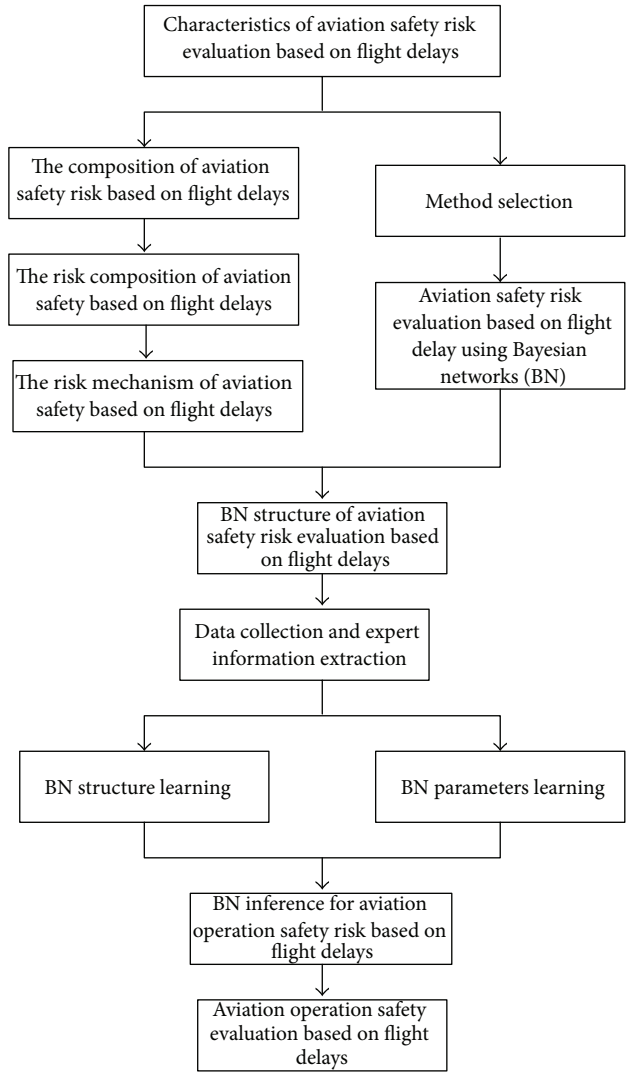

Figure 1: The diagram of civil aviation safety risk assessment based on flight delays.

(iii) The action mechanism and evolution law between civil aviation safety risk, which is induced by flight delays, and civil aviation operation system itself should be analyzed.

Figure 1 shows the diagram of civil aviation safety risk assessment based on flight delays.

3. The Civil Aviation Safety Risk Based on Flight Delays

3.1. The Composition of Civil Aviation Safety Risk Based on Flight Delays

(i) The Aggregation of Civil Aviation Safety Risk. The aggregation of civil aviation safety risk means that the actual risk of civil aviation safety consists of coinstantaneous and induced risks under flight delays. There are three main types of risk:

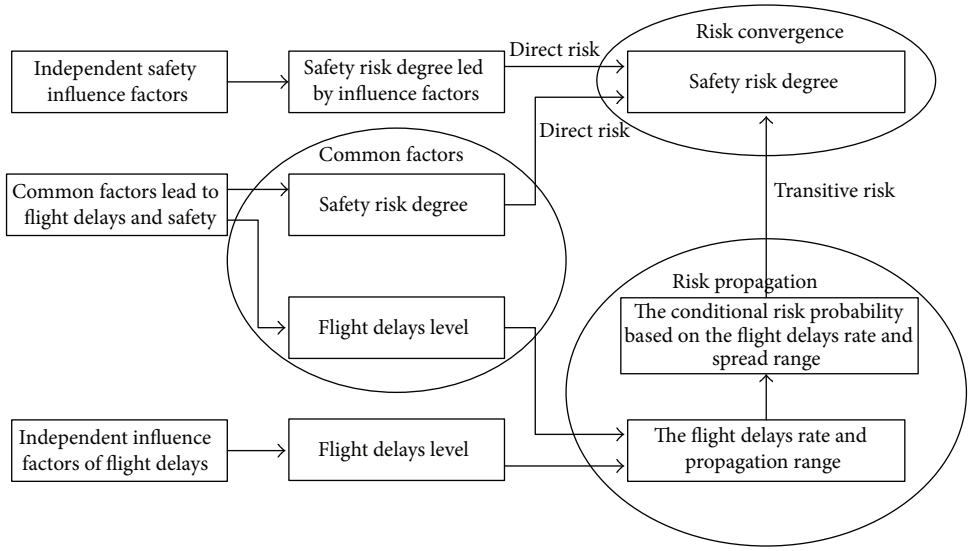

Figure 2: The entire constitute of civil aviation safety risk.

one is caused by the independent influence factors of civil aviation safety; the second is caused by the common factors which lead to flight delays and civil aviation safety risk; the third is caused by independent influence factors of flight delays.

(ii) The Transmission of Civil Aviation Safety Risk. The transmission of risk is from two aspects: one is the variation of the probability distribution of civil aviation safety risk according to different flight delays; the other is that the surging number of flight delay is caused by flight delays accumulation. The incensement of flight delays rate leads to the accumulation of civil aviation safety risk. Obviously, the civil aviation safety risk induced by flight delays changes with the rate and spread range of flight delays.

The entire constitute of civil aviation safety risk is shown in Figure 2.

3.2. The Randomness of Civil Aviation Safety Risk Variation. The civil aviation safety risk based on flight delays is random. The randomness is reflected as follows.

(i) Because the aviation accident is random, the civil aviation safety risk assessment is supposed to obey statistical probability distribution.

(ii) The appearance of flight delays is occasional. Although flight delays can be controlled to some extent, some flight delays caused by bad weather are generally unforeseeable and unavoidable. Therefore, some factors causing flight delay are random.

(iii) The occurrence of potential safety hazard factor is random. The potential safety hazard often appears as hidden factor, which is difficult to detect and will lead to safety risk when it is transformed into the dominant factor under some conditions.

(iv) As a special safety risk, the influence of flight delays on civil aviation safety risk is random. That is to say, the potential safety hazard which supervenes safety risk with hidden dangers is random. The concurrence probability is random, which is based on different delay rate and risk level.

(v) As a special safety risk, there is a causal relationship between different potential safety hazards to some extent. That is to say, as a potential safety hazard, it is uncertain and random that flight delays can induce and cause the variation of other dangers.

(vi) The influence of flight delays on civil aviation safety risk can be regarded as an increment risk, which belongs to the interaction between gradual accumulation and sudden surge of different random factors.

In conclusion, the source of random risk can be summarized as follows:

(i) the factors which induce flight delays and civil aviation safety are random;

(ii) the conditions which lead to flight delays and civil aviation safety are random;

(iii) the state of flight delays and civil aviation safety is random.

The randomness between factors, conditions, and states can be expressed in Figure 3.

3.3. The Analysis on Change Rules of Civil Aviation Safety Risk Based on Flight Delays

3.3.1. The Increase of Potential Safety Risks Leading to Civil Aviation Safety Risk. Flight delays are regarded as a kind of new safety risk. The characteristics of flight delays are that it exists when flight delay exists; otherwise, it disappears.

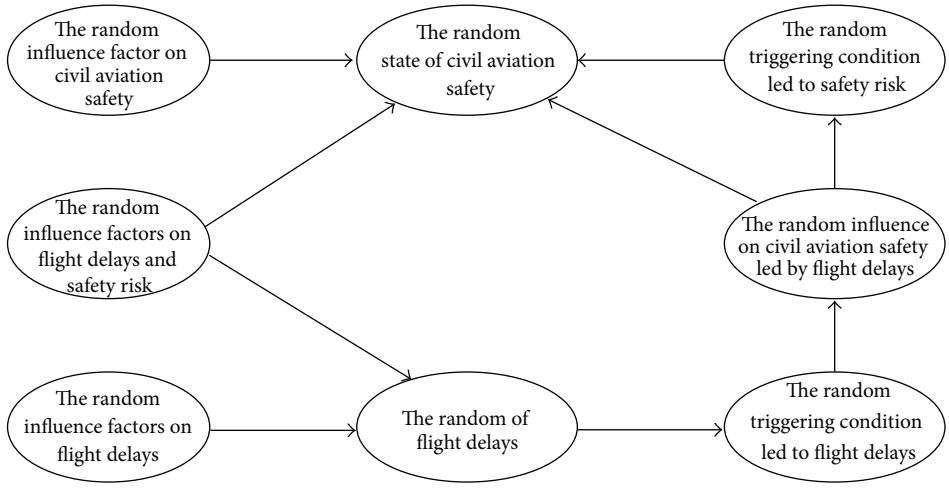

Figure 3: The diagram of random risk of civil aviation safety based on flight delay.

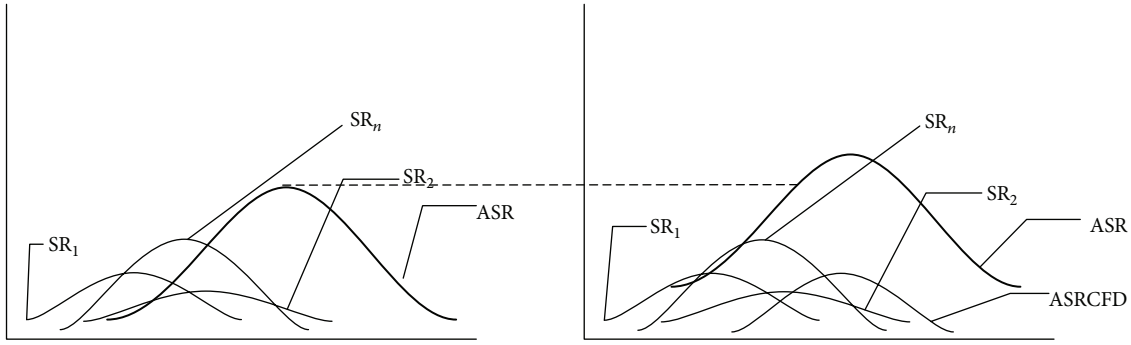

SR: safety risk

ASR: aviation safety risk

ASRCFD: aviation safety risk based on flight delays

Figure 4: The change rule of civil aviation safety risk considering flight delays as potential safety hazard.

Assuming that there are n hidden risks (n risk sources) when there are no flight delays, there are $n + 1$ hidden risks when flight delays occur. Even assuming that flight delays do not affect other hidden risks (e.g., civil aviation safety risk degree, which is caused by n hidden dangers, does not vary), the $n + 1$ hidden risks, including flight delay and safety risk induced by flight delays, will increase the degree of civil aviation safety risk.

The change rules of safety risk degree are shown in Figure 4.

(i) Assuming that potential safety risk and flight delays are independent when delays flights are acting as a potential safety risk;

(ii) The reason that safety risk increases is that flight delays act as an independent potential safety risk;

(iii) Regular flight is a normal state, and flight delays are abnormal state. The existence of flight delays can lead to the increase of civil aviation risk inevitably; this is a systemic risk;

(iv) As the change rule of potential safety risk in Figure 4, the paper has taken the randomness of risk change into account and assumes that the variation of risk obeys normal distribution.

3.3.2. The Common Causes of Safety Risk and Flight Delays Leading to Aviation Safety Risk. The factor which causes flight delays has an impact on civil aviation safety at the same time. Assuming that there are n potential safety risks (n risk sources) when flight delays do not occur. The common factors not only lead to flight delays but also have an influence on the risk variation rules of primary potential safety risk n. That is to say, flight delays are not the direct reason which leads to the increase of civil aviation safety risk.

The mechanism of risk is shown in Figure 5.

According to Figure 5, the explanations include the following.

(i) The risk caused by flight delays which act as an independent potential safety hazard should not be taken into account.

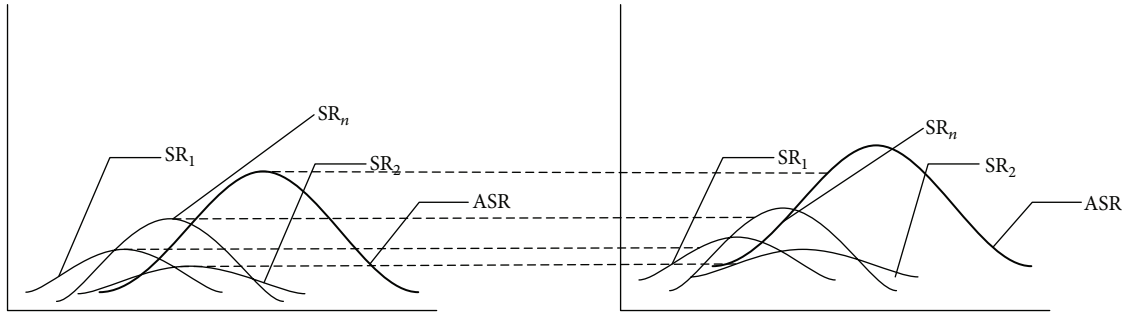

SR: safety risk

ASR: aviation safety risk

Figure 5: The change rule of civil aviation safety risk caused by the common causes of civil aviation and flight delays.

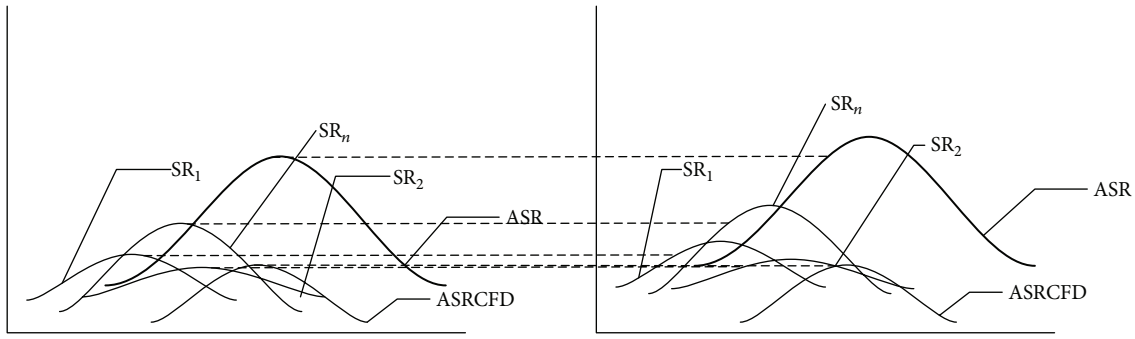

SR: safety risk

ASR: aviation safety risk

ASRCFD: aviation safety risk based on flight delays

Figure 6: The change rule of civil aviation safety risk under flight delay acting as inducement.

(ii) Figure 5 aims to analyze the influence on common factors of safety risk and flight delay on civil aviation safety risk. Compared with flight delay, the indications of safety risk (accident, accident symptom, and unsafe events) are much less sensitive to flight delay. That is to say, flight delay is the explicit index of common factors, and safety risk is shown as implicit index, usually.

(iii) The common factors of safety risk and flight delay lead to various change rules of risk on n safety potential safety hazard. Although the degree, time, and variation rules are different, the entire trend is to increase the civil aviation risk.

(iv) Considering the randomness of risk change, the paper assumes that risk change obeys normal distribution and the civil aviation safety risk sources are composed of different risk sources.

3.3.3. Flight Delays Leading to the Increase of Civil Aviation Safety Risk Degree as an Inducement. In addition to the common factors, flight delay as an inducement will further have an effect on civil aviation. The actual safety risk is overlapped between the above two kinds of influence and the superposition may lead to a sound increase in safety risk degree objectively.

Flight delays acted which as inducement increased the risk degree of civil aviation safety, and the change rule of risk is showed in Figure 6.

From Figure 6, we can draw some conclusions.

(i) Flight delays as an inducement in Figure 6 directly have an impact on potential safety risk, which acted as the occurrence of flight delay and stimulates and triggers the change of safety risk degree.

(ii) As the change rules of different potential safety risk in Figure 4, the paper has taken the randomness of risk change into account and assumes that risk change obeys the normal distribution.

It is worth mentioning that the risk change rule of civil aviation safety in Figures 4 and 6 has been assumed to obey normal distribution. The assumption is from general knowledge about civil aviation safety risk, which is not carefully calculated. The detailed calculation about safety risk of civil aviation can be seen in Section 4.

4. Risk Assessment Model of Civil Aviation Safety Based on BN

4.1. Overview of BN. BN is a directed acrylic graph for reasoning under uncertainty in which the nodes represent variables and are connected by means of directed arcs. The arcs denote dependencies or causal relationship between the link nodes and the conditional probability table assigned to the nodes determining how the linked nodes are dependent on each other [18].

Based on the conditional independency theorem and the chain rule, BN factorizes the joint probability distribution of a set of random variables $U = \{A_1, A_2, \ldots, A_n\}$ by considering local dependencies. The joint probability distribution can be decomposed as the product of the probabilities of the nodes given their immediate parents [19]:

$$P(U) = \prod_{i=1}^{n} P\left(A_i \mid Pa\left(A_i\right)\right), \tag{1}$$

where $P(U)$ is the joint probability distribution of variables and $Pa(A_i)$ is the parent set of variable A_i.

BN takes advantage of the Bayes theorem to update the probability of events given a new observation, called evidence E, to yield the posterior probability:

$$P(U \mid E) = \frac{P(U,E)}{P(E)} = \frac{P(U,E)}{\sum_U P(U,E)}. \tag{2}$$

Using (2) probability can be updated by versatile type of E.

BN is the method integrated by quality analysis and quantitative analysis, which can utilize many kinds of information. BN has the function of learning itself, backward reasoning, and inference in incomplete data sets. The above advantages make BN superior to other artificial intelligence methods in safety evaluation of civil aviation based on flight delays.

BN has been widely applied in engineering domain, such as risk analysis [20–22] and fault diagnosis [23, 24] and prediction [25, 26].

4.2. The BN Model for Civil Aviation Safety Risk Assessment. There are six steps in BN model to assess the civil aviation safety risk.

Step 1 (extract the key factors causing flight delays and civil aviation safety risk and determine the BN nodes). Determination of nodes is the foundation and key for determining the structure of BN. There are four categories of nodes to be taken into account. First, the common cause factors for flight delay and civil aviation safety should be taken into account. Second, the independent causing factors for flight delays and civil aviation safety should be taken into account. Third, the factors of flight delays which induced safety risk of civil aviation operation should be taken into account. Forth, the prorogation and spread of flight delay itself should be taken into account.

Step 2 (determine the risk assessment BN structure of civil aviation operation based on flight delays). The model should reflect the actual civil aviation safety. The nodes determined in Step 1 are connected with causality. So, the structure of BN consisted of causality chain, which can be required from logic analysis and expert experience. The determination of BN structure is the qualitative modeling in BN. The analyses of Sections 2 and 3 are used to build the BN structure of civil aviation safety risk.

Step 3 (instantiate the BN with probabilities). First, prior probabilities are assigned to the root nodes in the BN for civil aviation safety risk assessment. To root node X_i, $P(x_i = R)$ and $P(x_i = N)$ represent risk probability and normal probability of node x_i, respectively, and $P(x_i = R) + P(x_i = N) = 1$.

Next, conditional probabilities are assigned to other nodes. To a child node with n parents, 2^n conditional probabilities should be assigned. It is difficult to collect much information in actual civil aviation operation and management. Experts also have some difficulty in providing so much information. To overcome the problem, it is necessary to study the BN for civil aviation safety risk assessment for simplifying the conditional probabilities assignment.

Step 4 (learn BN structure). There are two contents in BN structure learning. One way is to decide BN structure by data reasoning. The other way is to verify structure of BN and delete weak connections between nodes by data if the initial structure of BN has been known. In the paper, the initial BN structure of civil aviation safety risk assessment has been decided based on the study of Sections 2 and 3. The emphasis of BN on civil aviation safety risk assessment is to simplify BN structure. Markov blanket is selected to BN in civil aviation operation risk.

Step 5 (learn BN parameters). Bayes method is the theory basis for BN. Bayes method uses prior density and posterior density to learn and assess parameters. BN also uses the above process to learn parameters after collecting and accumulating relevant data. In the practical application, the parameters learning of BN also use conjugate prior to simplify parameters learning.

Step 6 (infer BN). Civil aviation safety risk can be assessed by BN if the BN structure has been known and the nodes have been assigned. In the paper, GeNIe has been selected to compute because of large amount of calculation.

4.3. The BN Structure of Civil Aviation Safety Risk Assessment. The analysis on designing BN structure of civil aviation safety risk assessment bases on flight delay.

(i) Civil aviation safety system is the complex large system, which includes flight subsystem, maintenance subsystem, air traffic control subsystem, and airport subsystem. These subsystems are affected by flight delays in different degree. These subsystems also have an impact on civil aviation safety risk in different mode. So, it is necessary to use independent analysis for different subsystems.

Table 1: The description of node characteristics.

Meaning	Abbreviation
Weather	WE
Flow control	FC
Maintenance and engineering	ME
Airplane plan	AP
Airport design	AD
Airport order	AO
Scheduled flight time	SFT
ATC safety risk	ATSR
Airline safety risk	ALSR
Airport safety risk	APSR
Maintenance safety risk	MSR
Airport size	AS
Food supply	FS
Other reason	OR
Traveler	TR
Aircraft type	AT
Flight delay	FD
Station flight delay	SFD
Flight delay rate	FDR
Risk rate of aviation operation safety	AOSRR
Safety operation risk based on flight delay	SRBFD
ATC safety hidden danger	ATSHD
Airline safety hidden danger	ALSHD
Airport safety hidden danger	APSHD
Maintenance safety hidden danger	MSHD
Prohibited fly	PF
Air crew	AC
Security check	SC
Joint check	JC
Transport service	TS

(ii) Flight subsystem, maintenance subsystem, air traffic control subsystem, and airport subsystem are all affected by person, machine, environment, and management. To avoid large BN structure, modular structure has been introduced in the paper. The nodes of hidden risk and safety risk have been designed in different subsystems, the value of which can be calculated by BN inference.

(iii) In order to analyze the flight delays which propagated safety risk, the flight delays modeling should be emphasized, which include influence factors such as flight delays, flight delays propagation, flight delays rate, and risk assessment based on flight delays.

The initial risk assessment BN of civil aviation safety is shown in Figure 7. The meaning of nodes in Figure 7 is shown in Table 1.

4.4. BN Learning for Civil Aviation Safety Risk Assessment

4.4.1. BN Structure Learning of Civil Aviation Safety Risk Assessment. A novel idea of BN of significant feature selection is the Markov blanket (MB). In order to simplify BN structure of civil aviation safety risk assessment, Markov blanket is selected in BN structure learning.

MB is defined as the set of input features because all the other features are probabilistically independent of target features. In a Bayesian network, the Markov blanket [27] of a node X_i (which can be represented as $\mathrm{MB}(X_i)$ in short) is the set of nodes which is composed of its parent nodes, its child nodes, and parent nodes of its child nodes. The important property of Markov blanket is that Markov blanket of variable X_i is the set of nodes which makes X_i independent in the network. That is to say, the nodes belonging to the Markov blanket of X_i are the most relevant to X_i,

$$P\left(X_i \mid X_1, \ldots, X_{i-1}, X_{i+1}, \ldots, X_n\right) = P\left(X_i \mid \mathrm{MB}\left(X_i\right)\right). \tag{3}$$

The probability of the target node is influenced only by its Markov blanket. Therefore, MB (target node) is the most informative and relevant to risk assessment of civil aviation safety.

For example,

$$\begin{aligned}
&P\left(\mathrm{AOSRR} \mid \mathrm{MB}\left(\mathrm{AOSRR}\right)\right)\\
&= P\left(\mathrm{AOSRR} \mid \mathrm{SFD}, \mathrm{WE}, \mathrm{FFD}, \mathrm{ALSR}, \mathrm{APSR}, \mathrm{ARBR}, \mathrm{MSR}\right)\\
&= \frac{P\left(\mathrm{AOSSR}, \mathrm{SFD}, \mathrm{WE}, \mathrm{FFD}, \mathrm{ALSR}, \mathrm{APSR}, \mathrm{ARBR}, \mathrm{MSR}\right)}{P\left(\mathrm{SFD}, \mathrm{WE}, \mathrm{FFD}, \mathrm{ALSR}, \mathrm{APSR}, \mathrm{ARBR}, \mathrm{MSR}\right)}\\
&= \frac{\prod_{X_i \in \{\mathrm{SFD}, \mathrm{WE}, \mathrm{FFD}, \mathrm{ALSR}, \mathrm{APSR}, \mathrm{ARBR}, \mathrm{MSR}\}} P\left(X_i \mid \pi\left(X_i\right)\right)}{P\left(\mathrm{SFD}, \mathrm{WE}, \mathrm{FFD}, \mathrm{ALSR}, \mathrm{APSR}, \mathrm{ARBR}, \mathrm{MSR}\right)}\\
&= P\left(\mathrm{AOSRR} \mid \pi\left(\mathrm{AOSRR}\right)\right)\\
&\quad \cdot \prod_{X_i \in \mathrm{Children(AOSRR)}} P\left(X_i \mid \pi\left(X_i\right)\right)\\
&\quad \cdot \prod_{X_j \notin \mathrm{AOSRR} \cap X_j \notin \mathrm{Children(AOSRR)}} P\left(X_j \mid \pi\left(X_j\right)\right)\\
&\quad \times \left(P\left(\mathrm{SFD}, \mathrm{WE}, \mathrm{FFD}, \mathrm{ALSR}, \mathrm{APSR}, \mathrm{ARBR}, \mathrm{MSR}\right)\right)^{-1}.
\end{aligned} \tag{4}$$

4.4.2. BN Parameters Learning for Aviation Safety Risk Assessment. In the BN of civil aviation safety risk assessment, assuming that node has a multinomial distribution, we can parameterize it with the parameter vector $\theta_1, \theta_2, \ldots, \theta_S$, where S is the number of states of variable x and $\theta(k) = P(x = x_k \mid p)$, for $1 \le k \le S$.

(1) θ possess the Dirichlet distribution

$$\theta \sim D\left[\alpha_1, \alpha_2, \ldots, \alpha_S\right] \tag{5}$$

$\alpha_i > 0$; $i = 1, \ldots, S$, and $\sum_{i=1}^{S} \theta_i = 1$, we can act α_i as presenting counts of past cases which are stored as a summary of experience.

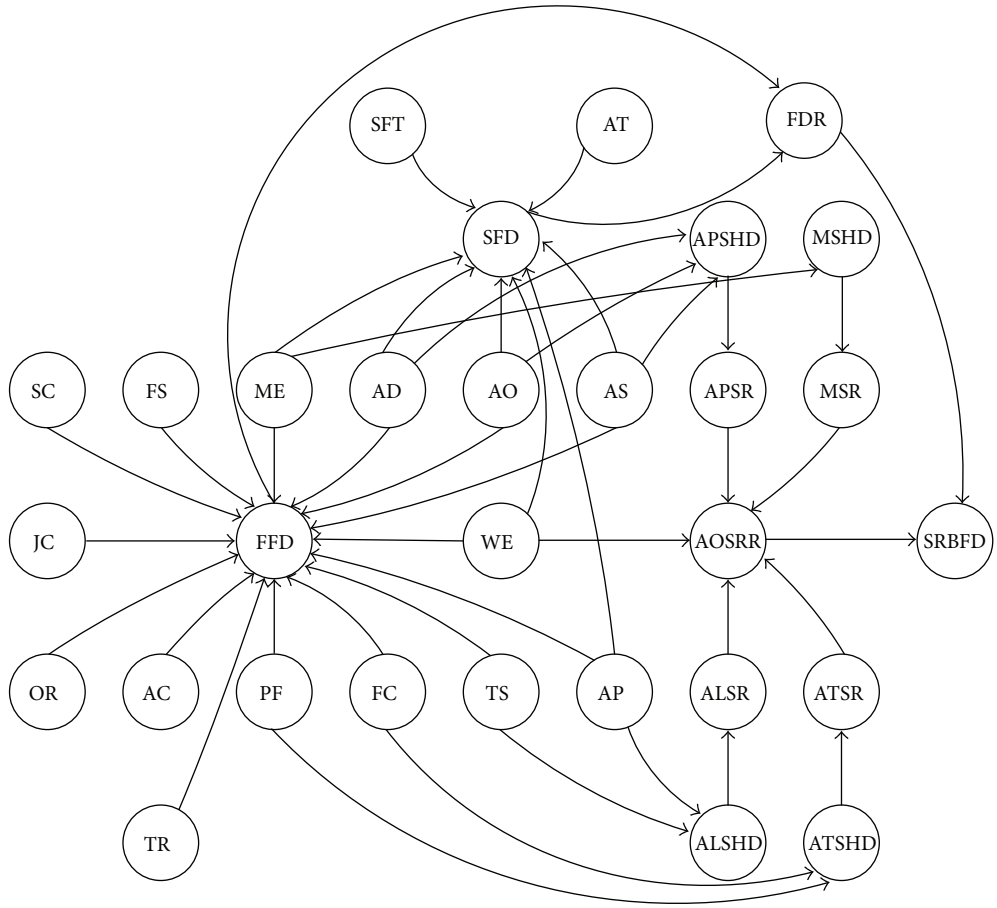

Figure 7: BN structure of civil aviation safety operation assessment based on flight delay.

(2) Let $\alpha_0 = \sum_{i=1}^{S} \alpha_i$ and let expected value, variance, and covariance of Dirichlet distribution be defined as follows:

$$E(\theta_i) = \frac{\alpha_i}{\alpha_0},$$

$$\mathrm{Var}(\theta_i) = \frac{\alpha_i(\alpha_0 - \alpha_i)}{\alpha_0^2(\alpha_0 + 1)}, \tag{6}$$

$$\mathrm{Cov}(\theta_i) = -\frac{\alpha_i \alpha_j}{\alpha_0^2(\alpha_0 + 1)}.$$

We assume that θ prior distribution is Dirichlet distribution; then posterior distribution is also Dirichlet distribution; they are conjunction distribution.

When the samples are $N = (N_1, N_2, \ldots, N_S)$, the posterior expected value of θ_k with $k = 1, 2, \ldots, S$ is given by

$$E(\theta_i \mid \alpha, N) = \frac{\alpha_i + N_i}{\sum_{i=1}^{S}(\alpha_i + N_i)}. \tag{7}$$

5. Examples

The paper selects an airline company in China to verify the model in the paper. The relevant data in Figure 7 were collected in 2012.

The data comes from the following sources.

(i) Some data is obtained by statistics analysis, such as FC node. The FC percentage can be calculated by statistics data.

(ii) Some data is difficult to collect directly, which is inferred by historical data and expert information.

(iii) Some data is obtained by other ways and analysis methods, such as hinder risk of airport. Because computation on hinder risk of airport is very complex, the result of airport safety audit of last year can be used to reduce the computation difficulty.

In the paper, calculation of time interval is a month. The data of 2011 can be used as prior information. After collecting the data of January 2012, the marginal posterior probability of each node in the risk assessment BN of civil aviation safety can be calculated for January 2012. Structure learning and parameter learning of BN are in the whole calculation process. Then posterior probability of each node in January 2012 can be used as the prior information of February 2012. After collecting data of February 2012, the marginal posterior probability of each node in the risk assessment BN of civil aviation safety can be calculated for February 2012. In the same way, the posterior marginal probability of each node in every month of 2012 can be calculated.

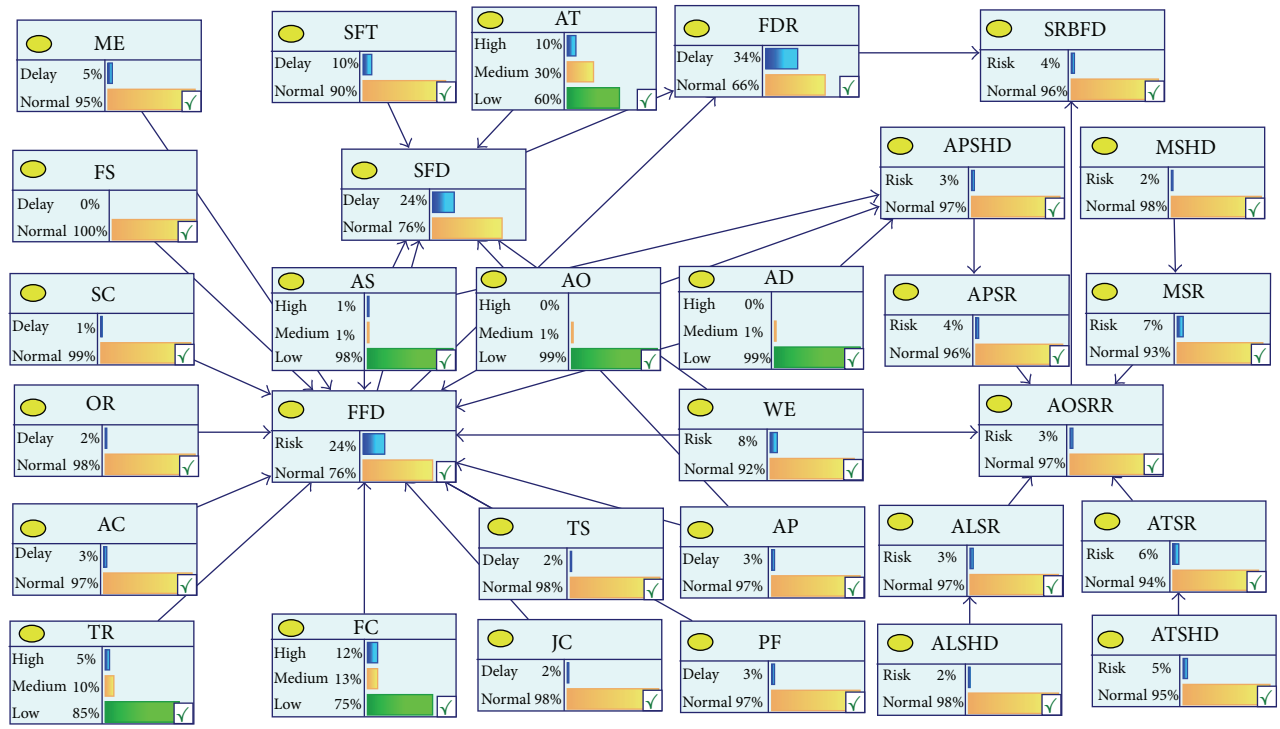

Figure 8: Posterior marginal probability of each node in January 2012.

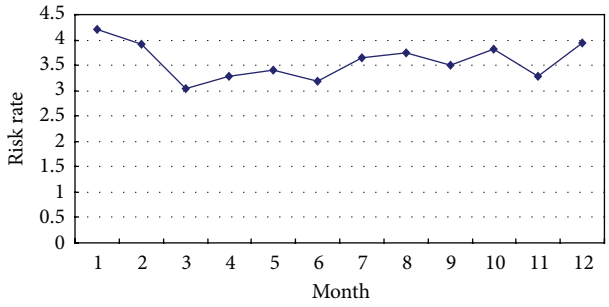

Figure 9: The safety risk probability of civil aviation operation in 2012.

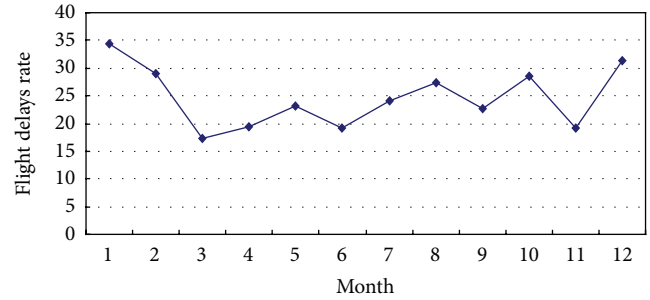

Figure 10: The civil aviation safety risk rate based on flight delay in 2012.

For example, the posterior margin probability of nodes in January 2012 is shown in Figure 8

From Figure 8, $P(\text{AOSRR} = R) = 2.960\%$ represents the safety risk of civil aviation operation system itself. $P(\text{SRBFD} = \text{Risk}) = 4.241\%$ represents the safety risk of civil aviation system based on flight delays. From the result in Figure 8, fight delays substantially increase in the safety risk probability of civil aviation, which increase the safety risk probability by 43.77%.

The safety risk probability of civil aviation for each month in 2012 has been calculated in Figure 9. Flight delays probability of civil aviation for each month in 2012 has been calculated in Figure 10. From Figures 9 and 10, the results demonstrate that there is a closer relationship between flight delays and safety risk of civil aviation; the trend is basically the same. When flight delays increase dramatically, safety risk probability greatly increases. So it is necessary to pay close attention to safety risk of civil aviation operation caused by flight delays.

The following conclusions can be drawn by the above results to strength the safety management of civil aviation in China.

(i) Fight delays are not related to the service quality and operation efficiency of civil aviation but do have a relatively great impact on civil aviation safety. The trend of flight delay rate and civil aviation risk rate is the same, which illustrates that flight delays have effect on civil aviation safety.

(ii) Partial factors which caused flight delays are controllable. The other factors which caused flight delays are not only uncontrollable but also unpredictable, which determines the difficulty of managing flight delays in China. With the development of Chinese civil aviation, the number of arrival and departure flights grows rapidly. If the managers cannot manage the flight delays effectively, the rate of flight delays will increase and the effect of flight delays will spread, which will lead to huge pressure on civil aviation safety.

(iii) It is an efficient way for strengthening the civil aviation by details management in China. The element state change in civil aviation safety system should be avoided and improved the safety management level of civil aviation in China.

6. Conclusions

The paper analyzes the relationship between flight delays and civil aviation safety risk. The problem of flight delays accompanied and propagated with civil aviation safety risk has been presented. The problem of flight delays leading to propagation and superposition of civil aviation safety risk has been analyzed. The BN has been used to model safety risk assessment of civil aviation safety. The example of some airlines in China has demonstrated the effectiveness and correctness of method. The countermeasures and suggestions have been put forward to solve the problems of Chinese civil aviation safety in the process of rapid development.

Acknowledgments

This work was supported by the National Natural Science Foundation and Aviation Fund of China (no. 60879001 and no. U1233115) and the Qinglan Project.

References

[1] M. Sachon and E. Paté-Cornell, "Delays and safety in airline maintenance," *Reliability Engineering and System Safety*, vol. 67, no. 3, pp. 301–309, 2000.

[2] M. V. McCrea, H. D. Sherali, and A. A. Trani, "A probabilistic framework for weather-based rerouting and delay estimations within an Airspace Planning model," *Transportation Research C*, vol. 16, no. 4, pp. 410–431, 2008.

[3] P. Zheng, S.-J. Hu, and C. Zhang, "Chaotic phenomena and quantitative analysis of aftereffect delay spread time on flights," *Journal of Transportation Systems Engineering and Information Technology*, vol. 10, no. 4, pp. 68–72, 2010.

[4] J.-T. Wong and S.-C. Tsai, "A survival model for flight delay propagation," *Journal of Air Transport Management*, vol. 23, pp. 5–11, 2012.

[5] S. Yan and C.-H. Tang, "A heuristic approach for airport gate assignments for stochastic flight delays," *European Journal of Operational Research*, vol. 180, no. 2, pp. 547–567, 2007.

[6] N. Pyrgiotis, K. M. Malone, and A. Odoni, "Modelling delay propagation within an airport network," *Transportation Research C*, vol. 27, pp. 60–75, 2013.

[7] G. Santos and M. Robin, "Determinants of delays at European airports," *Transportation Research B*, vol. 44, no. 3, pp. 392–403, 2010.

[8] J.-C. Ferrer, P. Rocha e Oliveira, and A. Parasuraman, "The behavioral consequences of repeated flight delays," *Journal of Air Transport Management*, vol. 20, pp. 35–38, 2012.

[9] H.-J. Shyur, "A quantitative model for aviation safety risk assessment," *Computers and Industrial Engineering*, vol. 54, no. 1, pp. 34–44, 2008.

[10] M. Janic, "An assessment of risk and safety in civil aviation," *Journal of Air Transport Management*, vol. 6, no. 1, pp. 43–50, 2000.

[11] C.-C. Chen, J. Chen, and P.-C. Lin, "Identification of significant threats and errors affecting aviation safety in Taiwan using the analytical hierarchy process," *Journal of Air Transport Management*, vol. 15, no. 5, pp. 261–263, 2009.

[12] K. B. Marais and M. R. Robichaud, "Analysis of trends in aviation maintenance risk: an empirical approach," *Reliability Engineering and System Safety*, vol. 106, pp. 104–118, 2012.

[13] P. Brooker, "Experts, Bayesian belief networks, rare events and aviation risk estimates," *Safety Science*, vol. 49, no. 8-9, pp. 1142–1155, 2011.

[14] M. Hadjimichael, "A fuzzy expert system for aviation risk assessment," *Expert Systems with Applications*, vol. 36, no. 3, pp. 6512–6519, 2009.

[15] W.-K. Lee, "Risk assessment modeling in aviation safety management," *Journal of Air Transport Management*, vol. 12, no. 5, pp. 267–273, 2006.

[16] A. Rose, "Measuring operational safety in aviation," *Aircraft Engineering and Aerospace Technology*, vol. 78, no. 1, pp. 26–31, 2006.

[17] C. V. Oster Jr., J. S. Strong, and C. Kurt Zorn, "Analyzing aviation safety: problems, challenges, opportunities," *Research in Transportation Economics*, vol. 43, no. 1, pp. 148–164, 2013.

[18] F. V. Jensen and T. D. Nielson, *Bayesian Networks and Decision Graphs*, Springer, New York, NY, USA, 2nd edition, 2007.

[19] J. Cheng, R. Greiner, J. Kelly, D. Bell, and W. Liu, "Learning Bayesian networks from data: an information-theory based approach," *Artificial Intelligence*, vol. 137, no. 1-2, pp. 43–90, 2002.

[20] P. Weber, G. Medina-Oliva, C. Simon, and B. Iung, "Overview on Bayesian networks applications for dependability, risk analysis and maintenance areas," *Engineering Applications of Artificial Intelligence*, vol. 25, no. 4, pp. 671–682, 2012.

[21] D. Zhang, X. P. Yan, Z. L. Yang et al., "Application of Bayesian belief networks in navigation risk estimation of the Yangtz river," *Reliability Engineering and System Safety*, vol. 118, pp. 93–105, 2013.

[22] M. J. Akhtar and I. B. Utne, "Human fatigue's effect on the risk of maritime groundings—a Bayesian network modeling approach," *Safety Science*, vol. 62, pp. 427–440, 2014.

[23] Y. Zhao, F. Xiao, and S. W. Wang, "An intelligent chiller fault detection and diagnosis methodology using Bayesian belief network," *Energy and Buildings*, vol. 57, pp. 278–288, 2013.

[24] C. H. Lo, Y. K. Wong, and A. B. Rad, "Bond graph based Bayesian network for fault diagnosis," *Applied Soft Computing Journal*, vol. 11, no. 1, pp. 1208–1212, 2011.

[25] S. Y. Sohn and A. S. Lee, "Bayesian network analysis for the dynamic prediction of early stage entrepreneurial activity index," *Expert Systems with Applications*, vol. 40, no. 10, pp. 4003–4009, 2013.

[26] Y. F. Xu, J. Choi, S. Dass et al., "Efficient Bayesian spatial prediction with mobile sensor networks using Gaussian Markov random fields," *Automatica*, vol. 49, no. 12, pp. 3520–3530, 2013.

[27] J. Pearl, *Probabilistic Reasoning in Intelligent Systems*, Morgan Kaufmann, 1988.

Hindawi Publishing Corporation
Mathematical Problems in Engineering
Volume 2013, Article ID 760604, 9 pages
http://dx.doi.org/10.1155/2013/760604

Research Article

Transport Turnover with Spatial Econometric Perspective under the Energy Conservation and Emissions Reduction in China

Zhongzhen Yang, Wensi Wang, Hongli Bao, Lu Kong, and Bin Yu

Management College, Dalian Maritime University, Dalian 116026, China

Correspondence should be addressed to Bin Yu; ybzhyb@163.com

Received 4 October 2013; Revised 13 October 2013; Accepted 14 October 2013

Academic Editor: Baozhen Yao

The method of spatial econometrics model is used to study the space correlation of road turnover (freight and passenger) among the 31 provinces (municipalities and autonomous regions) in China. Since some factors (such as the level of economic development, industrial structure, and population) may impact the road turnover (freight and passenger), these indexes are used as variables to reflect the influence in this model. The data of 31 provinces (municipalities and autonomous regions) in China in 2012 is collected to analyze the method. The results show that when the characteristics of turnover in a region are analyzed, it is necessary to consider the influence of its surrounding areas in space. Different scenarios were established according to different economic growth and degree of emission reduction to analyze the influence of the reduction of road turnover in regions with high spatial cluster effect to the whole country. We also carried out how to use the space effect of road turnover to the energy saving and emission reduction in the transportation industry.

1. Introduction

Since the Copenhagen conference [1], energy saving and emission reduction has become a hot issue around the world. The government of China has restated its commitment to achieving a 40–45% reduction in carbon emissions per unit of GDP by 2020 compared with 2005. With the increase of transport turnover in China, the scale of energy consumption in transportation industry increased year by year. Lots of cities attempt to solve the emission problem by improving urban public transportation [2–5]. However, the method cannot fundamentally solve the problem. The total energy consumption of transportation and related industries is 236.92 million tons of standard coal in 2009, accounting for 7.7% of the energy consumption of the whole country, just after industry and living consumption. Hence, it can be seen that if the target of carbon reduction can be achieved, transportation industry must take effective measures.

At present, many measures have been taken for the energy conservation in transportation industry all over the world, one of which is optimizing the structure of transportation. Many papers recommended that if part of the freight and passenger carried by road is transferred to railway and waterway, the energy consumption can be cut down. Authorities want to save energy and reduce emissions through transfer of the cargoes or passengers carried by road to water. So it is necessary to clear the characteristics and influencing factors of turnover first. Most of the current researches assumed that the turnover in each region is independent, and the influences of the surrounding areas are ignored. In fact, transportation industry is transport activities among different areas. This feature determines the dependence and spillover effects of turnover on geographical space. In addition, with the speeding up of the process of regional economic integration, regional cooperation will become increasingly frequent. The process will also make the data of transport turnover show some spatial dependence. Therefore, if this objective existence of spatial dependence is ignored, it is easy to produce model bias and make the conclusion of the study lack explanatory power. This paper argues that transport turnover is not only related to the region's economic and demographic factors, but also has a spatial effect. When the

transport structure of one region is adjusted, the interaction of the adjacent and close areas should be considered. Hence, in order to clear the influence to carbon reduction when turnover of road is decreased, studying the space correlation of transport turnover is of great significance.

In this paper, spatial econometrics model is used to find the relation between road turnover (freight and passenger) and the level of economic development, industrial structure, and population. The space correlation of the road turnover among 31 provinces (municipalities and autonomous regions) in China is also checked with the method. Different scenarios were established according to different economic growth and degree of emission reduction to analyze the influence of the reduction of road turnover in regions with high spatial cluster effect to the whole country. In order to achieve the emission reduction targets, China is bound to carry out macrocontrol. This paper provides a reference for the macrocontrol of China through analyzing the space correlation of the road turnover, and we also propose how to apply the characteristics of transport turnover to the energy conservation in the transportation industry.

2. Literature Review

During the past few decades, the concept of energy has received great attention from scientists, researchers, and engineers and has been applied to various industrial sectors and thermal processes. Saidur et al. [6] applied the useful energy and energy analysis models for different modes of transport in Malaysia and compared the result with a few countries. The result showed that the road subsector appeared to be the most efficient one compared to the air and marine subsectors. Jeffrey and Yanjia [7] examined trends in freight and passenger traffic to assess how growth in China's transport demand relates to growth in China's economy, as well as the energy intensity of transport. China's transport sector would likely raise world oil prices in 2020 by 1–3% in reference scenarios or by 3–10% if oil supply investment is constrained. Amekudzi et al. [8] presented a sustainability footprint framework and model that may be used in analyzing the impacts of transportation and other infrastructure systems on regional sustainable development.

Spatial econometrics is a rather recent methodological development in econometrics and has been rapidly growing as useful statistical tools for analysis of spatial dependence and spatial effect including externalities, spillovers, spatial interactions, social network effects, and peer effects in economic, demographic, political, and social studies [9, 10]. Rey and Montouri [11] considered the question of US regional economic income convergence from a spatial econometric perspective. A spatial econometric analysis of the familiar Baumol specification reveals strong evidence of misspecification due to ignored spatial error dependence. Brasington and Hite [12] estimate the relationship between house prices and environmental disamenities using spatial statistics, confirming that nearby point-source pollutants depress house price. There have been studies on spatial econometric models both for panel data ([13–16]: among others) and for cross-sectional data ([13, 17, 18]: among others).

3. Spatial Econometrics Model

According to the method and principle of spatial statistics and spatial econometrics, the basic idea for spatial econometric analysis of this paper is as follows. The Moran index method of spatial statistical analysis is used to test whether the spatial dependence of road turnover (the dependent variable) exists. If it exists, the spatial econometrics model will be established to proceed with spatial econometrics estimation and test.

3.1. Spatial Correlation. When studying the characteristics of an area, we usually depend on the sample data collected from each point in the space. But in general, because of the factors such as economy and culture, regions are not completely independent. There is, spatial correlation among spatial data of each region. Spatial correlation refers to the nonrandom spatial relevance between the observed values i and j $(i \neq j)$ in two regions, which can be expressed as

$$y_i = f\left(y_j\right), \quad j = 1, \ldots, n, \ \left(j \neq i\right). \tag{1}$$

We say that there is a spatial correlation between each two regions, but do not deny the relative independence between them. Generally, we believe that the spatial correlation between close regions is better than that of far away.

Moran derived spatial autocorrelation to study the spatial random distribution among two or higher dimension for the first time. By far, there are many methods to measure and test spatial correlation. This paper uses Moran's I index method which is mainly used to test whether the variables have spatial correlation on the whole, that is, the global spatial correlation. Global Moran's I index is defined as

$$\text{Moran's } I = \frac{\sum_{i=1}^{n}\sum_{j=1}^{n}\mathbf{W}_{ij}\left(Y_i - \overline{Y}\right)\left(Y_j - \overline{Y}\right)}{S^2\sum_{i=1}^{n}\sum_{j=1}^{n}\mathbf{W}_{ij}}, \tag{2}$$

where $S^2 = (1/n)\sum_{i=1}^{n}(Y_i - \overline{Y})$ and $\overline{Y} = (1/n)\sum_{i=1}^{n}Y_i$, Y_i represent the observed value in region i (such as freight and passenger turnover of road in this paper), n is the total number of the regions (it is 31 in this paper), and $\mathbf{W}_{ij}$ is spatial weight matrix to define the adjacent relation of spatial object.

The value of global Moran's I index is between −1 and 1. If it is greater than 0, there is a positive autocorrelation in space. And the higher the value is, the stronger the correlation is. If the value of global Moran's I index is less than 0, it means that the units do not have similar properties with their spatial adjacency. And the smaller value represents the greater difference among the units. The value of zero means that there is not any spatial correlation between various units, and they are subject to random distribution.

Through drawing Moran scatter plot which is a supplement to Moran's index, the spatial correlation in the local area can be revealed. In Moran scatter plot, the abscissa is the deviation of observed values in each area, and the ordinate is the value of spatial lag. Four different quadrants correspond to the four different types of local space link, respectively. Regions located in the first quadrant have larger observed values and their nearby areas also have larger observations. Such regions are called high-high areas and the quadrant they

locate in is defined as HH. Regions located in the second quadrant have smaller observations, but their nearby areas have larger observations. Such regions are called low-high areas and the quadrant they locate in is defined as LH. Similarly we call the third quadrant LL and the fourth HL. HH and LL quadrants indicate positive spatial autocorrelation and aggregation of close observed values in space, while LH and HL quadrants indicate that the regions in them are negatively correlated with their neighborhood. The oblique line through the first and the third quadrants expresses the value of global spatial autocorrelation. By Moran scatter plot, the phenomenon of spatial differentiation and agglomeration can be further understood.

Local spatial correlation is also known as local indicators of spatial association (LISA). This paper adopts a local Moran's Index, which is defined as

$$\text{Moran's } I = Z_i \sum_{j=1}^{n} \mathbf{W}_{ij} Z_j \quad (i \neq j), \tag{3}$$

where $Z_i = x_i - \overline{x}$ and $Z_j = x_j - \overline{x}$, respectively, mean the interest margin of the observed values and average values. x_i represents the observed value of spatial unit, and $\mathbf{W}_{ij}$ signifies spatial weight matrix. Thus, Moran's I Index can be indicated as the product of the deviation of observed values in space unit $i(Z_i)$ and the weighted average of deviation values observed in its adjacent space j.

When carried on the spatial correlation test, there are three methods to set the spatial weight matrix. One is by contiguity weight; that is, if geographic units a and b are adjacent, $\mathbf{W}_{ij} = 1$, otherwise, $\mathbf{W}_{ij} = 0$. Another is by distance weight; the upper limit of surrounding distance can be chosen autonomously according to the research content. The last is by K-nearest neighbor spatial weights. An appropriate matrix will be selected to be used in the space model through examining the contiguity weight and distance weight in our paper.

3.2. Spatial Model. According to the related theory of spatial panel model, relationships of spatial autocorrelation are in two forms: spatial lag model (SLM) and spatial error model (SEM). In the spatial lag model, the spatial relevance of variable is reflected by the space lag of the dependent variables. Spatial lag model is mainly focused on whether the variables in a region have diffusion effect (or spillover effect).

(1) Spatial Lag Model (SLM). Model as follows:

$$Y = \rho \times \mathbf{W}_y + X\beta + \varepsilon. \tag{4}$$

Y is explanatory variables. X is the exogenous variable matrix of $n \times k$. ρ is coefficient for spatial regression, which reflects the relationship among spatial units. That is to say, it is the degree of influence of the adjacent space units to one space unit (the degree of influence is vector with certain direction). $\mathbf{W}$ is spatial weight matrix of $n \times n$, and $\mathbf{W}_y$ is the spatially lagged dependent variables of $\mathbf{W}$. ε is the random error vector. Parameter β mainly reflects the influence of independent variable X to dependent variable Y. $\mathbf{W}_y$ is an endogenous variable, reflecting how the spatial distance affects each space unit.

(2) Spatial Error Model (SEM). Model as follows:

$$\begin{aligned} Y &= X\beta + \varepsilon, \\ \varepsilon &= \lambda \times \mathbf{W}\varepsilon + \mu. \end{aligned} \tag{5}$$

Y is dependent variables, and X is the exogenous variable matrix of $n \times k$. $\mathbf{W}$ is spatial weight matrix of $n \times n$. ε is the random error vector. μ is the random error vector of normal distribution. Parameter β is the influence coefficient of independent variable X to dependent variable Y. λ is the space error coefficient of dependent variable vector.

4. Empirical Analysis

In this paper, the space unit is 31 provinces in China. The measurement is freight and passenger turnover of each province from 1980 to 2012. Firstly, global spatial correlation index (Moran's I) is used to test whether road turnover (freight and passenger) of each province has self-correlation in space and cluster phenomenon. Then, by local indicators of spatial association (LISA), it is further analyzed to reveal the spatial correlation of road turnover (freight and passenger) in adjacent provinces. Moreover, spatial regression is used to search the relation between the turnover of road and the level of economic development, industrial structure, and population. And this section also puts forward an approach on how to apply the characteristics of turnover to energy conservation and emissions reduction in transport industry.

4.1. Data Collection and Process

4.1.1. TOV_i, the Freight and Passenger Turnover of Road Transportation. This paper studies the spatial relation of road turnover (freight and passenger) among 31 provinces in China. Hence, the data of freight and passenger turnover of road transportation of 31 provinces in China during 32 years (from 1981 to 2012) is collected. Meanwhile, to simplify the research, the passenger turnover of road, railway, airway, and waterway is transferred to freight turnover according to the general standards to reduce the unknown scalars.

4.1.2. GDP_i and People and RC (Route Coverage). Freight and passenger turnover is related to economic level, industry structure, and population in each province. In theory, the higher the level of economic development, the more population, and the more route coverage there is, the more transportation turnover there is. For the factor of industrial structure, the tertiary industry (service) impacts the transport turnover less than the first and the secondary industries. This paper chose GDP with different industries to be the measurement of local economic level and industry structure. The GDP of the primary, secondary, and tertiary industry and population of each province are collected to be exogenous explanatory variables in spatial econometric model.

4.2. Spatial Correlation Analysis. Before setting up the model, this paper tested the global spatial correlation of freight and passenger turnover of road firstly. The data of road turnover

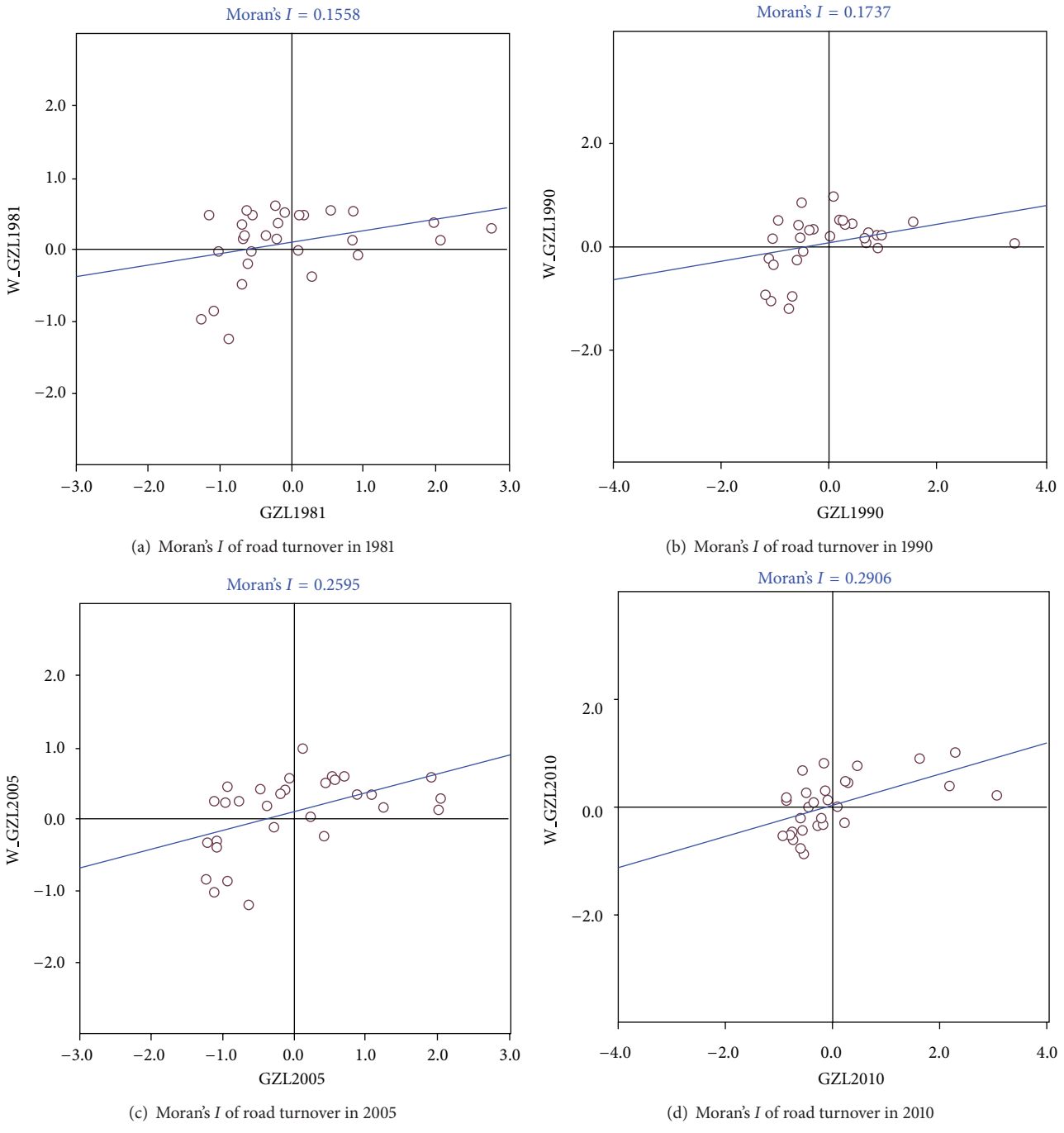

(a) Moran's I of road turnover in 1981

(b) Moran's I of road turnover in 1990

(c) Moran's I of road turnover in 2005

(d) Moran's I of road turnover in 2010

Figure 1: Moran's I of road turnover.

(freight and passenger) of 31 provinces from 1981 to 2012, a total 32 years, is adopted. Software package GeoDA is used to calculate Moran's I index. The result is shown in Figure 1.

Figure 2 shows that although the spatial correlation of road turnover (freight and passenger) fluctuates, the trend has been rising since 1981 on the whole. The initial figure is 0.1558 and increases to 0.2985 by 2012. The growth indicates that, with economic progress, road transportation system has developed rapidly. The relationship among provinces has become closer, and the degree of spatial dependence of road turnover (freight and passenger) among regions has been greater. The analysis of global spatial correlation in this section shows that whatever the space matrix is, the freight and passenger turnover of road between regions has strong spatial correlation. Thus, the influencing factors of space should be taken into consideration in the analysis.

In order to clear the influence of time and space on space correlation of the road turnover, it is necessary to perform

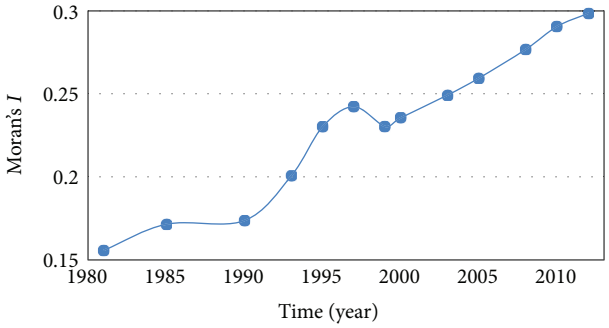

Figure 2: Tendency of Moran's I of road turnover (freight and passenger) during 32 years.

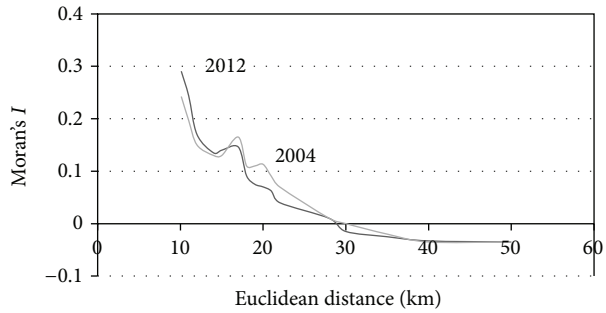

Figure 3: The space correlation of road turnover under different Euclidean distance.

a further study. This paper calculates the Moran's I of road turnover (freight and passenger) under different Euclidean distance in 2004 and 2012. The results are shown in Figure 3.

It can be seen from Figure 3 that the space correlation of road turnover among 31 provinces decreased with the increasing of Euclidean distance. With the distance below 15 km, the space correlation in 2012 is greater than that in 2004. But when the distance is more than 15 km, the space correlation in 2012 is weaker. It can be inferred that for the short-haul transportation, the space correlation of road turnover (freight and passenger) increased with the development of network and road infrastructure in the past 6 years. With the development of social economy and the process of location, many companies think more about local ingredients and reducing the long-haul transport, in order to reduce the transportation costs. So, for long-haul transportation, the space correlation debased.

4.3. Local Indicators of Spatial Association. Local indicators of spatial association (LISA analysis) is used to further study the spatial structure and cluster phenomenon of provincial road turnover (freight and passenger) as a supplement for global space correlation. The spatial matrix adopted is distance weight with the Euclidean distance of 1016.6 km. The result is shown in Figure 4.

As is seen visually from the figure, red areas represent regions with larger road turnover (freight and passenger); meanwhile the volumes in their surrounding regions are also high. These areas are Liaoning, Jiangsu, Shanghai, Zhejiang, and Jiangxi. Blue areas represent regions with smaller turnover of road, and the volumes in their surrounding regions are also low. These areas are Xinjiang, Gansu, Qinghai, and Sichuan. Light blue areas are regions of low turnover volume but with high volume in the adjacent areas. This is a negatively related relationship, and the areas are Anhui and Tianjin. The correlations of road turnover (freight and passenger) studied in this paper are mostly positive and only a few areas are negative.

Factors such as economy, industrial structure, and geographical conditions in each province are different, so is the transport structure. In order to reach the goal of energy conservation and emissions reduction, it is hard to adjust 31 provinces at the same time when the authorities take

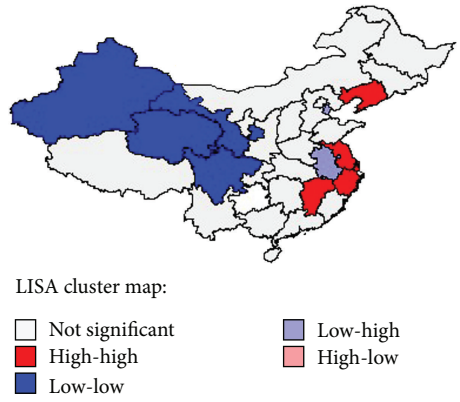

Figure 4: Local Indicators of spatial association.

measure to transfer the enterprise and resident performances of choosing transport modes. Thus, provinces that can be performed best should be selected through analysis so as to achieve the goal of maximum output with minimum input. The changes of turnover volume in one or more provinces would result in the corresponding change in its surrounding provinces. Highway transportation is usually transferred to waterway, while the integrated transport system structure is optimized. Thus, the regions with developed waterway and stronger spatial correlation should be considered for the macroeconomic regulation and control in order to reduce the proportion of road turnover, such as Liaoning, Jiangsu, Shanghai, and Zhejiang.

4.4. Spatial Relation Model. Based on the data of 2012, this part is mainly to set up two space models: spatial lag model (SLM) and spatial error correction model (SEM). Here we choose the Euclidean distance among each province (municipalities and autonomous regions) as spatial weight. Through the comparative analysis of above models, the space effects of road turnover (freight and passenger) and the influencing modes will be revealed. It is possible to provide reference for energy conservation and emission reduction.

As a whole, the amount of a region's freight and passenger turnover is the result of the comprehensive function of many factors. Since we could not describe all the relevant factors in detail, we only chose some representatives. (1) Economic

level: generally, the more developed a region's economy is, the more developed the transportation system is, and the more freight and passenger turnover is produced. (2) Industrial structure: the contribution of primary industry to cargo turnover is larger, while that of tertiary industry is small. (3) Population: without considering other factors, greater population means higher passenger traveling intensity. (4) Route coverage: the spatial lag model to examine provincial road transport volume is as follows:

$$\begin{aligned} \mathrm{RT}_i = {} & \rho \mathbf{W} \times \mathrm{RT}_i + \alpha_i + \beta_1 \mathrm{FGDP}_i + \beta_2 \mathrm{SGDP}_i \\ & + \beta_3 \mathrm{TGDP}_i + \beta_4 \mathrm{People}_i + \beta_5 \mathrm{RC}_i + \varepsilon_i. \end{aligned} \tag{6}$$

In formula (6), index i is for province. $\mathbf{W}$ is a spatial weight matrix of $31 * 31$. $\mathbf{W}_{ij}$ in $\mathbf{W}$ defines the spatial relationship which is known as Distance Weight. $\mathbf{W} \times \mathrm{RT}_i$ is dependent variable of spatial lag. ρ is the coefficient of spatial autoregressive, and its estimated value reflects the direction and size of the spatial correlation. β_x $(x = 1, 2, 3, 4, 5)$ is variable coefficient. a_i and ε_i represent the constant and the random error, respectively.

When the spatial correlation is transmitted through the variable ignored by explanatory variables of the model, it is assumed to be produced by error process. Space error model of road turnover (freight and passenger) is as follows:

$$\begin{aligned} \mathrm{RT}_i = {} & \alpha_i + \beta_1 \mathrm{FGDP}_i + \beta_2 \mathrm{SGDP}_i + \beta_3 \mathrm{TGDP}_i \\ & + \beta_4 \mathrm{People}_i + \beta_5 \mathrm{RC}_i \lambda \times \mathbf{W} \varepsilon_{ij} + \mu_i. \end{aligned} \tag{7}$$

In Formula (7), a_i is the intercept term. $\mathbf{W}\varepsilon_{ij}$ is the space lag error. λ is the spatial error autocorrelation coefficient which indicates the spatial correlation intensity between regression residuals. β_x $(x = 1, 2, 3, 4, 5)$ is the variable coefficient and μ_i represents the random error term.

FGDP means GDP of the first industry, SGDP means GDP of the second industry, and TGDP is GDP of the third. These three indexes indicate both the economic level and industrial structure. People is the total population in the region and RC is route coverage.

According to the data 2012, the above two spatial models and a conventional model (i.e., does not consider the spatial correlation) are used to study the relevance, and the results are shown in Table 1.

As is seen from the regression results, *R-squared* is greater than 0.8 in the three models and in SAM is the largest, nearly 0.9. Besides, the spatial regression for *R-squared* is superior to the traditional result. Under SLM model, the spatial autoregressive coefficient is 0.5578 which indicates that for a certain province, if the road turnover (freight and passenger) drops 1 unit in its adjacent province within 1016.6 km, it would decrease 0.5578 units. This is a strong correlation, while under SEM, spatial error autocorrelation coefficient is 0.597. It means that regional correlation impacted by unobserved factors in each province also plays a positive role in the road turnover.

The results also yield that the contribution of the primary and secondary industry to the turnover of road is greater than the tertiary industry. The government making efforts to optimize the industrial structure and increase the proportion of service industry is conducive to reducing turnover. And further, transport energy consumption could be reduced and the goal of energy conservation and emissions reduction would be also achieved.

Table 1: Road turnover regression results.

Model variable	Tradition	SAM	SEM
R-squared	0.845	0.894	0.853
FGDP	2.0867	1.8101	1.676
SGDP	0.205	0.1879	0.1738
TGDP	0.043	0.0015	0.0144
People	−0.933	−0.775	−0.716
RC	1.7904	1.3490	0.9962
α	992.135	212.91	1044.04
ρ		0.5578	
γ			0.597

5. Scenario Analysis

In this section, three scenarios are established according to different economic growth and degree of emission reduction to analyze the influence of the reduction of road turnover in regions with high spatial cluster effect to the whole country. We carry on a comparative analysis for the different states under each scenario and come up with how to use the space effect of road turnover to energy saving and emission reduction in transportation industry.

5.1. Scenarios and Hypothesis. As mentioned above, road turnover has relations with economic level, industrial structure, and population. At the same time, road turnover has spatial correlation. This paper sets three scenarios for economic development level in the future. According to the spatial relation model, the road turnover in 2013 under different scenarios can be calculated. On the basis of feasibility and regression fitting, the spatial lag model is chosen to calculate. Liaoning, Shanghai, Jiangsu, and Zhejiang are coastal regions; in each scenario, the authorities exert political pressure to the four regions and water transportation is developed rapidly. Jiangxi province is an inland area, so railway transportation is developed mainly. Therefore, the quantity of road turnover is reduced. Since the five regions are areas with high spatial cluster effect, the reduction of the road turnover in these areas will make the road turnover in the surrounding areas reduce. Then, we can get the percentage decline of road turnover in the whole country and observe the interaction effect of road turnover's spatial correlation.

In our model, with the availability of partial data and the feasibility of calculation with spatial lag model, the following assumptions are conducted for the model.

(1) When the road turnover is computed, only the economic level, industrial structure, and population are considered.

Table 2: Scenarios of economic growth and degree of emission reduction.

Scenarios	Introduction	Related parameters
High-growth scenario	The domestic economic development is good and the authorities of China adopt a high degree of macrocontrol. The road turnover of the five regions mentioned above transferred to waterway and railway largely. The philosophy of low-carbon is deep in the human mind and the implementation environment of low-carbon is fine.	GDP growth rate: 10%. The reduction rate of road turnover: 25%
Moderate-growth scenario	The domestic economic development is stable and the road turnover grows steadily. The authorities introduce relatively soft macro-control policies.	GDP growth rate: 8%. The reduction rate of road turnover: 15%
Low-growth scenario	A variety of uncertainties in the future are taken into account, so the domestic economic development is poor. In this economic environment, the increase in road turnover is small, and the measures adopted by authorities are slight.	GDP growth rate: 6%. The reduction rate of road turnover: 5%

(2) When we use the spatial lag model to compute the road turnover, if the turnover in the right and left of the equation is of the same period, the calculation is infeasible. Thus, this paper let the road turnover in the right of the equation release in time. It is assumed that the turnover in the left of the equation has the same spatial correlation with the date in the right of last period.

(3) The industrial structure does not change in the future.

The economic development level and degree of emission reduction are considered comprehensively to establish the scenarios. The scenarios are as follows: high-growth scenario, moderate-growth scenario, and low-growth scenario. The GDP growth rate of China during 1987 and 2012 is 8~12% and fluctuates up and down with the center of 10%. But the economics of domestic and overseas are both in depression, so the data of economic growth is set as follows. The details of each scenario are shown in Table 2.

5.2. Scenario Analysis. This paper lets the road turnover in the right of the equation of the Spatial Lag Model release in time with the data of road turnover in 2012. The data of GDP and population is in 2013. By the model, the road turnover of each province in 2013 can be calculated. According to polices and projections of Five-Year Plan (2011–2015) drafted by the provincial population and family planning commission, we collected the data of population in 2013. Under the three scenarios, the road turnover in Liaoning, Shanghai, Jiangsu, Zhejiang, and Jiangxi in 2012 is reduced by 25%, 15%, and 5%. With the Spatial Lag Model, the road turnover of other regions and the whole country in 2013 can be calculated again. The data before and after reduction are compared. We observe the reduction rate of road turnover in the regions that have spatial correlation with the five areas and the reduction rate in China. The lessening of the road turnover will carry out the reduction of energy consumption and carbon dioxide emissions. The results are shown as Figure 5.

It can be seen from Figure 5 that, in each scenario, the reduction of road turnover in the five regions (Liaoning, Jiangsu, Shanghai, Zhejiang, and Jiangxi) drives the road turnover of their adjacent areas decreasing at the same time. But the degrees of reduction in each region are different. Because for a province, apart from its adjacent areas, the quantity of its road turnover is also related with the economic level, industrial structure, and population of its own region. When the reduction rates of road turnover in the five regions are 25%, 15%, and 5%, respectively, the reduction rates in China are 6.4%, 3.3%, and 1.3%. Although the reduction rates in the whole country are less than the rates in the five regions, these are the achievements with the control of only certain areas. It is significant to reduce the carbon emissions all over the country through the emission reduction in part provinces.

Under the high-growth scenario, the road turnover increases rapidly with the quick development of the economy. Meanwhile, the degree of emission reduction is great. The reduction rates of road turnover in the regions with high spatial cluster effect are high, and the rates in their adjacent areas are relatively large. The reduction of the road turnover in the whole country is significant. Under the scenario of moderate-growth, the reduction rate of China is 3.3%. The number may seem to be unobvious, but it is the achievement of one year. If the authorities take measures of macro-control to partial regions every year, the road turnover will decrease year by year. When the quantity of road turnover in each province is changed, the local indicators of spatial association is used again to choice the appropriate areas, and the authorities take macroeconomic control to these new areas. The cumulative effect of road turnover reduction is considerable. Furthermore, these stable economic growth and gentle emission reduction efforts are suitable for the current economic development situation. In the low-growth scenario, the economic growth is slow, and the degree of emission reduction is low. Without taking other saving measures, the percentage of the total reduction in China is low, and the effect of emission reduction is unobvious. For the above three scenarios, the moderate-growth scenario is more coincident with the situation of China. On the basis of stable economic development, the degree of energy saving and emission reduction is gentle.

6. Conclusion and Prospect

In the era context of energy saving and emission reducing, transportation industry, a high energy consumption industry, should take measures actively to reduce carbon emissions. The quantities of carbon emission in transportation industry are directly related with transport turnover of comprehensive transportation system, so it is important to study the

(a) The reduction of road turnover under high-growth scenario

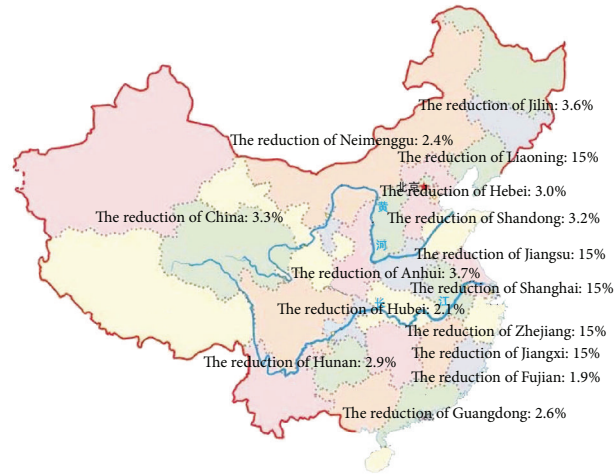

(b) The reduction of road turnover under moderate-growth scenario

(c) The reduction of road turnover under low-growth scenario

Figure 5: The reduction of road turnover.

characteristics of transport turnover. By the global spatial correlation, it can be found that road turnover (freight and passenger) has strong spatial correlation, and with the increasing of turnover the trend is rising year by year. Meanwhile, the examination with the local spatial correlation in each province shows that Liaoning, Jiangsu, Shanghai, Zhejiang, and Jiangxi have high spatial cluster effects in transport turnover. The spatial correlation should be considered when authorities take macroeconomic regulation and control to reduce the road turnover. However, macroeconomic regulation and control is difficult to be carried out nationally at the same time. Thus, this paper suggests to control the above five areas, making them drive the surrounding provinces and cities simultaneously.

Road turnover in certain region is positively related with its economic level, population, and transport volumes of surrounding areas. The spatial correlation is obvious. Meanwhile, the industrial structure also affects the volume of the turnover, and the influence of the primary and secondary industry to the road turnover (freight and passenger) is greater than the tertiary industry. The government making efforts to optimize the industrial structure and increase the proportion of service industry is conducive to reducing turnover. Through the scenario analysis, we find that with the reduction of road turnover in Liaoning, Jiangsu, Shanghai, Zhejiang, and Jiangxi, the turnover of their adjacent areas is also reduced. The moderate-growth scenario is more coincident with the situation of China. On the basis of stable economic development, the degree of energy saving and emission reduction is gentle. It can be seen that taking the space correlation of turnover into consideration for energy saving and emission reduction in transportation industry is an efficient way.

Acknowledgments

This work was supported by The National Natural Science Foundation of China (nos. 51078049 and 51108053), Humanities and Social Sciences Foundation from the Ministry of Education of China (09YJA790021), the Trans-Century

Training Program Foundation for Talents from the Ministry of Education of China (NCET-12-0752), and Liaoning Excellent Talents in University (LJQ2012045).

References

[1] "The United Nations Climate Change conference," Copenhagen, Danish, 2009.

[2] B. Z. Yao, P. Hu, M. H. Zhang, and S. Wang, "Artificial bee colony algorithm with scanning strategy for the periodic vehicle routing problem," *Simulation*, vol. 89, no. 6, pp. 762–770, 2013.

[3] B. Yu and Z. Z. Yang, "An ant colony optimization model: the period vehicle routing problem with time windows," *Transportation Research E*, vol. 47, no. 2, pp. 166–181, 2011.

[4] B. Yu, Z. Z. Yang, and L. I. Shan, "Real-time partway deadheading strategy based on transit service reliability assessment," *Transportation Research A*, vol. 46, no. 8, pp. 1265–1279, 2012.

[5] B. Yu, H. B. Zhu, W. J. Cai, N. Ma, and B. Z. Yao, "Two-phase optimization approach to transit hub location—the case of Dalian," *Journal of Transport Geography*, vol. 33, pp. 62–71, 2013.

[6] R. Saidur, M. A. Sattar, H. H. Masjuki, S. Ahmed, and U. Hashim, "An estimation of the energy and exergy efficiencies for the energy resources consumption in the transportation sector in Malaysia," *Energy Policy*, vol. 35, no. 8, pp. 4018–4026, 2007.

[7] S. Jeffrey and W. Yanjia, "China on the move: oil price explosion?" *Energy Policy*, vol. 35, no. 1, pp. 678–691, 2007.

[8] A. A. Amekudzi, C. Jotin Khisty, and M. Khayesi, "Using the sustainability footprint model to assess development impacts of transportation systems," *Transportation Research A*, vol. 43, no. 4, pp. 339–348, 2009.

[9] L. Anselin, "Spatial econometrics," A working paper, Center for Spatially Integrated Social Science, 1999.

[10] L. Anselin, "Spatial econometrics in RSUE: retrospect and prospect," *Regional Science and Urban Economics*, vol. 37, no. 4, pp. 450–456, 2007.

[11] S. J. Rey and B. D. Montouri, "US regional income convergence: a spatial econometric perspective," *Regional Studies*, vol. 33, no. 2, pp. 143–156, 1999.

[12] D. M. Brasington and D. Hite, "Demand for environmental quality: a spatial hedonic analysis," *Regional Science and Urban Economics*, vol. 35, no. 1, pp. 57–82, 2005.

[13] L. Anselin, *Spatial Econometrics: Methods and Models*, Kluwer Academic Publishers, Dordrecht, The Netherlands, 1988.

[14] J. P. Elhorst, "Specification and estimation of spatial panel data models," *International Regional Sciences Review*, vol. 26, no. 3, pp. 244–268, 2003.

[15] B. H. Baltagi, P. Egger, and M. Pfaffermayr, "Estimating models of complex FDI: are there third-country effects?" *Journal of Econometrics*, vol. 140, pp. 260–281, 2007.

[16] M. Kapoor, H. H. Kelejian, and I. R. Prucha, "Panel data model with spatially correlated error components," *Journal of Econometrics*, vol. 140, no. 1, pp. 97–130, 2007.

[17] H. H. Kelejian and I. R. Prucha, "A generalized moments estimator for the autoregressive parameter in a spatial model," *International Economic Review*, vol. 40, no. 2, pp. 509–533, 1999.

[18] B. Z. Yao, C. Y. Yang, and J. B. Yao, "Tunnel surrounding rock displacement prediction using support vector machine," *International Journal of Computational Intelligence Systems*, vol. 3, no. 6, pp. 843–852, 2010.

Hindawi Publishing Corporation
Mathematical Problems in Engineering
Volume 2013, Article ID 646241, 10 pages
http://dx.doi.org/10.1155/2013/646241

Research Article

Real-Time Gate Reassignment Based on Flight Delay Feature in Hub Airport

Huawei Wang, Yuxiao Luo, and Zhijian Shi

College of Civil Aviation, Nanjing University of Aeronautics and Astronautics, Nanjing 210016, China

Correspondence should be addressed to Huawei Wang; huawei678@163.com

Received 30 September 2013; Revised 30 October 2013; Accepted 31 October 2013

Academic Editor: Bin Yu

Appropriate gate reassignment is crucially important in efficiency improvement on airport sources and service quality of travelers. The paper divides delay flight into certain delay time flight and uncertain delay time flight based on flight delay feature. The main objective functions of model are to minimize the disturbance led by gate reassignment in the case of certain delay time flight and uncertain delay time flight, respectively. Another objective function of model is to build penalty function when the gate reassignment of certain delay time flight influences uncertain delay time flight. Ant colony algorithm (ACO) is presented to simulate and verify the effectiveness of the model. The comparison between simulation result and artificial assignment shows that the result coming from ACO is obvious prior to the result coming from artificial assignment. The maximum disturbance of gate assignment is decreased by 13.64%, and the operation time of ACO is 118 s. The results show that the strategy of gate reassignment is feasible and effective.

1. Introduction

Gate reassignment is a necessary procedure when its planned gate assignment is influenced by real-time operation situation and cannot be normally implemented. With the significant improvement of air transportation, gates become the key resources in airport, which are to be the bottleneck in maximizing operational efficiency. An appropriate gate assignment will make a difference in improving airport capacity and passenger satisfaction. However, in practice, disturbed by factors such as weather condition, flow control, flight schedule, and passengers, the advanced gate assignment plan cannot achieve original goal, so gate manager (or airport manager) must conduct gate reassignment timely to improve the operation effectiveness on airport surface. Rapid and effective gate reassignment plays an important role in improving operation efficiency and airport volume, decreasing operation cost of airlines, and improving service quality of passengers.

The characteristics of gate assignment based on flight delays should be described in following aspects.

(i) The difficulty in predicting the accurate flight delay, which is caused by the complicate delight delay, increases the complexity of gate assignment. Therefore, it is necessary to gate assignment on time.

(ii) Almost all the flights should be assigned proper gate under the condition of large-scale flight delay newly. The workload is very heavy, so that the traditional method of gate assignment is difficult to work effectively in gate assignment.

(iii) Large-scale flight delay can reduce the operation of airport. Constraint condition and multiobjective should be taken into account in the gate reassignment under the condition of large-scale delay in hub airport.

Considering the above characteristics of gate assignment, the intricate gate assignment under the condition of large-scale delay is a multiobject assign problem based on uncertain information.

Thus, gate reassignment is widely discussed in the worldwide research. In the way of gate preassigned, Yan and Chang [1] developed a multicommodity network flow to minimize passenger walking distances and utilized an algorithm based on the Lagrangian relaxation with subgradient methods.

Maharjan and Matis [2] presented a binary integer multicommodity gate flow network model with the objective of minimizing the fuel burn cost of aircraft taxi by type and expected passenger discomfort. Focusing mainly on maximum gate employment, Genç et al. [3] presented a stochastic neighborhood search approach for airport assignment, which combines the benefits of heuristic approaches with some stochastic approach to building a model to minimize the number of flights assigned to aprons and the total walking distances, Cheng et al. [4] presented a metaheuristics model for airport gate assignment, which generates good solutions in a reasonable timeframe. Considering the preference and robustness in flight assignment optimization, Dorndorf et al. [5] built a model to minimize the number of trailers in gage assignment and adapted search algorithm to verify the effectiveness of the model. Some researchers focus on real-time gate assignment. Tang and Wang [6] studied airport gate assignment for airline-specific gates, which is different from the traditional gate assignment and allocated flights to airline-specific gates is based on the perspective of the airline rather than that of the airport authority. Jaehn [7] used dynamic programming approach to building a gate assignment model based on flight number.

There are increasing researches on gate reassignment. For example, Maharjan and Matis [8] built a binary integer model for the optimal reassignment of planes to gates in response to flight delays. Gu and Chung [9] presented a genetic algorithm to minimize passenger walking distance. Some research concentrates on gate reassignment under stochastic or uncertain condition. Hou [10] built a gate reassignment model and classified flight types to minimize space and time disturbances based on flight delay feature. Tang et al. [11] built a gate reassignment model to decrease delay time and gate change, and then they calculated the disturbance by conversing delay time and designed a rapid heuristic algorithm to verify the model. Tang [12] added the influence of random factors and broadened some constraints in order to deal with delay. Yan and Tang [13] tried to build comprehensive gate assignment model at the same time based on Tang et al. [11] and Tang [12]. Some literature considered the interrelationship between planned assignment and reassignment. Şeker and Noyan [14] considered the gate assignment problem under uncertainty in flight arrival and departure times and developed stochastic programming models incorporating robustness measures based on the number of conflicting flights, idle and buffer times. Yan et al. [15] presented a simulation framework which could analyze the effects of stochastic flight delays, flexible buffer times, and real-time gate assignment rules. Some researches focused on reassignment in serious incidents such as airport closure. Taking a panoramic view of the domestic and foreign research status, most researches assigned the disturbed flight in passenger perspective. In practice, due to uncertainty and limitation of information obtained in real time, flights are possibly to be assigned more than once which will lead to increasing flight delay time and decreasing efficiency of airport resource. Therefore, both information certainty and reassignment urgency should be taken into account during gate reassignment in order to improve the efficiency of airport gates.

In the paper, the characteristics of gate reassignment based on flight delay in hub airport have been analyzed. The deposition of gate assignment and conformation of objective function are applied to reduce the complexity of research problems.

The paper divides delay flights into certain delay time flight and uncertain delay time flight base on flight delay feature. The main objective functions of model are to minimize the disturbance led by gate reassignment in the case of certain delay time flight and uncertain delay time flight, respectively. Ant colony optimization method, which is the representative method in discrete optimization, has been used to model real-time gate assignment and multiobjective optimization based on flight delay in hub airport. The remainder of paper is organized as follows. In Section 2, we describe the gate reassignment. In Section 3, we build optimization model. We design ACO to simulate the model in Section 4. In Section 5, a numerical test was performed with comparison to the artificial method. Finally, we conclude in Section 6.

2. Gate Reassignment Description

The purpose of gate reassignment is to obtain a new flight-to-gate scheme according to scheduled assignment to reassign the delay flights in order to avoid flight conflicts in view of operation safety. Therefore, in the course of gate reassignment, certainty information, stochastic issues, and reassignment disturbance should be taken into account.

2.1. Delay Features and Information. In practice, gate managers will constantly receive estimated time information of each delay flight. From the time point of gate reassignment operation, if the estimated time of the delay flight is more close to the actual operation time, the managers will get more certain information of delay flights. That is to say the managers can schedule the delay flights actually. Otherwise, the arrival-departure information of delay flights needed by managers is not easy to be gotten correctly, so the delay feature is difficult to be holed. In the paper, the authors classified the follow-up arrival-departure flights into certain delay time flight and uncertain delay time flight. Some scheduled time node after gate reassignment is a demarcation point to reassign the follow-up arrival-departure flights into the appropriate gate. The gate reassignment is based on the gate reassignment scheduled time. The time node is decided by the acquired information and operation condition the same day. If the delay time of delay flight is confirmed, the arrival-departure time is conformed, so the reassignment demand is urgent.

2.2. Stochastic Factors and Relax Constrains. Influenced by delay features, different flights have different uncertain degrees. Stochastic factors have a significant effect on unidentified flights, which will lead to varieties of uncertain situation. Assume that there are only 2 gates (Gate 1 and Gate 2) and 3 flights (Flight 1, Flight 2, and Flight 3), Figure 1 shows the scheduled gate assignment for 3 flights.

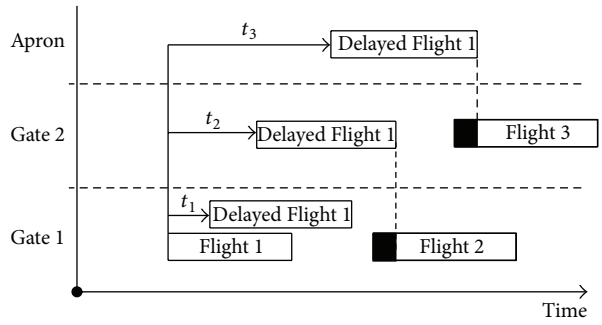

Figure 1: Influence on gate reassignment by stochastic factors.

From Figure 1, Flight 1 and Flight 2 are assigned to Gate 1 and Flight 3 is assigned to Gate 2 in the planned assignment stage. The probability of delay time of Flight 1 is one of t_1, t_2, or t_3. Assume that the probability of each delay scenarios is equal. If the delay time of Flight 1 is t_1, the planned assignment is still valid. If the delay time of Flight 1 is t_2, Flight 1 will have time overlap with Flight 2. To avoid this occasion, Flight 1 can be allocated to Gate 2 or the apron. If the delay time of Flight 1 is t_3, Flight 1 will have time overlap with Flight 2 and 3, and it can be only allocated to the apron. When Flight 1 is reassigned to Gate 2, the influence on airport operation cost and service level will be ignored, while when Flight 1 is reassigned to apron, the influence will be worse. At the real-time gate assignment stage, if avoiding occupancy conflict drastically is the main objective in gate reassignment, gate managers should consider all the three delay scenarios and assign Flight 1 to the apron.

From the point of minimizing the reassignment influence, it is just necessary to consider scenarios that delay time are t_1 and t_2 if some potential conflicts are acceptable. In this way, Flight 1 can be allocated to Gate 2. Gate managers need to balance the cost and influence caused by potential conflicts with small probabilities.

The influence coming from stochastic factors for uncertain delay information should be taken into consideration. Some constraints of unidentified delay flights are tolerable to be conflicted, which means that time overlap (or time violation) is allowable in one gate. Relax constraints can lead to infeasible solution in some scenarios, which needs penalty coefficients and functions to deal with. Details about penalty coefficients and functions will be described in Section 3. Uncertain flights are not in reassignment urgency, so this violation will not have actual influence on real-time airport operation in an operation framework repeatedly.

2.3. Reassignment Disturbance. There are three main processes for gate reassignment, allocating flights to aprons (apron disturbance), allocating flights to gates different from scheduled (gate disturbance), and making flights wait until gates are available (time disturbance). All of these processes will disturb the normal operation of airport and will have serious impact on passenger service level and stall scheduling. Thus, to maximize airport operation efficiency, benefits, and passenger service level, aforementioned constrains are necessary to be considered. The objective of research is to minimize the reassignment disturbance value and penalty value of certain and uncertain delay flight compared to planned gate assignment. Real-time gate reassignment is a continuous operation process. In order to obtain perfect reassignment scheme, the real-time operation process need a fixed time circle to complete all gate reassignment tasks in one day.

In order to avoid extra delay or propagation delay caused by airport operation for certain flight, only apron disturbance and gate disturbance are considered. On the contrary, for uncertain flight, because they lack reassignment urgency, it is better to delay their gate reassignment starting time rather than assign them to aprons when no gates are available. Thus, gate disturbance, time disturbance, and the penalty caused by relax constraints are considered. In actual airport operation, only the reassignment results of certain flights are released to gate managers, while the calculation results data of uncertain flights are key influence factors to improve the flexibility of certain flight gate reassignment results.

3. Real-Time Gate Assignment Model

3.1. Assumption. The assumptions used for the real-time gate assignment model are listed as follows.

(i) The result of planned gate assignment is known in advance.

(ii) The arrival-departure time distribution of each flight is known.

(iii) For simplicity, the research divides the minimum safety interval time and necessary buffer time between two consecutive flights into two parts and pluses them into gate occupation time of the two flights, respectively, according to aircraft type request. Thus, the minimum interval constrains need not to be considered.

(iv) For simplicity and maximum reassignment efficiency, constrains, such as airlines preference, are not considered.

(v) The aprons in airport, which includes three types, are sufficient. When a flight is assigned to the apron, it does not need to consider time overlap and aircraft type matching.

3.2. Mathematical Notation

$v_{i,k+1}$: The disturbance value, Flight i is assigned to apron

w_{ik}: The disturbance value, Flight i is assigned to gate k

C_i: The gate occupying time point of Flight i

T_i: The gate occupation time of Flight i, including minimum safety interval time and necessary buffer time

P_α: Probability of the ath stochastic scenario

d_{ij}: The delay disturbance value, the uncertain Flight i is assigned to gate at time point j

e_{kt}: The penalty value, gate conflict is emerged in the k gate at time point t for uncertain flight

MF: Set of certain flights in each gate reassignment stage

NF: Set of uncertain flights in each gate reassignment stage

VG_i: Set of all available gates assigned to certain Flight i

DG_i: Set of all available gates assigned to uncertain Flight i

TD_i: Set of available time points assigned to uncertain Flight i

k: Set of gates, including several gates

$k + 1$: Set of apron, including several aprons

M_i: Aircraft type of Flight i

N_k: Type of Gate k

B_{ij}^{α}: Set of available time point to assign uncertain Flight i to Gate k at stochastic scenario a

VF_{jk}: Set of certain flights assigned to Gate k at time point j

$\mathrm{DF}_{jk}^{\alpha}$: Set of uncertain flight assigned to Gate k at time point j at stochastic scenario a

H_S: Set of all available time point to assign uncertain flights

K_t: Set of all available gates at time point t

H: A sufficient large positive number to avoid time overlap in gate exclusive constraint

A: The number of all stochastic scenarios.

Consider

$$x_{i,k+1} = \begin{cases} 1, & \text{certain Flight } i \text{ assigned to apron} \\ 0, & \text{otherwise,} \end{cases}$$

$$x_{ik} = \begin{cases} 1, & \text{certain Flight } i \text{ assigned to gate } k \\ 0, & \text{otherwise,} \end{cases}$$

$$x_{ijk} = \begin{cases} 1, & \text{certain Flight } i \text{ assigned to Gate } k \text{ at time } j \\ 0, & \text{otherwise,} \end{cases}$$

$$y_{ijk} = \begin{cases} 1, & \text{uncertain Flight } i \text{ assigned to gate } k \text{ at time } j \\ 0, & \text{otherwise,} \end{cases}$$

$$h_{kt}^{\alpha} = \begin{cases} 1, & \text{at stochastic scenario } a, \\ & \quad \text{time violation occurs in gate } k \text{ at time } j \\ 0, & \text{otherwise.} \end{cases} \tag{1}$$

3.3. Objective Function. The basic ideology of the objective function in the paper deems that the original gate assignment is the optimal scheme under no flight delay. The objective function is consisting of three parts. The first part is the gate reassignment aimed at the certain information; the second part is the gate reassignment aimed at the uncertain information; the third part is to analyze the influence of gate assignment under certain information on the gate assignment under uncertain information. The objective function selected in the paper is to minimize the cost of gate assignment, which is caused by flight delay, rather than act the arrival-departure time as the input to gate reassignment. Therefore, the gate assignment schedule is not the optimal schedule aiming at some gates but the schedule ensuring the minimum number of flight delay accord with the basic principle of airport operation and management. The optimal schedule of gate assignment has not an effect on the normal order of airport operation and cannot lead to safety risk.

The First Part. Reassignment of certain flight is as follows:

$$\min Z_1 = \sum_{i \in \mathrm{MF}} V_{i,k+1} x_{i,k+1} + \sum_{i \in \mathrm{MF}} \sum_{k \in \mathrm{VG}_i} w_{ik} x_{ik}. \tag{2}$$

Objective function (2) aims to minimize apron disturbance value and gate disturbance value of certain flights gate reassignment. Assuming that gate number is m, space interval between reassigned gates and planned gates is n. To reduce the number of changed gates and the influence on additional distance of passengers and staffs, the authors set gate disturbance value as $m + n$. Due to larger influence on passenger service level and airport operation efficiency caused by reassigning the flights to apron, apron disturbance value is $2m$.

Part Two. Reassignment of uncertain flight is as follows:

$$\begin{aligned} \min Z_2 &= \sum_{\alpha=1}^{A} P_{\alpha} \left[\sum_{i \in \mathrm{NF}} \sum_{j = B_{jk}^1 \cup B_{jk}^2 \cdots B_{jk}^A} \sum_{k \in \mathrm{DG}_i} \left(w_{ik} + d_{ij} \right) y_{ijk} \right. \\ &\qquad \left. + \sum_{t \in T} \sum_{k \in K_t} e_{kt} h_{kt}^{a} \right]. \end{aligned} \tag{3}$$

Objective function (3) aims to minimize gate disturbance value, time disturbance value, and relax constraint penalty value of uncertain flights gate reassignment. Gate disturbance value is the same as in function (2). Assume that gate number is m, waiting time is t, considering influence on passenger service level and airline fuel consumption by delay gate starting time, and time disturbance coefficient is $(t/10)m$. To

minimize the infeasible situation caused by relax constraints under stochastic factors, penalty coefficient is $(4t/5)m$.

Part Three. Penalty functions of certain flights and uncertain flights are as follows:

$$\min Z_3 = \sum_{\alpha=1}^{A} P_\alpha \left\{ \sum_{i \in \mathrm{NF} \cup \mathrm{MF}} \sum_{j=B_{jk}^1 \cup B_{jk}^2 \cdots B_{jk}^A} \sum_{k \in \mathrm{VG}_i \cup \mathrm{DG}_i} e_{kt} \left[1 - \left(x_{ijk} - y_{ijk} \right)^2 \right] \right\}. \tag{4}$$

Penalty function (4) is designed to minimize the violation, by which the reassignment of certain flights may have disturbance on planned assignment of uncertain flights. The penalty value of the violation is the same as the relax constraint penalty value in function (3). The integrated objective function is the sum of all the three abovementioned functions:

$$\min Z = Z_1 + Z_2 + Z_3. \tag{5}$$

3.4. Constraints. Consider the following:

$$\sum_{k \in \mathrm{VG}_i \cup k+1} x_{ik} = 1, \quad \forall i \in \mathrm{MF}, \tag{6}$$

$$x_{ik} = \begin{cases} 1 \\ 0, \end{cases} \quad \forall i \in \mathrm{MF},\ \forall k \in \mathrm{VG}_i \cup k+1. \tag{7}$$

Constraint (6) is flight unique constraint. It indicates that each certain flight must be assigned to only one gate or assigned to apron. Constraint (7) indicates the certain flight variables are either zero or one:

$$\sum_{j=B_{ik}^\alpha} \sum_{k \in \mathrm{DG}_i} y_{ijk} = 1, \quad \forall i \in \mathrm{NF}, \tag{8}$$

$$y_{ijk} = \begin{cases} 1 \\ 0, \end{cases} \quad \forall i \in \mathrm{NF},\ \forall j \in B_{ik}^1 \cup B_{ik}^2 \cdots \cup B_{ik}^A,\ \forall k \in \mathrm{DG}_i. \tag{9}$$

Constraint (8) is flight unique constraint. It indicates that each uncertain flight must be assigned to only one gate at each stochastic scenario. Constraint (9) indicates that the uncertain flights variables are either zero or one:

$$\sum_{j=B_{ik}^\alpha} \sum_{k \in \mathrm{VG}_i} x_{ijk} = 1, \quad \forall i \in \mathrm{MF}, \tag{10}$$

$$x_{ijk} = \begin{cases} 1 \\ 0, \end{cases} \quad \forall i \in \mathrm{MF},\ \forall j \in B_{ik}^1 \cup B_{ik}^2 \cdots \cup B_{ik}^A,\ \forall k \in \mathrm{VG}_i. \tag{11}$$

Constraint (10) is flight unique constraint. It indicates that, in penalty function, each certain flight must be assigned to only one gate at each stochastic scenario. Constraint (11) indicates that the certain flights values are either zero or one:

$$C_{i'} \geq C_i + T_i + H\left(x_{i'k} + x_{ik} - 2\right), \quad i \leq i', \quad \forall i \in \mathrm{MF}, \quad \forall i' \in \mathrm{MF}, \quad \forall k \in \mathrm{VG}_i. \tag{12}$$

Constraint (11) is gate exclusive constraint. It indicates that, at one period of time, one gate can only serve less than or equal one certain flight. In the same gate, the gate starting time point of subsequent flight i' should be greater than the gate starting time point plus gate occupation time of front flight i. $H(x_{i'k} + x_{ik} - 2)$ is used to check if Flights i and i' are reassigned to the same gate:

$$\sum_{j \in H_s} \sum_{i \in \mathrm{VF}_{jk}} y_{ijk} - h_{kt}^\alpha \leq 1, \quad \forall k \in K_t,\ \forall t \in T, \tag{13}$$

$$h_{kt}^\alpha \geq 0, \quad \forall k \in K_t,\ \forall t \in T. \tag{14}$$

Constraint (13) is the relax gate exclusive constraint. It indicates that at one period of time, more than one uncertain flight are tolerable to be assigned to one gate. In one gate, the flight number minus violation number must be less than or equal to one. Constraint (14) is to ensure that the violation number is a positive number:

$$M_i \cdot x_{ik} \leq N_k, \quad \forall k \in \mathrm{VG}_i. \tag{15}$$

Constraint (15) is aircraft type matching constraint. The aircraft type of certain flights should be less than or equal to gate type:

$$M_i \cdot y_{ijk} \leq N_k, \quad \forall k \in \mathrm{DG}_i,\ \forall i \in \mathrm{NF},\ \forall j \in B_{ik}^1 \cup B_{ik}^2 \cdots B_{ik}^A. \tag{16}$$

Constraint (16) is aircraft type matching constraint. The aircraft type of uncertain flights should be less than or equal to gate type.

4. Ant-Based Heuristic Algorithms

4.1. Algorithm Selection. The paper selects Ant colony algorithm to solve the gate assignment problem. Ant colony optimization algorithm is a metaheuristic optimization method proposed by Dorigo et al. [16]. Dorigo presented the ant colony algorithm for the first time in 1992. The ant colony algorithm has the characteristic of solving the discrete combinatorial optimization problem. The typical combinatorial optimization problem includes: traveling salesman problem (TSP) [17, 18], machine scheduling problem (MSP) [19, 20], vehicle routing problem (VRP) [21, 22], and parallel machine scheduling (PMS) [23, 24].

There are some reasons to explain the selection of ant colony algorithm. First, ant colony algorithm is applied to solve combinatorial optimization problem, which accords with the characteristics of gate assignment. Second, the characteristics of ant colony algorithm are to add the solution to the solution system step by step until it acquires a complete solution. Therefore, it is superior to solve gate assignment relative to adjusting the part solution of algorithm.

4.2. Description of Ant Colony Algorithm. Our research designs an ant colony algorithm to solve the gate reassignment problem. The set of the number of ants is k, and the ant indicates the considered flight alignment. Ants firstly

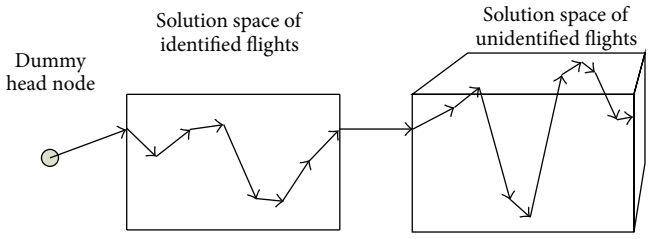

Figure 2: Integrated searching of ants.

walk through solution space of identified flights, then walk from one of the unidentified flights. After traversal of the two spaces, each ant releases suitable pheromone on each node passed, according to the target value of ant path. In reassignment process of identified flight, the space, which is a dimensional grid $m \times n$, consists of gate (apron) and flight alignment, and each node in grid indicates a possible result which is meant to assign a flight to a gate. Ants start form a dummy head node F_0, choose a node from the following row based on pheromone and heuristic information of each node, and then repeat until reach the last row. If a node cannot satisfy the constraints, ants will ignore this node. In reassignment process of unidentified flight, the space is a three-dimensional grid $m \times n \times t$ which consists of gate (apron), flight alignment, and available time point; each node in grid indicates a possible result which is meant to assign a flight to a gate at a time point. In unidentified flight solution space, the ants' searching method is similar to that of identified flight. Each time ants finish the above-mentioned stage, the ants will be deleted, and then a second iterative process will start. Figure 2 shows the ants' traversal process.

4.2.1. Heuristic Information Setting. Setting heuristic information as $\eta_i(t)$ means that the attractiveness of node i is at time t:

$$\eta_s(t) = \begin{cases} a, & a = P_{\text{assigned}} \cup (P,Q)_{\text{assigned}},\ a > b \\ b, & \text{otherwise}, \end{cases} \tag{17}$$

where P_{assigned} indicates sets of planned assignment gate alignment. $(P,Q)_{\text{assigned}}$ indicates sets of planned assignment gate and time point alignment. Gate assignment has a greater attractiveness to ants in order to enhance the probability of selecting scheduled gates.

4.2.2. State Transition Equation. When ants k ($k = 1, 2, \ldots, m$) search nodes, its state transition probability is based on the pheromone concentration and heuristic information of the following nodes. $p_i^k(t)$ indicates the state transition probability of ant k transferring from its located node into node i at time t. The expression is shown as follows:

$$p_i^k(t) = \begin{cases} \dfrac{[\tau_i(t)]^\alpha \cdot [\eta_i(t)]^\beta}{\sum_{s \in \text{allowed}} [\tau_s(t)]^\alpha \cdot [\eta_s(t)]^\beta}, & \text{if } s \in \text{allowed}_k, \\ 0, \end{cases} \tag{18}$$

where $\tau_i(t)$ indicates the pheromone concentration of node i at time point t and allowed_k indicates the available nodes for ant k to choose in the next stage, which satisfies the constraints of gate reassignment problem. Elements in set allowed_k may change according to the choice of ant k. Ants must select nodes in the following row or space in identified flights grid or unidentified flights grid, respectively, so reduplicative searching is avoided. Factors α and β determine the relative importance of pheromone accumulated on nodes when it has an impact on choice of ants.

4.2.3. Pheromone Update Methods. When ants complete an iteration, pheromone on each node should be updated. New pheromone will be added to nodes, while residual pheromone on each node should be volatilized. Therefore, the rule of pheromone modulation is shown as follows:

$$\tau_i(t+1) = \rho \tau_i(t) + \Delta \tau_i^{\text{best}},$$

$$\Delta \tau_i = \begin{cases} \dfrac{Q}{f(k^{\text{best}})}, & i \in k^{\text{best}} \\ 0, & i \notin k^{\text{best}}, \end{cases} \tag{19}$$

where ρ indicates volatile coefficient of pheromone, Q indicates pheromone strength, and $\Delta\tau_i$ indicates the total pheromone increment on node i at present iteration. Only the optimal ants release pheromone at each iteration.

4.3. Algorithm Flow. Figure 3 shows the algorithm flow.

The model can select PSO method to complete the relative parameters learning in ant colony algorithm in order to avoid the defects of ant colony algorithm itself under large-scale flight delay.

5. Simulation and Verification

In the numerical test, the starting and ending time of certain flights gate assignment are determined by two parts: one is the latest estimated time of departure (ETD) and arrival (ETA) delivered by airlines; the other is the minimum safety interval time and necessary buffer time according to aircraft types. The time of uncertain flights is also determined by the two parts as Table 1 shows; the difference between them is that certain flights utilize the scheduled time of depart (STD) and arrival (STA). In Table 1, the bold font represents the actual time of departure and arrival for the flight. The gate reassignment is based on the present gate occupation situation and sequencing of flights confirmed by updated gate starting time. Each time the gate reassignment aims at all flights, while only the reassignment scheme of identified flights can be released.

The simulation and verification in the paper is based on operation of a hub airport in China. The airport has a passenger throughput of more than 19 million and aircraft movements of 166 thousand, which is an important regional hub airport of East China. The Terminal B in the airport is domestic terminal, which has 41 gates and consists of 6 gates of type E, 7 gates of type D, and 28 gates of type C. In the simulation and verification, we assume that the gates and aprons have enough capacity such as sufficient runway and taxiway systems. Data is based on the timetable of May 20,

Table 1: Values of gate stating and ending time.

Flight type	Flight number	STA	ETA	STD	ETD
Identified flight	f1	1035	**1110**	1140	**1305**
	f2	1125	**1122**	1225	**1236**
Unidentified flight	f3	**1150**	—	**1245**	—
	f4	**1155**	—	**1300**	—

The bold font represents the actual time of departure and arrival for the flight.

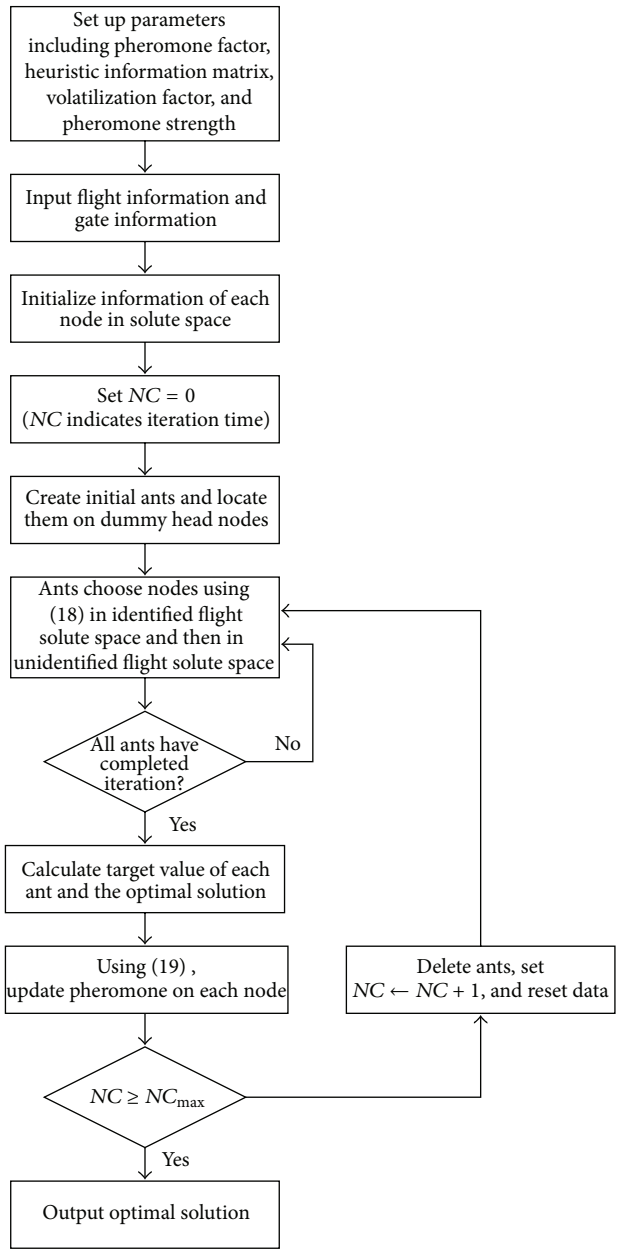

Figure 3: Algorithm flow.

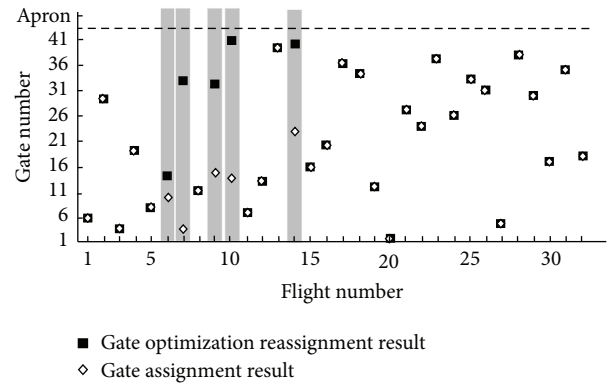

Figure 4: Gate optimization reassignment result at time point 9:00.

2013, of Terminal B, when there are 418 aircraft movements or 281 flight pairs, including departure, transferring, and arrival flights. The evaluation is based on the planned gate assignment of flights and the real-time tracked data between 6:00 and 15:00 which is used to be input information to gate reassignment. Affected by storm at that day, extensive flights delayed at about 12:00, and there was considerable deviation between flights schedule and real-time operation at airport.

This research selects time points 7:00, 9:00, 11:00, 13:00, and 15:00 to perform the test and has a comparison with manual reassignment methods. The manual method which based on experience operates can be used as follows: if there is a free gate when conflict occurs, assign the flight to the free gate, otherwise, assign to apron. The test is performed on an AMD TurionX2 2.2 GHz with 2 GB RAM in the environment of Microsoft Windows Vista and uses the C computer language to write the program.

Based on the case of gate reassignment of time point 9:00, the number of considered flights which needs to be allocated is 246, which includes 32 identified flights. Table 2 shows flight number, planned assignment result, manual reassignment result, and optimization reassignment result of identified flights at this time point.

Gate optimization and manual reassignment results are shown in Figures 4 and 5.

Figure 3 shows the test result of time point 9:00. At that time, 246 flights need to be reassigned, including 32 identified flights, which should display the specific reassignment result.

As shown in Figure 3, only Flights 6, 7, 9, 10, and 14 need to be reassigned, others keep their gates, and none of them are assigned to the apron. As shown in Figure 4, Flights 4, 7, 9, 10, 14, 16, and 29 need to be reassigned, and none of Flights 10, 14, and 16 are allocated to aprons. It is shown that gate optimization reassignment result causes less disturbances to aircraft, and the total disturbance value of identified flights and unidentified flights is 1535.642. The disturbance value of identified flights in optimization result is 1314.537 while being 1683 in manual result. Therefore, in actual situation, test

Table 2: Gate reassignment results of identified flight at time point 9:00.

Flight number	ETA	ETD	Planned assignment result	Manual reassignment result	Optimized reassignment result
1	900	1044	6	6	6
2	906	1025	29	29	29
3	911	1025	3	3	3
4	915	1106	19	19	19
5	924	1048	8	14	8
6	925	1113	10	10	14
7	929	1103	4	20	33
8	942	1109	11	11	11
9	945	1127	15	30	32
10	948	1154	14	Apron	41
11	954	1127	7	7	7
12	955	1105	13	13	13
13	956	1133	39	39	39
14	956	1130	23	Apron	40
15	1000	1100	16	16	16
16	1006	1136	20	Apron	20
17	1010	1050	36	36	36
18	1012	1310	34	34	34
19	1015	1136	12	12	12
20	1030	1200	2	2	2
21	1030	1155	27	27	27
22	1031	1208	24	24	24
23	1034	1200	37	37	37
24	1037	1318	26	26	26
25	1039	1148	33	33	33
26	1042	1227	31	31	31
27	1045	1220	5	5	5
28	1045	1213	38	38	38
29	1048	1217	30	25	30
30	1050	1210	17	17	17
31	1051	1213	35	35	35
32	1059	1156	18	18	18

results of optimization reassignment in our research have an obvious advantage over manual reassignment. In the test, the relative time we set for valid time of identified flights is long, so the influence of unidentified flights is low. The influence proportion of unidentified flights is adjustable according to real-time situation.

Table 3 and Figures 6 and 7 present the comparison results of optimization reassignment and manual reassignment of the above-mentioned 5 time points.

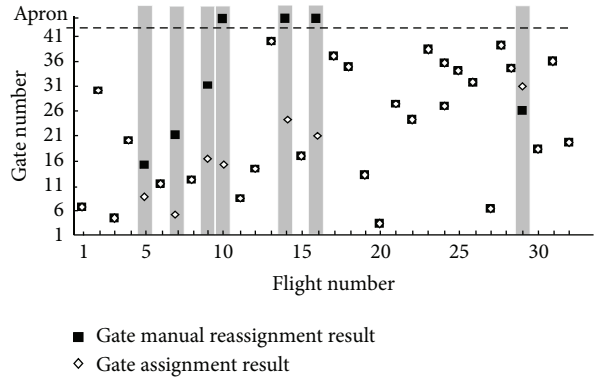

Figure 5: Gate manual reassignment result at time point 9:00.

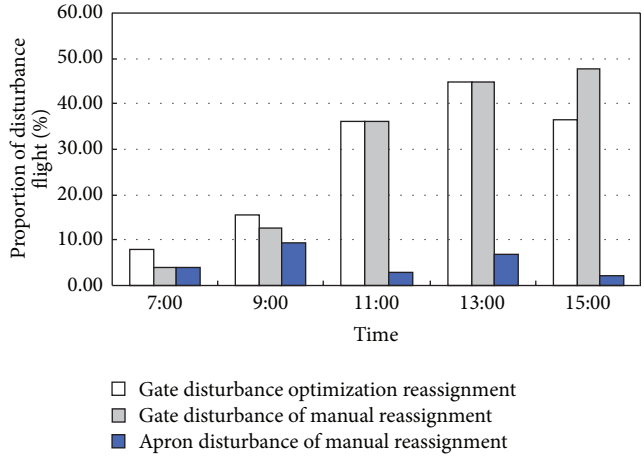

Figure 6: Comparisons of optimization and manual gate reassignment on disturbance proportion.

As shown in Figures 6 and 7, in operation day, the quantity of irregular flights largely increases, which leads to the more complex gate reassignment. Before time point 12:00, the situation in airport is relatively normal. The proportion of fights gate reassignment is less than 20% and disturbance value is small. After extensive delays happen, the disturbance value of reassignment largely increases. Although optimization result has considerable deviation compared to the planned gate assignment, the efficiency and systematic optimization are much better than manual reassignment. The proportion of disturbed flights in optimization result is less than 45%, while that of manual results is more than 50% with a larger disturbance value.

In the aforementioned tests of 5 time point, none of the flights are allocated to the aprons. Proportion and disturbance value of disturbed identified flights in optimization results are less than those of manual reassignment results. The maximum decrement of disturbed flights proportion reaches 13.64% at 15:00, while the maximum decrement of disturbance value is 327.093 at 9:00. As a consequence, the optimization gate reassignment strategy is better than the manuals, no matter in one operation or one day's operation. The resolving time for performing tests by ant-based

Table 3: Comparisons of optimization and manual gate reassignment.

Time point	Reassignment method	Gate disturbance proportion	Apron disturbance proportion	Total disturbance proportion	Identified flight number	Total considered flight number	Disturbance value	Time costs (s)
6:00	Optimization	8%	0	8%	50	281	2051.073	184.746
	Manual	4%	4%	8%	50	281	2173.52	
9:00	Optimization	15.60%	0	15.60%	32	246	1314.537	117.996
	Manual	12.50%	9.40%	21.90%	32	246	1686.63	
11:00	Optimization	36.11%	0	36.11%	36	207	1480.92	78.622
	Manual	36.11%	2.78%	38.89%	36	207	1604.34	
13:00	Optimization	44.80%	0	44.80%	29	173	1028.72	77.729
	Manual	44.80%	6.90%	51.70%	29	173	1317.35	
15:00	Optimization	36.36%	0	36.36%	44	151	1698.24	105.112
	Manual	47.73%	2.27%	50.00%	44	151	1931.66	

algorithm has a tendency to decrease with the decrease of considered flight. The longest resolving time is 184.746 s, which can reach the strict request of real-time operation.

Gate manual reassignment only considers recent flight information and actual gate utilization situation, while optimization reassignment can consider the long time in some degrees. Optimization reassignment will follow the airport delay trending order to look for more satisfied reassignment schemes. Therefore, it will largely decline the disturbance of gate reassignment.

Thus it can be seen that, in actual situation, test results of optimization reassignment in our research are much better than those in manual reassignment. The similarity between optimization gate reassignment and planned gate assignment is high.

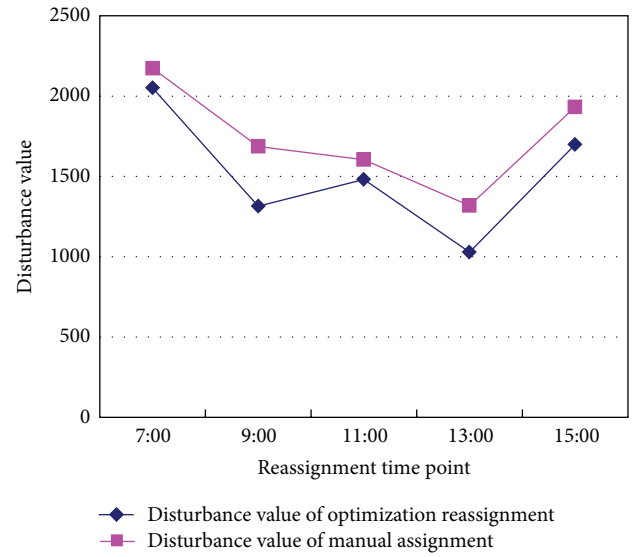

Figure 7: Comparisons of optimization and manual reassignment on disturbance proportion.

6. Conclusions

In the paper, airport gate reassignment problem under flight delay situation is studied. Flights are divided into different types considering delay feature. Real-time gate reassignment model has been presented, whose objective is to minimize the disturbance compared to planned gate assignment scheme. An ant-based heuristic algorithm is designed to solve the problem. With the numerical test, the method is proved to be effective and efficient, which can meet the request of real-time operation of hub airport.

Some conclusions can be drawn in the paper. First, the real-time gate assignment is very important in increasing the effectiveness and volume of airport. Second, the real-time gate assignment is difficult because that the flight delay is uncertain. Last, the gate reassignment schedule is decided by the selection of objective function directly. Airport operation and some kinds of influence factors should be taken into account in the actual gate assignment schedule. Therefore, the gate assignment is a typical a multiobjective optimization problem. It should be noted that the research only considers the general situation of gate reassignment. How to operate gate reassignment considering the tradition of gate assignment and importance of flight priority and the reassignment after situation as airport closures is worthy future research topics.

Acknowledgments

This work was supported by National Natural Science Foundation and Aviation Fund of China U1233115, Civil Aviation Science Fund of China (MHRD201127), and Qinglan Project.

References

[1] S. Yan and C.-M. Chang, "A network model for gate assignment," *Journal of Advanced Transportation*, vol. 32, no. 2, pp. 176–189, 1998.

[2] B. Maharjan and T. I. Matis, "Multi-commodity flow network model of the flight gate assignment problem," *Computers & Industrial Engineering*, vol. 63, no. 4, pp. 1135–1144, 2012.

[3] H. M. Genç, O. K. Erol, B. Eksin, M. F. Berber, and B. O. Güleryüz, "A stochastic neighborhood search approach for airport gate assignment problem," *Expert Systems with Applications*, vol. 39, no. 1, pp. 316–327, 2012.

[4] C. H. Cheng, S. C. Ho, and C. L. Kwan, "The use of meta-heuristics for airport gate assignment," *Expert Systems with Application*, vol. 39, no. 16, pp. 12430–12437, 2012.

[5] U. Dorndorf, F. Jaehn, and E. Pesch, "Modelling robust flight-gate scheduling as a clique partitioning problem," *Transportation Science*, vol. 42, no. 3, pp. 292–301, 2008.

[6] C. H. Tang and W. C. Wang, "Airport gate assignment for airline-specific gates," *Journal of Air Transport Management*, vol. 30, pp. 10–16, 2013.

[7] F. Jaehn, "Solving the flight gate assignment problem using dynamic programming," *Zeitschrift für Betriebswirtschaft*, vol. 80, no. 10, pp. 1027–1039, 2010.

[8] B. Maharjan and T. I. Matis, "An optimization model for gate reassignment in response to flight delays," *Journal of Air Transport Management*, vol. 17, no. 4, pp. 256–261, 2011.

[9] Y. Gu and C. A. Chung, "Genetic algorithm approach to aircraft gate reassignment problem," *Journal of Transportation Engineering*, vol. 125, no. 5, pp. 384–389, 1999.

[10] Y. Z. Hou, *An Approach for Dynamic Airport Gate Assignments for Stochastic Flight Delays*, National Central University, Jhongli, Taoyuan, 2007.

[11] C.-H. Tang, S. Yan, and Y.-Z. Hou, "A gate reassignment framework for real time flight delays," *4OR*, vol. 8, no. 3, pp. 299–318, 2010.

[12] C.-H. Tang, "A gate reassignment model for the taiwan taoyuan airport under temporary gate shortages and stochastic flight delays," *IEEE Transactions on Systems, Man, and Cybernetics A*, vol. 41, no. 4, pp. 637–650, 2011.

[13] S. Yan and C.-H. Tang, "A heuristic approach for airport gate assignments for stochastic flight delays," *European Journal of Operational Research*, vol. 180, no. 2, pp. 547–567, 2007.

[14] M. Şeker and N. Noyan, "Stochastic optimization models for the airport gate assignment problem," *Transportation Research E*, vol. 48, no. 2, pp. 438–459, 2012.

[15] S. Yan, C.-Y. Shieh, and M. Chen, "A simulation framework for evaluating airport gate assignments," *Transportation Research A*, vol. 36, no. 10, pp. 885–898, 2002.

[16] M. Dorigo, V. Maniezzo, and A. Colorni, "Ant system: optimization by a colony of cooperating agents," *IEEE Transactions on Systems, Man, and Cybernetics B*, vol. 26, no. 1, pp. 29–41, 1996.

[17] A. Uğur and D. Aydin, "An interactive simulation and analysis software for solving TSP using Ant Colony Optimization algorithms," *Advances in Engineering Software*, vol. 40, no. 5, pp. 341–349, 2009.

[18] C. García-Martínez, O. Cordón, and F. Herrera, "A taxonomy and an empirical analysis of multiple objective ant colony optimization algorithms for the bi-criteria TSP," *European Journal of Operational Research*, vol. 180, no. 1, pp. 116–148, 2007.

[19] V. T'kindt, N. Monmarché, F. Tercinet, and D. Laügt, "An Ant Colony Optimization algorithm to solve a 2-machine bicriteria flowshop scheduling problem," *European Journal of Operational Research*, vol. 142, no. 2, pp. 250–257, 2002.

[20] S. Marimuthu, S. G. Ponnambalam, and N. Jawahar, "Threshold accepting and Ant-colony optimization algorithms for scheduling m-machine flow shops with lot streaming," *Journal of Materials Processing Technology*, vol. 209, no. 2, pp. 1026–1041, 2009.

[21] Y. Gajpal and P. L. Abad, "Multi-ant colony system (MACS) for a vehicle routing problem with backhauls," *European Journal of Operational Research*, vol. 196, no. 1, pp. 102–117, 2009.

[22] J. F. Tang, Y. Y. Ma, J. Guan et al., "A Max-Min Ant System for the split delivery weighted vehicle routing problem," *Expert Systems with Applications*, vol. 40, no. 15, pp. 7468–7477, 2013.

[23] T. Keskinturk, M. B. Yildirim, and M. Barut, "An ant colony optimization algorithm for load balancing in parallel machines with sequence-dependent setup times," *Computers and Operations Research*, vol. 39, no. 6, pp. 1225–1235, 2012.

[24] J. Behnamian, M. Zandieh, and S. M. T. F. Ghomi, "Parallel-machine scheduling problems with sequence-dependent setup times using an ACO, SA and VNS hybrid algorithm," *Expert Systems with Applications*, vol. 36, no. 6, pp. 9637–9644, 2009.

Hindawi Publishing Corporation
Mathematical Problems in Engineering
Volume 2013, Article ID 490372, 7 pages
http://dx.doi.org/10.1155/2013/490372

Research Article

Damage Detection of Bridge Structure Based on SVM

Yaojin Bao,[1] Chenjin Song,[1] Wensi Wang,[2] Ting Ye,[2] Lu Wang,[3] and Lan Yu[4]

[1] *College of Civil Engineering, Beijing Jiaotong University, Beijing 100044, China*
[2] *Transportation Management College, Dalian Maritime University, Dalian 116026, China*
[3] *China Academy of Civil Aviation Science and Technology, Beijing 100028, China*
[4] *Yanching Institute of Technology, Beijing 065201, China*

Correspondence should be addressed to Yaojin Bao; bao_yaojin@163.com

Received 26 September 2013; Revised 17 October 2013; Accepted 17 October 2013

Academic Editor: Rui Mu

For bridge management and maintenance, it is important to detect the damage of bridge pier. Due to the complexity of damage detection, an effective method is very interesting. Support vector machine (SVM) is used to detect the damage of bridge pier in this paper. To improve the detection accuracy of SVM, Grubbs' test method is adopted to delete the outliers for SVM. Then, a numerical analysis is used to determine the input parameters for SVM. Lastly, the comparison results between the proposed SVM and the actual measure value suggested that the proposed SVM is a powerful tool for detecting damage of bridge pier.

1. Introduction

Many factors, like damage on the railway, may lead to the instability of railway bridge. The pier is a main part of bridge structure and its safety has been an essential element for the bridge. The state of generalized pier which includes the bridge pier and its base affects the safety of the entire bridge, as the important part supporting the upper structure. The pier in bad condition would affect the function of the entire bridge even though the beam is in good condition. There will be various damages on the railway pier because it not only bears the dynamic load of the train but also suffers from some outside influences such as flood erosion, material erosion caused by the ground and the groundwater, and sudden earthquake. These damages would break the pier base, reduce the stiffness, make the pier lack of durability and bearing capacity, and cause other problems. It will affect the safety of the entire bridge. Particularly, it will be a severe damage when a train is running on the bridge. In recent years, in order to increase the train speed and provide heavyweight freight train running successfully, a complete investigation on the line is often performed to find the potential damage in time and meet the requirement of speed increase and higher heavyweight. Thus, it is necessary to provide an effective method to identify the safety condition of the pier.

The damage of the pier usually exists in the ground or under the water surface; it is difficult to judge the safety condition of the pier only with the appearance inspection. Since this type of damage is expected to simulate the condition in which a bridge suffers from nonuniform pier settlement or hidden damage inside piles of buried foundations, this kind of damage is introduced by cutting one of the bridge piers at the footing level. Therefore, it is general to take a dynamic response of the pier under train excitation as an index to assess the safety condition. If the value of the index is beyond the threshold, it suggests that there would be some dangers about the pier [1–5].

The basic principle of the dynamic response can be described as follows: the damage would bring about changes in stiffness, quality, and damping of the pier structure, which will change the dynamic characteristic parameters of the structure (e.g., natural frequency and mode shape). Therefore, the changing condition of the structure damage can be detected based on the change of the dynamic characteristic parameters. However, it will cost quite a long time and enormous expenses using this method. In addition, the above safety assessment model needs to take many elements into consideration; however, most assessment models only consider some specific parameters. Therefore, it is very important

to develop a convenient and accurate safety assessment method for the pier.

In recent years, among all the damage detection methods of civil engineering structure, the damage detection method based on vibration modal analysis theory is the most widely used. The vibration modal analysis method involves many dynamic characteristic parameters such as modal frequency, modal type, curvature modal, and flexibility curvature. It is difficult to build the nonlinear relationship between the damage indicator and the structural breakage. This is because calculating the damage identification of modal structure is a complex mathematical problem.

Recently, support vector machine (SVM), which can be found in Vapnik [6–8], is a kind of statistical learning method which can achieve the best generalization effect by using a limit number of sample information to find the optimal compromise between the reasoning ability and the complexity of the model. The method has advantages in solving high-dimensional pattern recognition and nonlinear and small sample events and can be promoted and applied in regression analysis and other problems. Many studies show that SVM is an effective method to deal with systematical modeling and control of complex nonlinear problems [9–14]. It has also been proposed as a novel technique in detection problem, such as vehicle detection [15], traffic-pattern recognition [16], and head recognition [17]. These successful applications motivate us to apply SVM in damage detection of bridge pier.

The damage detection model of bridge pier based on Grubbs' test method and SVM mainly aims at getting the relative information from the input data and other aspects to solve damage detection problem of bridge pier. Before the application of SVM, data preprocessing is necessary for SVM to eliminate the abnormal data from input data. However, individual data often deviates from the expectation or a large number of statistical values in simple data processing. The results may be not accurate if these abnormal data are deleted as the input data. That is, if these abnormal data are simply rejected, the operation may delete the hidden useful information indicated by these abnormal data. Therefore, how to determine and eliminate the abnormal values is a key issue in data processing. Grubbs' test method is a statistical test used to detect outliers in a univariate data set, which has been proved in some literatures [18, 19]. Thus, Grubbs' test method is also used to detect outliers of SVM model.

To provide an effective method to detect bridge structure, this paper attempts to detect the damage of bridge pier based on Grubbs' test method and SVM. Therefore, this paper is organized as follows. Section 2 provides a brief introduction to the detected model based on Grubbs' test method and SVM; Section 3 presents numerical analysis and parameter selection. Section 4 reveals results of a numeral test and the prediction model. Lastly, the conclusions are stated in Section 5.

2. The Damage Detection Model of Bridge Pier

The damage detection model of bridge pier consists of two phases. One is the process of data processing in which Grubbs' test method is used and the other is the process of damage detection in which SVM is used. The model can be described as in Figure 1. Then, the two parts of the detection model are discussed, respectively.

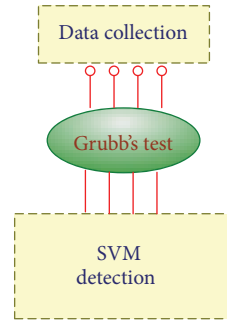

Figure 1: The structure of detection model.

2.1. Applying Grubbs' Test Method in Deleting Outliers. The abnormal data are processed based on Grubbs' criterion. It is greatly necessary to eliminate the abnormal data in data processing to improve the prediction accuracy. Therefore, the process of Grubbs' test method for deleting outliers is as follows. Firstly, the abnormal values usually would affect the prediction procedure; for example, there will be error codes if the abnormal values are added into the running code, so that the program cannot work normally. Secondly, the abnormal values usually would affect the prediction results. However, some undiscovered abnormal values may produce reasonable results under certain conditions. These abnormal values, if they have no regular variation and cannot affect the detection performance, are effective data samples and should be applied in the model rationally.

Grubbs' test method is usually used to detect outliers in small samples, where the number of outliers is unknown. Before the use of the method, all the data are assumed as normal distribution. In Grubbs' test method, only one abnormal value can be deleted every time. Thus, there are multiple eliminations for the data samples. Grubbs' test method will not come to an end until there are no abnormal values in the total samples. However, multistep iterative would affect the detection probability; the method is suitable for the samples with the number more than six.

Grubbs' test method is based on the following assumptions.

(H0) There is no abnormal value in the data set.

(Ha) There is at least one abnormal value in the data set.

Grubbs' test method can be described as follows:

$$G = \frac{\max_{i=1,\ldots,n} \left| Y_i - \overline{Y} \right|}{g}, \tag{1}$$

where $\overline{Y}$ and g represent the sample mean and the standard deviation, respectively. The statistic of Grubbs' test method is the deviation degree of the data with the maximum deviation compared with the standard value of unit sample.

Equation (1) reflects a double-sided test. Grubbs' test method can also be a one-sided test. In order to test whether the minimum value in the sample is an abnormal one or not, the following equation can be used:

$$G = \frac{\overline{Y} - Y_{\min}}{g}, \tag{2}$$

where $Y_{\min}$ represents the minimum value of the sample. In order to test whether the maximum value in the sample is an abnormal one or not, the following equation can be used:

$$G = \frac{Y_{\max} - \overline{Y}}{g}. \tag{3}$$

For the double-sided test, if the significance level a satisfies the following conditions in (4), it means that there exist abnormal values in the sample:

$$G > \frac{N-1}{\sqrt{N}} \sqrt{\frac{t^2_{a/(2N),N-2}}{N-2+t^2_{a/(2N),N-2}}}, \tag{4}$$

where $t^2_{a/(2N),N-2}$ represents the upper threshold of t-distribution under the premise of $N-2$ degrees of freedom and significance level $a/(2N)$. $a/(2N)$ can be substituted for a/N in the one-sided test.

2.2. The Basic Principle of SVM. Support vector machine is a learning linear machine which is based on the structural risk minimization (SRM) inductive principle, as opposed to the commonly used empirical risk minimization (ERM) approach. SRM attempts to minimize an upper bound of the generalization error which consists of the sum of the training error and a confidence level. ERM tries to minimize the training error. Therefore, SVM has a higher generalization performance.

Given a set of data points (x_1, y_1), (x_2, y_2), …, (x_i, y_i) $(x_i \in X \subseteq R^n,\ y_i \in Y \subseteq R)$, SVM can map x_i to a high-dimensional feature space H using nonlinear mapping ϕ and conduct the linear approximation in this space, which can be described as follows:

$$f(x) = \omega \cdot \phi(x) + b, \tag{5}$$

where ω is the weight vector of the hyperplane b is the bias term.

According to the statistical principles, the minimum and regular risk generic function can be attained under certain constraints to determine ω and b:

$$\min \quad \frac{1}{2}\|\omega\|^2 + C\frac{1}{l}\sum_{i=1}^{l}\left(\xi_i + \xi_i^*\right) \tag{6}$$

$$\text{s.t.} \quad y_i - \omega \cdot \varphi(x_i) - b \le \varepsilon + \xi_i \tag{7}$$

$$\omega \cdot \phi(x_i) + b - y_i \le \varepsilon + \xi_i^*, \quad i = 1, \ldots, l \tag{8}$$

$$\xi_i^* \ge 0. \tag{9}$$

The first term in formula (6) is named as the regular one, which makes the function more flat to improve its generic abilities; the second term is the experience risk generic function, which can be determined by different loss functions, among which the constraint $C > 0$ controls the punishment level for the samples beyond error ε. The meaning of formula (6) can be found in the literature [11].

Formula (6) is a convex quadratic optimization problem, which can be solved by introducing the Lagrange function, shown in the following equation:

$$\omega - \sum_{i=1}^{l}\left(a_i - a_i^*\right)x_i = 0. \tag{10}$$

Then,

$$f(x) = \sum_{i=1}^{l}\left(a_i - a_i^*\right)\phi(x_i) \cdot \phi(x) + b. \tag{11}$$

Let $K(x_i, x_j) = \phi(x_i) \cdot \phi(x)$; then,

$$f(x) = \sum_{i=1}^{l}\left(a_i - a_i^*\right)K(x_i, x) + b, \tag{12}$$

where $K(x_i, x_j)$ is the inner product of vectors x_i and x_j in feature spaces $\phi(x_i)$ and $\phi(x_j)$, which is named as the kernel function through which all the computations cannot be mapped to high-dimensional spaces but can be directly conducted in the input space. The kernel functions are the key parts of SVM; different SVMs consist of different kernel functions.

3. The Numerical Analysis of Natural Vibration Characteristics of the Pier

3.1. The FEM Analysis Model. The rectangular pier is made of reinforced concrete. The side soil mass of the concrete spread foundation is made of semidry and hard cohesive soil and the basal soil mass is made of pebble soil. The pier is 8 meters high and 3.6 meters and 1.6 meters width on average in the horizontal and longitudinal directions, respectively. The bottom 4 meters of the foundation is under the ground. The numerical analysis model of the pier is shown in Figure 2.

In order to simplify the calculation, some assumptions are made as follows.

(1) The pier body uses block units and the constraints imposed on the foundation by the soil mass are simulated through the linear spring.

(2) Ignoring the constraints imposed on the pier by the beam and the rail, the upper beam structure which is a one-hole beam including ballast, rail system, sidewalk panel, and other accessory structures is taken as the lumped mass to impose on the top of the pier.

3.2. The Computing Parameters of the Model. The constraints imposed on the pier by the soil mass include the transverse constraint for the side of the foundation and the longitudinal

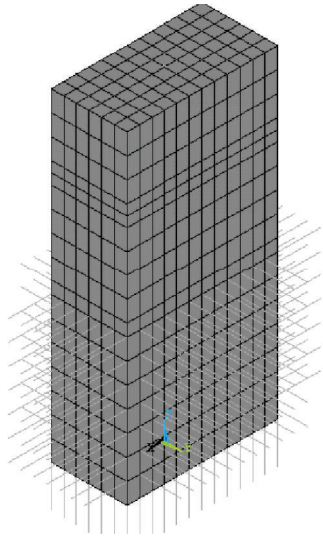

Figure 2: The FEM model of the fifth pier.

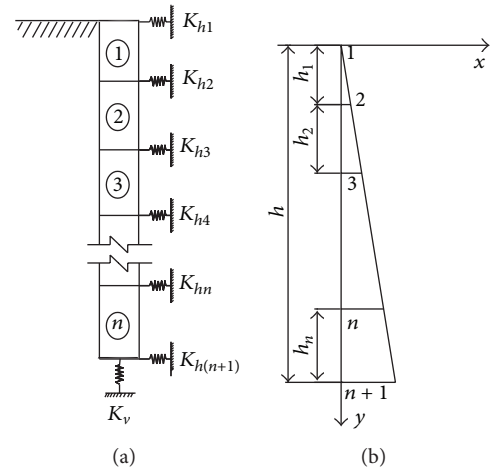

Figure 3: The calculation model of elastic coefficients.

constraint for the bottom of the foundation, which are simulated through horizontal spring k_h and vertical spring k_v. The spring coefficients based on the "m" method can be acquired in the literature [20].

(1) The Coefficient Calculation of the Lateral and Horizontal Springs. The pier foundation is discretized into n units and h_i meters each unit, as shown in Figure 3. The restriction imposed on the base by the foundation soil is equivalent to the spring applied to each node of the unit. If the effective width of the lateral base is b_0, then the spring coefficient of the nodes in the lateral base can be attained as follows.

The spring coefficient k'_{x1} of the lateral foundation soil within the range of unit ① is the product of the triangle area and the unit width b_0:

$$k'_{x1} = b_0\left(\frac{mh_1}{2}\right)h_1 = \frac{mb_0h_1^2}{2}, \tag{13}$$

where m is the scale factor of the horizontal spring coefficients of the soil changing with the depth.

The lateral spring coefficients imposed on node 1 and node 2 of unit ① shown in Figure 3 are determined based on the following equations:

$$\begin{aligned} k'_{x11} &= \frac{k'_{x1}}{3}, \\ k'_{x12} &= \frac{2k'_{x1}}{3}. \end{aligned} \tag{14}$$

In the same way, the lateral spring coefficients of other element nodes are as follows:

$$k'_{xn} = \frac{b_0m\left[2 * \left(h_1 + \cdots + h_{n-1}\right) + h_n\right]h_n}{2}. \tag{15}$$

Then,

$$\begin{aligned} k'_{xnn} &= \frac{k'_{xn}}{3}, \\ k'_{xn(n+1)} &= \frac{2k'_{xn}}{3}. \end{aligned} \tag{16}$$

Based on the above analysis, the equivalent spring coefficients of each node can be attained as follows:

$$\begin{aligned} K_{h1} &= k'_{x11} \\ K_{h2} &= k'_{x12} + k'_{x22} \\ &\vdots \\ K_{hn} &= k'_{x(n-1)n} + k'_{xnn} \\ K_{h(n+1)} &= F_{xn(n+1)}. \end{aligned} \tag{17}$$

(2) The Calculation of the Vertical Spring Coefficient of the Base Ground. The underside rotation of the pier base around the vertical plane can be considered, ignoring the horizontal vibration. The vertical spring coefficient of the underside of the base ground is calculated as follows:

$$k_v = C_0A_0, \tag{18}$$

where C_0 is the vertical foundation coefficient of the base bottom and A_0 is the stressed area of the base bottom.

(3) The Constraint Simulation in the State of Foundation Scouring. According to the literature [21], one meter depth of soil suffering from foundation scouring is taken as an example; the earth pressure in the scouring state is shown in Figure 4 in which $W_2, W_3, \ldots, W_n$ represent the weight of each layer of soil mass.

The influence of soil scouring of the base side on the base constraint is embodied in two aspects:

(a) after the soil scouring in the side of the base, the horizontal constraint of this layer of soil on the base can be deleted;

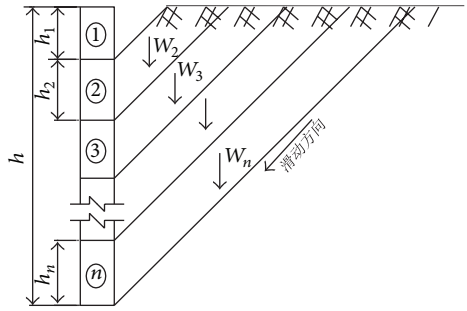

Figure 4: The distribution of soil pressure on the sliding surfaces.

Table 1: The calculation results of natural vibration frequency of the pier.

Working condition	Foundation depth (m)	Frequency (Hz)	Frequency reduction (Hz)	Relative frequency reduction (Hz)
Original state	4.0	7.02	/	/
Digging 1 m	3.0	6.67	0.34	0.34
Digging 2 m	2.0	6.45	0.57	0.23
Digging 3 m	1.0	6.31	0.71	0.14

(b) the lateral spring coefficient of the next layer of soil would change due to the soil scouring in this layer of soil.

From Figure 4, it can be found that it will have less influence on the lateral coefficient of the soil in the next layer if the side soil mass of the base is not much reduced because the soil is dug within a small range. The lateral spring coefficient of the base under the scoured region can still be calculated based on (13)–(17).

The lateral spring coefficients of the base are computed according to (19); the lateral spring coefficients with other scouring depth are calculated in the same way:

$$\begin{aligned} k'_{x1} &= 0, \\ k'_{x2} &= \frac{b_0 \left(2mh_1 + h_2\right) h_2}{2}, \\ K_{h1} &= 0, \\ K_{h2} &= k'_{x12} + k'_{x22} = 0 + k'_{x22}, \\ K_{h3} &= k'_{x23}. \end{aligned} \tag{19}$$

There will be less influence on the vertical coefficients of the base bottom if the side soil mass of the base is not much reduced, neglecting the change of the vertical spring coefficients of the base bottom caused by the scouring.

3.3. The Numerical Analysis Results. The natural vibration characteristics of the fifth pier in the original state and under different digging depths and the natural vibration frequency are shown in Table 1. Table 2 shows the amplitude ratio of the pier under four kinds of digging states.

Table 2: The amplitude ratio of the pier.

Working condition	Pier vertex	Pier midpoint	Pier subpoint
Original state	2.04	1.52	1
Digging 1 m	2.03	1.51	1
Digging 2 m	2.02	1.50	1
Digging 3 m	2.01	1.49	1

4. Case Studies

4.1. The Parameters for SVM. In fact, when SVM is training, the input parameters with enough high accuracy, the damage detection results will be accurate and effective. From the numerical analysis results, it can be found that the natural vibration frequency in different positions shows different results. Therefore, it is reasonable to choose depth, working condition, and natural vibration frequency as the input parameters for SVM model.

Before the application of SVM model, the data should be normalized firstly. Then, the normalized data will be divided into three parts of sets, which will be used for the training, testing, and inspection, respectively. That is, there are about 70% samples for training, 10% samples for testing, and the remaining samples for inspection. Thus, negative root mean squared error (NRMSE) is also adopted to reflect the prediction accuracy in this paper:

$$\text{fit} = -\left[\frac{\sum_{i=1}^{n}\left(V - \widehat{V}\right)}{n - p}\right]^{1/2}, \tag{20}$$

where $\widehat{V}$ is the prediction value by the model, V is the observed value, n is the number of observations, and p is the number of model parameters which refers to the literature [22].

The performance of SVM mainly referred to the ability of classifying unknown data samples correctly (i.e. the generalization ability). The kernel function is the key part for SVM. It is because the kernel function provides a simple bridge from linearity to nonlinearity for SVM. In general, the RBF kernel, as a nonlinearly kernel function, is a reasonable first choice [23]. There are three parameters while using RBF kernels: C, ε, and γ. The parameter selection is important for the performance of the algorithm. However, it is not known a priori which of C, ε, and γ is the best choice for the problem. To properly select the three parameters, there are several methods adopted to identify the best parameter value. Among these methods, grid search is frequently used. Therefore, the grid search is also used to determine the values of parameters (C, ε, and γ). At last, the three parameters are selected as 3.5423, 0.0064, and 1.0698.

4.2. The Detection Results Based on SVM. The damage degree of the pier structure was assumed as 3.05%, 6.15%, 11.5%, and 14.5%, respectively. After the samples have been trained

Table 3: The comparison results between the SVM and actual observation.

Working condition	Foundation depth (m)	Results of SVM	Actual results
Original state	4.0	14.5%	14.64%
Digging 1 m	3.0	11.5%	11.61%
Digging 2 m	2.0	6.15%	6.21%
Digging 3 m	1.0	3.05%	3.10%

in data processing by Grubbs' test method, the damage data with 20% were taken as the testing samples in this paper. The results of SVM can be seen in Table 3.

From the comparison results in Table 3, it can be found that the results of the proposed SVM are near to the measured values. This indicates that the proposed SVM is effective for damage detection of bridge structure.

5. Conclusions

For bridge management and maintenance, it is an important task to evaluate the working state of existing railway piers. It is also an important measure to ensure the safety of trains with increased speed or heavy loads. However, it is hard to detect the damage of bridge pier because the pier is under the water or there are lots of factors affecting the damage. SVM, as a learning machine, does not need a specific function and can reflect the relationship in nonlinear and real-time system of input and performance. Therefore, this paper attempted to use SVM to detect the damage of bridge pier. Considering that the data processing is important for the performance of SVM, Grubbs' test method is adopted to delete outliers for SVM. Since there are lots of factors which affect the damage of pier, a numerical analysis is used to determine the input parameters for SVM. The proposed SVM detection model was tested on the data from field experiments. The results show that the model has a good performance for detecting damage of bridge pier, by comparing with that of the measure values. Thus, the detection model is proved to be a powerful tool for detecting damage of bridge pier.

Acknowledgments

The research is sponsored by the Major State Basic Research Development Program of China ("973" Program: 2013CB036203), the Program for New Century Excellent Talents in University (NCET-10-0219) and Fundamental Research Funds for the Central Universities 3132013079.

References

[1] X. Luo, H. Haya, T. Inaba, T. Shiotani, and Y. Nakanishi, "Damage evaluation of railway structures by using train-induced AE," *Construction and Building Materials*, vol. 18, no. 3, pp. 215–223, 2004.

[2] H. Xia, N. Zhang, and G. De Roeck, "Dynamic analysis of high speed railway bridge under articulated trains," *Computers and Structures*, vol. 81, no. 26-27, pp. 2467–2478, 2003.

[3] H. Xia, N. Zhang, and R. Gao, "Experimental analysis of railway bridge under high-speed trains," *Journal of Sound and Vibration*, vol. 282, no. 1-2, pp. 517–528, 2005.

[4] H. Xia, G. De Roeck, N. Zhang, and J. Maeck, "Experimental analysis of a high-speed railway bridge under Thalys trains," *Journal of Sound and Vibration*, vol. 268, no. 1, pp. 103–113, 2003.

[5] D. M. Siringoringo, Y. Fujino, and T. Nagayama, "Dynamic characteristics of an overpass bridge in a full-scale destructive test," *Journal of Engineering Mechanics-ASCE*, vol. 139, no. 6, pp. 691–701, 2013.

[6] V. N. Vapnik, *The Nature of Statistical Learning Theory*, Springer, New York, NY, USA, 1995.

[7] V. N. Vapnik, "An overview of statistical learning theory," *IEEE Transactions on Neural Networks*, vol. 10, no. 5, pp. 988–999, 1999.

[8] V. N. Vapnik, *The Nature of Statistical Learning Theory*, Statistics for Engineering and Information Science, Springer, New York, NY, USA, 2nd edition, 2000.

[9] L. J. Cao and F. E. H. Tay, "Support vector machine with adaptive parameters in financial time series forecasting," *IEEE Transactions on Neural Networks*, vol. 14, no. 6, pp. 1506–1518, 2003.

[10] B. Z. Yao, C. Y. Yang, J. B. Yao, and J. Sun, "Tunnel surrounding rock displacement prediction using support vector machine," *International Journal of Computational Intelligence Systems*, vol. 3, no. 6, pp. 843–852, 2010.

[11] Y. Bin, Y. Zhongzhen, and Y. Baozhen, "Bus arrival time prediction using support vector machines," *Journal of Intelligent Transportation Systems*, vol. 10, no. 4, pp. 151–158, 2006.

[12] B. Yu, Z. Z. Yang, K. Chen, and B. Yu, "Hybrid model for prediction of bus arrival times at next station," *Journal of Advanced Transportation*, vol. 44, no. 3, pp. 193–204, 2010.

[13] B. Yu, W. H. K. Lam, and M. L. Tam, "Bus arrival time prediction at bus stop with multiple routes," *Transportation Research Part C*, vol. 19, no. 6, pp. 1157–1170, 2011.

[14] B. Yu, Z. Z. Yang, and S. Li, "Real-time partway deadheading strategy based on transit service reliability assessment," *Transportation Research Part A*, vol. 46, no. 8, pp. 1265–1279, 2012.

[15] Z. Sun, G. Bebis, and R. Miller, "Improving the performance of on-road vehicle detection by combining Gabor and wavelet features," in *Proceeding of the IEEE 5th International Conference Intelligent Transportation Systems*, pp. 130–135, 2002.

[16] J. T. Ren, X. L. Ou, Y. Zhang, and D. C. Hu, "Research on network-level traffic pattern recognition," in *Proceeding of the IEEE 5th International Conference Intelligent Transportation Systems*, pp. 500–504, 2002.

[17] R. Reyna, A. Giralt, and D. Esteve, "Head detection inside vehicles with a modified SVM for safer airbags," in *Proceeding of the IEEE Intelligent Transportation Systems*, pp. 268–272, Oakland, Calif, USA, August 2001.

[18] M. S. Srivastava, "Effect of equicorrelation in detecting a spurious observation," *The Canadian Journal of Statistics*, vol. 8, no. 2, pp. 249–251, 1980.

[19] J. K. Baksalary and S. Puntanen, "A complete solution to the problem of robustness of Grubbs's test," *The Canadian Journal of Statistics*, vol. 18, no. 3, pp. 285–287, 1990.

[20] W. M. Cai and Z. W. Hu, *Soil Mechanics and Foundation Engineering*, China Building Industry Press, Beijing, China, 1991 Chinese.

[21] A. Nishimura, "Examination of bridge substructure for integrity," *Japanese Railway Engineering*, no. 114, pp. 13–17, 1990.

[22] B. Dong, C. Cao, and S. E. Lee, "Applying support vector machines to predict building energy consumption in tropical region," *Energy and Buildings*, vol. 37, no. 5, pp. 545–553, 2005.

[23] S. S. Keerthi and C. J. Lin, "Asymptotic behaviors of support vector machines with gaussian kernel," *Neural Computation*, vol. 15, no. 7, pp. 1667–1689, 2003.

Hindawi Publishing Corporation
Mathematical Problems in Engineering
Volume 2013, Article ID 547904, 9 pages
http://dx.doi.org/10.1155/2013/547904

Research Article

Predicting Severity and Duration of Road Traffic Accident

Fang Zong,[1] Huiyong Zhang,[1,2] Hongguo Xu,[1] Xiumei Zhu,[2] and Lu Wang[3]

[1] *College of Transportation, Jilin University, 5988 Renmin Street, Changchun, Jilin 130022, China*
[2] *School of Management, Jilin University, 5988 Renmin Street, Changchun, Jilin 130022, China*
[3] *China Academy of Civil Aviation Science and Technology, Beijing 100028, China*

Correspondence should be addressed to Huiyong Zhang; jlu.zf@163.com

Received 22 September 2013; Accepted 27 October 2013

Academic Editor: Gang Chen

This paper presents a model system to predict severity and duration of traffic accidents by employing Ordered Probit model and Hazard model, respectively. The models are estimated using traffic accident data collected in Jilin province, China, in 2010. With the developed models, three severity indicators, namely, number of fatalities, number of injuries, and property damage, as well as accident duration, are predicted, and the important influences of related variables are identified. The results indicate that the goodness-of-fit of Ordered Probit model is higher than that of SVC model in severity modeling. In addition, accident severity is proven to be an important determinant of duration; that is, more fatalities and injuries in the accident lead to longer duration. Study results can be applied to predictions of accident severity and duration, which are two essential steps in accident management process. By recognizing those key influences, this study also provides suggestive results for government to take effective measures to reduce accident impacts and improve traffic safety.

1. Introduction

Traffic accidents are a significant source of deaths, injuries, property damage, and a major concern for public health and traffic safety. Accidents are also a major cause of traffic congestion and delay. Effective management of accident is crucial to mitigating accident impacts and improving traffic safety and transportation system efficiency. As two major steps of the accident response program (shown in Figure 1), severity prediction and duration estimation are, therefore, of great importance. Accurate predictions of severity and duration can provide crucial information for emergency responders to evaluate the severity level of accidents, estimate the potential impacts, and implement efficient accident management procedures.

To the authors' knowledge, most of the previous studies examined accident severity and duration separately, although they were found to have correlation between each other. Moreover, only one or two of the three aspects of accident severity, that is, number of fatalities, number of injuries, and property damage, were investigated by existing researchers. Therefore, the present study is aimed at developing a model system to estimate both accident severity and duration. Furthermore, three indicators for accident severity will be set, which represents number of fatalities, number of injuries, and property damage, respectively. In doing so, we will provide crucial information for emergency responders to take effective management measures.

The remainder of this paper is organized as follows. In Section 2, we present the literature review on predictions of severity and duration in general. The data are described in Section 3. Following is accident severity modeling in Section 4 and duration forecasting in Section 5. The paper concludes with a summary and directions for future research.

2. Existing Literature

As two major factors in accident analysis, severity and duration have long been important topics for research. Most of the previous studies examined only one of severity and duration. For example, with respect to severity analysis, Chang and Mannering [1] studied the relationship between injury severity and vehicle occupancy using Washington State accident data. Mannera and Wünsch-Ziegler [2] investigated

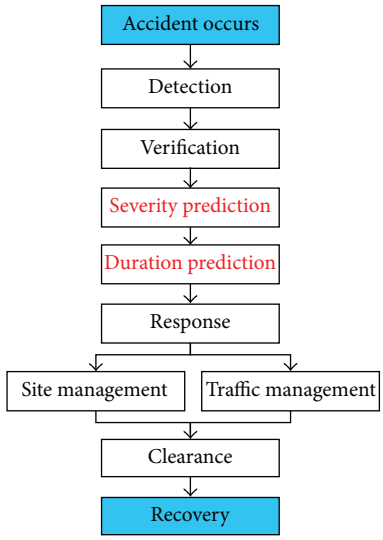

Figure 1: Accident response procedure.

accident severity and determined the important effects of related factors. As for duration, Chung [3] modeled accident duration with freeway accident data collected in Korea. Anastasopoulos et al. [4] presented a Bayesian network model that can be used to learn emerging patterns and predict accident clearance time. Nevertheless, accident severity was found to have influence on duration time by some researchers. For instance, Nam and Mannering [5] revealed that whether there is fatality or injury in accident impacts accident duration. Besides, as shown in Figure 1, severity prediction and duration estimation are connected procedures in the accident management system. Therefore, the two indicators should be considered together and combined in one model system.

Concerning severity analysis, which includes mainly three aspects, that is, number of fatalities, number of injuries, and property damage, most of the existing researchers investigated it as one comprehensive indicator; for example, Mannera and Wünsch-Ziegler [2]took accident severity as one independent variable with four alternatives, namely, fatal, severe injury, light injury, and property damage. Milton et al. [6] defined severity levels as property damage only, possible injury, and injury. Malyshkina and Mannering [7] modeled severity by using three alternatives, that is, fatality, injury, and property damage only. In addition, a number of researchers considered only one or two of the three aspects of severity. For instance, Stone and Broughton [8] and Sze and Wong [9] considered only the aspect of fatality by defining two levels of severity, that is, fatal and nonfatal accident. Delen et al. [10] defined injury severity levels as no injury, probable injury, nonincapacitating, incapacitating and fatality. Similarly, Ballesteros et al. [11] and Roudsari et al. [12] considered only number of fatalities and injuries but not property damage. In fact, different types of losses as well as the amount of losses lead to different response measures and last possibly for disparate amount of time. For example, either an accident resulting in $167–5000 property damage or an accident leading to 1–3 injuries will be defined as level 2 accident in Zhang's study [13]. However, the latter one needs rescue services but the former one does not. This indicates that any of the three indicators, that is, number of fatalities, number of injuries, and property damage, is crucial to making accident response decision and is therefore recommended to be modeled separately in order to provide more detailed information about accident management.

As mentioned above, most of the previous studies examined accident severity and duration separately, although they were found to have correlation between each other. Moreover, only one or two of the three aspects of accident severity, that is, number of fatalities, number of injuries, and property damage, were investigated by the existing studies. Therefore, the present work is aimed at developing a model system to estimate both accident severity and duration. Furthermore, three indicators for accident severity will be investigated, which represent number of fatalities, number of injuries, and property damage, respectively.

3. Data and Modeling Framework

The dataset for the study contains police-reported traffic accident records for Jilin province, China, in 2010. With records containing missing values eliminated, our final dataset consists of 3,914 cases, in which, 1,280 (32.70%) cases were pedestrian involved accidents and 387 (9.89%) cases were non-motor-vehicle-involved accidents. In addition to severity information, the data contains information regarding accident duration, accident characteristics (vehicle fire, crash type, accident occurrence time, and number of lanes affected), emergency services (police services, fire and rescue services, tow services, and emergency medical services), vehicle characteristics (vehicle type involved, debris involved, hazardous material involved, and disabled vehicles involved), environmental factors (weather conditions and visibility distance) and road conditions (number of lanes,

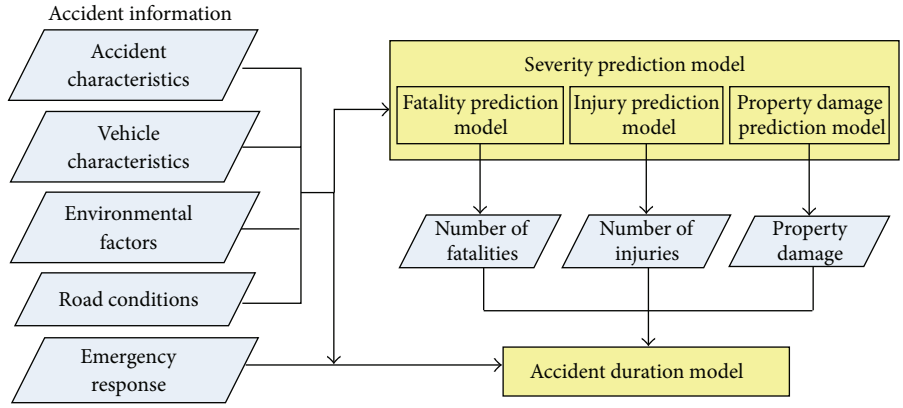

Figure 2: Accident severity and duration modeling framework.

pavement condition, road geometrics, and roadway surface condition, etc.).

Based on a preliminary correlation test, 4 independent variables and 26-candidate dependent variables were selected from the dataset, as shown in Table 1.

With *Nof*, *Noi*, and *Pd* as independent variables, three separate severity prediction models will be developed. Then, duration modeling will be conducted by taking accident severity as input. The modeling framework is shown in Figure 2.

4. Severity Modeling

Besides the Ordered Probit model [14], which is often used in discrete choice modeling, SVM will be introduced in this paper and be compared with the Ordered Probit model according to the prediction accuracies.

4.1. Ordered Probit Model. As shown in Table 1, the alternatives of the severity related dependent variables are all ordered. Since multinomial logit (MNL) model, which is commonly used in discrete choice modeling, would fail to account for the ordinal nature of the dependent variable and have the problem of Independence from irrelevant alternatives (IIA) [15], this study will employ Ordered multiple choice model for severity modeling.

The Ordered multiple choice model assumes the relationship:

$$\sum_{j=1}^{J} P_n(j) = F\left(\alpha_j - \beta_j X_n, \theta\right), \quad j = 1, \ldots, J-1,$$
$$P_n(J) = 1 - \sum_{j=1}^{J} P_n(j), \tag{1}$$

where $P_n(j)$ is the probability that alternative j happens in accident n ($n = 1, \ldots, N$), α_j is an alternative specific constant, X_n is a vector of the attributes of accident n, β_j is a vector of estimable coefficients, and θ is a parameter that controls the shape of probability distribution F. Therefore, F, can have various shapes of distribution based on different value of θ.

The Ordered Probit model, which assumes standard normal distribution for F is the most commonly used Ordered multiple choice model [16]. The Ordered Probit model has the following form:

$$P_n(1) = \Phi\left(\alpha_1 - \beta_j X_n\right),$$
$$P_n(j) = \Phi\left(\alpha_j - \beta_j X_n\right) - \Phi\left(\alpha_{j-1} - \beta_j X_n\right), \quad j = 2, \ldots, J-1, \tag{2}$$
$$P_n(J) = 1 - \sum_{j=1}^{J-1} P_n(j),$$

where $P_n(j)$ is the cumulative standard normal distribution function. For all the probabilities to be positive, we must have $\alpha_1 < \alpha_2 < \cdots < \alpha_{J-1}$.

4.2. Support Vector Machine Model. Support vector machine (SVM) is a type of learning algorithms based on statistical learning theory, which can be adjusted to map the input-output relationship for the nonlinear system [17–19]. SVM has been widely used in transportation modeling; for example, Bolbol et al. [20] employed SVM classification in travel behavior analysis, Apatean et al. [21] used it in road obstacle classification, and Abdel-Aty and Haleem [22] applied it to analyze angle crashes at unsignalized intersections. Previous studies indicate that SVM can conduct discrete choice modeling with acceptable accuracy. Therefore, it is chosen to be employed to model accident severity in this paper.

Given a set of input-output data pairs $D = (x_1, y_1), (x_2, y_2), \ldots, (x_l, y_l)$ ($x_i \in X \subseteq R^m, y_i \in Y \subseteq R^n$, and l being the number of training samples, that are randomly and independently generated from an unknown function, SVM estimates the function using the following equation [23]:

$$f(x) = w \cdot \Phi(x) + b \quad w, x \in R^m, \; b \in R^n, \tag{3}$$

Table 1: Variables and statistics based on survey data.

Factors	Variables	Values	Percentage (%)	Variables	Values	Percentage (%)
Accident severity	Number of fatalities: Nof	0	89.59	Number of injuries: Noi	0	9.86
		[1, 2]	10.38		[1, 3)	85.89
		More than 3	0.03		[3, 11)	4.14
	Property damage (yuan): Pd	Less than 1000	61.18		Over 11	0.11
		[1001, 30000)	37.19			
		Over 30000	1.63			
Duration	Duration (Continuous value)	Mean (min) 192.95	Standard deviation 111.63			
Accident characteristics	Motor-vehicle-only accident: Mvoa	Yes	57.41	Vehicle fire: Vf	Yes	8.93
		No	42.59		No	91.07
	Head-on type collision: Hotc	Yes	8.93	Weekend or festival: Wof	Yes	38.60
		No	91.07		No	61.40
	Rear-end type collision: Retc	Yes	19.64	Vehicle rollover: Vr	Yes	26.79
		No	80.36		No	73.21
	Time of day: Tod	[00:00, 6:00)	6.24	Number of lanes blocked: Nolb	0	3.57
		[6:00, 18:00)	69.12		1	62.50
		[18:00, 24:00)	24.64		over 1	33.93
Vehicle characteristics	Bus involved: Bi	Yes	16.07	Hazardous material involved: Hmi	Yes	1.79
		No	83.93		No	98.21
	Truck involved: Ti	Yes	89.29	Disabled vehicles involved: Dvi	Yes	27.27
		No	10.71		No	72.73
	Debris involved: Di	Yes	53.57			
		No	46.43			
Environmental factors	Weather conditions: Wc	Sunny	89.48	Visibility distance (meter): Vd	Less than 50	8.90
		Fog	0.23		[50, 100)	22.70
		Sleet	5.97		[100, 200)	19.86
		Other	4.32		Over 200	48.54
Road environment factors	Number of lanes in each direction: Nol	2	33.92	Accident location (horizontal): Alh	Motor vehicle lanes	71.68
		3	51.79		Bike lane	6.60
		Over 3	14.29		Shared motor vehicle and bike lane	13.71
	Pavement condition: Pc	Asphalt	96.95		Sidewalk	2.22
		Cement	2.85		Crosswalk	3.42
		Sand and gravel	0.07		Other	2.37
		Soil	0.07		Regular road section	60.01
		Other	0.06	Accident location (vertical): Alv	Four-way intersection	20.43
	Roadway surface condition: Rsc	Dry	85.16		Other road sections (narrow carriageway and tunnel, etc.)	1.09
		Wet	6.38		Other intersections	18.47
		Slippery (snowy or icy conditions)	6.76	Road geometrics: Rg	Flat and straight	98.57
		Other	1.70		Hill or bend	1.43
	Traffic signal control: Tsc	Yes	17.46			
		No	82.54			
Emergency services	Police services: Ps	Yes	71.43	Fire and rescue services: Frs	Yes	16.07
		No	28.57		No	83.93
	Tow services: Ts	Yes	98.21	Emergency medical services: Ems	Yes	33.93
		No	1.79		No	66.07

where $\Phi(x)$ represents the high-dimensional feature spaces which are nonlinearly mapped from the input space x, w denotes a parameter vector, and b is the threshold [24, 25].

If the domain of output space y only takes category values, that is, −1 and +1, the learning problem then refers to support vector classification (SVC) [26].

For classification about the training data D, SVM's linear soft-margin algorithm is used to solve the following primal quadratic programming problem:

$$\begin{aligned} \min_{w,b,\xi} \quad & \frac{1}{2}\|w\|_2^2 + C\sum_{i=1}^{l}\xi_i \\ \text{s.t.} \quad & y_i\left(w^T x_i + b\right) \geq 1 - \xi_i, \\ & \xi_i \geq 0, \quad i = 1, 2, \ldots, l, \end{aligned} \tag{4}$$

where C is a penalty parameter and ξ_i are the slack variables. The goal is to find an optimal separating hyperplane,

$$w^T x_i + b = 0, \tag{5}$$

where $x \in R^m$. The Wolfe dual, that is, (4), can be expressed as

$$\begin{aligned} \max_{\alpha} \quad & \sum_{j=1}^{l}\alpha_j - \frac{1}{2}\sum_{i=1}^{l}\sum_{j=1}^{l} y_i y_j \left(x_i \cdot x_j\right)\alpha_i\alpha_j \\ \text{s.t.} \quad & \sum_{i=1}^{l} y_i\alpha_i = 0, \quad 0 \leq \alpha_i \leq C, \ i = 1, \ldots, l, \end{aligned} \tag{6}$$

where $\alpha \in R^l$ are lagrangian multipliers. The optimal separating hyperplane of (5) can be given by

$$w = \sum_{i=1}^{l}\alpha_i^* y_i x_i, \quad b = \frac{1}{N_{sv}}\left(y_j - \sum_{i=1}^{N_{sv}}\alpha_i^* y_i\left(x_i \cdot x_j\right)\right), \tag{7}$$

where α^* is the solution of (6) and N_{sv} represents the number of support vectors such that $0 < \alpha < C$. A new sample is classified as +1 or −1 according to the finally decision function $f(x) = \text{sgn}((w \cdot x) + b)$.

In order to conduct multiclass classification (as SVC model is originally designed for binary classification), one-against-one method will be employed in this paper [27, 28].

4.3. Estimation Results. By using Stata and Matlab, the severity prediction models based on Ordered Probit and SVM are estimated, respectively. The estimation results as well as the prediction accuracies are shown in Table 2.

The last row shows the hit ratio for all the models. In general, higher value of hit ratio represents higher goodness-of-fit of the model. As all the hit ratio values of the Ordered Probit models are higher than that of SVM models, Ordered Probit-based models are chosen as the severity prediction models.

The results indicate that hazardous material involved in the accident, weather, and accident location are significant in all the three models. According to the estimation results, hazardous material involved will increase the probability of high property damage. The reason is that hazardous material will increase the probability of occurrence of fire or even explosion, which leads to high damage to the vehicles and goods.

Some of the variables have impact on only one or two indicators. For example, bus involved, truck involved, time of day, and traffic signal control are crucial to number of fatalities and injuries. The more buses or trucks are involved, the more fatalities and injuries the accident will cause. In addition, the factors of road geometrics, vehicle fire, and vehicle rollover are important for number of fatalities, while roadway surface condition has effect on number of injuries. The results also indicate that disabled vehicles involved, debris involved, visibility distance, pavement condition, and motor-vehicle-only accident are significant for property damage. The more disabled vehicles or debris is involved in the accident, the more property damage the accident will lead to. As for motor-vehicle-only accident, the results reveal that accidents with only vehicles involved cause more property damage than that with pedestrian or non-motor-vehicles involved.

5. Accident Duration Modeling

5.1. AFT Model and KM Estimator. As suggested by Nam and Mannering [5] and Stathopoulos and Karlaftis [29], hazard-based duration models have an advantage in that they allow the explicit study of duration effects of accidents (i.e., the relationship between how long an accident has lasted and the likelihood of it ending soon). Thus, hazard-based duration models, in particular the accelerated failure time (AFT) metric, were utilized in this study to model the accident duration. The reason that we choose AFT model is that, compared with other forms of hazard-based model, AFT model is predominately fully parametric; that is, a probability distribution is specified and it is also less affected by the choice of probability distribution [30, 31], and the results of AFT model are easily interpreted [32].

Let T be a nonnegative random variable representing the accident duration. The hazard at time t on the continuous time-scale $h(t)$ is defined as the instantaneous probability that the duration under study will end in an infinitesimal time period Δt after time t, given that the duration has not elapsed until time t. A mathematical definition for the hazard function is as follows:

$$h(t) = \lim_{\Delta \to 0^+} \frac{P\left(t \leq T < t + \Delta \mid T > t\right)}{\Delta}. \tag{8}$$

Let $f(\cdot)$ and $F(\cdot)$ be the density and cumulative distribution function for T, respectively. Then the probability of ending in an infinitesimal interval of range Δt, after time t is $f(t)\Delta t$. And the probability that the process lasts for at least t is given by the survival equation

$$S(t) = P(T > t) = 1 - F(t). \tag{9}$$

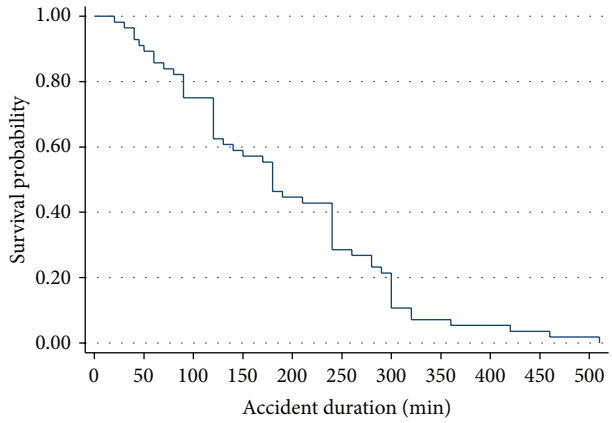

Figure 3: Survival curve of accident duration.

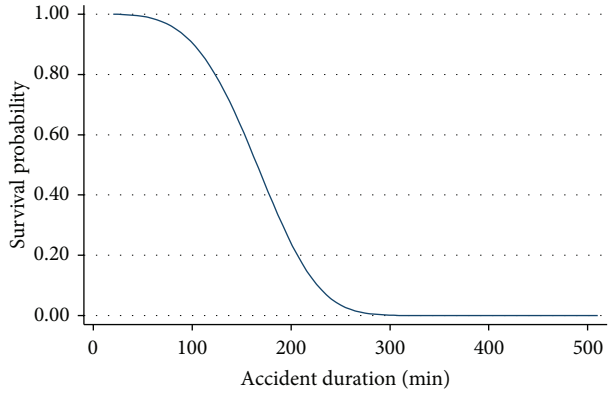

Figure 4: The estimated survival curve of accident duration.

Thus, the hazard function can be further expressed as

$$h(t) = \frac{f(t)}{S(t)} = \frac{dF(t)/dt}{S(t)} = \frac{-dS(t)/dt}{S(t)} = \frac{-d\ln S(t)}{dt}. \quad (10)$$

The distribution of the hazard can be assumed to be one of many parametric forms or to be nonparametric. Because the distribution of the accident duration is unknown, one of the nonparametric methods, the Kaplan-Meier (KM) product limit estimator, is conducted to explore the covariates effects and the potential distribution.

As a nonparametric method, the KM estimator, produces an empirical approximation of survival and hazard but hardly takes any covariate effects into consideration. It is similar to an exploratory data analysis. Denoting the distinct failure times of individuals n as $t_1 < t_2 < \cdots < t_m$, the KM estimator of survival at time t_i is computed as the product of the conditional survival proportions:

$$S_{KM}(t_i) = \prod_{k=1}^{i} \frac{r(t_k) - d(t_k)}{r(t_k)}, \quad (11)$$

where $r(t_k)$ is the total number of accidents at risk for ending at t_k and $d(t_k)$ is the number of accidents stopping at t_k.

By using the KM estimator, the survival function curves of the accident duration are estimated, which are shown in Figure 3. The results indicate that the survival probability decreases with duration, which implies an accelerated failure time model with Weibull or Exponential distribution should be employed. Therefore, the AFT model is developed to examine the linkages between duration and covariates relative to accident information.

The AFT model permits the covariates to affect the duration dependence. Its survival function is given as

$$S(t) = S_0\left[t \cdot \exp\left(-\beta' X\right)\right], \quad (12)$$

where $S_0(\cdot)$ is the baseline survival function. The corresponding hazard function is

$$h(t) = \frac{-\partial S(t)/\partial t}{S(t)} = h_0\left[t \cdot \exp\left(-\beta' X\right)\right]\exp\left(-\beta' X\right). \quad (13)$$

The AFT model can be expressed as a log-linear model:

$$\ln t = \beta' X + \varepsilon. \quad (14)$$

Assuming that the random error ε follows either a Weibull distribution or an Exponential distribution, one can get two kinds of AFT models, and both of them are often used in duration analysis.

5.2. Estimation Results. Assuming that the random error in (14) follows a Weibull distribution and an Exponential distribution, respectively, the accident duration models are established. The models are estimated by employing maximum likelihood estimation (MLE), and the estimation results are shown in Table 3.

The Mean absolute percentage error (MAPE), which looks at the average percentage difference between predicted values and observed ones, is adopted to examine the accuracy of the developed duration predication model. MAPE is calculated as

$$\text{MAPE} = \frac{1}{n}\sum_{i-1}^{n}\left|\frac{A_i - P_i}{A_i}\right|, \quad (15)$$

where A_i is the observed value and P_i is the predicted value for observation i.

The MAPE value of Weibull distribution (0.22) is less than that of the Exponential distribution (0.23), indicating that the values predicted by the AFT model with the Weibull distribution is more close to the actual accident duration [3]. Therefore, the Weibull distribution function is chosen.

The estimation results indicate that most of the results were consistent with the theoretical expectation. According to the results, the variables with respect to accident severity significantly affect accident duration: the more fatalities and injuries occur in the accident, the longer duration it will lead to. This supports the necessity of combining predictions of accident severity and duration in one model system. Besides, accident type is revealed to be crucial to duration: comparing with other types of accidents, the duration of rear-end type collision is 37% shorter, while that of rollover is 28% longer. The results also show that the duration of accident involving bus, truck, debris, or hazard material is 60%, 58%, 55%,

Table 2: Estimation results of severity prediction models.

Variables	Fatality model			Injury model			Property damage model		
	SVM	Ordered Probit		SVM	Ordered Probit		SVM	Ordered Probit	
		Coef.	Z-stat.		Coef.	Z-stat.		Coef.	Z-stat.
Dvi	—	—	—	—	—	—	√	0.23	1.99
Bi	√	0.75	8.82	√	0.28	4.37	—	—	—
Ti	√	0.64	7.93	√	0.29	4.61	—	—	—
Di	—	—	—	—	—	—	√	0.11	2.00
Hmi	√	0.04	1.34	√	0.04	1.65	√	0.21	1.96
Tod	√	0.12	2.94	√	0.04	1.21	—	—	—
Wc	√	0.12	2.3	√	−0.05	−2.3	√	0.04	2.46
Vd	—	—	—	—	—	—	√	0.10	5.92
Tsc	√	0.03	2.31	√	−0.02	−1.56	—	—	—
Alh	√	−0.03	−1.44	√	0.04	2.71	√	−0.03	−2.12
Alv	√	−0.11	−6.88	√	0.06	5	√	−0.13	−12.16
Rsc	—	—	—	√	0.11	4.03	—	—	—
Rg	√	−0.26	−1.71	—	—	—	√	−0.18	−2.01
Pc	—	—	—	—	—	—	√	−0.18	−2.09
Vf	√	0.73	7.70	—	—	—	√	0.13	1.98
Vr	√	0.04	1.32	—	—	—	—	—	—
Mvoa	—	—	—	—	—	—	√	0.45	11.66
α_1	—	0.63	—	—	−0.68	—	—	0.06	—
α_2	—	2.79	—	—	2.36	—	—	1.99	—
α_3	—	—	—	—	3.71	—	—	—	—
Hit ratio (%)	89.21	89.59		86.50	86.89		59.57	62.66	

Table 3: Estimation results of accident duration model.

Variables	Weibull distribution		Exponential distribution	
	Coef.	z-stat.	Coef.	z-stat.
Constant	5.12	13.99	4.71	11.76
Nof	0.51	4.14	0.51	1.43
Noi	0.33	4.45	0.34	1.28
Pd			−0.13	−1.01
Retc	−0.37	−2.62	—	—
Vr	0.28	2.06	—	—
Nolb	0.24	4.48	0.25	1.64
Bi	0.60	4.01	0.41	1.07
Ti	0.58	3.12	—	—
Di	0.55	5.28	0.45	1.35
Hmi	0.88	2.89	—	—
Wof	−0.14	−1.49	—	—
Alv	−0.57	−4.55	−0.43	−1.06
Nol	−0.18	−2.81	—	—
Ts	0.38	1.35	—	—
γ (shape parameter)	0.26	—	—	—
Prob > χ^2	0		0.0067	

Table 4: Goodness of fit index and estimated distribution statistics of accident duration model.

Model statistics	Mean (min)	Variance	Maximum (min)	Minimum (min)	MAPE value
Observed value	192.95	111.63	510	20	0.22
Predicted value	188.38	84.52	327.14	53.03	

or 88% longer than that of other accidents, respectively. Besides, according to the results, the accident which occurs in weekend or festival is found to be associated with shorter duration. The reason is that the traffic volume in nonworking day is lower than that in working day. As for accident location, the results reveal that the accident occurs at regular road section or 4-way intersection results in longer duration than that occuring at other locations. The reason may be that the traffic volume is higher at regular road section or intersection. Regarding emergency services, the accident which needs tow services has longer duration. Moreover, as the number of lanes occupied in the accident increases, duration increases.

By using the accident duration model, the survival curve of duration is estimated, which is shown in Figure 4. Comparing with observed value, the prediction accuracy of accident duration model is shown in Table 4.

6. Conclusions

In this paper, a severity prediction model system was constructed by employing Ordered Probit model, and a duration prediction model was established by applying Hazard model. Accident severity, including number of fatalities, number of injuries, and property damage, as well as accident duration was forecasted with the models.

Study results can be applied to severity and duration prediction, which are essential steps in accident response process. By comparing SVM and Ordered Probit model, it also makes a methodological contribution in enhancing prediction accuracy of severity estimation. In addition, by identifying the key effects of related factors on accident severity and duration, the results provide useful clues for government to take effective measures in order to reduce accident impacts and improve traffic safety.

One limitation of current study is that some factors, such as characteristics of the driver, passenger and pedestrian, and traffic condition, which have potential effects on accident severity and duration, are not considered because of the lack of suitable data. Further study should be done to collect the related information and investigate the impacts of these factors.

Acknowledgments

The research is funded by the National Natural Science Foundation of China (50908099) and China Postdoctoral Science Special Foundation (201104526).

References

[1] L.-Y. Chang and F. Mannering, "Analysis of injury severity and vehicle occupancy in truck- and non-truck-involved accidents," *Accident Analysis and Prevention*, vol. 31, no. 5, pp. 579–592, 1999.

[2] H. Mannera and L. Wünsch-Ziegler, "Analyzing the severity of accidents on the German Autobahn," *Accident Analysis and Prevention*, vol. 57, no. 8, pp. 40–48, 2013.

[3] Y. Chung, "Development of an accident duration prediction model on the Korean Freeway Systems," *Accident Analysis and Prevention*, vol. 42, no. 1, pp. 282–289, 2010.

[4] P. C. Anastasopoulos, V. N. Shankar, J. E. Haddock, and F. L. Mannering, "A multivariate tobit analysis of highway accident-injury-severity rates," *Accident Analysis and Prevention*, vol. 45, pp. 110–119, 2012.

[5] D. Nam and F. Mannering, "An exploratory hazard-based analysis of highway incident duration," *Transportation Research A*, vol. 34, no. 2, pp. 85–102, 2000.

[6] J. C. Milton, V. N. Shankar, and F. L. Mannering, "Highway accident severities and the mixed logit model: an exploratory empirical analysis," *Accident Analysis and Prevention*, vol. 40, no. 1, pp. 260–266, 2008.

[7] N. V. Malyshkina and F. L. Mannering, "Markov switching multinomial logit model: an application to accident-injury severities," *Accident Analysis and Prevention*, vol. 41, no. 4, pp. 829–838, 2009.

[8] M. Stone and J. Broughton, "Getting off your bike: cycling accidents in Great Britain in 1990–1999," *Accident Analysis and Prevention*, vol. 35, no. 4, pp. 549–556, 2003.

[9] N. N. Sze and S. C. Wong, "Diagnostic analysis of the logistic model for pedestrian injury severity in traffic crashes," *Accident Analysis and Prevention*, vol. 39, no. 6, pp. 1267–1278, 2007.

[10] D. Delen, R. Sharda, and M. Bessonov, "Identifying significant predictors of injury severity in traffic accidents using a series of artificial neural networks," *Accident Analysis and Prevention*, vol. 38, no. 3, pp. 434–444, 2006.

[11] M. F. Ballesteros, P. C. Dischinger, and P. Langenberg, "Pedestrian injuries and vehicle type in Maryland, 1995–1999," *Accident Analysis and Prevention*, vol. 36, no. 1, pp. 73–81, 2004.

[12] B. S. Roudsari, C. N. Mock, R. Kaufman, D. Grossman, B. Y. Henary, and J. Crandall, "Pedestrian crashes: higher injury severity and mortality rate for light truck vehicles compared with passenger vehicles," *Injury Prevention*, vol. 10, no. 3, pp. 154–158, 2004.

[13] H. Y. Zhang, *Analyzing Traffic Accident Situation with Bayesian Network [Doctor Dissertation]*, Jilin University, 2013.

[14] J. L. Bowman and M. E. Ben-Akiva, "Activity-based disaggregate travel demand model system with activity schedules," *Transportation Research A*, vol. 35, no. 1, pp. 1–28, 2000.

[15] P. Ray, "Independence of irrelevant alternatives," *Econometrica*, vol. 41, pp. 987–991, 1973.

[16] M. A. Quddus, R. B. Noland, and H. C. Chin, "An analysis of motorcycle injury and vehicle damage severity using ordered probit models," *Journal of Safety Research*, vol. 33, no. 4, pp. 445–462, 2002.

[17] B.-Z. Yao, C.-Y. Yang, J.-B. Yao, and J. Sun, "Tunnel surrounding rock displacement prediction using support vector machine," *International Journal of Computational Intelligence Systems*, vol. 3, no. 6, pp. 843–852, 2010.

[18] B. Yu, Z. Z. Yang, and B. Z. Yao, "Bus arrival time prediction using support vectormachines," *Journal of Intelligent Transportation Systems*, vol. 10, no. 4, pp. 151–158, 2006.

[19] F. Zong, H. Lin, and X. Pan, "Daily commute time prediction based on genetic algorithm," *Mathematical Problems in Engineering*, vol. 2012, Article ID 321574, 20 pages, 2012.

[20] A. Bolbol, T. Cheng, I. Tsapakis, and J. Haworth, "Inferring hybrid transportation modes from sparse GPS data using a moving window SVM classification," *Computers, Environment and Urban Systems*, vol. 36, no. 6, pp. 526–537, 2012.

[21] A. Apatean, A. Rogozan, and A. Bensrhair, "Visible-infrared fusion schemes for road obstacle classification," *Transportation Research C*, vol. 35, pp. 180–192, 2013.

[22] M. Abdel-Aty and K. Haleem, "Analyzing angle crashes at unsignalized intersections using machine learning techniques," *Accident Analysis and Prevention*, vol. 43, no. 1, pp. 461–470, 2011.

[23] K.-K. Sung and T. Poggio, "Example-based learning for view-based human face detection," *IEEE Transactions on Pattern Analysis and Machine Intelligence*, vol. 20, no. 1, pp. 39–51, 1998.

[24] J. B. Yao, B. Z. Yao, L. Li, and Y. L. Jiang, "Hybrid model for dispalcement prediction of tunnel surrounding rock," *Neural Network World*, vol. 22, no. 3, pp. 263–275, 2012.

[25] V. N. Vapnik, *The Nature of Statistical Learning Theory*, Springer, New York, NY, USA, 1995.

[26] Y. M. Li, S. G. Gong, and H. M. Liddell, "Support vector regression and classification based multi-view face detection and recognition," in *Proceedings of the IEEE International Conference on Automatic Face and Gesture Recognition*, pp. 300–305, 2000.

[27] C.-W. Hsu and C.-J. Lin, "A comparison of methods for multiclass support vector machines," *IEEE Transactions on Neural Networks*, vol. 13, no. 2, pp. 415–425, 2002.

[28] B. Yu, W. H. K. Lam, and M. L. Tam, "Bus arrival time prediction at bus stop with multiple routes," *Transportation Research C*, vol. 19, no. 6, pp. 1157–1170, 2011.

[29] A. Stathopoulos and M. G. Karlaftis, "Modeling duration of urban traffic congestion," *Journal of Transportation Engineering*, vol. 128, no. 6, pp. 587–590, 2002.

[30] P. Lambert, D. Collett, A. Kimber, and R. Johnson, "Parametric accelerated failure time models with random effects and an application to kidney transplant survival," *Statistics in Medicine*, vol. 23, no. 20, pp. 3177–3192, 2004.

[31] N. Keiding, P. K. Andersen, and J. P. Klein, "The role of frailty models and accelerated failure time models in describing heterogeneity due to omitted covariates," *Statistics in Medicine*, vol. 16, no. 1–3, pp. 215–224, 1997.

[32] R. Kay and N. Kinnersley, "On the use of the accelerated failure time model as an alternative to the proportional hazards model in the treatment of time to event data: a case study in influenza," *Drug Information Journal*, vol. 36, no. 3, pp. 571–579, 2002.

Hindawi Publishing Corporation
Mathematical Problems in Engineering
Volume 2013, Article ID 726194, 6 pages
http://dx.doi.org/10.1155/2013/726194

Research Article

An Improved Particle Swarm Optimization for the Automobile Spare Part Warehouse Location Problem

Zhen Yaobao,[1] Hu Ping,[2] and Yang Shu[2]

[1] *School of Mechanical Engineering, Dalian University of Technology, Dalian, 116024, China*
[2] *School of Automotive Engineering, Dalian University of Technology, Dalian 116024, China*

Correspondence should be addressed to Yang Shu; yangs_dl@126.com

Received 29 September 2013; Revised 2 November 2013; Accepted 2 November 2013

Academic Editor: Rui Mu

This paper deals with a real-life warehouse location problem, which is an automobile spare part warehouse location problem. Since the automobile spare part warehouse location problem is a very complex problem, particle swarm optimization is used and some improved strategies are proposed to improve the performance of this algorithm. At last, the computational results of the benchmark problems about warehouse location problems are used to examine the effectiveness of particle swarm optimization. Then the results of the real-life automobile spare part warehouse location problem also indicate that the improved particle swarm optimization is a feasible method to solve the warehouse location problem.

1. Introduction

The profitability of automobile spare part warehouse location for automobile spare part factories is important for several reasons. The last decade has witnessed greatly growth in the demand of automobile and commensurate with this growth is the large demand of automobile spare parts. The cost of the management and stock has been an excess burden for automobile spare part factories. Furthermore, the fixed cost of the vehicles involved in automobile spare part delivery is high enough. Automobile spare part warehouses are a part of an overall effort to gain place and time utility (a decision aid in warehouse site selection). It has some obvious advantages. For example, a warehouse can hold stocks to match the imbalance between supply and demand. And the travelling cost can be decreased by collecting from multiple sources into a single vehicle to the final destination. Therefore, these increasing pressures and the advantages of warehouse have caused these factories to look for an automobile spare part warehouse to minimize their management cost.

There have been many literatures on the location of warehouse. Michel and van Hentenryck [1] proposed a tabu search to solve the warehouse location problem which considered the fixed and the transportation costs from warehouse to stores. In the algorithm, a linear neighborhood was used to improve the performance of the tabu search. Khumawala [2] proposed an uncapacitated warehouse location problem which aimed to minimize the fixed cost of warehouse and the warehouse operating costs and transportation costs from the warehouse to customers. Then he attempted to solve the warehouse location problem by using of an efficient heuristic procedure which was derived from the branching decision rules. Baker [3] introduced a partial dual algorithm to solve the capacitated warehouse location problem which is based on the properties of transportation problems. Ozsen et al. [4] proposed a model of the capacitated warehouse location with risk pooling, in which the fixed facility location, transportation, and inventory carrying costs are considered simultaneously. Then, they tried to use a Lagrangian relaxation algorithm to solve this problem.

From the literatures, it can be attained that warehouse location problem has been recognized by academics and practitioners. Most of them paid attentions to the fixed cost of warehouse or transportation cost from warehouse to customers. However, in the real-life automobile spare part warehouse problem, the transportation cost from the factories to warehouse should also be considered. However, only few literature works attempted to incorporate routing

from the suppliers to the warehouse and the warehouse to customers in location analysis. This paper attempted to solve a real-life automobile spare part warehouse location problem, in which there are some automobile spare part factories and their customers.

Therefore, the objective of the warehouse location problem is to minimize the sum of the transportation cost from the factories to the warehouse and from the warehouse to the customers and the fixed cost of warehouse. Based on the objective, it can be attained that the automobile spare part warehouse location problem is a generalization of well-known and difficult location problems. It is therefore a large and complex problem. Many literature works suggested that heuristic algorithm was often a first choice to solve this kind of complicated problems [5–12]. Among heuristic algorithms, particle swarm optimization (PSO) is a heuristic which is a population-based search method developed by Kennedy and Eberhart [13]. PSO simulates the social behaviors from bee swarm, fish school, or bird flock. Thus, in PSO, each solution of optimization problem is corresponding to the position of one particle in the searching space. PSO attains the search for optimum based on the mechanism which adapts to the global and local exploration. Most applications of PSO have indicated that PSO have concentrated on the optimization in continuous space. In recent years, PSO has been a very popular optimization method due to that PSO does not need the calculation of derivatives, but the information from each particle and the information between the whole particle population. Thus, PSO is less sensitive to the nature of the objective function. which can be suitable for stochastic objective functions and can easily escape from local minima. PSO has been successfully applied to solving the complex problem [14–16]. Therefore, PSO is used to solve the automobile spare part warehouse location problem in this paper.

The remainder of the paper is organized as follows. Section 2 introduces the automobile spare part warehouse location problem. In Section 3, PSO and some improvement strategies are presented. Some computational results are discussed in Section 4 and, lastly, the conclusions are provided in Section 5.

2. The Automobile Spare Part Warehouse Location Problem

The automobile spare part warehouse location problem can be described as follows. There are a set of M potential warehouses and a set of N customers (repair station). Each warehouse has a fixed cost and the transportation cost from production factories to warehouse and from warehouse to customers. The automobile spare part warehouse location problem is to find a subset of warehouses and an assignment of warehouses to the customers aiming to minimize the fixed and the transportation costs. Once the locations of the warehouses are determinate, these warehouses should be assigned to serve their closest warehouse. Figure 1 described the network about the automobile spare part delivery.

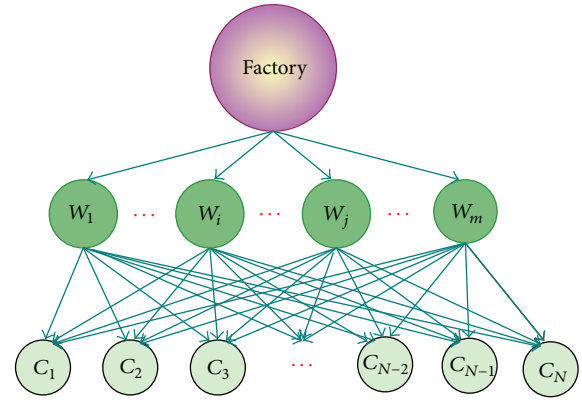

Figure 1: An example of the automobile spare part warehouse location problem.

From Figure 1, there are m depots for potential warehouse, that is, $w_1, \ldots, w_i, \ldots, w_j, \ldots, w_m$. it is assumed that w_j is selected as the warehouse which should serve the customers. And it is possible for any set among $w_1, \ldots, w_i, \ldots, w_j, \ldots, w_m$ to be the warehouse(s). Then, the automobile spare part warehouse location problem can be formulated as formulas (1a)–(1e):

$$\text{Min} \quad \left(\sum_{i=1}^{M} F_i y_i + \sum_{i=1}^{M} \sum_{j=1}^{N} C_{ij} \cdot d_{ij} \cdot x_{ij} + \sum_{i=1}^{M} \sum_{k=1}^{K} C_{ik} d_{ik} x_{ik} \right), \tag{1a}$$

$$\text{s.t.} \quad \sum_{i=1}^{M} F_i y_i \le B, \tag{1b}$$

$$\sum_{j=1}^{N} x_{ij} \ge \sum_{k=1}^{K} x_{ik}, \tag{1c}$$

$$\sum_{i=1}^{M} \sum_{j=1}^{N} x_{ij} \le 1, \tag{1d}$$

$$\sum_{i=1}^{M} \sum_{k=1}^{K} x_{ik} \le 1, \tag{1e}$$

where

$$y_i = \begin{cases} 1 & \text{point } i \text{ is selected for the warehouse} \\ 0 & \text{otherwise,} \end{cases} \tag{2}$$

B is the maximum operative budget; M is the number of potential warehouse; N is the number of customers; K is the number of factories; C_{ij} and C_{ik} in formulas (1a)–(1e) stand for the costs from point i to j and from point i to k, respectively;in this paper, it is the unit transportation cost of unit distance and unit quantity. x_{ij} is the demand of customer i supplied from warehouse i. x_{ik} is the demand of warehouse i supplied from factory k. F_i is the fixed cost associated with warehouse i, where formulas (1a)–(1e) represent the objective function, as described above. Constraint (1b) ensures that

the fixed cost from selected warehouse cannot exceed the total planned budget. Constraint (1c) ensures the reliability of production of part factories. Constraints (1d)-(1e) ensure that each customer can be visited at most once.

3. Improved Particle Swarm Optimization for the Automobile Spare Warehouse Location Problem

3.1. Particle Swarm Optimization. PSO is a population-based search method, proposed by Kennedy and Eberhart [13], in which each individual is taken as a particle. Each particle has a position in the space of solutions and fly at a certain speed. The particles can dynamically adjust their position according to the fly experiences from themselves and their populations, that is, three possible directions that a particle can follow: one is its own path, the second is its best position, and the third is the best position of the population. In this way, the particle's personal best position and the global best position can be always updated and kept. Thus, the principles of the algorithm can be described as follow.

In PSO, the position of each particle is a solution of the problem. The fitness of each particle is based on the objective function of the problem. The position (X_i) and the speed (V_i) of particle i can be denoted as $(X_{i1}, X_{i2}, \ldots, X_{iD})$ and $(X_{i1}, X_{i2}, \ldots, X_{iD})$, respectively. At the iteration t, if the best fitness of particle i is p_i^t and the best fitness of the whole population is p_g^t, then, the velocity and the position of the particle i are updated using the following formula:

$$v_i^{t+1} = wv_i^t + c_1 \text{rand1}\left(p_i^t - X_i\right) + c_2 \text{rand2}\left(p_g^t - X_i\right), \quad (3)$$

$$X_i^{t+1} = X_i^t + v_i^{t+1}, \quad (4)$$

where t is the iteration counter; c_1 and c_2 are the acceleration coefficients which determine the effect the experiences from the particle and the population. w is the inertia weight which is used to control the impact of previous histories of velocities on current velocity. The inertia weight is a parameter which affects the trade-off between exploration and exploitation.

3.2. Random Inertia Weight. According to (3), it can be found that inertia weight is one of the most important parameters of PSO algorithm. In order to balance the global search ability and local search ability, the value of the inertia weight should be adjusted to achieve the goal. If the value of the inertia weight w was larger, the particle would have stronger global searching ability. While the value of the inertia weight w was smaller, the local searching ability of the particle would be enhanced. If the value of the inertia weight can obey a certain distribution of random number, it will randomize particle movement according to (3). Hence, two different particles may move to different position in the subsequent iteration even though they have similar position, personal best, and global best. It is common to have high inertia weight at the beginning of PSO iteration to lead to the particles exploring larger solution space, and low weight at the end allows the population following the cognitive and social term to exploit the personal best and global best in the final phase. Based on the above analysis, the proposed random inertia weight ω can be described as the following formula:

$$w = \lambda_{\min} + \left(\lambda_{\max} - \lambda_{\min}\right) \cdot \text{rand}() + \sigma \cdot \text{rand}n() \cdot \frac{t}{T_{\max}}, \quad (5)$$

where $\lambda_{\min}$ is the minimum value of the proposed random inertia weight ω; $\lambda_{\max}$ is the minimum value of the proposed random inertia weight ω; rand() denotes the uniformly distributed random numbers between 0 and 1; σ is deviation, which is used to measure the deviation degree between the random inertia and its average value and can control the direction of the random inertia to expected value. rand$n$() is a random of normal distribution. t is the number of the current iteration, and $T_{\max}$ is the maximum number of the iterations.

3.3. Acceleration Coefficients. From the formula (3), the acceleration coefficients c_1 and c_2 can also be attained which are used to control the acceleration weight for each particle to the best fitness p_i^t and the best fitness p_g^t of the whole population, respectively. Thus, acceleration coefficient with low value allows particles to roam far from target regions before being tugged back, while high values for high value easily result in abrupt movement towards, or past, target regions [13]. If $c_1 = c_2 = 0$, the particles are directed where their velocity indicates, which will lead to the algorithm fail in finding the optimal solution. If $c_1 > 0$ and $c_2 = 0$, all the particles follow the best particle. There is not social information exchange between particles and then the model becomes a cognition-only model. Thus it is difficult for the model to find the optimal solution. In most literature works, $c_1 = c_2$ is selected.

The functions of c_1 and c_2 are changed so that the influence of the two factors can vary during the iterations. Therefore, the value of acceleration coefficient is also optimized to improve the performance of the algorithm. The following formulas for c_1 and c_2 can be used in this paper [17]:

$$c_1 = c_1^{\min} + \frac{c_1^{\max} - c_1^{\min}}{T_{\max}} \times t,$$
$$c_2 = c_2^{\min} + \frac{c_2^{\max} - c_2^{\min}}{T_{\max}} \times t, \quad (6)$$

where, $c_1^{\min}$, $c_1^{\max}$, $c_2^{\min}$, and $c_2^{\max}$ denote the minimum and maximum values of c_1 and c_2, respectively. t is the number of the current iteration and $T_{\max}$ is the maximum number of the iterations.

3.4. Crossover Operation. Crossover operation is a reproduction operation in GA, which is used to exchange genetic information between two parent chromosomes at a predefined probability [10, 18, 19]. In this paper, crossover operation is used to help PSO algorithm to reach further solution space. In the crossover operation, half of the particles with better fitness are selected to enter into the next generation in each iteration. Simultaneously, the positions and speeds

of the former half-particles with better fitness substitute the corresponding vectors of the latter half-particles with worse fitness. However, during the crossover operation, the individual extrema of the latter is unchanged. In the crossover operation, any two of the latter half-particles will perform the crossover operation like genetic algorithm to children. Then half of the latter with better fitness enter into the next generation again. The crossover operation can increase the particle diversity, jump out of the local optimum, and accelerate the convergence speed.

The positions and speed vectors of the children particles are shown as follows:

$$\begin{aligned} \text{child}_1(x) &= p \times \text{parent}_1(x) + (1.0 - p) \times \text{parent}_2(x), \\ \text{child}_2(x) &= p \times \text{parent}_2(x) + (1.0 - p) \times \text{parent}_1(x). \end{aligned} \tag{7}$$

Among them, x is a D-dimensional position vector. $\text{Child}_k(x)$ and $\text{parent}_k(x)$ show the positions of the child particles and the parent particles, respectively. p is a D-dimensional even-distributed random vector, that is, crossover probability which is between 0 and 1.

Crossover operation can help the PSO algorithm to search in a larger space; however, in the late iteration, frequent crossover operation will make the algorithm run with more computing time and hard to be converged. Therefore, an adaptive method to adjust the crossover probability is used in this paper. The adaptive method can be found as follow:

$$P_c = P_{c0} + \sum_{k=1}^{N} \left[\frac{\left| f' - \overline{f} \right|}{\left(f_{\max} - \overline{f} \right)} \right]^{[(t\times 2)/T_{\max}]+1}, \tag{8}$$

where P_{c0} is the initial value of the crossover probability. $f_{\max}$ and $\overline{f}$ represent the best fitness and the average fitness of the population until now. f' is the current best fitness.

4. Case Studies

This paper attempts to use an improved PSO algorithm to solve the automobile spare part warehouse location problem. To examine the feasibility of the improved PSO algorithm (IPSO), some benchmarks for uncapacitated warehouse location from the standard OR library are selected in this paper. Then, the IPSO is used to solve a real-life automobile spare part warehouse location problem. The following will describe the two examples, respectively.

4.1. The Well-Known Uncapacitated Warehouse Location. In order to examine the performance of the proposed IPSO in this paper, the instances from the standard OR library [1] are selected. The information of the test problems can be shown in Table 1. VC++.NET 2003 is used to achieve the IPSO proposed in this paper, operating environment is the Pentium IV 2.93 GHz processor and 3 GB for the Windows platform. Large number of experiments to determine the parameters is set to the following: the number of particle is 50. The maximum number of the iterations is set to 1000. Also $c_1^{\min} = 0.5c_2^{\min} = 0.5c_2^{\max} = 2c_1^{\max} = 2$, $\lambda_{\min} = 0.5\lambda_{\max} = 0.95$, and $P_{c0} = 4$. In order to test the performance of the algorithm, the results of the proposed IPSO algorithm are compared with those of tabu search [1]. Table 2 is the results from these algorithms for solving the warehouse location problems from the standard OR library.

Table 1: The information of the test problems.

Bench	Size	Bench	Size	Bench	Size
Cap71	16 × 50	MO1	100 × 100	MR1	500 × 500
Cap72	16 × 50	MO2	100 × 100	MR2	500 × 500
Cap73	16 × 50	MO3	100 × 100	MR3	500 × 500
Cap74	16 × 50	MO4	100 × 100	MR4	500 × 500
Cap101	25 × 50	MO5	100 × 100	MR5	500 × 500
Cap102	25 × 50	MP1	200 × 200	MS1	1000 × 1000
Cap103	25 × 50	MP2	200 × 200	MS2	1000 × 1000
Cap104	25 × 50	MP3	200 × 200	MS3	1000 × 1000
Cap131	50 × 50	MP4	200 × 200	MS4	1000 × 1000
Cap132	50 × 50	MP5	200 × 200	MS5	1000 × 1000
Cap133	50 × 50	MQ1	300 × 300	MT1	2000 × 2000
Cap134	50 × 50	MQ2	300 × 300	MT2	2000 × 2000
Cap a	100 × 1000	MQ3	300 × 300	MT3	2000 × 2000
Cap b	100 × 1000	MQ4	300 × 300	MT4	2000 × 2000
Cap c	100 × 1000	MQ5	300 × 300	MT5	2000 × 2000

From Table 2, it can be found that most results of IPSO algorithm have been close to the ones of tabu search, which indicate that the proposed IPSO algorithm is suitable for solving a warehouse location problem.

4.2. The Automobile Spare Part Warehouse Location Problem. The PSO algorithm is examined by the warehouse location problems from the standard OR library, which indicates that IPSO algorithm is suitable for solving the warehouse location problem. Then a real-life automobile spare part warehouse location problem needs to be solved by the PSO algorithm. In the real-life warehouse location problem, there is one automobile company that wants to large its business. Thus, the company wants to build some warehouses in a chosen area. Then the automobile spare parts will be sent from the company to the warehouses and from the warehouses to customers (e.g., repair station). There is one warehouse in the chosen area and three alternative points for selection. In the chosen area, there are four potential points for selection and ten customers need to be served. If the horizontal and vertical coordinates of the factory are assumed as (0,0), then, the information of the problem is shown in Tables 3, 4, and 5.

Then, the improved PSO continues calculating the automobile spare par warehouse location problem ten times. However, in the real-life seafood product delivery routing problems, the distance between two points is based on the length of the routes. The results are shown in Figure 2. It can be found that the optimization results are stable and the difference between the optimum and the worst plan is less than 2.1%. Furthermore, the computing time is from 320 to 410 seconds, which is acceptable for the larger real-life problem. Therefore, the proposed PSO has an excellent convergence performance to solve the automobile spare part

Table 2: Computational results using IPSO algorithm and tabu search.

Bench	Tabu search	IPSO	Bench	Tabu search	IPSO
Cap71	932 615.75	932 615.75	MP4	2633.56	2633.56
Cap72	977 799.40	977 799.40	MP5	2290.16	2290.16
Cap73	1 010 641.45	1 010 641.45	MQ1	3591.27	3591.27
Cap74	1 034 976.97	1 034 976.98	MQ2	3543.66	3543.66
Cap101	796 648.44	796 648.44	MQ3	3476.81	3476.82
Cap102	854 704.20	854 704.20	MQ4	3742.47	3742.47
Cap103	893 782.11	893 782.11	MQ5	3751.33	3751.33
Cap104	928 941.75	928 941.75	MR1	2349.86	2349.86
Cap131	793 439.56	793 439.56	MR2	2344.76	2344.76
Cap132	851 495.32	851 495.33	MR3	2183.24	2183.24
Cap133	893 076.71	893 076.71	MR4	2433.11	2433.11
Cap134	928 941.75	928 941.75	MR5	2344.35	2344.35
Cap a	17 156 454.4	17 156 454.48	MS1	4378.63	4378.63
Cap b	12 979 071.5	12 979 071.58	MS2	4658.35	4658.35
Cap c	11 505 594.3	11 505 594.33	MS3	4659.16	4659.16
MO1	1156.91	1156.91	MS4	4536.00	4536.01
MO2	1227.67	1227.67	MS5	4888.91	4888.91
MO3	1286.37	1286.37	MT1	9176.51	9176.51
MO4	1177.88	1177.88	MT2	9618.85	9618.85
MO5	1147.60	1147.61	MT3	8781.11	8781.11
MP1	2460.10	2460.10	MT4	9225.49	9225.49
MP2	2419.32	2419.32	MT5	9540.67	9540.67
MP3	2498.15	2498.15			

Table 3: The information of warehouse.

Item	$W1$	$W2$	$W3$	$W4$
Horizontal coordinate	23	88	72	45
Vertical coordinate	74	46	90	16
Land price	1.95	1.8	1.35	2.25

Table 4: The transportation cost from warehouses to customers and factories (Yuan/T).

Item	$W1$	$W2$	$W3$	$W4$
1	45	37.5	28.5	30
2	39	32.25	49.5	27
3	38.25	40.5	30	34.5
4	29.25	30.75	34.5	32.25
5	46.5	40.5	38.25	31.5
6	33.6	35.4	39.6	39
7	42	24	52	24.5
8	28	30	30	36
9	35	16	32	35
10	36	18	38	30
Factory	33.6	300	39.6	240

warehouse location problem. The optimized results of the problem can be seen in Table 6.

Table 5: The information of customers.

Customers	Horizontal	Vertical	Demand
1	25	80	3
2	30	23	0.8
3	70	60	0.75
4	92	51	3
5	42	64	1.05
6	87	45	2.1
7	39	7	1.5
8	28	71	3
9	55	20	4.5
10	14	56	1.5

Table 6: The optimized results of the automobile spare part warehouse location problem.

Item	$W1$	$W2$	$W3$	$W4$
The served customers	(1,5,8,10)	(3,4,6)	()	(2,7,9)
The treatment capability	5.2	3.9	0.0	4.6

From Table 6, it can be attained that the potential warehouse 3 is not suitable for warehouse and the potential warehouses 1, 2, and 4 are selected for warehouse location.

5. Conclusions

The automobile spare part warehouse location problem is the warehouse selection in potential depots in order to meet the demand of the customers and keep the automobile spare part factory competitiveness in a chosen area. Thus, the automobile spare part warehouse location problem is attempted to minimize the total cost which includes the transportation cost (from factories to warehouse and from warehouse to customers) and the fixed cost while meeting the constraints. Since the automobile spare part warehouse location problem is difficult to be solved. PSO is selected in this paper and some improved strategies are used to improve the performance of PSO. The computational results of some benchmark instances for uncapacitated warehouse location problem from the standard OR library suggest that the improved PSO is effective to solve the warehouse location problem. The results of the automobile spare part warehouse location problem can also indicate that the improved PSO is an effective method for the automobile spare part warehouse location problem.

The main contribution of this paper is to test the feasibility of PSO for the automobile spare part warehouse location problem. Our future research work will be on the models with stochastic demand, model and solve the model by other convenient methods, and possibly have added a capacity constraint on the multiple central warehouses.

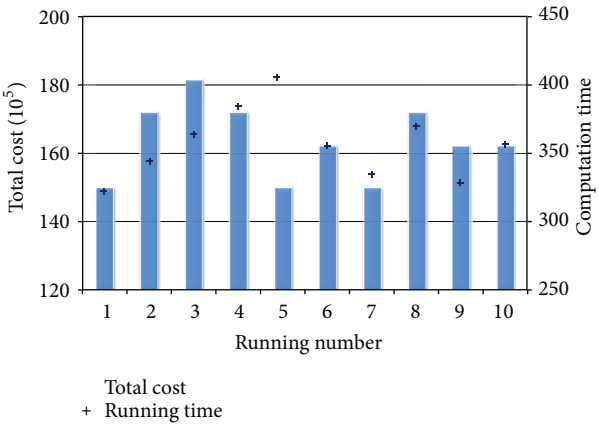

Figure 2: Computing results of the improved PSO after running 10 times.

Acknowledgments

This work was supported by the National Science Foundation for Postdoctoral Scientists of China 2013M530924 and the National Natural Science Foundation of China 51208079 and 11272075.

References

[1] L. Michel and P. van Hentenryck, "A simple tabu search for warehouse location," *European Journal of Operational Research*, vol. 157, no. 3, pp. 576–591, 2004.

[2] B. M. Khumawala, "An efficient heuristic procedure for the capacitated warehouse location problem," *Naval Research Logistics Quarterly*, vol. 21, no. 4, pp. 609–623, 1974.

[3] B. M. Baker, "A partial dual algorithm for the capacitated warehouse location problem," *European Journal of Operational Research*, vol. 23, no. 1, pp. 48–56, 1986.

[4] L. Ozsen, C. R. Coullard, and M. S. Daskin, "Capacitated warehouse location model with risk pooling," *Naval Research Logistics*, vol. 55, no. 4, pp. 295–312, 2008.

[5] G. Chen, K. Govindan, and Z. Yang, "Managing truck arrivals with time windows to alleviate gate congestion at container terminals," *International Journal of Production Economics*, vol. 141, no. 1, pp. 179–188, 2012.

[6] G. Chen and Z. Yang, "Optimizing time windows for managing export container arrivals at Chinese container terminals," *Maritime Economics & Logistics*, vol. 12, no. 1, pp. 111–126, 2010.

[7] B. Y. Chen, W. H. K. Lam, A. Sumalee, and H. Shao, "An efficient solution algorithm for solving multi-class reliability-based traffic assignment problem," *Mathematical and Computer Modelling*, vol. 54, no. 5-6, pp. 1428–1439, 2011.

[8] B. Y. Chen, W. H. K. Lam, A. Sumalee, Q. Q. Li, H. Shao, and Z. X. Fang, "Finding reliable shortest paths in road networks under uncertainty," *Networks & Spatial Economics*, vol. 13, no. 2, pp. 123–148, 2013.

[9] B.-Z. Yao, C.-Y. Yang, J.-B. Yao, and J. Sun, "Tunnel surrounding rock displacement prediction using support vector machine," *International Journal of Computational Intelligence Systems*, vol. 3, no. 6, pp. 843–852, 2010.

[10] B. Yu and Z. Z. Yang, "An ant colony optimization model: the period vehicle routing problem with time windows," *Transportation Research E*, vol. 47, no. 2, pp. 166–181, 2011.

[11] B. Yu, Z.-Z. Yang, and B. Yao, "An improved ant colony optimization for vehicle routing problem," *European Journal of Operational Research*, vol. 196, no. 1, pp. 171–176, 2009.

[12] B. Yu, Z.-Z. Yang, P.-H. Jin, S.-H. Wu, and B.-Z. Yao, "Transit route network design-maximizing direct and transfer demand density," *Transportation Research C*, vol. 22, pp. 58–75, 2012.

[13] J. Kennedy and R. Eberhart, "Particle swarm optimization," in *Proceedings of the IEEE International Conference on Neural Networks*, pp. 1942–1948, Perth, Aystralia, December 1995.

[14] A. W. Mohemmed, N. C. Sahoo, and T. K. Geok, "Solving shortest path problem using particle swarm optimization," *Applied Soft Computing Journal*, vol. 8, no. 4, pp. 1643–1653, 2008.

[15] T.-L. Lin, S.-J. Horng, T.-W. Kao et al., "An efficient job-shop scheduling algorithm based on particle swarm optimization," *Expert Systems with Applications*, vol. 37, no. 3, pp. 2629–2636, 2010.

[16] T. J. Ai and V. Kachitvichyanukul, "A particle swarm optimization for the vehicle routing problem with simultaneous pickup and delivery," *Computers & Operations Research*, vol. 36, no. 5, pp. 1693–1702, 2009.

[17] Y. Marinakis, G. R. Iordanidou, and M. Marinaki, "Particle swarm optimization for the vehicle routing problem with stochastic demands," *Applied Soft Computing*, vol. 13, no. 4, pp. 1693–1704, 2013.

[18] B. Yu, Z. Yang, and C. Cheng, "Optimizing the distribution of shopping centers with parallel genetic algorithm," *Engineering Applications of Artificial Intelligence*, vol. 20, no. 2, pp. 215–223, 2007.

[19] B. Yu, Z. Yang, and C. Cheng, "Optimizing the distribution of shopping centers with parallel genetic algorithm," *Engineering Applications of Artificial Intelligence*, vol. 20, no. 2, pp. 215–223, 2007.

Hindawi Publishing Corporation
Mathematical Problems in Engineering
Volume 2013, Article ID 361031, 7 pages
http://dx.doi.org/10.1155/2013/361031

Research Article

Multiobjective Gate Assignment Based on Passenger Walking Distance and Fairness

Yu Jiang, Linyan Zeng, and Yuxiao Luo

Nanjing University of Aeronautics and Astronautics, College of Civil Aviation, Nanjing 210016, China

Correspondence should be addressed to Linyan Zeng; znlnyn@nuaa.edu.cn

Received 29 August 2013; Accepted 21 October 2013

Academic Editor: Baozhen Yao

Passenger walking distance is an important index of the airport service quality. How to shorten the walking distance and balance the airlines' service quality is the focus of much research on airport gate assignment problems. According to the problems of airport passenger service quality, an optimization gate assignment model is established. The gate assignment model is based on minimizing the total walking distance of all passengers and balancing the average walking distance of passengers among different airlines. Lingo is used in the simulation of a large airport gate assignment. Test results show that the optimization model can reduce the average walking distance of passenger effectively, improve the number of flights assigned to gate, balance airline service quality, and enhance the overall service level of airports and airlines. The model provides reference for the airport gate preassignment.

1. Introduction

Airport gate is a main component of airport resource. Rational and efficient gate assignment is an important way to improve airport operation efficiency and passenger service level. Airport gate is divided into contact gate (a gate with an aerobridge) and remote stand (on the apron). The type and layout lead to different distance from gate to security check, baggage hall, and transit counters. The distance between different areas has a direct impact on passenger activities in the terminal. How to optimize the gate assignment from the perspective of passengers becomes a hot research area at home and abroad.

At present, the main research findings of gate assignment from the perspective of passengers took the shortest passenger walking distance and the minimum embarking and transit time as objective function to optimize gate assignment; for example, Braaksma, [1], Babic et al. [2], Mangoubi and Mathaisel [3], Yan and Huo [4], Bolat [5], Yan et al. [6], and Cheng's [7] research findings showed that reasonable gate assignment could reduce passenger walking distance appropriately. In 1998, Haghani and Chen [8] took the number of transfer passengers of different flights and the distance between different gates into account comprehensively while minimizing passenger walking distance in a terminal. Assuming that all passengers were converted into transit passengers and had taken the shortest transit time as the objective function, Xu and Bailey [9] established quadratic mixed 0-1 integer programming model of gate assignment through virtual assumption. In further research, some scholars began to consider minimizing the number of flights, which are assigned to remote stands, and the passenger walking distance/time, such as Pintea et al. [10], Ding et al. [11, 12], and so on; some scholars considered minimizing walking distance together with delay costs, like Zhu et al. [13], balancing usage of airport gates, like Wei and Liu [14, 15], passenger waiting time, like Hu and Paolo [16], and fuel consumption of aircraft taxiing, like Maharjan and Matis [17], respectively.

Optimization gate assignment from the perspective of passengers can reduce passenger walking distance and improve passenger service levels to a certain extent. However, there are some deficiencies in research findings. Firstly, in some large hub airporsts, the proportion of transit passengers is large and the actual walking distance of transit passengers is not equal to the actual distance between two gates. The walking distance is related with the layout of transit counters and transit halls. In the research, ignoring transit passengers can cause the model to be inaccurate. Secondly, civil airport service quality issued by the Civil Aviation Administration

in 2006 requires that the number of passengers embarking/disembarking through aerobridges should be above 80%. But in most current research, the proportion of passengers is not taken into account. Thirdly, most current researches do not consider the balance of passenger walking distance between different airlines, which can lead to reducing the passenger service level and can be unfair for some airlines, especially for small airlines.

Optimizing gate assignment can improve passengers' satisfaction and balance the service quality of each airline. In this research, we propose a new model which is different from previous researches; the gates are categorized into contact gate and remote stand in the mode, the proportion of passenger embarking/disembarking through aerobridges is taken into account, and the model considers the fairness between airlines besides reducing the overall passengers' walking distance.

The paper is organized as follows. The gate assignment model is detailed in Section 2. Section 3 briefs the simulation software and analyzes the results under different conditions in detail. Some conclusions are drawn in the last section.

2. Gate Assignment Model

2.1. Description of Gate Assignment. Gate assignment is to arrange a reasonable gate for each arrival-departure flight timely according to the flight plan, which is submitted by every airline. Safety operation of aircraft and gate is the premise of gate assignment.

Passenger walking distance in a large airport is composed of three parts: arrival passenger walking distance, departure passenger walking distance, and transit passenger walking distance. The arrival passenger walking distance refers to the distance from gate to baggage hall; the departure passenger walking distance refers to the distance from security check to gate; the transit passenger walking distance refers to the distance from gate to transit counter and then to the next flight gate. The arrival-departure transit passengers are known collectively as transit passengers in the paper. The walking distance of transit counter passengers includes the arrival passengers' distance from gate to transit counter and the departure passengers' distance from transit counter to gate.

Minimizing and balancing the walking distance of all passengers from different airlines are goals to model gate assignment in the paper. Then Lingo software is adopted to verify the effectiveness of a model in order to improve the service level of airport and airline.

2.2. Model Assumptions

(1) Gate assignment is a continuous operation course. In order to reduce the scale of the problem, the paper selects some time intervals for gate assignment.

(2) The capacity of gates can meet the demand of all flights in the research time; it means that every flight can be assigned to a gate.

(3) The arrival-departure flight performed by the same aircraft is assigned to the same gate and it used the same flight number.

(4) All information, such as flight plan, aircraft basic information, the usage status of gates, and so on, is known in research time.

(5) Only the gate assignment of domestic flights is considered in the paper.

2.3. Symbol Definition

F: flight set, $F = \{f_1, f_2, \ldots, f_m\}$, m is the total number of flights in research period. f_i $(1 \le i \le m)$ is flight number which is ordered by the arrival time of flights; the bigger i means the later flight f_i arrives at the airport.

c_{f_i}: size of the aircraft which executes flight f_i. The bigger c_{f_i} is, the larger aircraft is. The smaller c_{f_i} is, the smaller aircraft is.

L: airline set, $L = \{l_1, l_2, \ldots, l_q\}$, q is the total number of airlines in research period. l_a $(1 \le a \le q)$ is airline code.

F_{l_a}: the flights set of airline l_a.

G: gate set, $G = \{g_1, g_2, \ldots, g_n\}$, n is the total number of gates. g_k $(1 \le k \le n)$ is gate code.

Assuming that the number of gates is x, if $k \le x$, it means that g_k gate is a contact gate; otherwise, it is a remote stand.

c_{g_k}: size of gate g_k; the bigger c_{g_k} means the larger aircraft can be parked on the gate; the smaller c_{g_k} means the smaller aircraft can be parked.

a_{f_i}: arrival time of flight f_i; the unit is minute.

d_{f_i}: departure time of flight f_i; the unit is minute.

T: minimum time interval of two flights which are assigned to the same gate; the unit is minute.

$S^a_{g_k}$: distance of arrival passenger walking from gate g_k to baggage hall.

$S^d_{g_k}$: distance of departure passenger walking from security checking to gate g_k.

$S^m_{g_k}$: distance between gate g_k and transit counter.

$N^a_{f_i}$: number of arrival passengers of flight f_i.

$N^d_{f_i}$: number of departure passengers of flight f_i.

$N^m_{f_i}$: number of transit passengers of flight f_i.

Consider

$$y_{f_i,g_k} = \begin{cases} 1, & \text{if flight } f_i \text{ is assigned to gate } g_k, \\ 0, & \text{otherwise,} \end{cases}$$

$$z_{f_i,f_j} = \begin{cases} 1, & \text{if flight } f_i \text{ and } f_j \text{ are assigned} \\ & \text{to the same gate,} \\ 0, & \text{otherwise.} \end{cases} \quad (1)$$

2.4. Modeling. Minimizing the total walking distance of all passengers in research period is one of the goals in the paper.

Consider

$$\min Z_1 = \sum_{f_i \in F} \sum_{g_k \in G} y_{f_i,g_k} \left(N_{f_i}^a S_{g_k}^a + N_{f_i}^d S_{g_k}^d + N_{f_i}^m S_{g_k}^m \right), \quad (2)$$

where $N_{f_i}^a S_{g_k}^a$ represents the total walking distance of arrival passengers of flight f_i walking from gate g_k to baggage hall; $N_{f_i}^d S_{g_k}^d$ represents the total walking distance of departure passengers of flight f_i walking from security checking point to gate g_k; $N_{f_i}^m S_{g_k}^m$ represents the total walking distance of transit passengers of flight f_i.

According to the objective function (2), gate assignment may result in longer walking distance of some airlines' passengers while some others are shorter. The objective function (2) can lead to unbalanced passenger walking distance among airlines and reduce the airlines' service quality. Therefore, in order to improve the service quality of the entire airport, it is necessary to balance passenger walking distance of each airline from the viewpoint of airline fairness.

Consider

$$\min Z_2 = \max_{l_a \in L} Z_{S_{l_a}}, \quad (3)$$

$$\overline{S_{l_a}} = \frac{\sum_{f_i \in F_{l_a}} \sum_{g_k \in G} y_{f_i,g_k} \left(N_{f_i}^a S_{g_k}^a + N_{f_i}^d S_{g_k}^d + N_{f_i}^m S_{g_k}^m \right)}{\sum_{f_i \in F_{l_a}} \left(N_{f_i}^a + N_{f_i}^d + N_{f_i}^m \right)}, \quad (4)$$

$$\overline{S} = \frac{\sum_{f_i \in F} \sum_{g_k \in G} y_{f_i,g_k} \left(N_{f_i}^a S_{g_k}^a + N_{f_i}^d S_{g_k}^d + N_{f_i}^m S_{g_k}^m \right)}{\sum_{f_i \in F} \left(N_{f_i}^a + N_{f_i}^d + N_{f_i}^m \right)}, \quad (5)$$

$$Z_{S_{l_a}} = \frac{\left| \overline{S_{l_a}} - \overline{S} \right|}{\overline{S}}, \quad l_a \in L. \quad (6)$$

The objective function (3) is to minimize the ratio between the difference and the average walking distance of all passengers, where $\overline{S_{l_a}}$ represents the average passenger walking distance of airline l_a in research period; $\overline{S}$ represents the average walking distance of all passengers in research period; $Z_{S_{l_a}}$ represents the ratio of the difference and walking distance of all passengers, where the difference is the average passenger walking distance of airline l_a and all passengers.

Subject to

$$\frac{\sum_{f_i \in F} \sum_{k \le x, g_k \in G} y_{f_i,g_k} \left(N_{f_i}^a + N_{f_i}^d + N_{f_i}^m \right)}{\sum_{f_i \in F} \left(N_{f_i}^a + N_{f_i}^d + N_{f_i}^m \right)} \ge 0.8, \quad (7)$$

$$\sum_{g_k \in G} y_{f_i,g_k} = 1, \quad \forall f_i \in F, \quad (8)$$

$$y_{f_i,g_k} \in \{0, 1\}, \quad (9)$$

$$z_{f_i,f_j} = \sum_{f_i \in F} \sum_{j>i, f_j \in F} \sum_{g_k \in G} \left(y_{f_i,g_k} \times y_{f_j,g_k} \right), \quad (10)$$

$$a_{f_j} - d_{f_i} + \left(1 - z_{f_i,f_j}\right) M \ge T, \quad i < j, \quad (11)$$

$$c_{f_i} \le c_{g_k} + \left(1 - y_{f_i,g_k}\right) M, \quad (12)$$

$$i, j, a, q, k, x \in Z^+. \quad (13)$$

Equation (7) is to restrain the proportion of passengers who are required to embark/disembark aircraft through aerobridges. Civil airport service quality, which was issued by the Civil Aviation Administration in 2006, requires that the number of passengers that embark/disembark through aerobridges should be above 80%.

Equations (8) and (9) indicate that each flight has one and only one gate to be assigned. That is, for flight f_i, in the gate set G, there is only one gate g_k to make $y_{f_i,g_k} = 1$.

Equation (10) is used to judge whether the two flights are assigned to the same gate. When $y_{f_i,g_k} \times y_{f_j,g_k} = 1$, $z_{f_i,f_j} = 1$, it indicates that the later arrival flight f_j and the front flight f_i are arranged in the same gate; otherwise, $z_{f_i,f_j} = 0$.

Equation (11) requires that the two flights which were assigned to the same gate should meet certain safety interval. According to (10) when $z_{f_i,f_j} = 1$, it needs to meet $a_{f_j} - d_{f_i} \ge T$; the front and later flights should meet the minimum safety interval. When $z_{f_i,f_j} = 0$, the two flights are not assigned in the same gate; it need not meet safety interval. Therefore, value M, which is big enough, is introduced to ensure the inequality holds.

Equation (12) means that the gate type should match the aircraft type. When $y_{f_i,g_k} = 1$, flight f_i is assigned to gate g_k; it should meet $c_{f_i} \le c_{g_k}$. When $y_{f_i,g_k} = 0$, there is no relationship between flight f_i and gate g_k.

Equation (13) is a positive integer constraint.

3. Simulations

The decision variables in the gate assignment model are 0 and 1, belonging to 0-1 planning of integer programming problem. Due to nonlinear constraints involved in the model, the model is called integer nonlinear programming (INLP). The paper uses Lingo software to simulate and verify the model. The Global (global optimization algorithm) and Multistart (more initial point algorithm) built-in Lingo are specifically used to solve nonlinear programming (Scharge [18]). In addition, Lingo can be connected with EXCEL, database, and other software conveniently; it also can easily input and output the simulation results. Another important superiority of Lingo is convenient to describe large-scale optimization problems concisely and intuitionisticly. Therefore, the paper uses Lingo software to simulate and verify the effectiveness of the model.

The simulation data of domestic flights to be assigned in a typical time interval (8:00–11:00) in a large airport is shown in Tables 1 and 2. The minimum time interval $T = 15$ minutes; this is the time when the two flights are to be assigned to the same gate continuously. The constant value $M = 300$.

Table 1: Domestic flight to be assigned from 8:00 to 11:00.

Flight no.	Type	Airline	Arr. time	Dep. time	Number of arr. passengers	Number of dep. passengers	Number of transit passengers	Total passengers
F101	M	A1	08:00	08:55	35	48	174	257
F102	M	A2	08:15	09:20	129	142	36	307
F103	L	A4	08:30	09:50	132	136	169	437
F104	M	A3	08:45	09:55	97	101	86	284
F105	M	A1	09:00	10:10	106	89	128	323
F106	L	A2	09:10	10:30	206	189	64	459
F107	M	A1	09:15	10:20	72	96	72	240
F108	S	A2	09:30	10:15	41	46	98	185
F109	M	A3	09:40	10:40	128	114	29	271
F110	M	A4	10:00	11:30	154	146	65	365
F111	S	A3	10:05	10:55	49	63	32	144
F112	M	A2	10:20	11:20	143	136	40	319
F113	M	A3	10:30	11:25	98	92	108	298
F114	L	A2	10:35	11:55	246	238	63	547
F115	L	A4	10:55	12:00	182	168	57	407
F116	M	A2	11:00	11:50	118	115	20	253

Note: L, M, and S represent large, middle, and small aircrafts, respectively. A1~A4 represent different airlines.

Table 2: Data of available gates.

Gate no.	Gate size	Distance to the baggage hall (unit: m)	Distance to the security check points (unit: m)	Distance to the transit counter (unit: m)	Average distance (unit: m)	Contact gate or remote stand
G001	M	150	245	215	203.3	C
G002	L	240	270	245	251.7	C
G003	M	220	260	230	236.7	C
G004	M	190	235	210	211.7	C
G005	L	135	170	115	140.0	C
G006	S	530	585	440	518.3	C
G007	M	520	580	425	508.3	C
G008	L	400	220	230	283.3	C
G009	L	920	960	975	951.7	R
G010	L	1000	1100	1050	1050.0	R

Note: L, M, and S represent large, middle, and small gates, respectively.

The paper uses Lingo 11.0 and selects Global Solver (Global optimization solve) and Global set strategy (Branching: Rel Violation; Box Selection: Worst Bound; Reformulation: High) to verify the effectiveness of models.

The paper uses Lingo to simulate the results of the random assignment, the objective function (2) (Z_1 optimal) and the objective function (3) (Z_2 optimal), respectively. The simulation result is shown in Table 3, where Z_1 and Z_2 represent the value of the objective function (2) and the objective function (3), respectively. The smaller Z_1 is, the shorter passenger walking distance is. The smaller Z_2 is, the fairer between airlines is. Q represents the proportion of passengers embarking/disembarking through aerobridge (referring to passing rate); the larger Q is, the more passengers embarking/disembarking through aerobridge are. S represents the overall average passenger walking distance. S_{A1}–S_{A4} represents the average passenger walking distance of four airlines, respectively. $S_{\max}$ represents the maximum difference of average passenger walking distance between airlines. (the unit of Z_1, S, S_{A1}–S_{A4}, and $S_{\max}$ is meters.)

With Table 3 and Figures 1 and 2, we can draw the conclusions.

(1) When Z_1 is optimal, the value of Z_1 is a minimum. It means that the total passenger walking distance is the shortest. The maximum value of Q is 1, which means the passing rate is 100%. But the difference of average passenger walking distance between four airlines is

Table 3: Comparison of simulation results between random assignment, optimization Z_1, and optimization Z_2.

Results	Z_1	Z_2	Q	S	S_{A1}	S_{A2}	S_{A3}	S_{A4}	$S_{\max}$
Random assignment	2089750	0.238	0.831	410.1	351.1	351.9	461.2	507.6	156.5
Z_1 optimal	1244430	0.299	1.000	244.2	206.9	243.6	317.3	210.2	110.4
Z_2 optimal	2165555	0.003	0.800	425.0	423.8	424.4	426.1	425.7	2.3

comparatively large and the value of Z_2 (0.299) is also the largest; it means that the ration between the average and total passenger walking distance of airlines is large; the largest ration is approaching 30%.

(2) When Z_2 is optimal, the value of Z_2 is approximately zero and the average passenger walking distance of four airlines (Figure 2) is basically flat. That is, the gate assignment is the fairest. But the average passenger distance is 180.8 meters higher than the value of optimal Z_1. and the passing rate is only 80% (Q = 0.800), which is the lowest in the three simulation groups.

(3) The three values of Z_1, Z_2, and Q in random gate assignment are relatively concentrated. But compared with the value of optimal Z_1, the value of Z_1 in random gate assignment is high and the value of Q is low. Compared with the value of optimal Z_2, the value of Z_2 in random gate assignment is high. And the difference of average passenger walking distance between airlines is the largest, which is 156.5 meters. The gate assignment schedule is much unfair to airline A_4 because the average walking distance is larger than other airlines distinctly.

From the above simulation results, the three groups all have shortcomings. To find a set of ideal solution, the paper takes the objective function (2) as primary objective and transfers the objective function (3) into constraint. Assuming $Z_2 \leq 0.10$ and $Z_2 \leq 0.20$, the simulation results can be acquired (Table 4).

According to Table 4 and Figures 3 and 4, when the objective function (2) is the objective and $Z_2 \leq 0.10$, all the indexes of simulation are in the state of ideal according to the five group simulation results. Compared with the random gate assignment, the simulation result of $Z_2 \leq 0.10$ is as follows. (1) The total walking distance of passengers is 1,368,320 meters and decreases by 34.5%; (2) the passing rate is 96.4% and improves by 13.3%; (3) the total average passenger walking distance is 268.5 meters and decreases by 141.6 meters; (4) the simulation results show that it is relatively fair among airlines. The largest difference of average walking distance among airlines is only 20.3 meters; it is more inferior to the random gate assignment.

Flight Gantt chart of the random gate assignment and the situation of $Z_2 \leq 0.10$ are shown in Figures 5 and 6. Distribution of passengers and the average distance of gate are shown in Figure 7.

It is convenient for passengers to embark/disembark the aircraft through aerobridge because the distance is close and passengers will not be influenced by weather. The average distance from gate to baggage hall, security check, and transit

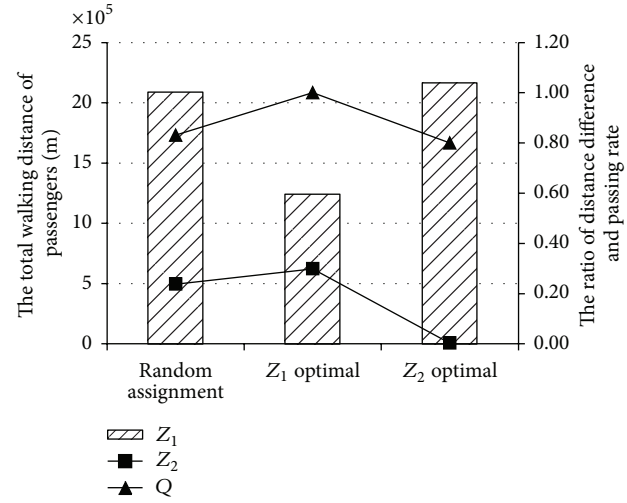

Figure 1: Comparison of Z_1, Z_2, and Q.

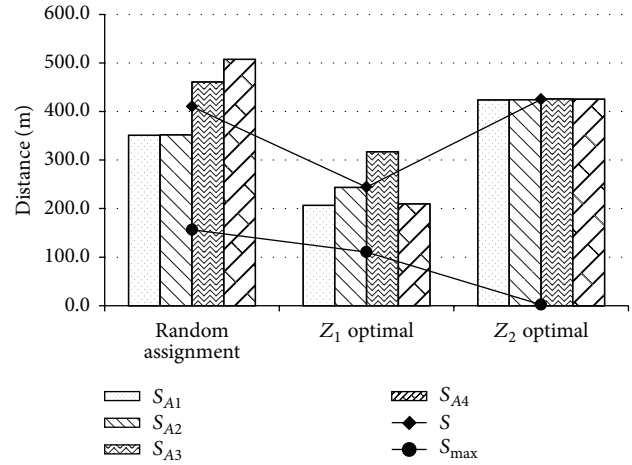

Figure 2: Comparison of S and S_{A1}–S_{A4}.

counter is shorter; the total walking distance of passengers assigned to the gate is shorter. Thus the passenger will feel comfortable. We can draw the conclusions from Figure 5 to Figure 7: (1) the number of flights assigned to the remote stands (G009, G010) is only one, and this gate assignment schedule can improve the passing rate; (2) two flights are reduced to be assigned to gate which is near the remote stand; one flight is added to be assigned to G001, G003, G004, and G008 gate, respectively; (3) the gate, where the average walking distance is short, is assigned efficiently. Making

Table 4: Comparison of simulation results under five different conditions.

Results	Z_1	Z_2	Q	S	S_{A1}	S_{A2}	S_{A3}	S_{A4}	$S_{\max}$
Random assignment	2089750	0.238	0.831	410.1	351.1	351.9	461.2	507.6	156.5
Z_1 optimal	1244430	0.299	1.000	244.2	206.9	243.6	317.3	210.2	110.4
Z_2 optimal	2165555	0.003	0.800	425.0	423.8	424.4	426.1	425.7	2.3
$Z_2 \le 0.10$	1368320	0.041	0.964	268.5	278.1	267.7	275.6	257.6	20.5
$Z_2 \le 0.20$	1272690	0.199	1.000	249.7	204.0	252.0	222.5	299.3	95.3

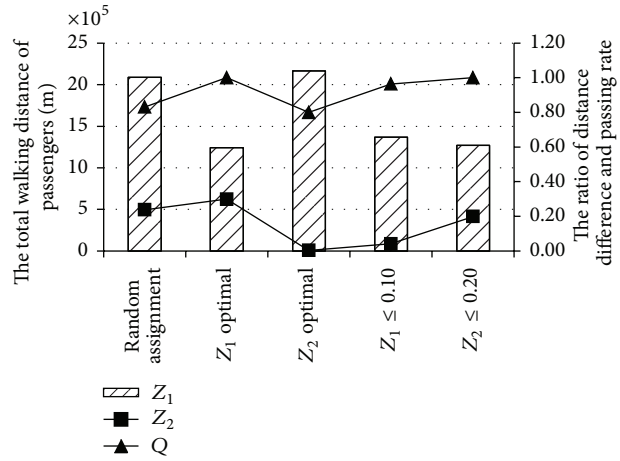

Figure 3: Comparison value of Z_1, Z_2, and Q in five groups.

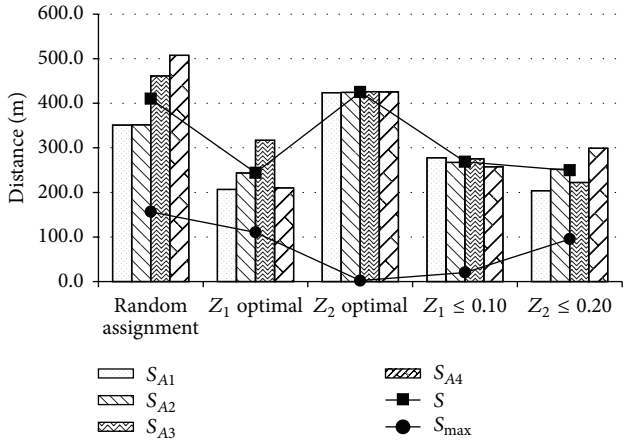

Figure 4: Comparison value of S, S_{A1}–S_{A4}, and $S_{\max}$ in five groups.

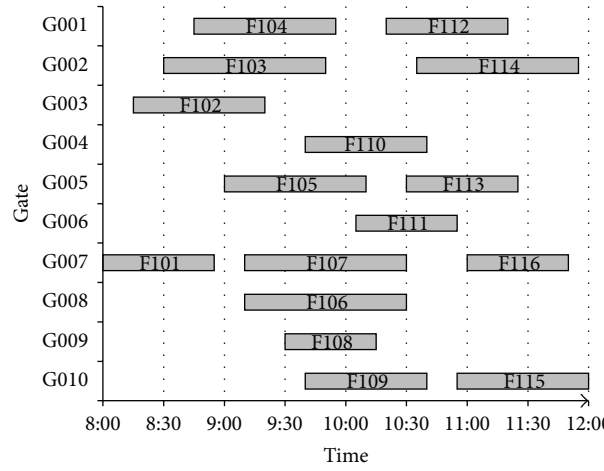

Figure 5: The flight Gantt chart of random gate assignment.

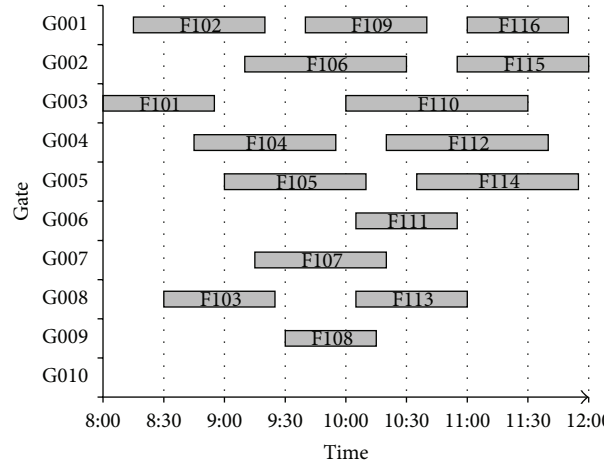

Figure 6: The flight Gantt chart of $Z_2 \le 0.10$.

effective use of a gate can reduce the walking distance and improve the service level of passengers.

In summary, the simulation optimization results can not only reduce the average passenger walking distance effectively and improve passing rate, but also reduce the difference of average walking distance of passengers among airlines and enhance the overall passenger service quality of airports and airlines.

4. Conclusions

The paper presents a new idea for the airport gate assignment problem. Unlike the previous researches, it takes the restraint of passenger passing rate and airlines' fairness into account under the premise of airport safety operation. Combining with the objective of minimizing the whole passengers' walking distances, the paper builds a multiobjective optimization model of gate assignment. Lingo software is used to verify the effectiveness of model by simulating a large airport gate

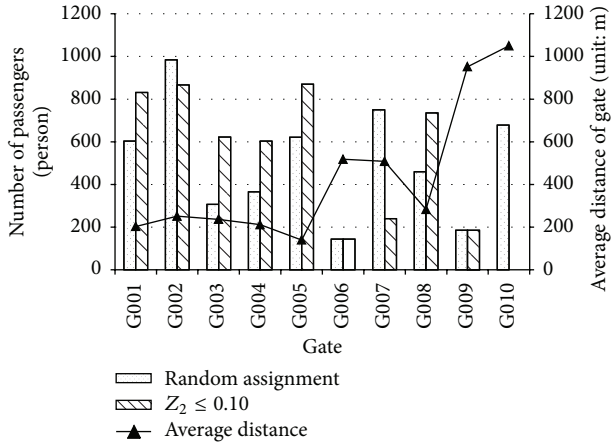

Figure 7: Distribution of passengers and the average distance of gate.

assignment. According to the test results, we can draw some conclusions.

(1) The assignment can ensure the passengers passing rate by setting (7).

(2) The two objectives are interactional between each other. And decision makers can get a set of suitable results by adjusting the value range of the second objective.

(3) Compared to the random assignment, this model can reduce the whole passengers' walking distances and improve the fairness between airlines at the same time.

(4) The research scope of the paper is only part of the domestic flights. How to combine with international flights and effective resource schedule should be further researched.

Acknowledgments

This work was supported by the National Natural Science Foundation of China and Civil Aviation Administration of China (no. U1333117), China Postdoctoral Science Foundation (no. 2012M511275), and the Fundamental Research Fund for the Central Universities (nos. NS2013067, NN2012019, and NS2012115).

References

[1] J. P. Braaksma, "Reducing walking distance at existing airports," *Airport Forum*, no. 7, pp. 135–142, 1977.

[2] O. Babic, D. Teodorovic, and V. Tosic, "Aircraft stand assignment to minimize walking," *Journal of Transportation Engineering*, vol. 110, no. 1, pp. 55–66, 1984.

[3] R. S. Mangoubi and D. F. X. Mathaisel, "Optimizing gate assignments at airport terminals," *Transportation Science*, vol. 19, no. 2, pp. 173–188, 1985.

[4] S. Yan and C.-M. Huo, "Optimization of multiple objective gate assignments," *Transportation Research Part A*, vol. 35, no. 5, pp. 413–432, 2001.

[5] A. Bolat, "Procedures for providing robust gate assignments for arriving aircrafts," *European Journal of Operational Research*, vol. 120, no. 1, pp. 63–80, 2000.

[6] S. Yan, C.-Y. Shieh, and M. Chen, "A simulation framework for evaluating airport gate assignments," *Transportation Research Part A*, vol. 36, no. 10, pp. 885–898, 2002.

[7] Y. Cheng, "Solving push-out conflicts in apron taxiways of airports by a network-based simulation," *Computers and Industrial Engineering*, vol. 34, no. 2, pp. 351–369, 1998.

[8] A. Haghani and M.-C. Chen, "Optimizing gate assignments at airport terminals," *Transportation Research Part A*, vol. 32A, no. 6, pp. 437–454, 1998.

[9] J. Xu and G. Bailey, "The airport gate assignment problem: mathematical model and a tabu search algorithm," in *Proceedings of the 34th Annual Hawaii International Conference on System Sciences*, pp. 1–10, January 2001.

[10] C.-M. Pintea, P. C. Pop, C. Chira, and D. Dumitrescu, "A hybrid ant-based system for gate assignment problem," in *Proceedings of the 3rd International Workshop on Hybrid Artificial Intelligence Systems*, vol. 5271 of *Lecture Notes in Computer Science*, pp. 273–280, Burgos, Spain, 2008.

[11] H. Ding, A. Lim, B. Rodrigues, and Y. Zhu, "Aircraft and gate scheduling optimization at airports," in *Proceedings of the 37th Hawaii International Conference on System Sciences*, pp. 1185–1192, January 2004.

[12] H. Ding, A. Lim, B. Rodrigues, and Y. Zhu, "The over-constrained airport gate assignment problem," *Computers and Operations Research*, vol. 32, no. 7, pp. 1867–1880, 2005.

[13] Y. Zhu, A. Lim, and B. Rodrigues, "Aircraft and gate scheduling with time windows," in *Proceedings of the 15th IEEE International Conference on Tools with Artificial Intelligence*, pp. 189–193, Sacramento, Calif, USA, November 2003.

[14] D. Wei and C. Liu, "Optimizing gate assignment at airport based on genetic-tabu algorithm," in *Proceedings of the IEEE International Conference on Automation and Logistics (ICAL '07)*, pp. 1135–1140, Jinan, China, August 2007.

[15] D.-X. Wei and C.-Y. Liu, "Fuzzy model and optimization for airport gate assignment problem," in *Proceedings of the IEEE International Conference on Intelligent Computing and Intelligent Systems (ICIS '09)*, pp. 828–832, Shanghai, China, November 2009.

[16] X.-B. Hu and E. Di Paolo, "A ripple-spreading genetic algorithm for the airport gate assignment problem," in *Proceedings of the IEEE Congress on Evolutionary Computation (CEC '09)*, pp. 1857–1864, Trondheim, Norway, May 2009.

[17] B. Maharjan and T. I. Matis, "Multi-commodity flow network model of the flight gate assignment problem," *Computers & Industrial Engineering*, no. 63, pp. 1135–1144, 2012.

[18] L. Scharge, *Optimization Modeling with LINGO*, LINDO Systems Inc., 2004.

Hindawi Publishing Corporation
Mathematical Problems in Engineering
Volume 2013, Article ID 418303, 8 pages
http://dx.doi.org/10.1155/2013/418303

Research Article

Accurate Multisteps Traffic Flow Prediction Based on SVM

Zhang Mingheng,[1] Zhen Yaobao,[2] Hui Ganglong,[3] and Chen Gang[4]

[1] *School of Automotive Engineering, Dalian University of Technology, Dalian 116024, China*
[2] *School of Mechanical Engineering, Dalian University of Technology, Dalian 116024, China*
[3] *School of Navigation, Dalian Maritime University, Dalian 116026, China*
[4] *Department of Mechanical and Manufacturing Engineering, Aalborg University, 169220 Aalborg, Denmark*

Correspondence should be addressed to Zhang Mingheng; gloriazhang@163.com

Received 29 August 2013; Accepted 12 September 2013

Academic Editor: Rui Mu

Accurate traffic flow prediction is prerequisite and important for realizing intelligent traffic control and guidance, and it is also the objective requirement for intelligent traffic management. Due to the strong nonlinear, stochastic, time-varying characteristics of urban transport system, artificial intelligence methods such as support vector machine (SVM) are now receiving more and more attentions in this research field. Compared with the traditional single-step prediction method, the multisteps prediction has the ability that can predict the traffic state trends over a certain period in the future. From the perspective of dynamic decision, it is far important than the current traffic condition obtained. Thus, in this paper, an accurate multi-steps traffic flow prediction model based on SVM was proposed. In which, the input vectors were comprised of actual traffic volume and four different types of input vectors were compared to verify their prediction performance with each other. Finally, the model was verified with actual data in the empirical analysis phase and the test results showed that the proposed SVM model had a good ability for traffic flow prediction and the SVM-HPT model outperformed the other three models for prediction.

1. Introduction

1.1. Backgrounds. Accurate traffic flow prediction is an important research content in intelligent transportation system (ITS). The traffic flow information predicted rapidly and accurately is essential for traffic control, guidance, and providing traffic information services to the public. Especially in recent years, urban traffic congestion are now becoming the major problems in the traffic management all over the world, which produce a series influence hindering the social sustainable development and people's daily work. The transit agencies also have realized that the rapid and accurate traffic information can help them efficiently make reasonable and effective traffic guidance strategy. Thus, there is a growing demands in providing accurate traffic flow duration and diffusion prediction over a period of time.

The urban transport system has the characteristics such as nonlinear, stochastic, and time-varying. In order to achieve accurate prediction, some scholars applied traffic flow model to explain the dynamic changes and evolution of traffic flow. However, the traffic flow model is relatively complex in construction and has some difficulties with practical application. Therefore, the models based undetermined predictive method encounters the problems with model construction and solving. In contrast, nonmathematical models such as nonparametric regression, neural networks, and SVM are now widely applied to the traffic flow prediction due to their characteristics of self-learning and without complicated mathematical model construction.

On the other hand, most of the traditional prediction is based on the single-step method, which can only provide the current or single-step traffic parameters with obtained traffic data. The information provided is not enough for the public or traffic agencies' making decision. Thus, multisteps traffic flow prediction is essential for obtaining the traffic state trends over a certain period in the future. From the perspective of dynamic decision, the development trends of traffic states within a certain time in the future are more important than the current traffic state. For example, the traffic congestion is considered occurred with the significant

differences between the obtained traffic data and prediction trends. So we can estimate the range of possible spread of congestion and duration according to the traffic parameters of multistep prediction results.

However, accurate prediction of traffic flow is very difficult due to many stochastic variables involved (e.g., traffic conditions). Therefore, the deployment of traffic flow prediction model is a challenging task.

1.2. Literature Review. Accurate real-time traffic flow prediction is prerequisite and key to realize intelligent traffic control and guidance, and it is also the objective requirement to intelligent traffic management. Over the past decades, various sophisticated techniques and algorithms have been developed for traffic flow prediction. These methods can be roughly categorized as prediction methods based on mathematics and physics, including the historical average model, time series model, Kalman filter model, and exponential smoothing model; the other methods based on nonmathematical models such as artificial neural network (ANN), nonparametric regression (NPR), and SVM. Here, only a brief introduction about the typical method is made, more detailed information is found in their literature, respectively.

1.2.1. Kalman Filter Models. The Kalman filter, also known as linear quadratic estimation (LQE), is an efficient recursive procedure that estimates the future states of dependent variables. It is originated from the state-space representations in modern control theory. Wang et al. [1] developed a traffic state estimator model based on stochastic macroscopic traffic flow modeling and extended Kalman filtering. One major innovative feature of the traffic state estimator is the online joint estimation of important model parameters (free speed, critical density, and capacity) and traffic flow variables (flows, mean speeds, and densities). Hage et al. [2] proposed and validated an algorithm for estimating the urban links travel times based on an unscented Kalman filter (UKF). The algorithm integrates stochastically the vehicle count data from underground loop detectors at the end of every link and the travel times from probe vehicles. Their results showed that the proposed methodology can be used for estimating travel time in real time. Yuan et al. [3] proposed a state estimator based on the EKF technique, in which observation models for both Eulerian and Lagrangian sensor data (from loop detectors and vehicle trajectories, resp.) are incorporated. The results indicate that the Lagrangian estimator is significantly more accurate and offers computational and theoretical benefits over the Eulerian approach.

1.2.2. Support Vector Machine Models. Support vector machine, a novel supervised learning method used for classification and regression, has been recently proved to be a promising tool for both data classification and pattern recognition [4–6]. SVM shows very resistant to the overfitting problem, achieving high generalization performance in solving various time series forecasting problems, which has been applied in prediction of time series [7, 8]. These successful applications motivate researchers to apply SVM in the intelligent traffic system (ITS). Yang and Yu [9] proposed a freeway dynamic traffic flow forecasting model bases on SMO support vector machine. With the analysis of the freeway macroscopic dynamic traffic flow model and carrying out detail research on selecting parameter of SMO support vector machines, a test experiment was carried out and the result showed that the average relative error of forecasting was less than 3.84%. Yu et al. [6, 10] developed the SVM-based models to predict bus arrival time. In the models, travel speeds of the preceding buses of the same bus route were used to estimate traffic conditions. Their results showed that the SVM-based models outperformed the ANN and historic mean prediction models, and SVM seemed to be a powerful alternative for bus arrival time prediction. With versatile parallel distributed structures and adaptive learning processes, ANN and SVM have recently been gaining popularity in bus travel/arrival time prediction. Yu et al. [11] applied the SVM to predicting bus travel times. In which, a decay factor was introduced to adjust the weights between new and old data and the test results showed that the SVM with the decay factor and the adaptive algorithm had better prediction accuracy and dynamic performance than other existing algorithms.

In summary, due to the characteristics of urban traffic state such as uncertainty, nonlinearity and complexity, some researchers use traffic flow model to illustrate the dynamic changes of traffic state, to predict the evolution of the traffic flow, and then achieved the short-term traffic flow prediction model. However, the structure of the traffic flow model is complex relatively, which brings difficulty to the practical application. The method based on mathematical model is hard to meet the practical real-time requirements and the need for accuracy due to its difficulties in model building and solving. In contrast, the method based on nonmathematical model does not need complex model building, the prediction accuracy can meet the requirements of the intelligent transportation system. Therefore, these methods have been widely applied to the traffic flow prediction.

1.3. Contributions. Urban road traffic conditions are not only closely related to historical period conditions, but also to the upstream and downstream road state. At present, most of the accurate traffic flow prediction methods are focusing on the relation analysis between the traffic conditions and the historical traffic data from the time dimension of view. While the spatial dimension such as the upstream and downstream traffic condition and the traffic mode changes daily are ignored. In addition, most of the current traffic flow predictions are concentrated on the single-step prediction, less in the multisteps prediction. In other words, the prediction concentrates more on the coming traffic flow estimation for a specific time point, not concerns with the traffic condition changing trends in the next certain time periods. But in fact, from the perspective of dynamic decision making, the traffic condition changing trends are more important than the current traffic situation for the traffic management. Therefore, it is absolutely essential to establish a multisteps model for the traffic flow prediction, which can be used for estimating

the road traffic status trends accurately and the prediction result can be applied in improving rationality of the traffic management and the travel decisionmaking.

This paper seeks to make two contributions to the literature. Firstly, it attempts to develop the models to predict multisteps traffic flow with multiple steps using real-world data. It is expected to help the transit agencies efficiently make reasonable and effective traffic guidance strategy. Secondly, in order to improve the prediction accuracy, not only the historical traffic data but also the daily space-time sequences data are taken into consideration during the input state vector constructing. The performance of the proposed model can provide valuable insight for researchers as well as practitioners.

The structure of this paper is organized as follows: Section 2 provides the accurate real-time prediction model for predicting traffic flow with multisteps; Section 3 presents a case study together with results and analysis including performance evaluation of the proposed model; and lastly, the conclusions are given in Section 4 together with suggestions for further study.

2. Methodologies

2.1. Support Vector Machine Models. SVM is a type of learning algorithm based on statistical learning theory, which can be adjusted to map the complex input-output relationship for the nonlinear system without dependent on the specific functions. Unlike other nonlinear optimization methods, the solution of SVM always can achieve the global optimal solution without limitation to a local minimum point and it shows the strong resistance to the over-fitting problem and the high generalization performance.

Given the samples $(x_1, y_1), (x_2, y_2), \ldots, (x_i, y_i)$ $(x_i \in X \subseteq R^n,\ y_i \in Y \subseteq R)$, SVM make use of a nonlinear mapping ϕ to map x into a high-dimensional feature space H in which linear approximation is conducted to find the mapping function so that we can get a better approximation for the given data samples. Based on the statistical learning theory, we can get the function as follows:

$$f(x) = \omega\phi(x) + b. \tag{1}$$

Regression can be defined as a problem that minimized the risks for a loss function. The optimal regression function is the minimum and regularized generic function Q under certain constraints:

$$Q = \frac{1}{2}\|\omega\|^2 + \frac{C}{l}\sum_{i=1}^{l} L_\varepsilon\left(y_i, f(x_i)\right), \tag{2}$$

where, ω is a standard vector. The first item is named as the regularized term, which makes the function flat and improve its generalization ability; the second item is named as the experience risk generic functional, which can be determined by different loss functions; C is used to balance the relationship between structure risks and experience risks $(C > 0)$. When the insensitive loss function is defined with

$$L_\varepsilon\left(y_i, f(x_i)\right) = \max\left(\left|y_i - f(x_i)\right| - \varepsilon, 0\right). \tag{3}$$

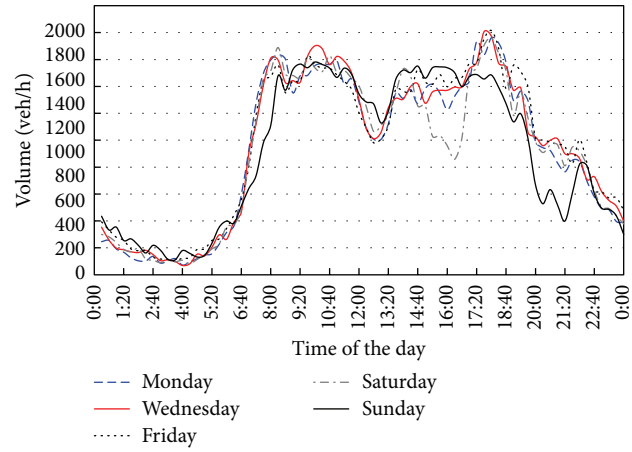

Figure 1: Traffic volume diurnal variation trends.

The minimization of (2) is a convex quadratic optimization problem, and then the problem can be inferred with the Lagrange multipliers a_i and a_i^*, shown as following:

$$\omega - \sum_{i=1}^{l}\left(\alpha_i - \alpha_i^*\right)x_i = 0. \tag{4}$$

Then, the SVM decision function is

$$f(x) = \operatorname{sgn}\left(\sum_{i=1}^{l}\left(\alpha_i - \alpha_i^*\right)\phi\left(x_i\right)\cdot\emptyset(x) + b\right). \tag{5}$$

The following equation can be obtained:

$$f(x) = \sum_{i=1}^{l}\left(\alpha_i - \alpha_i^*\right)K\left(x_i, x_j\right) + b, \tag{6}$$

where $K(x_i, x_j) = \phi(x_i)$ denotes the inner product of the vector in the feature space. All of the kernel functions can be directly computed in the input space.

2.2. Multisteps Prediction Methods Based on SVM. Traffic flow data are time-series data which have the characteristics such as autocorrelation and historical changes with similarity. Figure 1 shows the traffic volume changes for a certain road section during a few days in a week. In which, during the week days, the traffic volume changes gradually. That is to say the traffic volume data have the autocorrelation properties which can be demonstrated with the relationships between the traffic flow data at time t and before. Therefore, the prediction of the traffic flow can be conducted according with this autocorrelation properties.

Furthermore, other some cues can be inferred. Firstly, the traffic volume changes with similarity each day due to the inhabitant regular daily traveling. The data waveform presents like a saddle and the peak/valley of the wave appeared in the same time. In this paper, this regular changing pattern is named as the historical change of similarity, which can be used for establishing the traffic flow changing model to predict future multisteps traffic state.

Secondly, although the daily traffic volume has the same changing trends, the models have different properties from each other. For example, the traffic volume curve are similar from Monday to Friday, but on Saturday and Sunday, the curve presents different pattern from the week-days, the peak/valley of traffic volume curve is not obvious for distinguishing.

Therefore, a historical data model for prediction should be constructed which can be used for predicting the traffic flow historical models for every day (from Monday to Sunday). When the database is not enough for predicting, we also can establish the models for week-days and week ends, respectively. In addition, the trends of traffic flow data also can be influenced by weather or holidays.

Besides the above demonstration about the traffic flow properties in time domain, the data are also correlated in space domain. The traffic flow data has some correlations between the upstream and downstream for a certain road section. The upstream traffic flow will reach the downstream after a while; therefore, we can predict the future traffic flow condition of the downstream based on this correlation.

Given the traffic volume $q_{i,j}(t)$ of road section i, time t and day j, the observation volume sequence $Q_{i,j} = \{q_{i,j}(1), q_{i,j}(2), \ldots, q_{i,j}(t), \ldots\}$, the prediction of the traffic volume $\widehat{q}_{i,j}(t)$, then the forecasting traffic volume sequence of road section in the future n steps are expressed as $\widehat{Q}_{i,j} = \{\widehat{q}_{i,j}(t), \widehat{q}_{i,j}(t+1), \ldots, \widehat{q}_{i,j}(t+n)\}$. The historical pattern data sequence is defined as $HQ_{i,k} = \{hq_{i,k}(1), hq_{i,k}(2), \ldots, hq_{i,k}(t), \ldots\}$, in which $hq_{i,k}(t) = (1/w)\sum q_{i,j}(t)$ is the historical data of section i on the kth day (from Monday to Sunday), and w is the number of weeks for the data included.

Based on the description above and the space-time characteristics of the traffic flow data, in order to predict the traffic flow for the n steps $(t+1, \ldots, t+n)$ at section i, time t, three input feature vectors are designed for the prediction model:

(1) autocorrelation time feature vector: $Q_{i,j} = \{q_{i,j}(t-m), \ldots, q_{i,j}(t)\}$;

(2) historical model feature vector: $HQ_{i,k} = \{hq_{i,k}(1), \ldots, hq_{i,k}(t-1), hq_{i,k}(t), hq_{i,k}(t+1), \ldots, hq_{i,k}(t+n)\}$, $k = 1, 2, \ldots, 7$, which represents from Monday to Sunday, respectively;

(3) space correlation feature vector: $Q_{i-1,j} = \{q_{i-1,j}(t-m), \ldots, q_{i-1,j}(t)\}$, $Q_{i-2,j} = \{q_{i-2,j}(t-m), \ldots, q_{i-2,j}(t)\}, \ldots$. The number of time sequence m is determined by the time consumption from the upstream to the current road section.

The relationship between each input vector and output vector is shown in Figure 2.

From the aspect of theoretical analysis, for the single-step mode, accurate results can be obtained with only consideration of the time state and space state vectors due to the gradient traffic flow characteristics. On the contrary, for the multisteps mode, the traffic flow changing trends play a more important role in prediction; therefore, more accurate results can be achieved by taking the historical data into account.

Based on the above analysis, the combination of three state vectors is used as the input data for SVM, which are as follows:

(1) the combination of one-dimensional data for the specified road section in the previous intervals (T): $Q_{i,j} = \{q_{i,j}(t-m), \ldots, q_{i,j}(t)\}$, which describes the traffic volume changing property with the time intervals, this property is similar to the single-step prediction method;

(2) the combination of multidimensional space-time data of the upstream and the specified road section (PT): $Q_{i-1,j} = \{q_{i-1,j}(t-m), \ldots, q_{i-1,j}(t)\}$, $Q_{i-2,j} = \{q_{i-2,j}(t-m), \ldots, q_{i-2,j}(t)\}$, which describes the correlation of the traffic flow changing in time domain, especially the correlations between the upstream and downstream for a certain road section;

(3) the combination of the time-series data and the historical pattern data for the specified road section in the current interval (HT): $Q_{i,j} = \{q_{i,j}(t-m), \ldots, q_{i,j}(t)\}$, $HQ_{i,k} = \{hq_{i,k}(1), \ldots, hq_{i,k}(t-1), hq_{i,k}(t), hq_{i,k}(t+1), \ldots, hq_{i,k}(t+n)\}$, which describes the historical similarity of the traffic volume changing property demonstrated in the Figure 1;

(4) the combination of the time-series data for the upstream and the specified road section in the current interval and the historical pattern data for the target road section (HPT).

Each of the combination vectors above are used as the input variable of the SVM model, and $\widehat{Q}_{i,j} = \{\widehat{q}_{i,j}(t), \widehat{q}_{i,j}(t+1), \ldots, \widehat{q}_{i,j}(t+n)\}$ as the output variable, the SVM-T, SVM-TP, SVM-TH and SVM-TPH can be achieved respectively during the SVM training process.

3. Case Study

3.1. Evaluation of Model Performance. As an indicator to reflect the accuracy and availability of the prediction model, error plays an important role in evaluating the prediction model. Common error indictors include absolute prediction error and relative prediction error, which can be calculated as follows, respectively:

$$E_a(t) = q_i(t) - \widehat{q}_i(t),$$
$$E_r(t) = \frac{q_i(t) - \widehat{q}_i(t)}{q_i(t)}, \tag{7}$$

where $E_a(t)$ denotes the absolute prediction error at time t, $E_r(t)$ denotes the relative prediction error, $q_i(t)$ denotes the measured value, and $\widehat{q}_i(t)$ denotes the prediction value. $E_a(t)$ and $E_r(t)$ are the errors of the single-step prediction, while for the dynamic multisteps prediction, both the value and error can be achieved during each prediction process, which can be described with $\widehat{q}_i(t+1), \widehat{q}_i(t+2), \ldots, \widehat{q}_i(t+n)$. $\widehat{q}_i(t+1)$ is the prediction value of $(t+1)$ at the current time t, where n is the prediction step size. The greater the n, the more prediction

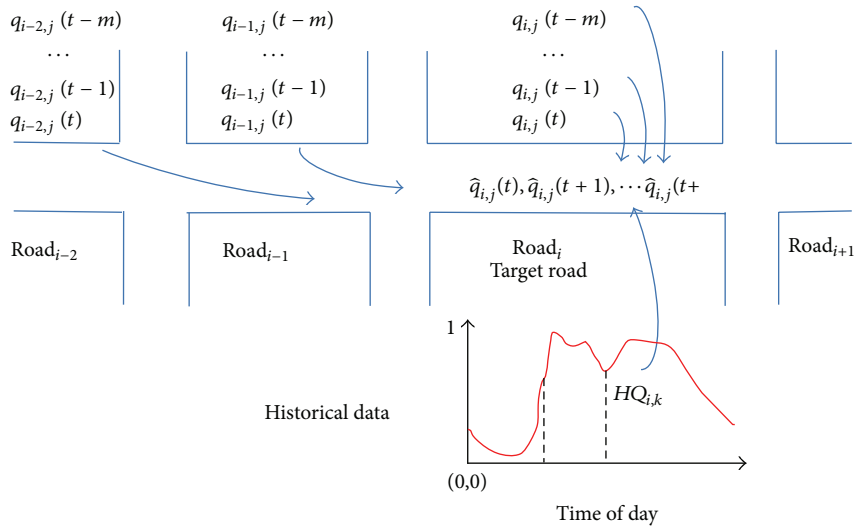

Figure 2: Prediction mechanism based on the traffic flow space-time characteristics.

error we can achieve. But a maximum theoretical limit $n_{\max}$ exists for avoiding unlimited prediction loop.

In order to obtain an objective and accurate evaluation of the prediction effect, the mean value of all the errors is used as the evaluation index for multisteps prediction, the formulas are as follows:

$$ME_a(t) = \frac{1}{n}\sum_{t=t+1}^{n}\left(q_i(t) - \hat{q}_i(t)\right),$$
$$ME_r(t) = \frac{1}{n}\sum_{t=t+1}^{n}\left(\frac{q_i(t) - \hat{q}_i(t)}{q_i(t)}\right), \quad (8)$$

where $ME_a(t)$ is the mean value of the absolute error for multisteps prediction at time t, $ME_r(t)$ is the mean value of the relative error. In fact, for multisteps prediction, the time-series synthetical error is more important for the prediction result. Therefore, $ME_a(t)$ and $ME_r(t)$ are the direct sum rather than the sum of absolute values of $E_a(t)$ and $E_r(t)$.

3.2. Data Collection and Processing. The presented SVM model for traffic flow prediction was tested with the actual survey data of Gaoerji Road in Dalian, China, dated from May 14 (Monday) to 20 (Sunday), 2012. Gaoerji road is a one-way lane with several imports/exports and goes from Zhongshan road to Yierjiu street through the city center with a distance of 3.8 km. The traffic state is highly congested in the morning and afternoon peaks. In this research, the actual survey started from 7:00 in the morning. The collected data was obtained with SCOOT (Split, Cycle, and Offset Optimization Technology) and consist of the traffic volume during the peak time (PT; 0700–0830 h) and off-peak time (OT; 1000–1200 h) with recording data once every 5 minutes.

There are some influence factors including missing, error and random noise in the raw datasets which is obtained with SCOOT. Therefore, the data must be identified, repaired and smoothed firstly. Then the time-series data is achieved with normalization method. The main advantage of data normalization is to accelerate convergence velocity of iteration during the SVM training. Another advantage is to facilitate subsequent data processing. Singular value sample data might cause numerical problems because the kernel values usually depend on the inner products of feature vectors such as the linear kernel or the polynomial kernel. Therefore, it is recommended that each attribute should be linearly scaled to the range [−1, +1] or [0, +1]. In this research, the data sets were scaled to the range between 0 and 1.

Table 1: Four popular kernel functions.

Kernel function	Expression	Comment
Linear kernel	$K(x_i, x_j) = x_i^T x_j$	
Polynomial kernel	$K(x_i, x_j) = (\gamma x_i^T x_j + r)^d$	$\gamma > 0$
Radial basis function (RBF) kernel	$K(x_i, x_j) = e^{-\gamma\|x_i - x_j\|^2}$	$\gamma > 0$
Sigmoid kernel	$K(x_i, x_j) = \tanh(\gamma x_i^T x_j + r)^d$	

x_i, x_j are input vectors and γ, r, and d are kernel parameters.

3.3. Model Identification. In Section 2.2 demonstrated above, the input vectors for traffic flow prediction model have been discussed and constructed. Here, we only give an introduction to SVM briefly. More detailed descriptions can be found in [12]. Given a training set of instance-label pairs, the input vectors can be mapped implicitly and hence very efficiently into high-dimensional space (maybe infinite) by the kernel function Φ, and SVM finds a linear separating hyper plane with the maximal margin in this higher dimensional space. At present, new kernel functions are proposed by researchers, some popular kernel functions are as Table 1.

The previous researches [13, 14] suggested that radial basis function (RBF) kernel had less numerical difficulties with application and was efficient for traffic state and traffic

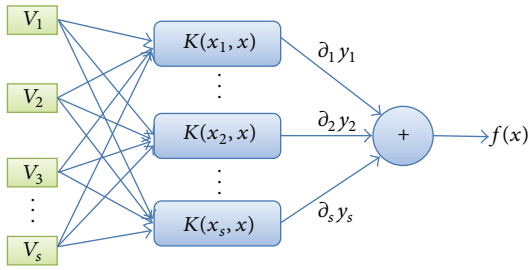

Figure 3: Structure of the SVMs model for traffic flow prediction.

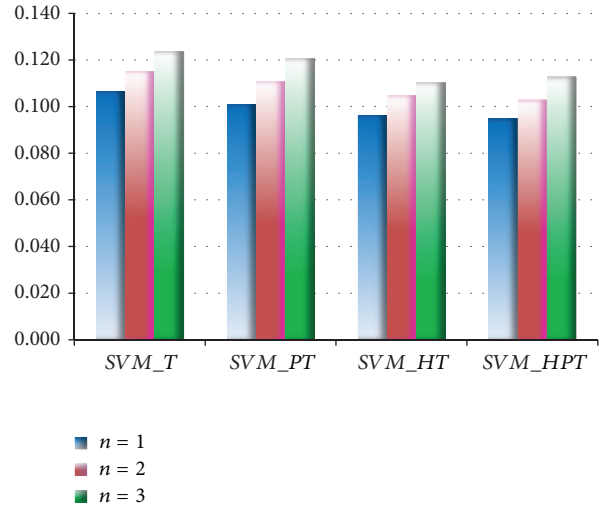

Figure 4: Prediction error results of the SVM model with different input vectors.

flow prediction. Thus, RBF kernel function is used for the SVM model in this study. Before the RBF kernel is being used, three parameters associated should be determined: (C, ε, γ). Parameter C is a regularization constant or penalty parameter which is assigned in advance before each SVM model training process. This parameter allows striking a balance between the two competing criteria of margin maximization and error minimization, whereas the slack variables ε indicate the distance of the incorrectly classified points from the optimal hyper plane [15]. The larger the C value, the higher the penalty associated to misclassified samples. Parameter γ is the parameter of RBF function kernel. In summary, the entire SVM model training process is a process that the parameters are optimized and determined by simulation. Kavzoglu and Colkesen [16] pointed out that the parameters determination was a practical way to identify good parameters. Thus, in this research, they are calibrated by grid-search method. During the search process, all possible combinations of (C, ε, γ) are tested and the one with the best performance is chosen. After conducting the grid search on the training dataset, the optimal parameters were selected as $(2^{-2}, 2^{-5}, 1.22)$, and a cross validated on validation dataset is conducted. The various SVMs are implemented with Libsvm (National Taiwan University, available at: http://www.csie.ntu.edu.tw/~cjlin/libsvm/) on a Microsoft Windows platform.

The structure of the SVMs model for *SVM-T*, *SVM-PT*, *SVM-HT*, and *SVM-HPT* is shown as Figure 3. In this structure, the feature vector v is composed with the different dimensions of each SVM model, respectively. For example, in *SVM-T model*, $v = (V_1, V_2, \ldots, V_s)$ denotes the traffic volume of road section i and day j at different times $\{q_{i,j}(t - s - 1), \ldots, q_{i,j}(t)\}$. The features vector definitions for each SVMs model are demonstrated in Section 2.2.

To determine the SVM's inputs vector for practical application, some comparison tests have been conducted between the models with different input variables (T, PT, HT, and HPT) which have been calibrated based on the data collected. The comparison of prediction errors about the four models on off-peak period and peak period prediction error results are shown as Figure 4.

During the whole prediction process, the data processing was divided into three steps: respectively for training, cross-validation, and testing. Firstly, about 10% of samples data were set as testing data. Then, 70% of the remaining samples data were assigned to training and the others to cross-validation. In particular, the training and testing processes were conducted with the same datasets for the four models in order to have the same basis of comparison.

3.4. Results Analysis. From the comparison results of the four models (*SVM-T*, *SVM-PT*, *SVM-HT,* and *s-HPT*) in Section 3.3, some conclusions can be drawn as follows.

(1) Firstly, in the case of single-step prediction, the number of prediction steps $n = 1$. The prediction error curves in Figure 4 indicate that the results of the prediction error are similar with each other for the four models and *SVM_PT* has more accuracy than *SVM_T*. The reason of this case is that the upstream of the traffic volume can reach the current road section after a while, so a more accurate prediction result can be obtained with the introduction of upstream traffic volume into *SVM-T*.

(2) Secondly, in the case of multisteps prediction, the number of prediction steps $n > 1$. For the case of $n = 2$, the prediction error has the similar characteristics to single-step model. For the case of $n > 2$, the prediction error of *SVM_T* increases significantly with the steps n increasing. The reason for this is that in *SVM_T* model, the traffic volume data is time-series data, the distance between the predicted points and observing data has the different impact effect for the prediction accuracy, the more closely the more important for prediction result. Furthermore, for the multisteps prediction, the *SVM_HT* and *SVM_HPT* have a good prediction performance compared with the *SVM_T* which only uses the time-series data for predicting. The reason for this is mainly that the historical data can represent the traffic trends changing mode with traffic volume for the current road section, so the prediction result can be better with the introduction

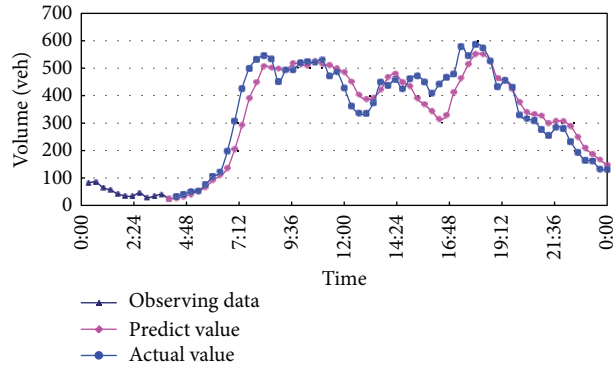

Figure 5: Example of dynamic multisteps prediction results of *SVM_PT*.

of upstream traffic volume data and historical data into *SVM-T*.

(3) It is important to note that the execution performance of *SVM_HPT* and *SVM_HT* is different due to the complicated input vector dimensions in upstream traffic volume data and historical data. Therefore, in practical application, the *SVM_HT* model is a priority selection for prediction under the condition of meeting the requirement prediction accuracy in order to reduce the time-consumption of the whole system.

In order to verify the actual performance of the prediction model presented above, a test was conducted with *SVM_HT* and the result was shown as Figure 5. In this test, a certain whole day traffic volume data were used for predicting the traffic trends and the sample interval was assigned to 20 minutes so as to simplify the computation process. From the result, it can be seen that the prediction curves agree well with the actual observing data. Test of the prediction error found that the traffic volume mean error is 16.8 vehicles and the mean relative error is 12.8%. Thus it can be seen that there seems to be a strong potential effectiveness to be used to the practical application.

4. Conclusions

The urban transport system has the characteristics such as nonlinear, stochastic, and time-varying. Therefore, artificial intelligence methods are now receiving more and more attentions in ITS. In order to predict traffic flow with multisteps accurately, this paper proposed a SVM model for the prediction. In the present research, the traffic volume data with actual observation surveys in urban area of Dalian was used to predict the traffic flow by SVM models. In order to obtain the prediction effect with different input vectors, some comparison tests are conducted with different input variables (T, PT, HT, and HPT). The test results showed that the proposed SVM model had a good ability for traffic flow prediction and the comparison of different input vectors indicated that the *SVM-HPT* model outperformed the other three models for prediction.

In this paper, only the traffic volume data was used to estimate the current traffic conditions. Further study will consider more factors analysis such as the input vectors dimensions and the prediction steps so as to enhance the performance of the proposed prediction models.

Acknowledgments

This work was jointly supported by grants from the Humanities and Social Sciences Foundation of the Ministry of Education in China (Project no. 12YJCZH280), the Ph.D. Programs Foundation of Ministry of Education of China (Project no. 20112125120004), and National Natural Science Foundation of China (Project no. 11272075).

References

[1] Y. Wang, M. Papageorgiou, and A. Messmer, "Real-time freeway traffic state estimation based on extended Kalman filter: adaptive capabilities and real data testing," *Transportation Research A*, vol. 42, no. 10, pp. 1340–1358, 2008.

[2] R. M. Hage, D. Betaille, F. Peyret, and D. Meizel, "Unscented Kalman filter for urban network travel time estimation," *Procedia—Social and Behavioral Sciences*, vol. 54, no. 4, pp. 1047–1057, 2012.

[3] Y. Yuan, J. W. C. van Lint, R. E. Wilson, F. van Wageningen-Kessels, and S. P. Hoogendoorn, "Real-time lagrangian traffic state estimator for freeways," *IEEE Transactions on Intelligent Transportation Systems*, vol. 13, no. 1, pp. 59–70, 2012.

[4] V. N. Vapnik, "An overview of statistical learning theory," *IEEE Transactions on Neural Networks*, vol. 10, no. 5, pp. 988–999, 1999.

[5] B. Yu, Z. Z. Yang, and B. Z. Yao, "Bus arrival time prediction using support vector machines," *Journal of Intelligent Transportation Systems*, vol. 10, no. 4, pp. 151–158, 2006.

[6] B. Yu, W. H. K. Lam, and M. L. Tam, "Bus arrival time prediction at bus stop with multiple routes," *Transportation Research C*, vol. 19, no. 6, pp. 1157–1170, 2011.

[7] L. J. Cao and F. E. H. Tay, "Support vector machine with adaptive parameters in financial time series forecasting," *IEEE Transactions on Neural Networks*, vol. 14, no. 6, pp. 1506–1518, 2003.

[8] B. Z. Yao, C. Y. Yang, J. B. Yao, and J. Sun, "Tunnel surrounding rock displacement prediction using support vector machine," *International Journal of Computational Intelligence Systems*, vol. 3, no. 6, pp. 843–852, 2010.

[9] J. H. Yang and X. N. Yu, "The support vector machines prediction model of freeway dynamic traffic flow," *Journal of Xi'an Technological University*, no. 3, pp. 280–284, 2009.

[10] B. Yu, Z. Z. Yang, K. Chen, and B. Yu, "Hybrid model for prediction of bus arrival times at next station," *Journal of Advanced Transportation*, vol. 44, no. 3, pp. 193–204, 2010.

[11] B. Yu, T. Ye, X. M. Tian, G. B. Ning, and S. Q. Zhong, "Bus travel-time prediction with forgetting factor," *Journal of Computing in Civil Engineering*, 2012.

[12] C. Cortes and V. Vapnik, "Support-vector networks," *Machine Learning*, vol. 20, no. 3, pp. 273–297, 1995.

[13] V. Tyagi, S. Kalyanaraman, and R. Krishnapuram, "Vehicular traffic density state estimation based on cumulative road acoustics," *IEEE Transactions on Intelligent Transportation Systems*, vol. 13, no. 3, pp. 1156–1166, 2012.

[14] Q. Li, "Short-time traffic flow volume prediction based on support vector machine with time-dependent structure," in *Proceedings of the IEEE Intrumentation and Measurement Technology Conference (I2MTC '09)*, pp. 1730–1733, May 2009.

[15] T. Oommen, D. Misra, N. K. C. Twarakavi, A. Prakash, B. Sahoo, and S. Bandopadhyay, "An objective analysis of support vector machine based classification for remote sensing," *Mathematical Geosciences*, vol. 40, no. 4, pp. 409–424, 2008.

[16] T. Kavzoglu and I. Colkesen, "A kernel functions analysis for support vector machines for land cover classification," *International Journal of Applied Earth Observation and Geoinformation*, vol. 11, no. 5, pp. 352–359, 2009.

Hindawi Publishing Corporation
Mathematical Problems in Engineering
Volume 2013, Article ID 475194, 9 pages
http://dx.doi.org/10.1155/2013/475194

Research Article

Prediction for Traffic Accident Severity: Comparing the Bayesian Network and Regression Models

Fang Zong, Hongguo Xu, and Huiyong Zhang

College of Transportation, Jilin University, 5988 Renmin Street, Changchun, Jilin 130022, China

Correspondence should be addressed to Huiyong Zhang; jlu.zf@163.com

Received 29 August 2013; Accepted 22 September 2013

Academic Editor: Baozhen Yao

The paper presents a comparison between two modeling techniques, Bayesian network and Regression models, by employing them in accident severity analysis. Three severity indicators, that is, number of fatalities, number of injuries and property damage, are investigated with the two methods, and the major contribution factors and their effects are identified. The results indicate that the goodness of fit of Bayesian network is higher than that of Regression models in accident severity modeling. This finding facilitates the improvement of accuracy for accident severity prediction. Study results can be applied to the prediction of accident severity, which is one of the essential steps in accident management process. By recognizing the key influences, this research also provides suggestions for government to take effective measures to reduce accident impacts and improve traffic safety.

1. Introduction

As a significant cause of deaths, injuries, and property loss, traffic accident is a major concern for public health and traffic safety. According to statistics from the Ministry of Public Security of China between 2009 and 2011, traffic crashes resulted in an average of 65 123 people dead and 255 540 cases injured annually in China (China Statistical Yearbook of Road Traffic Accidents, 2009–2011). It was reported that the cost of medical care and productivity losses associated with motor vehicle crash injuries was over $99 billion, or nearly $500, for each licensed driver in the United States (Centers for Disease Control and Prevention, 2010). Being one of the major steps of accident management, accident severity prediction can provide crucial information for emergency responders to evaluate the severity level of accidents, estimate the potential impacts, and implement efficient accident management procedures.

In recent years, increased attention has been directed at accident severity prediction, for which Bayesian network and Regression model are two widely used modeling techniques. However, to the authors' knowledge, there is no study that presents quantitative comparison of the two methods. Therefore, the present work focuses on conducting an accident severity modeling by employing both Bayesian network and Regression model. The accuracies of the two methods will then be compared and a better one will be selected for accident severity prediction. By carrying out accident severity analysis, the risk factors and their effects will also be identified in the work.

The remainder of this paper is organized as follows. In Section 2, the literature review on predictions of severity is presented in general. The data are described in Section 3. This is followed by accident severity modeling with Bayesian network and Regression models in Sections 4 and 5, respectively. The paper concludes with a summary and directions for future research.

2. Literature Review

Regression analysis has been widely used to accident severity prediction and contributing factors determination. The most commonly used Regression models are Logistic Regression model and Ordered Probit model [1–6]. However, some researchers [7, 8] pointed out that most of the Regression models have their own assumptions and predefined underlying relationships between dependent and independent variables (i.e., linear relations between the variables).

If these assumptions are violated, the model could lead to erroneous estimations of the likelihood of severe injury.

Some researchers carried out traffic accident analysis by employing Bayesian network. For instance, de Oña et al. [8] applied Bayesian network to the identification of the factors affecting injury severity, which was classified into slightly injured and killed/severely injured. Based on Bayesian network, the factors associated with a killed/severely injured accident were identified to be accident type, driver age, lighting, and number of injuries. The results indicate that Bayesian network is capable of making predictions without the need for preassumptions and can make graphic representations of complex systems with interrelated components. Simoncic [9] constructed a Bayesian network for analysis of injury severity. The results showed that Bayesian network can be applied in road accident modeling. It also presented some advantages of Bayesian network, such as being able to involve more variables and larger data set than Regression model. Ozbay and Noyan [10]'s work constructed a Bayesian network and applied it to predicting incident duration and understanding factors associated with incident clearance time. The results indicated that Bayesian network can represent the stochastic nature of incidents. Gregoriades [11] highlighted the interest of using Bayesian network to model traffic accidents and discussed the need to not consider traffic accidents as a deterministic assessment problem, but model the impacts of the factors that could lead to traffic accidents.

Although previous works presented the advantages of adopting Bayesian network in accident severity modeling, there is no contribution that conducts a quantitative comparison of Bayesian network and Regression model. Therefore, both Bayesian network and Regression model will be applied to accident severity modeling in this work and the accuracy of the two models will be compared.

3. Data

The data set for this work contains police-reported traffic accident records for Jilin province, China, in 2010. With records containing missing values eliminated, our final data set consists of 2,246 cases, which are all motor-vehicle involved accidents. In addition to severity information, the data contains information regarding accident characteristics (accident occurrence time and accident location), vehicle characteristics (vehicle type involved and vehicle condition), environmental factors (weather condition and visibility distance), and road conditions (pavement condition, road geometrics and roadway surface condition, etc.).

Previous studies [7, 12] indicated that the factors associated with accident severity mainly include road characteristics, accidents characteristics, vehicle characteristics, driver characteristics, and environmental factors. However, driver characteristics related variables are not involved since suitable records for driver characteristics are not available in the data set. Based on a preliminary correlation test, 3 dependent variables and 14 candidate independent variables were selected from the data set, shown in Table 1. In the process of accident severity modeling, 50% of the total records are selected as training data to calibrate the prediction models, and the left 50% are set aside as testing data.

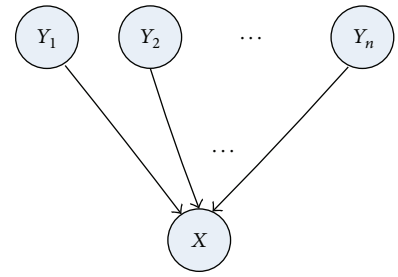

Figure 1: An example of Bayesian network.

4. Accident Severity Modeling

4.1. Accident Severity Modeling with Bayesian Network

4.1.1. A Brief Overview of the Bayesian Network. Over the last decade, Bayesian network has become a popular representation for encoding uncertain expert knowledge in expert systems. It has been applied to many fields, such as medicine, document classification, information retrieval, image processing, data fusion, and decision support systems [13].

Bayesian network is a graphical model representing random variables and their conditional dependencies. Figure 1 shows a simple Bayesian network, in which $Y_1, Y_2, \ldots, Y_n$ and X are random variables represented by nodes. $Y_1, Y_2, \ldots, Y_n$ are called parents of X and X is called the child of $Y_1, Y_2, \ldots, Y_n$. The directed edge from $Y_1, Y_2, \ldots, Y_n$ to X indicates the dependence of X on its parent node.

4.1.2. Structure Learning. In most cases, the graphical structure of a Bayesian network needs to be automatically learnt from the data. This learning process can be described as follows. Let a random variable S be the structure of a Bayesian network and let $P(S)$ be its prior probability distribution. Given data set D, which consists of all the variables represented by nodes in the Bayesian network (e.g., X and $Y_1, Y_2, \ldots, Y_n$ in Figure 1), based on the Bayesian theorem, the posterior probability of S can be calculated as

$$P(S \mid D) = \frac{P(S, D)}{P(D)} = \frac{P(S)\,P(D \mid S)}{P(D)}, \tag{1}$$

where $P(S \mid D)$ is the posterior probability of structure S, $P(S)$ is the prior probability distribution of S, and $P(D)$ is the probability distribution of data set D.

The posterior probability $P(S \mid D)$ is also called Bayesian score, and (1) is called Bayesian score function. The structure that maximizes the Bayesian score will be chosen as the final structure of the Bayesian network.

4.1.3. Parameter Learning. In order to fully specify a Bayesian network, it is necessary to specify the conditional probability of each node upon its parent nodes in the network,

Table 1: Variables and statistics based on survey data.

Factors	Variables	Values	Percentage (%)
Accident severity	Number of fatalities: Nof	0 : 1	89.59
		≥1 : 2	10.41
	Number of injuries: Noi	0 : 1	9.86
		[1, 3) : 2	85.89
		[3, 11) : 3	4.14
		≥11 : 4	0.11
	Property damage (Yuan): Pd	<1000 : 1	61.18
		[1000, 30000) : 2	37.19
		≥30000 : 3	1.63
Accident characteristics	Time of day: Tod	day [6:00, 18:00) : 1	69.12
		night [18:00, 6:00) : 2	30.88
	Location-Motor vehicle lanes: L-Mvl	Yes: 1	71.68
		No: 2	28.32
	Location-Crosswalk: L-C	Yes: 1	3.42
		No: 2	96.58
	Location-Regular road section: L-Rrs	Yes: 1	60.01
		No: 2	39.99
	Location-Intersection: L-I	Yes: 1	38.90
		No: 2	61.10
Vehicle characteristics	Motorcycle involved: Mi	Yes: 1	16.97
		No: 2	83.03
	Bus or truck involved: Bti	Yes: 1	95.30
		No: 2	4.70
	Vehicle condition: Vc	Good: 1	73.79
		Poor: 2	26.21
Environmental factors	Weather condition: Wc	Sunny: 1	89.48
		Other: 2	10.52
	Visibility distance (meter): Vd	<50 : 1	8.90
		[50, 100) : 2	22.70
		[100, 200) : 3	19.86
		≥200 : 4	48.54
Roadway characteristics	Pavement condition: Pc	Asphalt or cement: 1	99.80
		Other: 2	0.20
	Roadway surface condition: Rsc	Dry: 1	85.16
		Other: 2	14.84
	Road geometrics: Rg	Flat and straight: 1	98.57
		Hill or bend: 2	1.43
	Traffic signal control: Tsc	Yes: 1	17.46
		No: 2	82.54

given the structure S and the data set D. Parameter learning refers to the process of identifying the parameters in the conditional distribution of any child nodes on the joint distribution of its parent nodes. Bayesian estimation is one of the methods for parameter learning, which assumes that parameter θ_i is a random variable with prior distribution $P(\theta_i)$. According to the Bayesian theorem, the posterior probability for the parameter ($P(\theta_i \mid D)$) given data set D is computed as

$$P(\theta_i \mid D) = \frac{P(\theta_i, D)}{P(D)} = \frac{P(\theta_i) P(D \mid \theta_i)}{P(D)}, \quad (2)$$

where $P(\theta_i)$ is the prior probability distribution of parameter θ_i and $P(D)$ is the probability distribution of data set D.

4.1.4. Learning Results. Since the number of possible structures grows exponentially as a function of the number of variables, it is computationally infeasible to find the most probable network structure, given the data, by exhaustively enumerating all possible network structures. Cooper and Herskovits [14] and Herskovits [15] proposed a greedy algorithm, called the K2 algorithm, which becomes one of the most popular methods for structure learning of Bayesian network. Besides the basic Bayesian theories, the K2

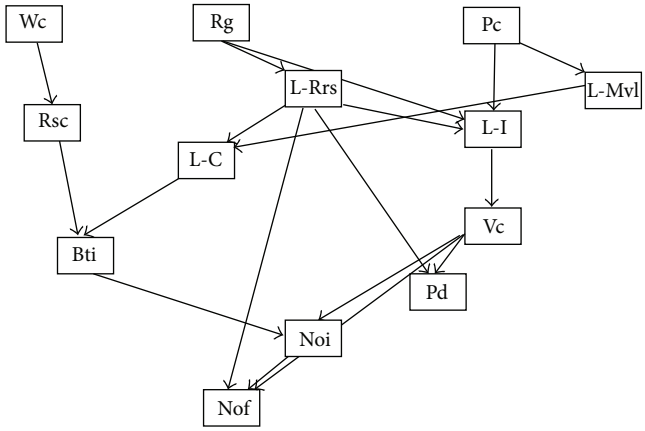

Figure 2: The structure of the Bayesian network.

algorithm uses two assumptions, namely, that there is an ordering available on the variables and that, a priori, all structure are equally likely. The K2 algorithm considers each node in the order given to it as input and determines its parents as follows. Initially, assume that each node has no parent. Then, add parents for some nodes when the score (computed by using (1)) of the resulting structure could be increased. Try to add parents for each node until no more parents can increase the score. Then the structure of the highest score is the final structure [14].

The structure of the severity prediction Bayesian network is learned by employing the K2 algorithm and the Full-BNT toolbox, which is an open-source Matlab package for directed graphical models [16]. The final network structure is shown in Figure 2. The results indicate that Bayesian network for accident severity analysis is composed of 13 nodes and the concerned edges, which represent the relationships between the nodes.

Based on the developed structure, the parameters are learned by employing the method of Bayesian estimation. The prior distributions of all the variables are assumed to be Dirichlet distribution, which is a kind of conjugate distribution allowing closed form for posterior distribution of parameters and closed-form solution for prediction. The Full-BNT toolbox of Matlab is employed to realize the algorithm of Bayesian estimation.

As the parent nodes gather the impacts of the indirect nodes and deliver them to the child nodes, the influence of parent nodes will be focused on. Under the impact of the parent nodes, that is, factors which have direct edge to the severity indicators in this structure, the parameter learning results of number of fatalities (Nof), number of injuries (Noi), and property damage (Pd) are shown in Tables 2, 3, and 4 respectively. The indicators of Mean Absolute Percentage Error (MAPE) and *Hit ratio* are adopted to examine the accuracy of the models.

MAPE, which looks at the average percentage difference between predicted values and observed ones, is calculated as

$$\text{MAPE} = \frac{1}{n}\sum_{i-1}^{n}\left|\frac{A_i - P_i}{A_i}\right|, \tag{3}$$

where A_i is the observed value and P_i is the predicted value for observation i.

The MAPE value of the fatality forecasting model is 0.0226, and the *Hit ratio* is 100%, which recommend that this model has a high accuracy [17, 18].

According to the developed structure, Nof's parent nodes are L-Rrs, Vc, and Noi. The estimation results indicate that the probability of occurrence of fatal accident increases when the condition of the involved vehicle gets worse. Moreover, higher number of deaths is associated with higher number of injuries. The accident that occurs at normal section of road, but not at abnormal section or intersection, tends to cause more fatalities. The reason may be that the involved vehicle usually speeds down when going through intersection or abnormal section of road.

The MAPE value of the injury forecasting model is 0.0013, and the *Hit ratio* is 100%, which presents a high accuracy of the model.

Two parent nodes, namely, Bti and Vc, have direct impacts on number of injuries in the accident. The estimation results show that bus or truck involved accident tends to cause more injuries. In addition, the worse the vehicle condition is, the more injuries are in the accident.

The MAPE value of the property damage forecasting model is 0.0019, and the *Hit ratio* is 100%, which shows a high accuracy of the model.

Two parent nodes, that is, L-Rrs and Vc, have direct impact on property damage. The results indicate that, like the influences of Vc on Nof and Noi, poor vehicle condition is associated with large amount of property damage and vice versa. In addition, the accident that occurs at irregular section of road or intersection tends to cause large amount of property damage. Combining the effects of L-Rrs on Pd and Nof, it can be deduced that the accident that occurs at regular section of road tends to result in high number of deaths but small amount of property damage.

4.2. Accident Severity Modeling with Regression Models. The most commonly used Regression models in traffic injury analysis are the Logistic Regression model and the Ordered Probit model [1–6]. Since the alternatives of Noi and Pd are all ordered and the Logistic Regression model would fail to account for the ordinal nature of the dependent variable and have the problem of independence from irrelevant alternatives (IIA) [19], Ordered Probit model will be employed in forecasting of Noi and Pd. Besides, one of the Logistic Regression models-Binary Logit model, will be adopted in prediction of Nof, which has two discrete alternatives.

4.2.1. Binary Logit Model. As one of the Binomial choice models, Binary Logit model is commonly used in discrete choice modeling. According to the random utility theory [20], the utility of alternative i ($i = 1$ or 2 for Nof $= 0$ or Nof ≥ 1, resp.) for accident n can be specified as

$$U_{in} = V_{in} + \varepsilon_{in}, \tag{4}$$

where V_{in} denotes the deterministic component of U_{in}, and ε_{in} is the random component of U_{in}.

Table 2: Parameter learning results of the fatality forecasting model.

No.	Variables			Estimation results								N
	L-Rrs	Vc	Noi	Nof ≥ 1				Nof = 0				
				Bayesian	Test	Absolute error	Relative error	Bayesian	Test	Absolute error	Relative error	
1	1	1	1	0.0052	0.0000	0.0052	1.0000	0.9948	1.0000	0.0052	0.0052	1123
2	1	1	2	0.9995	1.0000	0.0005	0.0005	0.0005	0.0000	0.0005	1.0000	
3	1	1	3	0.6622	0.6667	0.0045	0.0068	0.3378	0.3333	0.0045	0.0133	
4	1	2	1	0.2628	0.2626	0.0002	0.0008	0.7372	0.7374	0.0002	0.0003	
5	1	2	2	0.9855	0.9855	0.0000	0.0000	0.0145	0.0145	0.0000	0.0000	
6	1	2	3	0.9994	1.0000	0.0006	0.0006	0.0006	0.0000	0.0006	1.0000	
7	2	1	1	0.2012	0.2000	0.0012	0.0060	0.7988	0.8000	0.0012	0.0015	
8	2	1	2	0.9369	0.9375	0.0006	0.0006	0.0631	0.0625	0.0006	0.0095	
9	2	1	3	0.5000	0.0000	0.5000	1.0000	0.5000	0.0000	0.5000	1.0000	
10	2	2	1	0.2601	0.2601	0.0000	0.0000	0.7399	0.7399	0.0000	0.0000	
11	2	2	2	0.9575	0.9575	0.0000	0.0000	0.0425	0.0425	0.0000	0.0000	
12	2	2	3	0.9087	0.9091	0.0004	0.0004	0.0913	0.0909	0.0004	0.0044	

Table 3: Parameter learning results of the injury forecasting model.

Variables	No.		1	2	3	4
	Bti		1	1	2	2
	Vc		1	2	1	2
Estimation results	Noi = 0	Bayesian	0.1299	0.0907	0.2444	0.1813
		Test	0.1295	0.0906	0.2439	0.1812
		Absolute error	0.0004	0.0001	0.0005	0.0001
		Relative error	0.0031	0.0011	0.0020	0.0006
	1 ≤ Noi < 3	Bayesian	0.8552	0.8643	0.7293	0.7542
		Test	0.8561	0.8644	0.7317	0.7544
		Absolute error	0.0009	0.0001	0.0024	0.0002
		Relative error	0.0011	0.0001	0.0033	0.0003
	Noi ≥ 3	Bayesian	0.0150	0.0450	0.0263	0.0646
		Test	0.0144	0.0450	0.0244	0.0645
		Absolute error	0.0006	0.0000	0.0019	0.0001
		Relative error	0.04	0.0000	0.0722	0.0015
	N		1123			

Table 4: Parameter learning results of the property damage forecasting model.

Variables	No.		1	2	3	4
	L-Rrs		1	1	2	2
	Vc		1	2	1	2
Estimation results	Pd < 1000	Bayesian	0.7905	0.6802	0.4402	0.4641
		Test	0.7917	0.6803	0.4405	0.4641
		Absolute error	0.0012	0.0001	0.0003	0.0000
		Relative error	0.0015	0.0001	0.0006	0.0000
	1000 ≤ Pd < 30000	Bayesian	0.1983	0.3072	0.5470	0.5093
		Test	0.1979	0.3072	0.5476	0.5093
		Absolute error	0.0004	0.0000	0.0006	0.0000
		Relative error	0.0019	0.0000	0.0011	0.0000
	Pd ≥ 30000	Bayesian	0.0113	0.0126	0.0129	0.0266
		Test	0.0104	0.0125	0.0119	0.0266
		Absolute error	0.0009	0.0001	0.0010	0.0000
		Relative error	0.0782	0.0048	0.0772	0.0002
	N		1123			

Here V_{in} can be written as

$$V_{in} = \sum_{k=1}^{K} \theta_k X_{kin}, \tag{5}$$

where X_{kin} is attribute k ($k = 1, \ldots, K$) for accident n and alternative i, and θ_k is the estimable coefficients, which can be estimated by adopting the Maximum Likelihood method.

Assuming ε_{in} follows Gumbel distribution, the choice probability of alternative i ($i = 1$) for accident n is then

$$P_{1n} = \frac{\exp(V_1)}{\exp(V_1) + \exp(V_2)}, \tag{6}$$

and the choice probability of alternative i (i=2) for accident n is

$$P_{2n} = 1 - P_{1n}. \tag{7}$$

4.2.2. Ordered Probit Model. The Ordered multiple choice model assumes the relationship

$$\sum_{j=1}^{J} P_n(j) = F\left(\alpha_j - \beta_j X_n, \theta\right), \quad j = 1, \ldots, J-1,$$
$$P_n(J) = 1 - \sum_{j=1}^{J} P_n(j), \tag{8}$$

where $P_n(j)$ is the probability that alternative j happens in accident n ($n = 1, \ldots, N$), α_j is an alternative specific constant, X_n is a vector of the attributes of accident n, β_j is a vector of the estimated coefficients, and θ is a parameter that controls the shape of probability distribution F. Therefore, F can have various shapes of distribution based on different value of θ.

The Ordered Probit model, which assumes standard normal distribution for F, is the most commonly used ordered multiple choice model [21]. The Ordered Probit model has the following form:

$$P_n(1) = \Phi\left(\alpha_1 - \beta_j X_n\right)$$
$$P_n(j) = \Phi\left(\alpha_j - \beta_j X_n\right) - \Phi\left(\alpha_{j-1} - \beta_j X_n\right), \quad j = 2, \ldots, J-1,$$
$$P_n(J) = 1 - \sum_{j=1}^{J-1} P_n(j), \tag{9}$$

where $P_n(j)$ is the cumulative standard normal distribution function. For all the probabilities to be positive, it must satisfy that $\alpha_1 < \alpha_2 < \cdots < \alpha_{J-1}$.

4.2.3. Estimation Results. By using logistic and probit procedure in SAS [22], the Binary Logit model and Ordered Probit models are estimated, and the results are shown in Table 5.

5. Discussions

By comparing the test results of MAPE and *Hit ratio* with respect to the predictions of the three severity indicators, it can be concluded that the goodness of fit of Bayesian network is higher than that of Regression models. This suggests that Bayesian network is more suitable in accident severity prediction than Regression models regarding modeling accuracy.

Besides goodness of fit, there is also difference between Bayesian network and Regression models regarding the interactions between the variables in the model. In Bayesian network, indirect nodes (or variables), which are related to the dependent variable, affect their own child nodes first, and then the impacts are delivered to the related edges and nodes until they arrive the dependent variable [23, 24]. As shown in Figure 3(1), every indirect node's change will cause dependent variable's change. The impact of indirect node on dependent variable can be obtained by inference based on the constructed Bayesian network. For instance, the impacts of L-C on the three accident severity variables are inferred according to the Bayesian network for accident severity analysis, and the results are shown in Table 6. Comparing with Bayesian network, all the independent variables, either indirect node, child node or direct node in the Bayesian network, affect the dependent variable directly in the Regression models [25, 26]. The interactions between variables in the Regression models are shown in Figure 3(2).

Moreover, for Regression models, two independent variables cannot exist in one model if they are related to each other. This causes the missing of some influences between variables. Also, Regression models will fail to present the impact between dependent variable and dependent variable as well as the interaction between independent variable and independent variable, such as the impact of Noi on Nof and the effect of Rsc on Bti in this study, respectively, which can be presented by the Bayesian work shown in Figure 2.

Furthermore, as mentioned above, most of the Regression models have their own assumptions and predefined underlying relationships between dependent and independent variables (i.e., linear relations between the variables or independence between variables) [7, 8]. The differences between Regression models and Bayesian network also reflect the methods of probabilistic reasoning [27–29]. That is, Bayesian network can reason under uncertainty, but Regression models cannot. In addition, for parameter estimation, Regression models need complete (without missing values) and quantitative data, while Bayesian network can be constructed with incomplete data or qualitative information [30, 31].

The above characteristics of Bayesian network prove that, compared with Regression models, Bayesian network is more suitable to be adopted in accident severity analysis.

6. Conclusions

In this paper, two modeling techniques, that is, Bayesian network and Regression models, are investigated in accident severity modeling. The goodness of fit of the two methods is compared according to the test results, and the differences

Table 5: Estimation results of the Regression models.

Variables	Fatality forecasting model		Injury forecasting model		Property damage forecasting model	
	Coef.	Z-stat.	Coef.	Z-stat.	Coef.	Z-stat.
Constant	−2.57	−12.53				
Mi	0.44	3.36	−0.14	−2.50	−0.09	−1.85
Bi	1.11	8.82	−0.30	−4.99		
Wc	−0.27	−1.66	0.23	2.70	−0.12	−1.85
Tod	−0.44	−4.03			−0.15	−3.29
Vd					0.10	4.88
Pc			−0.38	−5.24		
Tsc	0.22	2.06	−0.07	−1.57	0.11	2.76
L-Mvl			−0.08	−1.57		
L-C	−0.52	−1.39			−0.40	−3.51
L-Rrs	0.73	5.98			0.72	4.07
L-I			0.23	4.94	0.20	1.10
α_1			−1.50		0.80	
α_2			1.47		2.77	
MAPE	0.0530		0.0415		0.0698	
Hit ratio (%)	84.65		80.20		60.23	

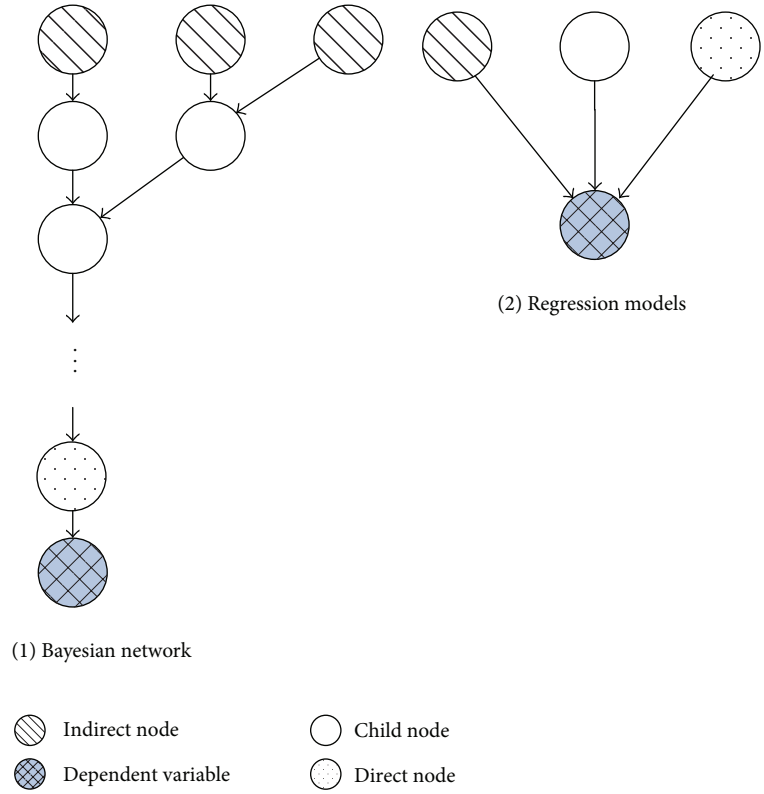

Figure 3: Comparison of Bayesian network and Regression models with respect to the interactions between variables.

between the two methods are analyzed. The results suggest that, comparing with Regression models, Bayesian network is more suitable for accident severity prediction.

Study results can be applied to predicting traffic accident severity and identifying the key effects of contributed factors on accident severity. By comparing Bayesian network and Regression models, it also makes a methodological contribution in enhancing prediction accuracy of severity estimation.

It should be pointed out that both the structure and the parameter of the proposed Bayesian network will change when there are specific numbers of new reported cases added into the data set. According to the study by Zhang [32],

Table 6: Impact of L-C on accident severity.

Accident severity		At crosswalk	Not at crosswalk
Noi	Noi = 0	0.0578	0.0881
	1 ≤ Noi < 3	0.8864	0.8883
	Noi ≥ 3	0.0558	0.0237
Nof	Nof > 0	0.9080	0.8990
	Nof = 0	0.0920	0.1010
Pd	Pd < 1000	0.7484	0.7313
	1000 ≤ Pd < 30000	0.2439	0.2614
	Pd ≥ 30000	0.0077	0.0074

the structure and the parameter of the Bayesian network will change when the amount of new records reaches 10% and 5% of the number of the original cases, respectively.

One limitation of current work is that some factors, such as driver characteristics and traffic condition, which have potential effects on accident severity, are not considered because of the lack of suitable data. Further study should be conducted to examine the impacts of these factors on accident severity.

Acknowledgments

The research is funded by the National Natural Science Foundation of China (50908099 and 51078167) and the Doctoral Program of Higher Education of China (201104493).

References

[1] A. S. Al-Ghamdi, "Using logistic regression to estimate the influence of accident factors on accident severity," *Accident Analysis and Prevention*, vol. 34, no. 6, pp. 729–741, 2002.

[2] J. C. Milton, V. N. Shankar, and F. L. Mannering, "Highway accident severities and the mixed logit model: an exploratory empirical analysis," *Accident Analysis and Prevention*, vol. 40, no. 1, pp. 260–266, 2008.

[3] M. Bédard, G. H. Guyatt, M. J. Stones, and J. P. Hirdes, "The independent contribution of driver, crash, and vehicle characteristics to driver fatalities," *Accident Analysis and Prevention*, vol. 34, no. 6, pp. 717–727, 2002.

[4] K. K. W. Yau, H. P. Lo, and S. H. H. Fung, "Multiple-vehicle traffic accidents in Hong Kong," *Accident Analysis and Prevention*, vol. 38, no. 6, pp. 1157–1161, 2006.

[5] T. Yamamoto and V. N. Shankar, "Bivariate ordered-response probit model of driver's and passenger's injury severities in collisions with fixed objects," *Accident Analysis and Prevention*, vol. 36, no. 5, pp. 869–876, 2004.

[6] K. M. Kockelman and Y. Kweon, "Driver injury severity: an application of ordered probit models," *Accident Analysis and Prevention*, vol. 34, no. 3, pp. 313–321, 2002.

[7] L. Chang and H. Wang, "Analysis of traffic injury severity: an application of non-parametric classification tree techniques," *Accident Analysis and Prevention*, vol. 38, no. 5, pp. 1019–1027, 2006.

[8] J. de Oña, R. O. Mujalli, and F. J. Calvo, "Analysis of traffic accident injury severity on Spanish rural highways using Bayesian networks," *Accident Analysis and Prevention*, vol. 43, no. 1, pp. 402–411, 2011.

[9] M. Simoncic, "A Bayesian network model of two-car accidents," *Journal of Transportation and Statistics*, vol. 7, no. 2-3, pp. 13–25, 2004.

[10] K. Ozbay and N. Noyan, "Estimation of incident clearance times using Bayesian Networks approach," *Accident Analysis and Prevention*, vol. 38, no. 3, pp. 542–555, 2006.

[11] A. Gregoriades, "Towards a user-centred road safety management method based on road traffic simulation," in *Proceedings of the 39th Conference on Winter Simulation: 40 years! The Best is Yet to come*, pp. 1905–1914, Washington, DC, USA, December 2007.

[12] P. Kopelias, F. Papadimitriou, K. Papandreou, and P. Prevedouros, "Urban freeway crash analysis geometric, operational, and weather effects on crash number and severity," *Transportation Research Record*, vol. 2015, pp. 123–131, 2007.

[13] A. Mittal, A. Kassim, and T. Tan, *Bayesian Network Technologies: Applications and Graphical Models*, IGI Publishing, New York, NY, USA, 2007.

[14] G. F. Cooper and E. Herskovits, "A Bayesian method for the induction of probabilistic networks from data," *Machine Learning*, vol. 9, no. 4, pp. 309–347, 1992.

[15] E. Herskovits, *Computer-based probabilistic-network construction [Ph.D. dissertation]*, Medical Information Sciences, Stanford University, Stanford, Calif, USA, 1991.

[16] D. Eaton and K. Murphy, "Bayesian structure learning using dynamic programming and MCMC," in *Proceedings of the 23rd Conference on Uncertainty in Artificial Intelligence (UAI '07)*, pp. 101–108, July 2007.

[17] F. Zong, H. Y. Lin, B. Yu, and X. Pan, "Daily commute time prediction based on Genetic algorithm," *Mathematical Problems in Engineering*, vol. 2012, Article ID 321574, 20 pages, 2012.

[18] F. Zong, Z. C. Juan, and H. F. Jia, "Examination of staggered shifts impacts on travel behavior: a case study of Beijing," *Transport*, vol. 28, no. 2, pp. 175–185, 2013.

[19] P. Ray, "Independence of irrelevant alternatives," *Econometrica*, vol. 41, pp. 987–991, 1973.

[20] J. L. Bowman and M. E. Ben-Akiva, "Activity-based disaggregate travel demand model system with activity schedules," *Transportation Research A*, vol. 35, no. 1, pp. 1–28, 2000.

[21] M. A. Quddus, R. B. Noland, and H. C. Chin, "An analysis of motorcycle injury and vehicle damage severity using ordered probit models," *Journal of Safety Research*, vol. 33, no. 4, pp. 445–462, 2002.

[22] R. A. Hanneman, 2013, Ordered Logit and Probit Models with PROC LOGIST and PROC PROBIT. The course in Generalized Linear Models. University of California, http://faculty.ucr.edu/~hanneman/soc271/ologit.html.

[23] B. Z. Yao, C. Y. Yang, and J. B. Yao, "Tunnel surrounding rock displacement prediction using support vector machine," *International Journal of Computational Intelligence Systems*, vol. 3, no. 6, pp. 843–852, 2010.

[24] J. B. Yao, B. Z. Yao, L. Li, and Y. L. Jiang, "Hybrid model for displacement prediction of tunnel surrounding rock," *Neural Network World*, vol. 22, pp. 263–275, 2012.

[25] Y. Bin, Y. Zhongzhen, and Y. Baozhen, "Bus arrival time prediction using support vector machines," *Journal of Intelligent Transportation Systems*, vol. 10, no. 4, pp. 151–158, 2006.

[26] B. Yu, W. H. K. Lam, and M. L. Tam, "Bus arrival time prediction at bus stop with multiple routes," *Transportation Research C*, vol. 19, no. 6, pp. 1157–1170, 2011.

[27] B. Yu, Z. Yang, and B. Yao, "An improved ant colony optimization for vehicle routing problem," *European Journal of Operational Research*, vol. 196, no. 1, pp. 171–176, 2009.

[28] B. Yu, Z.-Z. Yang, and J.-X. Xie, "A parallel improved ant colony optimization for multi-depot vehicle routing problem," *Journal of the Operational Research Society*, vol. 62, no. 1, pp. 183–188, 2011.

[29] B. Yu, Z. Z. Yang, and S. Li, "Real-time partway deadheading strategy based on transit service reliability assessment," *Transportation Research A*, vol. 46, no. 8, pp. 1265–1279, 2012.

[30] B. Y. Chen, W. H. K. Lam, A. Sumalee, Q. Q. Li, H. Shao, and Z. X. Fang, "Finding reliable shortest paths in road networks under uncertainty," *Networks and Spatial Economics*, vol. 13, no. 2, pp. 123–148, 2013.

[31] B. Y. Chen, W. H. K. Lam, A. Sumalee, and H. Shao, "An efficient solution algorithm for solving multi-class reliability-based traffic assignment problem," *Mathematical and Computer Modelling*, vol. 54, no. 5-6, pp. 1428–1439, 2011.

[32] H. Y. Zhang, *Analyzing traffic accident situation with Bayesian network [Doctoral dissertation]*, Jilin University, Changchun, China, 2013, (Chinese).